1-1-2016

Structural Characterization And Therapeutic Utility Of The Proton-Coupled Folate Transporter

Michael Roy Wilson
Wayne State University,

STRUCTURAL CHARACTERIZATION AND THERAPEUTIC UTILITY OF THE PROTON-COUPLED FOLATE TRANSPORTER

by

MICHAEL ROY WILSON

DISSERTATION

Submitted to the Graduate School

of Wayne State University,

Detroit, Michigan

in partial fulfillment of the requirements

for the degree of

DOCTOR OF PHILOSOPHY

2016

MAJOR: CANCER BIOLOGY

Approved By:

_____

Advisor Date

_____

_____

_____

_____

DEDICATION

This dissertation is dedicated to my family, who have given me so much love and support throughout my life and throughout my career.

To my grandmother, Sue, who has survived chronic lymphoblastic leukemia and non-Hodgkin's lymphoma, and to my grandfather, Lee, who lost his battle with metastatic prostate cancer. They have been my inspiration to research new cancer therapies.

To my siblings, Marissa and Lucas, who have always been my biggest fans and best friends.

To my fiancé, Shannon, who has provided so much encouragement, patience and love.

To my father, Roy, who was my first mentor and role model. He gave me the work ethic and ambition that has been so vital to my career.

And to my mother, Jill, who was my first teacher. She gave me the thirst for knowledge that has always driven me. They have always believed in me, and I owe them so much. This path in life would never have been possible without them.

ACKNOWLEDGEMENTS

I would like to thank my mentor, Dr. Larry Matherly, without whom this project would not have been possible. Dr. Matherly has helped me to think both critically and creatively in science. He has dedicated countless hours to my education and to my career, despite so many other obligations. Dr. Matherly has always encouraged me to learn new methods and to test every idea. Without his expertise and ambition, my graduate studies could not have been so successful. I feel that wherever my career takes me, Dr. Matherly has prepared me for it.

I would like to thank Dr. Zhanjun Hou, who has taught me so many scientific techniques. Zhanjun has taught me to think carefully and critically when it comes to experimental design, and has consulted on nearly every experiment I performed. Without his patience in teaching me and his eye for detail, I could not have produced such quality work.

I would like to thank the past and present members of the Matherly lab, including Christina George, Steve Orr, Dr. Sita Kugel, Dr. Eric Hales, Erika Etnyre, Jenny Huang, Lucas Wilson, Dr. Leda Gattoc, Aamod Dekhne, Carrie O'Connor, and Adrianne Wallace-Povirk, who have all been extremely helpful and kind throughout my time in the lab.

I would like to thank Dr. Aleem Gangjee and his laboratory for the synthesis of the antifolate compounds studied in this dissertation project. I would like to thank Dr. Lisa Polin, Juiwanna Kushner and Kathryn White for the many hours they spent teaching me to work with mice. I would like to thank my committee members, Dr. Manohar Ratnam, Dr. George Brush, Dr. Zengquan Yang, and Dr. Bharati Mitra, who have provided much insight and guidance.

Finally, I would like to thank my funding, T-32 CA009531 from the NIH and the Rumble Fellowship from Wayne State University.

TABLE OF CONTENTS

LIST OF TABLES

LIST OF FIGURES

LIST OF ABBREVIATIONS

AICAR	5-aminoimidazole-4-carboxamine ribonucleotide
AICARFTase	5-aminoimidazole-4-carboxamine ribonucleotide formyltransferase
ALL	Acute lymphoblastic leukemia
AMT	Aminopterin
AMPK	AMP-activated protein kinase
CL	Cysteine-less
CHO	Chinese hamster ovary cells
Dex	Dexamethasone
DHF	Dihydrofolate
DHFR	Dihydrofolate reductase
dTMP	Thymidylate
DMEM	Dulbecco's modified Eagle's medium
DTT	Dithiothreiotol
dTTP	Deoxythymidine triphosphate
dUMP	Deoxyuridine monophosphate
dUTP	Deoxyuridine triphosphate
EC145	Vintafolide
ECFP	Enhanced cyan fluorescent protein
EGFR	Epidermal growth factor receptor
FBS	Fetal bovine serum
FDA	Food and Drug Administration
FPGS	Folylpoly-γ-glutamate synthase

FR	Folate receptor
FRET	Fluorescence resonance energy transfer
GAR	Glycinamide ribonucleotide
GARFTase	Glycinamide ribonucleotide formyltransferase
GlpT	Glycerol-3-phosphase transporter
GPI	Glycosyl phosphatidylinositol
GR	Glucocorticoid receptor
HA	Hemagglutinin
HBS	HEPES-buffered saline
HEPES	4-(2-hydroxyethyl)-1-piperazineethanesulfonic acid
HFM	Hereditary folate malabsorption
IC_{50}	Fifty percent inhibitory concentration
IHC	Immunohistochemistry
IMP	Inosine monophosphate
KD	Knockdown
LacY	Lactose permease
LCV	Leucovorin
LMX	Lometrexol
MEM	Minimal essential media
MES	2-(*N*-morpholino)ethanesulfonic acid
MFS	Major facilitator superfamily
MRP	Multidrug resistance protein
MTHFD	Methylenetetrahydrofolate dehydrogenase

MTHFR	5,10-MethyleneTHF reductase
MTS-1-MTS	1,1- methanediyl bismethanethiosulfonate
MTS-6-MTS	1,6-hexanediyl bismethanethiosulfonate
MTSEA	2-aminoethyl methanethiosulfonate
MTSES	2-sulfonatoethyl methanethiosulfonate
MTSET	2-(Trimethylammonium)ethyl methanethiosulfonate
MTX	Methotrexate
NSCLC	Non-small cell lung cancer
NS-NSCLC	Non-squamous non-small cell lung cancer
NTC	Non-targeted control
OAT	Organic anion transpoter
PBS	Phosphate buffered saline
PCFT	Proton-coupled folate transporter
PDX	Pralatrexate
PIPES	Piperazine-N,N'-bis(2-ethanesulfonic acid)
PMX	Pemetrexed
PRPP	Phosphoribosyl pyrophophaste
PT523	Talotrexin
RFC	Reduced folate carrier
RTX	Raltitrexed
RT-PCR	Reverse transcription-polymerase chain reaction
SAR	Structure activity relationship
SCAM	Substituted cysteine accessibility methods

SCID	Severe-combined immunodeficient
SHMT	Serine hydromethyltransferase
SLC	Solute Carrier
THF	Tetrahydrofolate
TMD	Transmembrane domain
TS	Thymidylate synthase
WT	Wild-type
Ypet	Yellow fluorescent protein
ZD9331	Plvitrexed
ZMP	5-aminoimidazole-4-carboxamine ribotide

CHAPTER 1- INTRODUCTION

1.1 Introduction to Folate Biology

Folates are B9 vitamins required for cellular growth (Stokstad, 1990). Mammalian cells cannot synthesize folates *de novo*, and must obtain these cofactors from exogenous sources. Folates contribute to several one-carbon transfer reactions in the synthesis of serine, methionine, thymidylate, and purine nucleotides. In its contribution to methionine synthesis, folates are required for the synthesis of S-adenosyl methionine, which is necessary for DNA, histone, and lipid methylation (Lu, 2000).

The major circulating form of folate is 5-methyl tetrahydrofolate (THF) (Figure 1.1), which is converted to several other polyglutamylated forms (the preferred forms for metabolic single-carbon transfer reactions) following uptake of the monoglutamyl forms into cells (Moran, 1999; Shane, 1989). Mammals must obtain folates through the diet. Dark green leafy vegetables and liver are foods which are high in folate content, although several other foods including bread, grains, and cereal have been fortified with folic acid, a synthetic form of folate not found in tissues (Jacques et al., 1999).

At physiological pH, folates are hydrophilic anions and are unable to diffuse across membranes. Over time, two major facilitative transporters have evolved in mammals in order to facilitate transport of folates into cells, the reduced folate carrier (RFC; Solute Carrier (SLC) 19A1) and the proton-coupled folate transporter (PCFT; SLC46A1) (Goldman et al., 1968; Matherly and Goldman, 2003; Qiu et al., 2006; Zhao et al., 2011a), as well as three isoforms of folate receptors (FRs) (α, β, and γ) (Elwood, 1989; Lacey et al., 1989; Ratnam et al., 1989; Sadasivan and Rothenberg, 1989; Shen et al., 1994; Shen et al., 1995).

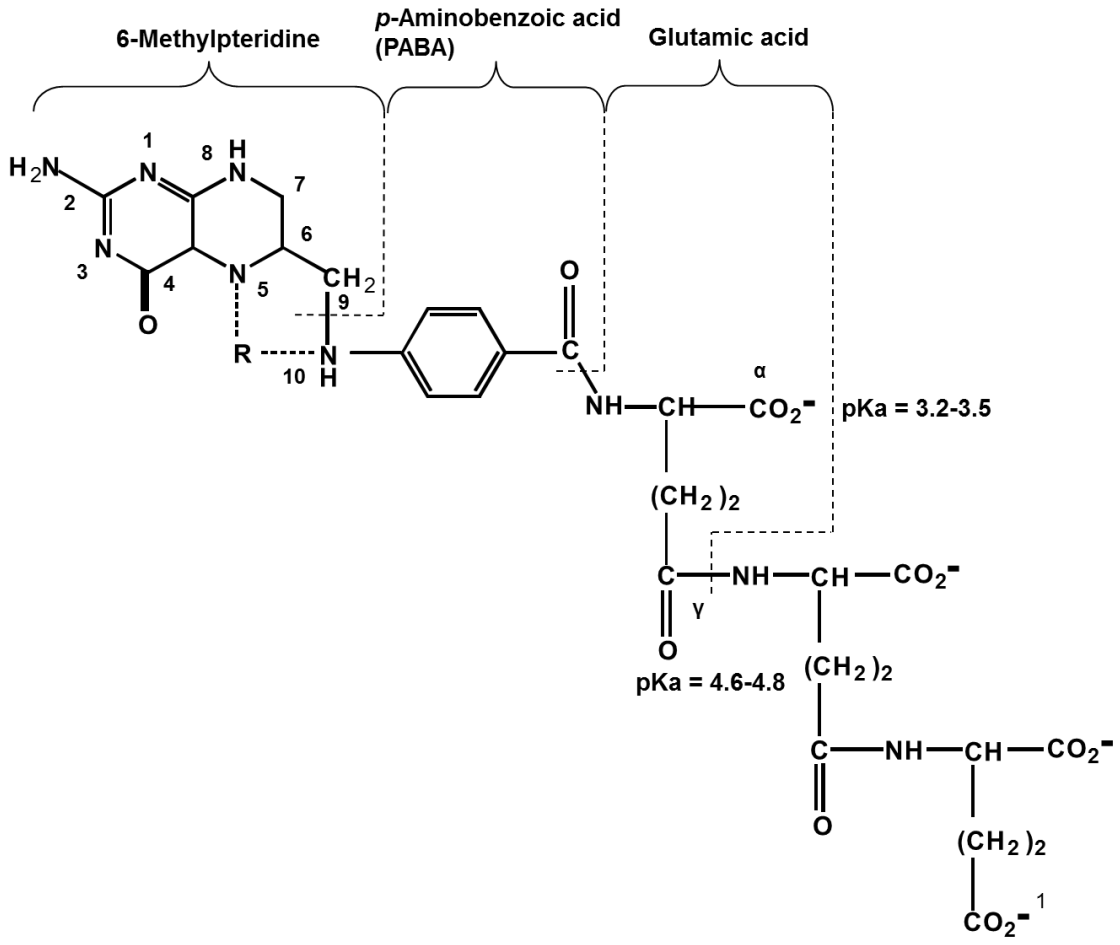

Figure 1.1 Structure of tetrahydrofolate. THF is the major form of dietary folate. The N5 and N10 position can associate with several one-carbon moietys including methyl, formyl, methylene and methenyl, which can be used in biosynthetic reactions. THF can have additional glutamate groups added by FPGS, contributing to cellular retention.

RFC is an anion exchange transporter and a member of the major facilitator superfamily (MFS), which serves as the major folate uptake mechanism at neutral physiological pH and is ubiquitously expressed in tissues and tumors. PCFT is a proton/folate symporter and also an MFS protein, which serves as the primary mechanism of dietary folate uptake and with a specificity for acidic pH folate uptake and distinct transport specificities from RFC. PCFT shows substantial expression in the duodenum and jejunum, kidney, liver, and the choroid plexus (Inoue et al., 2008; Qiu et al., 2006; Umapathy et al., 2007; Zhao et al., 2009a; Zhao et al., 2009b). FRα and β are embedded in the plasma membrane by a glycosyl phosphatidylinositol (GPI) anchor in certain cells including renal cells and macrophages, respectively (Elnakat and Ratnam, 2004; Leamon and Low, 2001; Weitman et al., 1992b). FRs mediate uptake of folates into cells via receptor-mediated endocytosis (Kamen et al., 1988; Leamon and Low, 1991; Turek et al., 1993; Wu et al., 1997). FRα expression is found in the uterus, placenta, proximal renal tubules, and choroid plexus, while FRβ shows expression in hematopoietic cells, activated macrophages, and the placenta (Nakashima-Matsushita et al., 1999; Ratnam et al., 1989; Ross et al., 1994; Ross et al., 1999; Weitman et al., 1992b). There is also FRγ, which is secreted and serves an unknown purpose (Elnakat and Ratnam, 2004; Shen et al., 1995).

In addition to their role as facilitative transporters of folates, RFC and PCFT serve critical roles in the transport of antifolates for used in cancer chemotherapy (Figure 1.2). Antifolates including methotrexate (MTX), pemetrexed (PMX), raltitrexed (RTX) and pralatrexate (PDX) are transported by both RFC and PCFT, although RFC transport dominates under neutral pH conditions characterizing most tissues (Nakai et al., 2007; Sierra et al., 1997; Zhao and Goldman, 2007). Both RFC and PCFT were shown to be abundantly expressed in a wide variety of solid

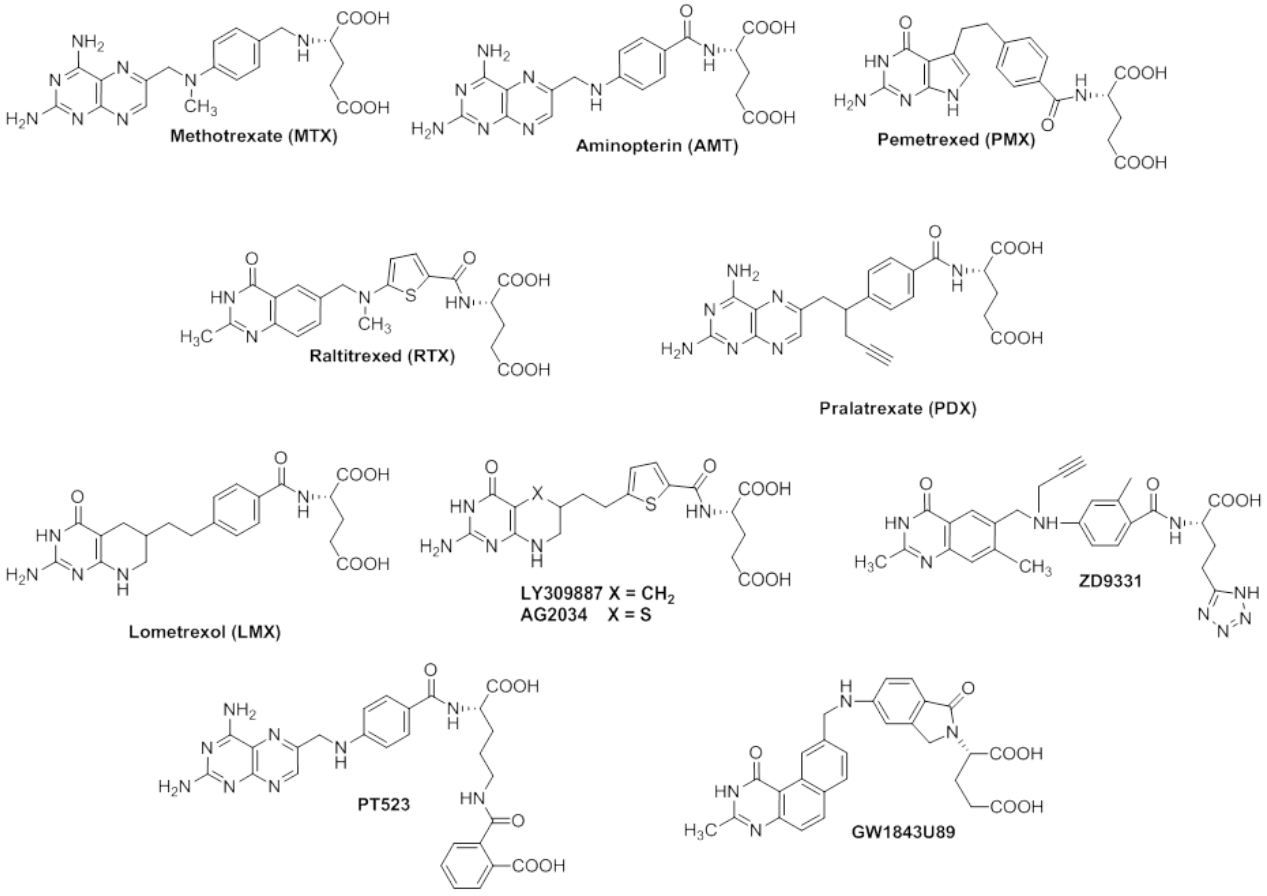

Figure 1.2 Structures of classical antifolate molecules. Structures for clinically relevant antifolates: MTX, PMX, RTX, PDX, and AMT, as well as antifolates which had clinical trials: LMX, ZD9331, GW1843U89, PT523, LY309887, AG2034. All drugs are described in Chapter 1.6.1-1.6.4.

tumor cell lines, although gene expression data in primary tumors is still emerging (Desmoulin et al., 2012b; Kugel Desmoulin et al., 2011) (also see Chapter 5). Notably, PCFT is characterized by an acidic pH optimum and is well suited to transport in the acidic tumor microenvironment (Nakai et al., 2007; Zhao and Goldman, 2007). Because of the ubiquitous expression of RFC in normal tissues as well as tumors, there has been a recent interest in developing novel antifolate molecules targeting the tumor microenvironment via PCFT over RFC (Cherian et al., 2013; Desmoulin et al., 2012a; Golani et al., 2014; Wang et al., 2012; Wang et al., 2010; Wang et al., 2011; Wang et al., 2015) (also see Chapters 5 and 6). While progress has been made in the development of PCFT-specific antifolate compounds, these have been developed entirely without PCFT structural modeling, due to the limited availability of PCFT structural data. Molecular modeling using x-ray crystal structures from other MFS proteins has provided an estimate of PCFT structure. Experimental manipulations of PCFT protein sequence have contributed to our understanding of PCFT topology and key structural determinants of PCFT function, in some cases validating and in other cases correcting the molecular models which have been developed (Hou et al., 2012; Shin et al., 2011; Shin et al., 2010; Shin et al., 2013; Shin et al., 2012; Subramanian et al., 2008; Unal et al., 2009a; Unal et al., 2009b; Unal et al., 2008; Visentin et al., 2015; Zhao et al., 2007; Zhao et al., 2011b; Zhao et al., 2012; Zhao et al., 2010) (also see Chapters 2, 3, and 4). A comprehensive understanding of PCFT structure is essential to understanding the mechanism of transport and is complementary to the development of novel cancer therapeutics targeting PCFT. This chapter serves as a review of the biology of folate transport and metabolism, as well as to deseribe the history of antifolate drug development leading to a novel series of PCFT-selective antifolate molecules as tumor-targeted drugs.

1.2 Reduced Folate Carrier

RFC has been well established as the main cellular and tissue folate uptake mechanism (Matherly and Hou, 2008; Matherly et al., 2007). RFC is ubiquitously expressed, and serves as the primary delivery system for both folates and antifolates throughout the body (Matherly et al., 2007). RFC is a folate/anion antiporter in the MFS, and was first characterized in terms of its kinetic and thermodynamic properties more than 40 years ago (Goldman, 1969; Goldman, 1971; Goldman et al., 1968; Sirotnak et al., 1968). Murine *RFC* was first cloned in 1994 (Dixon et al., 1994), while human *RFC* was cloned by multiple labs the following year (Moscow et al., 1995; Prasad et al., 1995; Williams and Flintoff, 1995; Wong et al., 1995). Human *RFC* is located on chromosome 21q22.3 (Moscow et al., 1995) and is regulated by multiple promotors spanning 35 kb upstream from the major AUG translation start point, as well as many noncoding exons (Matherly et al., 2007). RFC is additionally regulated by promoter methylation and chromatin structure (Liu et al., 2004; Payton et al., 2005a; Payton et al., 2005b; Whetstine et al., 2002b). These mechanisms likely guarantee the ubiquitous expression of RFC. Measurements of RFC transcriptional expression in various tissues and tumor cell lines revealed the highest RFC expression in the placenta and liver, with additional high expression in kidney, lung, leukocytes, bone marrow and small intestine, and low levels in heart and skeletal muscles (Whetstine et al., 2002a). Although the function of RFC in the small intestine is unclear, as RFC function is dramatically decreased in acidic pH, folate deficiency in rodents resulted in increased RFC transcript and protein levels (Liu et al., 2005).

As an anion-folate antiporter, RFC functions optimally at neutral physiological pH, and transport activity decreases dramatically at pHs below 7 (Sierra et al., 1997). While RFC has a low affinity for folic acid, (6S)5-formyl THF and (6S)5-methyl THF are excellent RFC

substrates (Goldman et al., 1968; Westerhof et al., 1995). Although transport of (6S)5-formyl THF is favored over the (6R) stereoisomer (Sirotnak et al., 1979), RFC displays no stereospecificity for 5-methyl THF (Chello et al., 1982; White et al., 1978). Additionally, many clinically used antifolates have strong affinity for RFC transport, including MTX, PMX, PDX and RTX (Jansen, 1999; Matherly and Hou, 2008; Matherly et al., 2007; Sirotnak et al., 1998; Visentin et al., 2013). Novel antifolates PT523 (talotrexin) and GW1843U89 are among the best RFC substrates yet described (Jansen, 1999; Rhee et al., 1994; Rosowsky et al., 1994; Wright et al., 2000).

As with all MFS transport proteins (Abramson et al., 2003; Huang et al., 2003), hydropathy plot analysis of RFC amino acid sequence (591 amino acids) predicted twelve transmembrane domains (TMDs) with both carboxyl and amino termini located within the cytosol (Figure 1.3) (Matherly and Hou, 2008; Matherly et al., 2007). Thease features have been confirmed by scanning cysteine accessibility methods (SCAM), N-glycosylation mutagenesis and hemagglutin epitope insertion (Cao and Matherly, 2004; Ferguson and Flintoff, 1999; Liu and Matherly, 2002). RFC is glycosylated at Asn58 on the first extracellular loop connecting TMDs 1 and 2, and mutation of this residue to Gln abolishes N-glycosylation without major effects on membrane targeting or transport activity (Matherly et al., 1991; Wong et al., 1998). As with many MFS proteins, RFC contains a long intracellular loop connecting the long distances between TMDs 6 and 7 (Figure 1.3). For RFC, this TMD6-7 loop shows the lowest amount of sequence conservation between species (human and rodents). Deletion of large segments of this loop region (amino acid residues 215-263 or 204-263) abolished transport, while replacement of this region with the MFS homolog SLC19A2 (thiamine transporter ThTr1) restored transport (Liu et al., 2003). Removal of the C- and N- termini had minimal effects on trafficking and

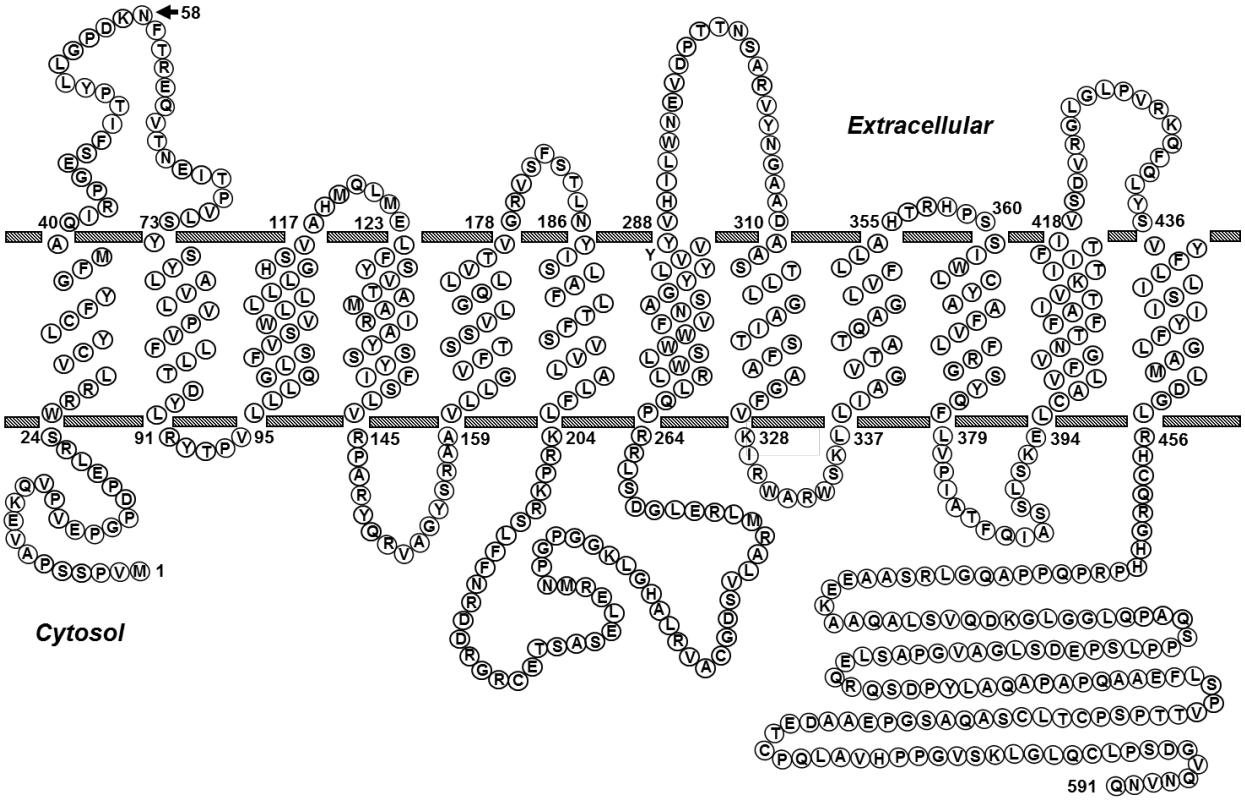

Figure 1.3 Membrane topology of the human reduced folate carrier. This figure shows the predicted topology for RFC, much of which has been experimentally confirmed. EL, extracellular loop; IL, intracellular loop.

function of RFC (Liu et al., 2003). RFC was expressed as two distinct half-molecules (amino acid residues 1-301 or 302-591) and while each half-molecule was non-functional, co-transfection of both half-molecules restored RFC function (Witt et al., 2004). These results suggest that the TMD6-7 loop region of RFC plays a primarily structural role, connecting the long gap between TMDs 6 and 7.

In order to perform SCAM to characterize the RFC protein structure, a "cys-less" RFC was developed using mutagenesis to replace the 11 cysteine residues with serine (Cao and Matherly, 2003). In total, 282 RFC cysteine mutants were developed from cys-less RFC and used for 2-sulfonatoethyl methanethiosulfonate (MTSES) scanning via transfection into RFC-null Hela (R5) cells. Based on patterns of MTSES transport inhibition, it was determined that TMDs 4, 5, 7, 8, 10 and 11 comprise the membrane translocation pathway for folate substrates (Hou et al., 2005; Hou et al., 2006), confirming models predicted by hydropathy modeling and MFS comparisons. Of the 282 cysteine mutants, only 10 were inactive for transport activity, including residues on TMD4 (Arg133, Ile134, Ala135, Tyr136, Ser138), TMD7 (Tyr281), TMD8 (Ser313) and TMD10 (Arg373). Arg133, Arg373 and Ser313 had been previously shown to be functionally important (Liu and Matherly, 2001; Sadlish et al., 2002; Sharina et al., 2001; Zhao et al., 1999).

RFC exists as a homo-oligomer (Hou and Matherly, 2009), although RFC monomers function independently (Hou et al., 2010). Cofolding of RFC monomers is necessary for intracellular trafficking and surface activity, such that RFC displays a dominant-negative effect (Hou and Matherly, 2009). When wild-type RFC and inactive mutant S138C RFC were co-transfected into RFC-null (R5) HeLa cells, both RFC proteins displayed decreased cell surface

expression due to impaired cellular trafficking, as observed by confocal microscopy and surface biotinylation.

1.3 Folate Receptors

Folate receptors (FRs) are high affinity folate binding proteins, which bind folic acid, reduced folates, and many antifolate molecules with low-nanomolar affinities, and bring them into the cell using an endocytosis mechanism (Rijnboutt et al., 1996; Sabharanjak and Mayor, 2004). FRs exist in three isoforms; α, β, and γ (Elwood, 1989; Lacey et al., 1989; Ratnam et al., 1989; Sadasivan and Rothenberg, 1989; Shen et al., 1994; Shen et al., 1995), which are each encoded by unique genes located at chromosome 11q13.3-q13.5 (Elnakat and Ratnam, 2004). Human FRs share 68-79% amino acid sequence identity. FRα contains three N-glycosylation sites, while FRβ and FRγ have only two. While FRα and FRβ are GPI-anchored glycoproteins, FRγ does not contain a signal for GPI-anchoring and is instead a secretory protein with an unknown function (Elnakat and Ratnam, 2004).

Membrane-bound (α and β) FRs function to mediate cellular folate uptake via endocytosis. Folates bind FRα/β at the plasma membrane, followed by invagination, formation, and budding-off of an endosome (Rijnboutt et al., 1996; Sabharanjak and Mayor, 2004). Release of folate ligand from FR ensues upon acidification of the endosome. Exit of the folate molecule from the endosome involves either diffusion out of the intact vesicle or pH-dependent transport processes (Kamen et al., 1988). PCFT has been implicated to play a role in the export of endosomal folates (Zhao et al., 2009b).

FRα shows expression primarily in the choroid plexus, retinal pigment epithelium, and proximal tubules in uterus, placenta, fallopian tubes, and kidney (Elnakat and Ratnam, 2004). In these tissues, FRα is expressed on the apical (luminal) surface of polarized epithelial cells, and

therefore does not come into contact with circulating folates (Chancy et al., 2000), a feature which protects these tissues from circulating FRα-targeted antifolate molecules (Weitman et al., 1992b). FRβ is expressed in the placenta and hematopoietic cells (Elnakat and Ratnam, 2004). Expression of FRβ in normal bone marrow and peripheral blood cells is limited to the myelomonocytic lineage, such as mature neutrophils, and is reported as non-functioning (Pan et al., 2002; Reddy et al., 1999).

1.4 Proton-Coupled Folate Transporter

Although an additional transport mechanism other than RFC was previously recognized as capable of intestinal folate uptake, it was not until 2006 that this transporter, PCFT, was identified and cloned, providing the molecular basis for low pH folate transport activity (Assaraf et al., 1998; Henderson and Strauss, 1990; Kuhnel et al., 2000; Sierra and Goldman, 1998; Zhao et al., 2004a; Zhao and Goldman, 2007). PCFT plays a critical role in absorption of dietary folates into the intestine, as demonstrated by hereditary folate malabsorption (HFM) patients harboring loss-of-function mutations, as well as by PCFT knockout mice (Atabay et al., 2010; Borzutzky et al., 2009; Diop-Bove et al., 2009; Lasry et al., 2008; Mahadeo et al., 2010; Mahadeo et al., 2011; Meyer et al., 2010; Min et al., 2008; Qiu et al., 2006; Salojin et al., 2011; Shin et al., 2011; Shin et al., 2010; Zhao and Goldman, 2007). PCFT knockout mice had undetectable levels of serum folate (Salojin et al., 2011). PCFT plays a major role in intestinal folate absorption, and has been shown to be expressed in certain other tissues (Desmoulin et al., 2012a).

1.4.1 PCFT Tissue Expression

PCFT has been identified as a folate transporter which operates at an acidic pH optimum, consistant with its main function of transporting dietary folates (Zhao and Goldman, 2007).

PCFT levels are highest at the apical brush border membrane of the proximal jejunum and the duodenum, but expression in other segments of the intestine and colon is dramatically decreased (Inoue et al., 2008; Qiu et al., 2006; Qiu et al., 2007; Urquhart et al., 2010). PCFT is also expressed in the choroid plexus and plays a role in folate transport into the central nervous system, where it may function in conjunction with FRs to release folates from endosomes (Wollack et al., 2008; Zhao et al., 2009b). While high levels of PCFT gene expression were detected in other tissues, in particular liver and kidney, its role in these tissues has not been explored (Desmoulin et al., 2012a).

1.4.2 Hereditary Folate Malabsorption

Mutations in PCFT can cause HFM, a rare autosomal-recessive disease which results in loss of the low pH intestinal absorption of dietary folates by PCFT (Atabay et al., 2010; Borzutzky et al., 2009; Geller et al., 2002; Lasry et al., 2008; Mahadeo et al., 2010; Meyer et al., 2010; Min et al., 2008; Qiu et al., 2006; Shin et al., 2011; Shin et al., 2010; Unal et al., 2009b; Zhao et al., 2007). HFM leads to systemic folate deficiency, and is associated with developmental delay, peripheral neuropathies, seizures, gait disorders, anemia, hypoimmunoglobulinemia, and *Pneumocyctis jiroveci* pneumonia (Geller et al., 2002). Loss of PCFT function in HFM also results in impaired transport of folates across the choroid plexus into the central nervous system (Wollack et al., 2008; Zhao et al., 2009b). Infants who present HFM display neurological defects, revealing the importance of PCFT function in the central nervous system. The existence of HFM implies the importance of PCFT folate transport in both the intestine and the nervous system.

1.4.3 PCFT Function

PCFT exhibits an acidic pH optimum, transporting folates most effectively at pH 5-5.5,

with transport becoming less effective as pH increases (Inoue et al., 2008; Qiu et al., 2006; Zhao and Goldman, 2007; Zhao et al., 2009a). Above pH 7, PCFT is nearly incapable of folate transport, although specific transport efficiencies with increasing pH vary for particular (anti)folate molecules, largely reflecting differences in substrate binding (Zhao and Goldman, 2007). Unlike RFC, PCFT shows similar binding affinities (K_t) for reduced folates (5-formyl and 5-methyl THF) as for folic acid, and is stereospecific for (6*S*)5-formyl THF. PCFT shows stereospecificity for L- aminopterin over D-aminopterin, due to differences in binding affinity (K_t) (Menter et al., 2012). PCFT is known to transport MTX, RTX, LMX and PDX (Deng et al., 2009; Desmoulin et al., 2012a; Qiu et al., 2007; Zhao et al., 2008), while PMX is widely considered to be the best PCFT substrate (Zhao and Goldman, 2007; Zhao et al., 2008). However, a novel series of 6-substituted pyrrolo[2,3-d]pyrimidine antifolates have been shown to have similar or stronger affinities for PCFT as PMX (Cherian et al., 2013; Kugel Desmoulin et al., 2011; Kugel Desmoulin et al., 2010; Wang et al., 2010; Wang et al., 2011; Wang et al., 2015) (also see Chapters 5 and 6).

PCFT transport of folates is electrogenic, producing a net positive charge, indicating that more than two protons are transported alongside bivalent folate anions (Qiu et al., 2006). PCFT couples downhill proton influx with uphill anion influx, and PCFT transport results in intracellular acidification (Zhao et al., 2009a). Under acidic conditions, PCFT displays channel-like functions. Removal of Na^+, K^+, Ca^{2+}, Mg^{2+}, or Cl^- does not effect PCFT transport, while carbonylcyanide p-trifluoro-methoxyphenylhydrazone (a proton ionophore) or nigericin (a K^+/H^+-exchanging ionophore) treatment does reduce PCFT transport activity (Inoue et al., 2008; Qiu et al., 2006). PCFT is capable of functioning without a proton gradient, in which case transport is dependent on membrane potentials (Qiu et al., 2006; Umapathy et al., 2007). An

"alternate access model," similar to other previously studied MFS proteins was described (Abramson et al., 2003; Hou et al., 2012; Inoue et al., 2008; Qiu et al., 2006; Unal et al., 2009b). According to this model, PCFT is predicted to exist in two distinct conformations, an inward-facing and an outward-facing form. In the outward-facing (extracellular) form, PCFT binds a proton first, followed by the folate molecule. The binding of folate causes a conformational change in PCFT, resulting in the inward-facing (intracellular) form, in which the folate molecule is released from PCFT first, followed by the release of the proton (the rate-limiting step) and then another conformational change back into the outward-facing form. In the absence of protons, the transformation from inward-facing to outward-facing conformation is the rate limiting step (Unal et al., 2009b). In the inward-facing conformation, TMDs 1, 2, 7 and 11 form an extracellular gate (Zhao et al., 2016).

Additionally, PCFT exists as an oligomer (Hou et al., 2012). PCFT dimers are the most common form, although higher-order oligomers have been identified. PCFT dimers are capable of restoring folate transport activity to inactive variants of PCFT, such that wild-type PCFT is capable of restoring activity to inactive PCFT mutants (such as the P425R mutation) via oligomerization (possibly explaining the recessive nature of HFM) (Geller et al., 2002; Hou et al., 2012).

1.4.4 PCFT Structure

The human PCFT protein is made up of 459 amino acid residues, with a predicted molecular mass of 49.8 kDa (Figure 1.4). By molecular modeling with MFS proteins, including the glycerol-3-phosphate transporter and lactose permease (Abramson et al., 2003; Huang et al., 2003), hPCFT is predicted to have twelve transmembrane domains (TMDs), with both the N- and C- termini located in the cytosol. This basic structure has been verified experimentally by

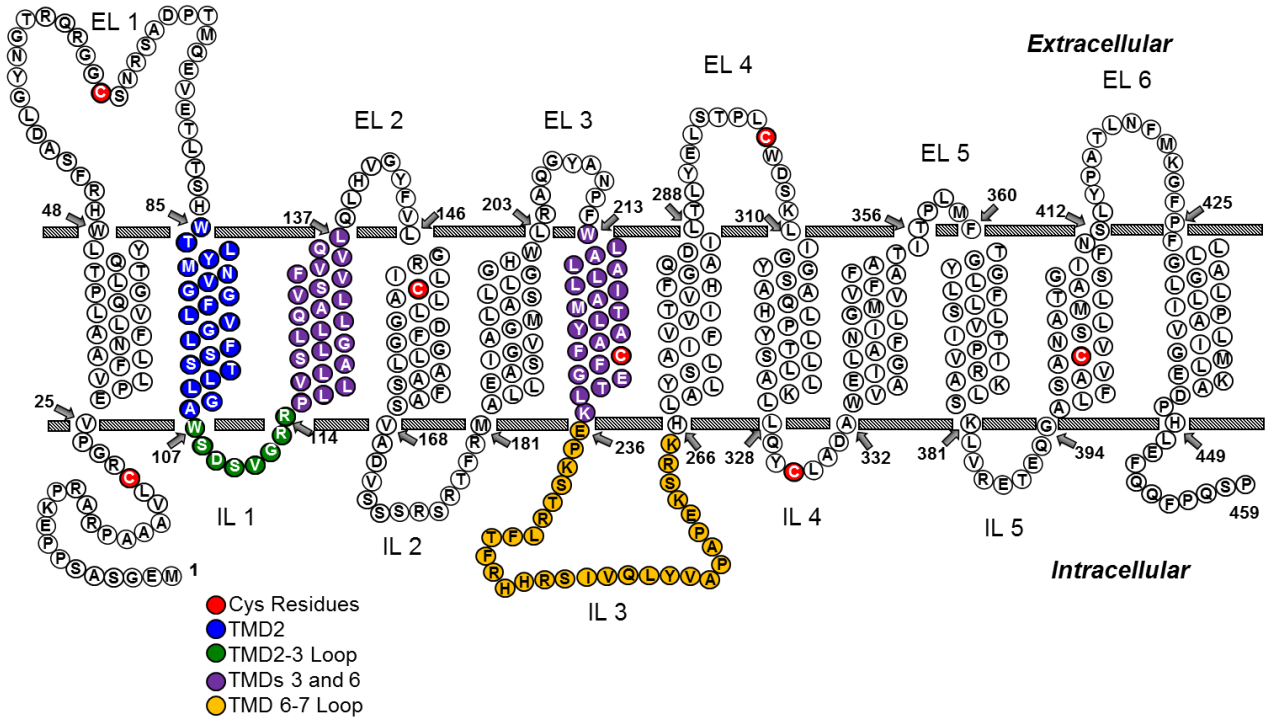

Figure 1.4 Membrane topology of the human proton-coupled folate transporter. This figure shows the predicted topology for PCFT, much of which has been experimentally confirmed. Domains of interest in this dissertation have been highlighted. The 7 cys residues of PCFT are highlighted in red. TMD2 is highlighted in blue, while the TMD2-3 connecting loop is highlighted in green. TMDs 3 and 6 are highlighted in purple. The TMD6-7 connecting loop is highlighted in orange. EL, extracellular loop; IL, intracellular loop.

SCAM using MTSEA (2-aminoethyl methanethiosulfonate)-biotin in order to identify intra- and extracellular TMD-connecting loop regions (Unal et al., 2008; Zhao et al., 2010). On the first extracellular loop region (connecting TMDs 1 and 2), PCFT contains two N-glycosylation sites at Asn58 and Asn68, and loss of both of these residues by mutation to glutamine did not impact protein expression or transport function (Unal et al., 2008). Two cysteine residues, Cys66 (first extracellular loop) and Cys298 (fourth extracellular loop), form a disulfide bond which is not essential to transport function (Zhao et al., 2010). The first predicted intracellular loop region (connecting TMDs 2 and 3) is thought to contain a functionally important β-turn structure, although this has not been experimentally determined (Lasry et al., 2009; Lasry et al., 2008; Subramanian et al., 2008) (see Chapter 2). The third predicted intracellular loop, which connects TMDs 6 and 7, contains a long sequence of 30 amino acid residues, necessary to span the long gap between these two domains (see Chapter 4). The ten residues found on the C-terminus of PCFT (450 to 459) seem to play no obvious role, as experimental removal of these residues from PCFT sequence had no effect on transport function or membrane expression (Subramanian et al., 2008).

Much work has been done to identify key amino acid residues of PCFT protein sequence. Often, these residues are characterized by expression of DNA vectors containing PCFT mutant coding sequence via transfection into PCFT-null cell lines, epitomized by the R1-11 HeLa cell line which lacks both PCFT and RFC expression (Diop-Bove et al., 2009). Transfected cells can be used to measure uptake of tritiated folates (folic acid, MTX, PMX) at pH 5.5 and 37^{o}C in order to determine the functional impact of mutagenesis of the PCFT residue of interest. Via this method, experimental characterization of PCFT mutants identified in HFM patients has revealed several key residues in PCFT function (Zhao et al., 2007). One such residue, His281 (TMD7)

(Figure 1.4), faces the extracellular region of TMD7 and plays an important role in PCFT protonation, a feature which contributes to folate substrate binding (the H281A mutant PCFT displayed a 11.3-fold increase in K_t for [^{3}H]folic acid compared to wild-type) (Unal et al., 2009a). Residue Glu185 (TMD5) plays a role in proton coupling, and mutations in Glu185 (including Ala, Leu, Cys, Asp, His, Gln) drastically decreased PCFT transport activity at acidic pH, while the E185A mutant showed no significant decrease in transport activity at pH 7.4 compared to wild-type PCFT and was capable of trans-stimulation (increased transport activity when pre-incubated with substrate) (Unal et al., 2009b). Arg376 (TMD10) contributes to both proton coupling and substrate binding, as mutation to glutamine resulted in an increased K_m (14-fold increase over wild-type) for PMX as well as a "proton slippage" effect, observed via electrophysiological analysis (*Xenopus* oocytes were used to measure currents associated with folate transport) (Mahadeo et al., 2010). Mutation of Pro425 (TMD12) to arginine had an impact on transport efficiency, although this effect was variable between different substrates (Shin et al., 2012). In a kinetic comparison between MTX and PMX, P425R displayed decreased V_{max} for both substrates, while the K_t value for MTX increased and the PMX K_t decreased (4.98-fold and 0.68-fold relative to wild-type, respectively) (Shin et al., 2012). The dietary folate 5-methylTHF had the most notable loss in uptake of any substrate, suggesting a role for P425R in HFM (Shin et al., 2012). Asp156 (TMD4) mutation to tyrosine was discovered in an HFM patient, and side-directed mutagenesis of Asp156 to several other residues (including Asn, Lys, Trp, Phe, Val) resulted in dramatic losses in cell surface protein expression, revealing the critical role of Asp156 in PCFT protein stability (Shin et al., 2010).

Mutation of Arg113 (Figure 1.4) was also identified in multiple HFM patients. The R113C mutant protein cannot transport folate molecules due to protein misfolding, with a lack of

protein translocation to the apical membrane (Shin et al., 2011). One group predicted that Arg113 could protrude into the membrane cavity formed by TMDs 1, 3, 4, and 6, as shown by molecular modeling, due to a β-turn structure formed by residues 109-114 (DSVGRR sequence) in the TMD 2-3 connecting loop region, similar to other DXXGRR structures found within other MFS proteins (Lasry et al., 2008). However, this was not experimentally tested (see Chapter 2). Complete replacement of residues 109-114 with alanine resulted in endoplasmic reticulum retention and a loss of transport activity (Subramanian et al., 2008). Additionally, a study of aspartic acid residues in PCFT found that Asp109 is essential for transport function, and cannot be replaced with other residues (Shin et al., 2010).

Other functionally important residues have been identified by random mutagenesis (via manipulation of both manganese and dGTP concentrations in PCR reactions) (Zhao et al., 2011b). One study found that only 4.5% of all mutations had a direct impact on PCFT function, which is plausible given the rarity of HFM (Zhao et al., 2011b). In total, 26 independent loss-of-function mutations were isolated. This study identified M222R (TMD6), V134E (TMD3) and L31P (TMD1) as mutations which dramatically decreased PCFT protein expression by ectopic expression and western blotting (Zhao et al., 2011b). The E232G (TMD6) mutatant protein was unable to form a structural conformation to facilitate folate transport, while the L161R (TMD4) mutation resulted in a reduced V_{max} and I304F (TMD8) showed a decreased binding affinity (increased K_t) (Zhao et al., 2011b). While neither F426V (TMD12) nor L432H (TMD12) mutations showed any effect on transport activity, these mutations completely inhibited transport activity in combination, likely due to an instability of the protein structure rather than an interaction between the two residues (Zhao et al., 2011b).

A systematic study of all tyrosine residues of PCFT identified several residues in TMDs

which face the substrate translocation pathway [Tyr291 (EL4), Tyr315 (TMD7), and Tyr362 (TMD10)], as shown by cysteine mutant accessibility to MTSEA-biotin (Visentin et al., 2015). Interestingly, the mutant Y414C (EL6) showed transport which could be inhibited by MTSET (2-(Trimethylammonium)ethyl methanethiosulfonate, bromide), despite its extracellular position (Visentin et al., 2015). Tyr291 (EL4), Tyr362 (TMD10), and Tyr414 (EL6) all displayed enhanced transport compared to wild-type PCFT for 50 μM MTX (but not 0.5 μM MTX) when mutated to alanine, cysteine, or phenylalanine, while Tyr315 (TMD7) displayed this phenomenon only when alanine mutation was introduced (Visentin et al., 2015). Conversely, Tyr315 mutants for alanine, cysteine, and phenylalanine all displayed enhanced transport for 50 μM PMX, a phenomenon explained by an increased V_{max}, accompanied by a decreased K_t compared to wild-type PCFT.

In another study, Zhao et. al. identified point mutation c.575G>A, an inactivating PCFT mutation of G192V, which led to the evaluation of the evolutionally conserved $G^{189}XXG^{192}$ domain of TMD5, as "GXXG" domains have been shown to serve as RNA binding domains without a known function in membrane transporters (Zhao et al., 2012). Inactivating mutations in both glycine residues (G189A, G192V) were identified, while additional residues lining the substrate binding domain were also identified (Zhao et al., 2012). When mutated to cysteine, both Ile188 and Met193 interacted with MTSET (as indicated by loss of transport activity), indicating their aqueous accessibilities (Zhao et al., 2012). I188C MTSET transport inhibition was abolished by PMX co-incubation at 0°C, suggesting its direct role in substrate binding. M193C did not display this phenomenon, indicating its position in the substrate binding cavity without a direct role in substrate binding.

As with all MFS proteins, PCFT forms two distinct halves composed of TMDs 1-6 on

one side, and TMDs 7-12 on the other. These two halves are linked by a TMD6-7 connecting loop (residues 236 to 265), the longest of PCFT's transmembrane loop domains, containing 30 amino acids (see Chapter 4). This region contains the functionally important residue His247, which has been suggested to interact with Ser172, another intracellular residue, and serve as a functional gatekeeper for transport substrate access to the substrate binding site (Unal et al., 2009a). Mutation of His247 to alanine resulted in increased binding affinities (decreased K_t, K_i) for several substrates, while influx (V_{max}) was decreased, and transport of folate and protons also became uncoupled (Unal et al., 2009a).

A recent study characterized an extracellular "gate" in PCFT. While in the inward-facing conformation, TMDs 1, 2, 7, 11 come within close proximity to one another toward the extracellular ends of each TMD (Zhao et al., 2016). This was confirmed via crosslinking experiments using single- and double-cysteine mutants of Q45C, N90C, L290C, S407C and N411C (Zhao et al., 2016). In many combination double-cysteine mutants, disulfide bonds formed between cysteine residues, preventing the labeling with MTSEA-biotin which was observed in single-cysteine mutants (Zhao et al., 2016). Treatment of these mutants with dithiothreiotol (DTT) to break disulfide bonds enhanced transport, while chemical crosslinking using CuPh or $CdCl_2$ inhibited transport. Chemical crosslinking could be blocked by incubation of PCFT with folic acid, restoring transport activity (Zhao et al., 2016).

1.4.5 PCFT Oligomerization

Several studies have identified PCFT homo-oligomers (Hou et al., 2012; Zhao et al., 2012). One study demonstrated oligomerization by protein crosslinking using 1,1- methanediyl bismethanethiosulfonate (MTS-1-MTS, a chemical which crosslinks nearby cysteine residues together) (Zhao et al., 2012) (also see Chapter 3), while another showed fluorescence resonance

energy transfer (FRET) between co-expressed YPet- and ECFP*-tagged PCFT monomers and co-binding of HA- and His_{10}-tagged PCFT monomers to nickel-affinity columns (Hou et al., 2012). As previously mentioned, PCFT dimers displayed a dominant-positive functional phenotype. Wild-type PCFT can restore activity to the inactive PCFT mutant P425R, such that when wild-type PCFT was cotransfected with P425R in equal amounts, the transport of [^{3}H] MTX was greater than that of wild-type alone, and equal to that of two wild-type PCFT transfectants (Hou et al., 2012). Confocal microscopy also revealed that cotransfection with wild-type PCFT increased trafficking of P425R PCFT to the surface membrane (Hou et al., 2012).

Studies have attempted to identify the dimerization interface for PCFT. The human PCFT sequence contains two "GXXXG" motifs, which are analogous to previously described dimerization motifs found in other proteins, and which form a flat surface and allow for a tight interaction between two transmembrane α-helicies (Duan et al., 2011; Gerber and Shai, 2001; Lebovka et al., 2014; McClain et al., 2003; Melnyk et al., 2002; Mendrola et al., 2002; Mueller et al., 2014; Overton et al., 2003; Polgar et al., 2004; Russ and Engelman, 2000; Whittington et al., 2001; Wilson et al., 2015; Zhao et al., 2012). For human PCFT, these groups are found from Gly^{93} to Gly^{97} (TMD2), which is highly conserved, and from Gly^{155} to Gly^{159} (TMD4) which is not conserved (Figure 1.4). An initial study of this region found that mutations G93A and G97A did not inhibit protein crosslinking by MTS-1-MTS (a measure of PCFT oligomerization), although this study did not include the TMD4 GXXXG motif (Zhao et al., 2012). Further investigation of this region by Gly-to-Leu mutations revealed that disruptions of either or both of the GXXXG motifs had no effect on PCFT oligomerization, reflected in protein crosslinking, and rather decreased protein stability and intramolecular packing (Wilson et al., 2015).

Other studies have utilized cysteine-less PCFT to crosslinking of PCFT monomers. By replacing each individual cysteine residues with serine (Figure 1.4), and examining cysteine-crosslinking via MTS-1-MTS treatment, localization of a putative dimerization domain of PCFT could be determined (Zhao et al., 2012). Of the seven cysteine residues of PCFT, only Cys229 was implicated as important for MTS-1-MTS crosslinking (thus, in forming an oligomer interface), suggesting a possible role for TMD6 in PCFT oligomerization (Zhao et al., 2012) (see Chapter 3).

1.5 The Metabolic Role of Folates

The biological significance of folates relates to their participation in one-carbon transfer reactions which are critical to the *de novo* synthesis of thymidylate and purine nucleotides, the catabolism of formic acid and histidine, the conversion of homocysteine to methionine and interconversions between glycine and serine (Stokstad, 1990; Tibbetts and Appling, 2010). Via synthesis of methionine, a precursor of S-adenosyl methionine, folates contribute to the methylation of DNA, histones, lipids, and neurotransmitters (Lu, 2000). Folate molecules consist of three structural components: the pteridine ring, the p-aminobenzoic acid, and the *L*-glutamine (Assaraf, 2007; Zhao et al., 2009a) (Figure 1.1). Folic acid is the synthetic form of metabolically important folates, which vary in the level of oxidation of the pteridine ring, the single-carbon moieties (formyl, methyl, methylene, methenyl) bound to the N^5 and/or N^{10} positions, and the level of polyglutamylation (Stokstad, 1990). 5-Methyl THF is the major circulating folate form. Following cellular uptake 5-methyl THF is polyglutamylated by folylpoly-γ-glutamate synthase (FPGS), a process by which between 2 and 8 glutamyl residues are linked to the γ-carboxyl of the *p*-aminobenzoic acid of THF, which contributes to the cellular retention of THF (Shane,

1989) (Figure 1.1). Then, THF can be converted to various forms bound to single-carbon units to contribute to metabolic reactions (Stokstad, 1990).

1.5.1 One-Carbon Metabolism

The main source of single-carbon units comes from the conversion of serine to formate in the mitochondria (Barlowe and Appling, 1988; Barlowe and Appling, 1990; Davis et al., 2004; Garcia-Martinez and Appling, 1993; Gregory et al., 2000; Herbig et al., 2002; Kastanos et al., 1997; Pasternack et al., 1994; Pasternack et al., 1996; Patel et al., 2003; Quinlivan et al., 2005; Tibbetts and Appling, 2010). In the mitochondria, carbon 3 of serine is transferred to THF in a relation catalyzed by serine hydromethyltransferase (SHMT), which produces 5,10-methyleneTHF and glycine (Figure 1.3) (Tibbetts and Appling, 2010). 5,10-MethyleneTHF is converted to 10-formylTHF by either methylenetetrahydrofolate dehydrogenase (MTHFD) 2 (MTHFD2) (embryonic tissues) (Mejia and MacKenzie, 1985) or MTHFD2-like (MTHFD2L) (adult tissues) (Bolusani et al., 2011) (Figure 1.5). 10-FormylTHF can be reduced to formate and THF by MTHFD 1-like (MTHFD1L) 10-formyl THF synthase (Prasannan et al., 2003), after which formate can be exported to the cytoplasm and react with unsubstituted THF via MTHFD1 to form 10-formylTHF (cytosolic) (Figure 1.5) (Hum et al., 1988; Paukert et al., 1977; Schirch, 1978; Smith et al., 1980).

MTHFD1 can also convert 10-formyl THF to 5,10-methenyl THF or, subsequently, 5,10-methylene THF (Hum et al., 1988; Paukert et al., 1977; Schirch, 1978; Smith et al., 1980; Thigpen et al., 1990). 5,10-MethyleneTHF donates its methylene group to deoxyuriine monophosphate (dUMP) to synthesize thymidylate (dTMP) in a reaction catylized by thymidylate synthase (TS) (Figure 1.5) (Friedkin and Roberts, 1956; Phear and Greenberg, 1957). In this reaction, 5,10-methylene THF is converted to dihydrofolate (DHF), which can be

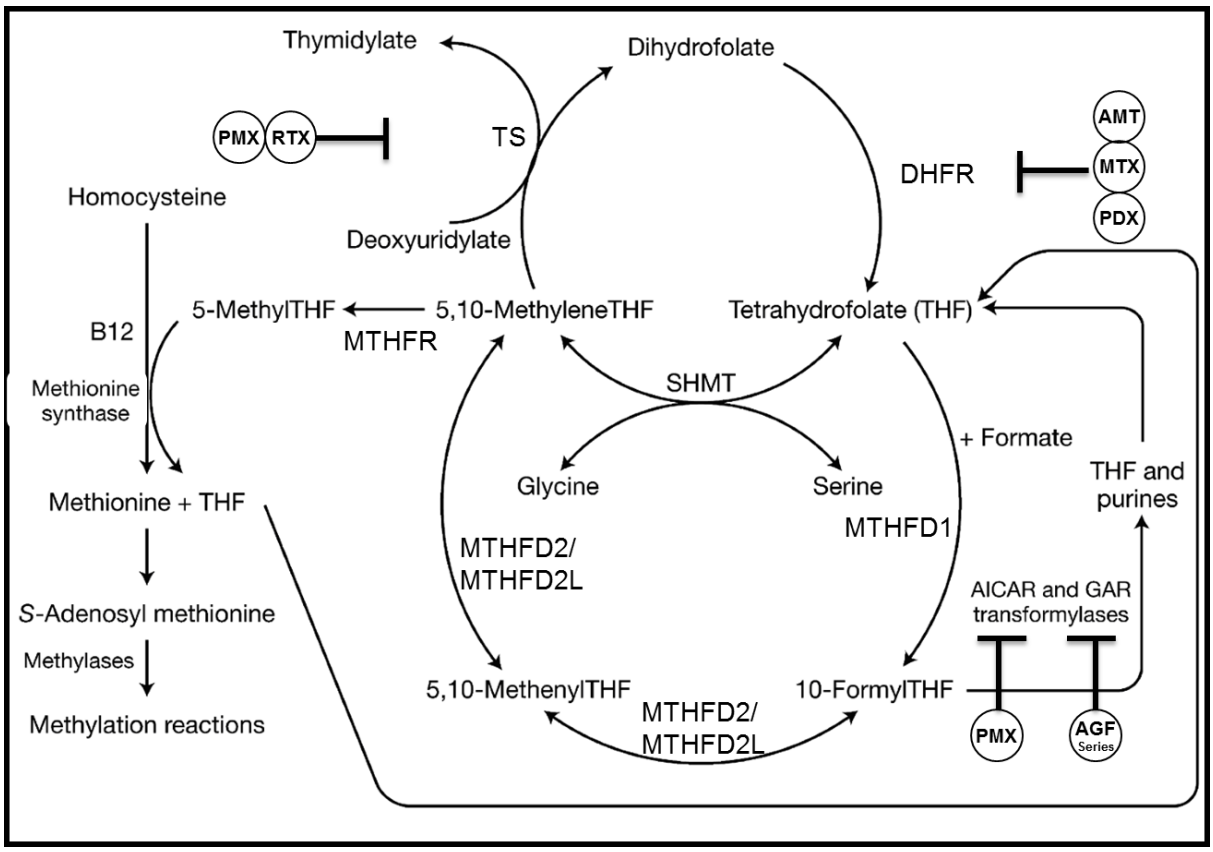

Figure 1.5 Folate metabolic pathways. The schematic shows metabolic steps which are metabolized by folates, resulting in the synthesis of purines, thymidine, methionine, serine and glycine.

converted to unsubstituted THF by DHF reductase (DHFR) (Figure 1.5) (Humphreys and Greenberg, 1958; McDougall and Blakley, 1960). An alternate route for 5,10-methyleneTHF is to be reduced to 5-methylTHF by 5,10-MethyleneTHF reductase (MTHFR) (Figure 1.5), which can donate its methyl group to homocysteine, synthesizing methionine via methionine synthase and regenerating unsubstituted THF (Hatch et al., 1961).

1.5.2 Purine Biosynthesis

Purines are an essential component of both DNA and RNA, while also regulating enzymatic activity and serving to mediate energy transfer in the cell as components of ATP, cyclic AMP, NADH and coenzyme A (King et al., 1983). Differentiated adult cells can usually satisfy purine requirements through purine salvage mechanisms, while proliferating cells usually rely on *de novo* purine biosynthesis in order to meet the demands of DNA and RNA synthesis (Denkert et al., 2008; Fairbanks et al., 1995; Howell et al., 1981; Jackson and Harkrader, 1981; King et al., 1983; Kondo et al., 2000; LeLeiko et al., 1983; Mackinnon and Deller, 1973) *De novo* purine biosynthesis inhibitors prevent lymphocyte and tumor cell growth, suggesting that purine salvage pathways are insufficient in these rapidly-dividing cell types (Christopherson et al., 2002; Hovi et al., 1976).

10-FormylTHF can be used in the *de novo* synthesis of purine nucleotides (Figure 1.6). The formate group of 10-formylTHF can be dontated to β-glycinamide ribonucleotide (GAR) formyltransferase (GARFTase) and 5-aminoimidazole-4-carboxamide (AICA) ribonucleotide formyltransferase (AICARFTase), catalyzing the third and ninth, respectively, of the ten steps in *de novo* purine biosynthesis from phosphoribosyl pyrophosphate (PRPP) to inosine monophosphate (Figure 1.6). This leads to a net transfer of two one-carbon units transferred from

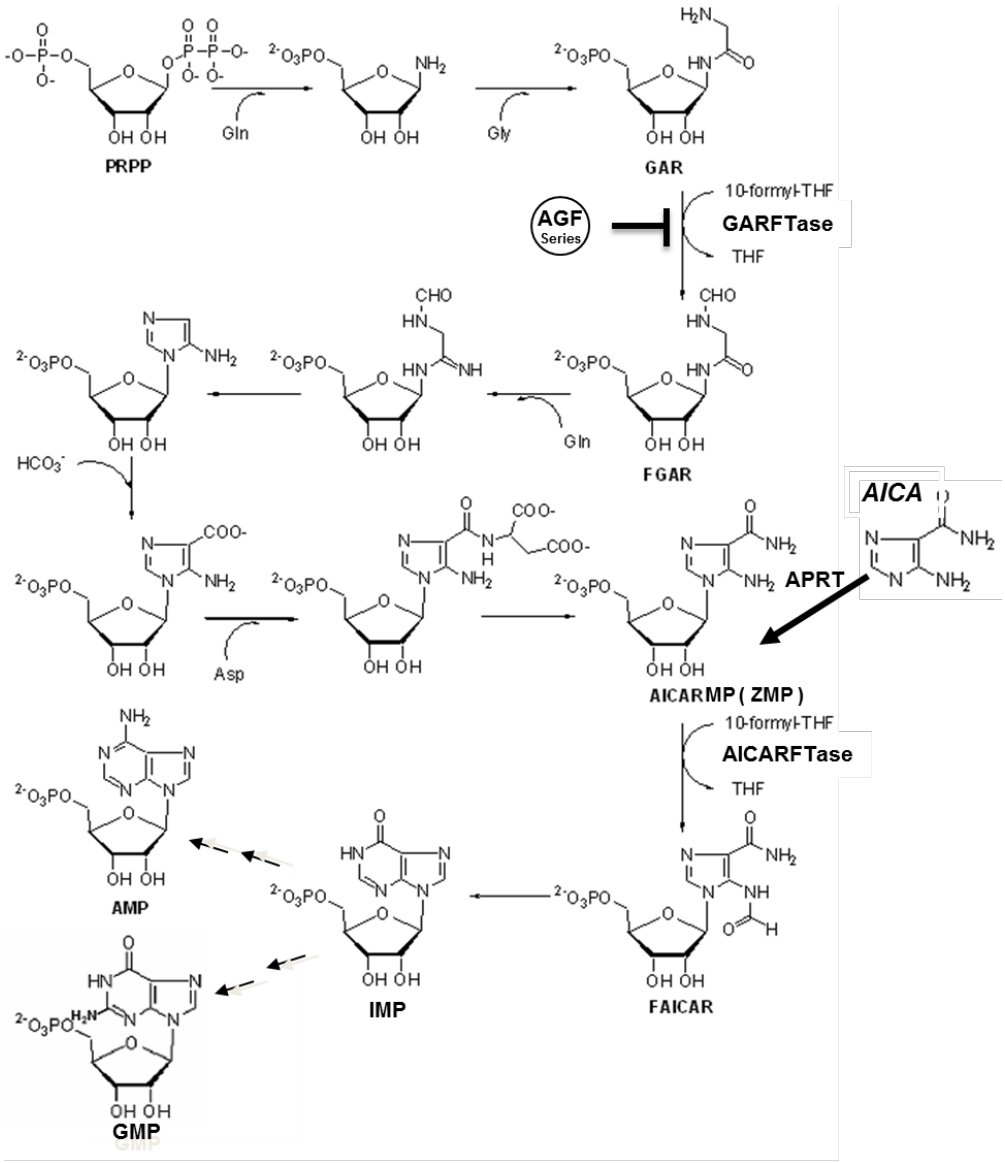

Figure 1.6 ***De novo*** **purine biosynthesis.** The 10 steps from PRPP to inosine monophosphate are detailed. Two steps are catalyzed by 10-formylTHF, step 3 (catalyzed by GARFTase) and step 9 (catalyzed by AICARFTase). The AGF series of compounds discussed in this dissertation inhibit GARFTase.

10-formylTHF and to the C-2 and C-8 of the purine ring and the regeneration of two molecules of unsubstituted THFs (Hartman and Buchanan, 1959b; Smith et al., 1981; Smith et al., 1980).

Hypoxanthine PRPP is also required in purine salvage. Hypoxanthine phosphoribosyl transferase converts guanine and hypoxanthine into GMP and IMP (inosine monophosphate), respectively, while adenine is converted to AMP by adenosine phosphorribosyl transferase; both reactions require PRPP (Murray, 1971). This pathway was characterized in avian models, and has since been shown to be conserved across all nearly all species (Hartman and Buchanan, 1959a).

1.5.3 Polyglutamylation of Folates

In the blood, folates exist primarily in the monoglutamate form (Assaraf, 2007; Stokstad, 1990). However, upon transport into the cell, folates are polyglutamylated by FPGS. FPGS can be located in both the cytosol and the mitochondria (McGuire et al., 2000), and catalyzes an ATP-dependent reaction to add glutamic acid groups to the γ-carboxyl group of folates. This reaction can occur multiple times, sequentially, such that multiple glutamates can be bonded to a single folate molecule (Figure 1.1). The primary purpose of polyglutamylation is to contribute to the cellular retention of folate molecules (Baugh et al., 1973; McBurney and Whitmore, 1974; Moran, 1999; Moran et al., 1976). Following polyglutamylation, folates become better substrates for folate-dependent enzymes, including TS, GARFTase and AICARFTase (Allegra et al., 1985; Allegra et al., 1987; Baggott et al., 1986; Jackman et al., 1991b; Schirch and Strong, 1989; Shih et al., 1997). Additionally, long chain (n>3) polyglutamate folates are no longer substrates for RFC or several efflux proteins including multidrug resistance proteins (MRPs) and breast cancer resistance protein, which contributes to their cellular retention (Assaraf, 2006; Matherly and Goldman, 2003; Volk and Schneider, 2003; Wielinga et al., 2005; Zeng et al., 2001).

1.6 Antifolate Treatment of Cancer

Rapidly proliferating tumor cells have specific metabolic requirements, as excessive nutrient quantities are needed to support synthesis of macromolecules required for cell division. Folates are required to contribute to the *de novo* synthesis of purine nucleotides and thymidylate necessary for DNA replication (Scotti et al., 2013) (Figure 1.5). In order to keep up with the folate requirements, tumors have been shown to express folate transporters and receptors (Kugel Desmoulin et al., 2011). Membrane transport of circulating folates is essential, as folates exist as anions at physiological pH. Both PCFT and RFC have been shown to be expressed in a wide variety of human tumor cell lines (Gonen et al., 2008; Kugel Desmoulin et al., 2011; Matherly et al., 2007; Zhao et al., 2004a). For 29 of 32 human tumor cell lines including cell lines from the National Cancer Institute 60 cell line panel, [^{3}H]MTX uptake was shown to be increased at pH 5.5 compared to pH 7.4, suggesting PCFT-mediated uptake (Zhao et al., 2004a). FRα overexpression has been shown in several cancer types including ependymal brain tumors and non-mucinous adenocarcinomas of ovary, cervix, and uterus (Bueno et al., 2001; Buist et al., 1995; Campbell et al., 1991; Elnakat and Ratnam, 2004; Evans et al., 2001; Garin-Chesa et al., 1993; Ross et al., 1994; Veggian et al., 1989; Weitman et al., 1994; Weitman et al., 1992a; Wu et al., 1999). FRα expression increases with tumor stage in ovarian cancer (Buist et al., 1995; Garin-Chesa et al., 1993; Veggian et al., 1989). FRα is expressed in some non-small cell lung cancer patients (NSCLC), although expression levels are highly variable (Christoph et al., 2013; Nunez et al., 2012; O'Shannessy et al., 2012) (also see Chapter 5). FRβ expression was found in chronic myelogenous leukemia and acute myelogenous leukemia, but not in acute lymphoblastic leukemia (ALL) (Pan et al., 2002; Ross et al., 1999).

1.6.1 DHFR Inhibitors

Based on observations which established the importance of folates in cancer progression, Sidney Farber and colleagues at Harvard hypothesized in 1947 that cancer cell proliferation could be inhibited via folate antagonists, based on the observation that folic acid stimulated leukemic cell growth (Farber et al., 1947). Aminopterin (AMT) (Figure 1.2), an antifolate synthesized by Yellapragada Subbarow, was the first ever chemotherapeutic compound shown to cause remission of ALL (Farber and Diamond, 1948). AMT was later improved through the synthesis of MTX (Figure 1.2), which could be used to treat ALL with fewer side effects and less toxicity (Farber, 1949). MTX remains relevant today as a treatment for ALL, lymphomas, and several solid tumors (Jolivet et al., 1983; Monahan, 2001; Pui and Evans, 2006), as well as non-malignant diseases such as rheumatoid arthritis, psoriasis and Crohn's disease (Chladek et al., 1998; Feagan et al., 1995; Wessels et al., 2008). AMT, too, has found new interest in therapy of cancer and inflammatory diseases (Cole et al., 2008; Menter et al., 2012). As such, antifolate compounds have remained an essential class of cancer chemotherapeutic for nearly 70 years. However, the therapeutic utility of MTX is limited by its lack of tumor specificity and the existence of both *de novo* and acquired resistance (Matherly et al., 2007; Zhao and Goldman, 2003).

Both MTX and AMT are highly potent inhibitors of DHFR (Gonen and Assaraf, 2012; Zhao and Goldman, 2003). DHFR inhibition causes accumulation of DHF, generated by TS. DHF is reduced to THF by DHFR, and the buildup of DHF as a result of DHFR inhibition causes net depletion of unsubstituted THF and termination of THF-dependent carbon transfer reactions in the biosynthesis of thymidylate, purine nucleotides, methionine and serine (Matherly et al., 1987; Seither et al., 1989). AMT has a much stronger affinity than MTX for both RFC and FPGS,

which adds additional glutamates to folate molecules and contributes to cellular retention (Matherly et al., 1985). Thus, AMT enters the cell and is polyglutamylated much more quickly than MTX, resulting in much higher levels of AMT polyglutamates (Matherly et al., 1985), and displays far more potent antitumor activity than MTX (Goldin et al., 1955; Sirotnak et al., 1984). However, this may also be the reason for the increased toxicity of AMT in patients, reflecting the ubiquitous expression of RFC.

PDX (10-propargyl-10-deaza-AMT) (Figure 1.2) was the product of a collaboration between F. M. Sirotnak of Memorial Sloan-Kettering Cancer Center and J. I. Degraw of Southern Research Institute to improve cellular pharmacology of antifolate compounds. PDX precursors 10-deaza-AMT and 10-ethyl-10-deaza-AMT were more potent than MTX (Schmid et al., 1985; Sirotnak et al., 1984; Sirotnak et al., 1993). PDX, the third generation in this series of compounds, was found to be 3-fold less potent at DHFR inhibition than MTX, but displayed 10-fold higher transport rates by RFC and higher polyglutamylation by FPGS, ultimately resulting in increased drug efficacy toward breast cancer, NSCLC and leukemia cell lines both *in vitro* and *in vivo* (DeGraw et al., 1993; Sirotnak et al., 1998; Visentin et al., 2013). In phase I and II trials, which included non–small-cell lung cancer and peripheral T-cell lymphoma patients, PDX showed both efficacy and safety, leading to the Food and Drug Administration (FDA) approval for the treatment of relapsed, refractory peripheral T-cell lymphoma in 2009 (Krug et al., 2003; Marchi et al., 2013; O'Connor et al., 2009; Thompson, 2009). Since 2009, PDX has been tested in combination with other therapies in several different cancer types with promising results (Azzoli et al., 2007; Marchi et al., 2010; Toner et al., 2006; Zain and O'Connor, 2010a; Zain and O'Connor, 2010b).

PT523 (Figure 1.2) is a hemiphthaloylornithine antifolate synthesized by A. Rosowsky and colleagues at Dana-Farber Cancer Institute (Rosowsky et al., 1988). PT523 is a strong inhibitor of DHFR with a submicromolar K_t for RFC, while also being a very poor substrate for PCFT (Kugel Desmoulin et al., 2010; Rhee et al., 1994; Rosowsky et al., 1988; Wang et al., 2010; Wright et al., 2000; Zhao and Goldman, 2007). PT523 lacks a terminal glutamate, and is not a substrate for polyglutamylation, which decreases the impact of intracellular THF levels on PT523 compared to MTX. In a phase I study including 18 patients with relapsed or refractory NSCLC, PT523 displayed acceptable toxicity and efficacy (2 partial responses, 9 stable disease) after multiple chemotherapy cycles (Lima et al., 2006).

1.6.2 TS Inhibitors

RTX (Tomudex; ZD1694; (S)-2-(5-methyl((2-methyl-4-oxo-1,4-dihydroquinazolin-6-yl)methyl)amino)thiophene-2-carboxamido)pentanedioic acid) (Figure 1.2) is a quinazoline antifolate and an inhibitor of TS. RTX was designed by scientists at the Institute for Cancer Research and Astra Zeneca (Hughes et al., 1999; Jackman and Calvert, 1995). Earlier attempts to develop a TS-targeted antifolate resulted in CB3717 (N_{10}-propargyl-5,8-dideazafolic acid; N-[4-[N-[(2-amino-4-hydroxy-6-quinazo-linyl)methyl]prop-2-ynylamino] benzoyl]-*L*-glutamic acid), which showed efficacy against ovarian, liver and breast cancers in phase I/II clinical trials but also resulted in hepatic toxicity and dose-limiting nephrotoxicity in 70% of patients given doses above 450 mg/m^2 (Jackman and Calvert, 1995). In order to reduce toxicity and increase solubility, CB3717 was modified by substitution of the 2-amino group with 2-desamino-2-methyl, replacement of benzoyl ring with thiophene ring, and replacement of N_{10}-propargyl with a methyl (Jackman et al., 1996; Jackman et al., 1991a; Jackman et al., 1991b). These modifications resulted in RTX, which is a poorer TS inhibitor than CB3717. RTX is a greater

RFC and FPGS substrate than CB3717, resulting in enhanced antitumor efficacy *in vivo* and *in vitro* as well as increased water solubility (Hughes et al., 1999; Jackman et al., 1991b). RTX has been approved for use in the treatment of advanced colorectal cancer in Australia, Canada, and Europe, and for treatment of malignant pleural mesothelioma in combination with cisplatin in several European countries (Chu et al., 2003; Surmont and van Meerbeeck, 2011). RTX represents the success of developing structure activity relationships (SAR) through careful testing of chemical modifications made to antifolate compounds.

ZD9331 (Plvitrexed, BGC9331) (Figure 1.2) is a quinazoline antifolate with a γ tetrazole. ZD9331 lacks FPGS activity but remains an excellent RFC substrate and inhibitor of TS (Jackman and Calvert, 1995; Jackman et al., 1997). While RFC is the primary mechanism of transport, ZD9331 is also a substrate for FRs and PCFT (Jansen, 1999; Matherly and Gangjee, 2011). ZD9331 was developed with the intention of circumventing polyglutamylation-based resistances tumors can develop during antifolate treatment, associated with low FPGS or high γ-glutamyl hydrolase activity (Zhao and Goldman, 2003), and ZD9331 activity was preserved in RTX-resistant L1210 murine leukemia cells with low FPGS activity (Jackman et al., 1997). Phase II clinical trials of ZD9331 showed some efficacy in patients with metastatic colorectal, ovarian, and pancreatic cancers with a manageable toxicity profile (Hainsworth et al., 2003; Louvet et al., 2004; Rader et al., 2003; Schulz et al., 2004; Smith and Gallagher, 2003).

GW1843U89 (Figure 1.2) was discovered at the Burroughs Wellcome Company in an attempt to identify antifolates which might be useful as antimicrobial agents (Smith et al., 1999). GW1843U89 is an extremely potent TS inhibitor, with a K_i of 0.09 nM, while also being an excellent RFC substrate (Duch et al., 1993). GW1843U89 is a good FPGS substrate, but the diglutamyl GW1843U89 is a poor FPGS substrate, leading to diglutamyl GW1843U89 being the

major cellular form (Duch et al., 1993; Hanlon and Ferone, 1996). Polyglutamylation status of GW1843U89 seemed to have no effect on TS inhibition (Hanlon and Ferone, 1996). GW1843U89 was later encapsulated in liposomes, forming the new drug OSI-7904L, which was shown to be well tolerated in patients and effective in patients with advanced gastric cancer or gastroesophageal cancers (Falk et al., 2006) but not patients with advanced biliary cancer (Ciuleanu et al., 2007).

In the case of antifolates that target either TS or DHFR, cell death occurs due to a lack of thymidylate and accumulation of dUMP (Matsui et al., 1996; Yin et al., 1997). The net effect is a decrease in the level of deoxythymidine triphosphate (dTTP), which results in the misincorporation of deoxyuridine triphosphate (dUTP) into DNA synthesis. This causes DNA strand breaks, as dUTP incorporation into DNA is recognized as incorrect and cycles of unsuccessful excision-repair occur, leading to cell death (Bronder and Moran, 2003)

1.6.3 Inhibitors of *De Novo* Purine Biosynthesis

Lometrexol (LMX) (Figure 1.2) is a (6R) diastereomer of 5,10-dideaza THF which was developed by E.C. Taylor of Princeton University and Chuan (Joe) Shih of Eli Lilly in an attempt to develop antifolates which have enzyme targets other than DHFR (Mendelsohn et al., 1999b; Moran et al., 1989; Taylor et al., 1985). LMX is structurally identical to THF, with the exception that carbons 5 and 10, which participate in carbon transfer reactions and have been replaced with nitrogens. LMX is an RFC substrate, although it can also be transported by PCFT and FRs (Desmoulin et al., 2012a; Jansen, 1999; Matherly et al., 1993; Westerhof et al., 1995). LMX is polyglutamylated by FPGS (Baldwin et al., 1991; Matherly et al., 1993; Moran et al., 1989), and polyglutamyl forms of LMX are potent GARFTase inhibitors, depleting cells of ATP and GTP (Beardsley et al., 1989; Mendelsohn et al., 1999b; Moran et al., 1989). Because loss of ATP

renders p53 transcriptionally inert, LMX displayed cytotoxicity in a p53-independent manner (Bronder and Moran, 2003). Based on *in vivo* and *in vitro* models, LMX was considered a promising anticancer agent (Beardsley et al., 1989; Mendelsohn et al., 1999b; Moran et al., 1989). However, in Phase I clinical trials, LMX treatment resulted in severe toxicity, with dose-limiting myelosuppression and mucositis (Ray et al., 1993). Clinical toxicity can be reduced by the co-administration of folic acid with LMX, allowing for a ten times greater dose than LMX treatment without folic acid (Roberts et al., 2000a). It was hypothesized that the high toxicity may be caused by a gradual release of LMX metabolites from the liver (Taber et al., 1991), that folate depletion increased liver FR expression, contributing to increased uptake (Mendelsohn et al., 1996; Pohland et al., 1994) and that polyglutamate forms of LMX are essentially impossible to eliminate from circulation (Jackman, 1999).

In an attempt to reduce the toxicities of LMX, LY309887 [(2S)-2-[[5-[2-[(6R)-2-amino-4-oxo-5, 6, 7, 8-tetrahydro-1H-pyrido [2,3-d] pyrimidin-6-yl] ethyl] thiophene- 2-carbonyl] amino] pentanedioic acid] (Figure 1.2) was synthesized. LY309887 was designed to have lower FR affinity, lower polyglutamylation, and increased affinity for GARFTase compared to LMX (Budman et al., 2001; Mendelsohn et al., 1996; Mendelsohn et al., 1999b; Wang et al., 1992). Another compound, AG2034 [N-[(5-(2-[(6S)-2-amino-4-oxo-4,6,7,8-tetrahydro-1H-pyrimido[5,4-b][1,4]thiazin-6-yl]ethyl)thiophen-2-yl)carbonyl]-*L*-glutamic acid] (Figure 1.2) was designed based on the X-ray crystal structure of GARFTase, and AG2034 was shown to be a potent GARFTase inhibitor (Almassy et al., 1992; Boritzki et al., 1996) and exhibited reduced FR affinity (Boritzki et al., 1996). However, in phase I clinical trials, both LY309887 and AG2034 showed similar cumulative toxicities to those observed in LMX-treated patients (Bissett et al., 2001; Boritzki et al., 1996; Budman et al., 2001; Kisliuk, 2003; Roberts et al., 2000b).

1.6.4 Multitargeted Antifolate

PMX (LY231514;Alimta;N-[4-[2-(2-amino-4,7-dihydro-4-oxo1H-pyrrolo[2,3d] pyrimidin-5-yl)ethyl]benzoyl]-*L*-glutamic acid) (Figure 1.2) was synthesized by Eli Lilly in an attempt to meet FDA requirements of purity and to eliminate chirality at the 6 position of the 5-deazapteridine ring of LMX by replacement with a pyrrolo[2,3-*d*]pyrimidine ring (Taylor, 1993; Taylor et al., 1992). *In vitro* experiments revealed that PMX was a potent TS inhibitor, and additionally was a weak inhibitor of DHFR, GARFTase and AICARFTase (Shih et al., 1997; Taylor et al., 1992). PMX is also an excellent substrate for both PCFT and RFC, being among the best substrates for PCFT (Wang et al., 2004; Westerhof et al., 1995; Zhao et al., 2008). Unlike MTX or RTX, the antitumor efficacy of PMX is maintained or even enhanced in cells with low RFC expression, so long as PCFT is expressed (Zhao et al., 2008). PMX is highly polyglutamylated and is among the best known FPGS substrates, although polyglutamylation is negatively affected by intracellular folate status (Desmoulin et al., 2012b; Shih et al., 1997; Zhao et al., 2001; Zhao et al., 2004b). PMX polyglutamylation enhanced TS inhibition, as PMX pentaglutamate showed a TS K_i value of 1.3 nM compared to 109 nM for parent PMX. K_i values for GARFTase and AICARFTase were much higher, suggesting decreased inhibition potency of these enzymes, although polyglutamates were still more potent inhibitors than non-polyglutamyl drug (Shih et al., 1997; Taylor et al., 1992). Additionally, PMX has a very low affinity for DHFR. Potent TS inhibiton by PMX would obviate any effect on DHFR, as dihydrofolate would not be generated once TS is inhibited.

Recently, it has been suggested that AICARFTase may be a more important secondary target for PMX than originally realized (Racanelli et al., 2009; Rothbart et al., 2010). Treatment with PMX results in an accumulation of the purine synthesis intermediate 5-aminoimidazole-4-

carboamide ribotide (ZMP), the AICARFTase substrate (Racanelli et al., 2009). ZMP is an AMP mimetic and can activate AMP-activated protein kinase (AMPK), which phosphorylates proteins involved in initiation of energy metabolism, cap-dependent translation, and lipid synthesis (Mihaylova and Shaw, 2011). AMPK phosphorylation due to PMX treatment results in inhibition of mTOR signaling in lung and colon cancer cells (Gwinn et al., 2008; Inoki et al., 2003; Racanelli et al., 2009; Rothbart et al., 2010). However, in the absence of direct TS inhibition, AMPK activation by PMX or by direct AMPK activators (metformin) did not produce an antiproliferatve effect in KB tumor cells (Mitchell-Ryan et al., 2013). PMX was found to act synergistically with the multi-kinase inhibitor sorafenib by promoting autophagy which led to activation of apoptosis pathways, thereby enhancing antitumor effects (Bareford et al., 2011).

PMX was approved by the FDA in 2004 for treatment of malignant pleural mesothelioma in combination with cisplatin (Hazarika et al., 2005). In 2008, PMX was approved as a primary treatment for non-squamous NSCLC (NS-NSCLC) coadminstered with cisplatin (Cohen et al., 2009) and in 2009 for maintenance therapy in patients with local advanced or metastatic NS-NSCLC (Cohen et al., 2010). Randomized clinical trials have revealed that PMX is superior to other chemotherapy agents in the treatment of NS-NSCLC, while being inferior to other drugs in squamous cell lung cancer either as monotherapy or in combination with platinum-based chemotherapies (Ciuleanu et al., 2009; Hanna et al., 2004; Scagliotti et al., 2009; Scagliotti et al., 2008).

Despite widespread use in the treatment of NS-NSCLC, the utility of PMX in the treatment of these patients is modest, as the median progression free survival of these patients is only 3.5 months when treated with PMX and carboplatin in combination and 3.6 months when treated with PMX monotherapy (Ardizzoni et al., 2012). This suggests that there is a high

amount of variability in the efficacy of PMX between patients. As a standard practice, patients who will be treated with PMX are given dexamethasone (Dex) in order to reduce the possibility of a severe skin rash caused by PMX treatment. Patients are given 4 mg Dex twice the day before treatment, once the day of and once the day after. The effects of Dex are mediated by the glucocorticoid receptor (GR), a transcription factor which can regulate cell proliferation, apoptosis, immune response, inflammation, and cellular senescence (Ge et al., 2012; Mangelsdorf et al., 1995; Vilasco et al., 2011). An immunohistochemical analysis of GR expression in NSCLC showed heterogeneity of GR expression, with approximately half of the tumors showing a relatively high GR expression (Lu et al., 2006). *In vitro* studies of NS-NSCLC cell lines revealed that Dex treatment suppresses cell progression into S-phase, causes down-regulation of TS, DHFR, RFC and PCFT and reduces the efficacy of PMX in cells with high GRα expression (Patki et al., 2014). These effects were p53-independent and could be restored within 24 hours, suggesting that Dex treatment before, during, and after PMX treatment can drastically reduce the efficacy of PMX in patients with high tumor GR expression (Patki et al., 2014).

1.6.5 Antifolate Resistance

Resistance to MTX via impaired RFC function has been identified *in vitro* (Hill et al., 1979; Niethammer and Jackson, 1975; Sirotnak et al., 1968; Sirotnak et al., 1981) and in many disease types, including ALL, osteosarcoma, colorectal cancer and primary central nervous system lymphoma (Belkov et al., 1999; Ferreri et al., 2004; Gorlick et al., 1997; Guo et al., 1999; Ifergan et al., 2003; Levy et al., 2003; Wettergren et al., 2005; Yang et al., 2003). This impaired RFC function can be the result of either decreased RFC expression or reduced RFC function (Assaraf, 2007; Matherly and Goldman, 2003; Matherly et al., 2007), results which can be

produced by a variety of mutations including promoter methylation, point mutations, frameshift mutations, genomic deletions and loss of RFC alleles (Chattopadhyay et al., 2006; Ding et al., 2001; Rothem et al., 2002; Worm et al., 2001; Zhao et al., 2004b; Zhao et al., 1999).

Reduced polyglutamylation can also result in antifolate resistance (Drake et al., 1996; Li et al., 1992; Liani et al., 2003; Mauritz et al., 2002; McCloskey et al., 1991; McGuire et al., 2000; Pizzorno et al., 1989; Pizzorno et al., 1988; Pizzorno et al., 1995). Folate-dependent enzymes, such as TS and DHFR, can aquire mutations which reduce the impact of antifolates, either via enzyme mutations resulting decreased drug affinities or increased enzyme expression (Albrecht et al., 1972; Alt et al., 1978; Dolnick et al., 1979; Drake et al., 1996; Flintoff and Essani, 1980; Freemantle et al., 1995; Goldie et al., 1980; Haber et al., 1981; Horns et al., 1984; Jackman and Calvert, 1995; Jackson and Harrap, 1973; Jackson et al., 1976; Kitchens et al., 1999; McIvor and Simonsen, 1990; Melera et al., 1984; Melera et al., 1988; Mini et al., 1985; Miyachi et al., 1995; Nunberg et al., 1978; O'Connor et al., 1992; Sigmond et al., 2003; Srimatkandada et al., 1989; Tong et al., 1998; Trent et al., 1984; Wang et al., 2001; White and Goldman, 1981). MTX resistance can be acquired through DHFR gene amplification (Alt et al., 1978) which has been observed clinically in various cancers following treatment with MTX (Horns et al., 1984; Trent et al., 1984). Additionally, overexpression of MRPs may also contribute to antifolate resistance (Assaraf, 2006; Assaraf, 2007). MRP1, MRP2 and MRP3 have been shown to be methotrexate transporters (Assaraf, 2006)

1.6.6 Utility of FRα Overexpression in Cancer for Therapy and Imaging

Because of the ubiquitous expression of RFC, which causes the non-specific action of classical antifolates toward normal tissues as well as tumors, there has been an increased interest in utilizing FRα overexpression in cancer (and limited normal tissue expression) for a variety of

purposes, including both therapeutics and imaging. This concept has been demonstrated by the development of ONX0801 (previously BGC 945), a FRα-specific TS inhibitor with a low affinity for RFC (Gibbs et al., 2005; Theti et al., 2003). This compound displays a 70% binding affinity compared to folic acid, and a K_i of 1.2 nM for TS (Gibbs et al., 2005) and an IC_{50} of 3.6 nM in KB cells (Theti et al., 2003). This compound was licensed by Onyx Pharmacuticals for a Phase I study, laying the groundwork for numerous FRα-targeted molecules.

In addition to therapeutics, FRα-targeted imaging agents are also being developed. A radiolabeled derivitave of folic acid, ^{111}In-DPTA-folate, was shown to detect new ovarian cancer in mice as well as patients in a phase I/II clinical study (Siegel et al., 2003). A version of folic acid conjugated with ^{99m}Techneitum, called EC20, uses a more cost effective label with a shorter half-life, and has demonstrated higher specificity to FRα and a higher clearance rate from the blood and kidneys (Leamon et al., 2002). EC20 has been used to image over 200 ovarian cancer patients (Sega and Low, 2008).

Recently, there has been an interest in utilizing FR overexpression in various cancer types to deliver cytotoxic drugs via conjugation with folic acid. The first of these to be evaluated in tumor therapy was EC131, a folate-maytansinoid conjugate (Reddy et al., 2007). Maytansinoid, a microtubule-inhibiting agent, was shown to be tumor-targeted to FR-positive M109 tumors in BALB/c mice and tumor growth was inhibited.

A conjugate of folate and desacetylvin-blastinemonohydrazide (a derivative of microtubule destabilizing agent vinblastine), Vintafolide (or EC145), has been shown to be safe in a phase I clinical study (Lorusso et al., 2012; Vlahov et al., 2006). Multiple phase II and III clinical trials have been performed in lung and ovarian cancer (Edelman et al., 2012; Lorusso et al., 2012). One phase II clinical study showed that ovarian cancer patients with higher FRα

expression displayed longer progression free survival when treated with vintafolide compared to patients treated with PEGylated liposomal doxorubicin (Naumann et al., 2013). However, the subsequent phase III clinical trial failed because the vintafolide-treated patients did not meet the preliminary outcome for progression free survival (Merck, 2014). An additional phase II clinical study in lung adenocarcinoma patients failed to demonstrate a firm conclusion on efficacy of vintafolide due to non-random study design (Hanna et al., 2014).

Another folate conjugate, EC0225, is a folate linked to both a vinca alkaloid and mitomycin, has had a phase I clinical trial to determine the maximum tolerated dose (Sharma et al., 2010). Additional folate conjugates including Epofolate [a folate and epothilone A (microtubule stabilizing agent) conjugate], EC0489 (a vintafolide analogue), and EC1456 (a folic acid-tubulysin small-molecule drug conjugate) all had a phase I clinical trials (Gokhale et al., 2013; Leamon et al., 2011; Lee et al., 2002; Peethambaram et al., 2015; Reddy et al., 2009).

1.6.7 Tumor Targeted Antifolates with PCFT and FR Selectivity

Cancer cells have an increased need for energy and biosynthesis of nucleotides due to enhanced rates of growth and proliferation. In order to meet this demand, cancer cells become reliant on the altered metabolism known as the "Warburg effect," or aerobic glycolysis, in which cells become highly glycolytic despite the presence of normal oxygen levels (Lunt and Vander Heiden, 2011). In order to maintain a normal intracellular pH, glycolytically-produced acids must be flushed out of the cell, which cells achieve by increasing expression and/or activity of plasma membrane ion pumps and transporters. Examples include H^+-ATPases and vacuolar ATPases (Hinton et al., 2009; Martinez-Zaguilan et al., 1993; Sennoune et al., 2004), the Na^+/K^+ exchanger (Chiang et al., 2008; Kumar et al., 2009; McLean et al., 2000; Miraglia et al., 2005), and the monocarboxylate H^+ efflux symporter (Chiche et al., 2012; Kennedy and Dewhirst, 2010;

Pinheiro et al., 2008a; Pinheiro et al., 2008b; Pinheiro et al., 2010). Increased activity of these transporters allows cells to maintain an intracellular pH of ≥7.4, while creating a tumor microenvironment of extracellular pH ranging from ~6.7-7.1. This is opposed to normal differentiated adult cells, which have an intracellular pH of ~7.2 and an extracellular pH of ~7.4 (Busco et al., 2010; Gallagher et al., 2008; Gillies et al., 2002; Stuwe et al., 2007; Webb et al., 2011). This acidic tumor microenvironment creates an H^+-electrochemical gradient which acts as a driving force for proton-coupled solute transporters at the cell membrane, while also increasing substrate affinity and broadening substrate specificity for these transporters (Leuthold et al., 2009; Nozawa et al., 2004; Qiu et al., 2006; Rubio-Aliaga et al., 2003).

There is a precedent for tumor targeting using chemotherapeutics which are specifically transported by proton-coupled transporters (Anderson and Thwaites, 2010). Proton-coupled di/tripeptide transporters PepT1 and PepT2 have shown increased tumor expression and activity and provide utility in transporting cancer therapies, including prodrugs floxuridine and cytarabine (Sun et al., 2009), photodynamic therapy and the imaging agent 5-aminolevulinic acid (Anderson et al., 2010), and bestatin, an aminopeptidase inhibitor (Nakanishi et al., 2000; Rubio-Aliaga and Daniel, 2002). A proton-coupled amino acid transporter, PAT1, has also been shown to mediate uptake of 5-aminolevulinic acid and L-cycloserine in low pH conditions (Anderson et al., 2004; Anderson et al., 2010). Several members of the organic anion transporter (OAT) family displayed low pH polypeptide transport (Leuthold et al., 2009). OATP1A2 has been shown to transport MTX at low pH (Badagnani et al., 2006), while OATP2B1 has also demonstrated low pH antifolate transport (Visentin et al., 2012).

PMX is a 5-substituted 2-amino-4-oxo-pyrrolo[2,3-*d*]pyrimidine antifolate with a p-amino-benzoyl glutamate attached by a 2-carbon bridge region. The 6-substituted regioisomer of

PMX has no activity against tumor cells (Shih, 1993), but 6-substituted regioisomers with an elongated carbon bridge region connecting the heterocycle and the p-aminobenzoate including three (AGF17) or four (AGF23) (Figure 1.7) carbons were cabable of inhibiting proliferation of KB and IGROV1 cells at nanomolar drug concentrations (Deng et al., 2008). These compounds were later characterized in Chinese hamster ovary (CHO) (Flintoff et al., 1976) cells engineered to express either human RFC (PC43-10) (Wong et al., 1995) or human PCFT (R2/PCFT4) (Deng et al., 2009), and it was reported that AGF17 and AGF23 were selective for PCFT over RFC and were active at nanomolar concentrations (Kugel Desmoulin et al., 2010), while also being inhibitors for FRα- and β-expressing CHO cells (RT16 and D4, respectively) (Deng et al., 2008).

Following AGF17 and AGF23, 6-substituted pyrrolo[2,3-*d*]pyrimidine with thienoyl-for-benzoyl substitutions were synthesized, designated AGF94 (three carbon bridge) and AGF71 (four carbon bridge) (Figure 1.7). This thienoyl replacement of the side-chain phenyl moiety was inspired by the same substitution used in the creation of LY309887 (Mendelsohn et al., 1999b) and AG2034 (Boritzki et al., 1996). AGF94 and AGF71 are PCFT-selective antifolates (Kugel Desmoulin et al., 2011; Wang et al., 2010; Wang et al., 2011) with IC_{50} values for R2/PCFT4 CHO cells of 3.34 nM and 43 nM, respectively (Wang et al., 2010; Wang et al., 2011). Both AGF94 and AGF71 showed significant inhibition of tumor growth *in vivo* in IGROV1 xenografts (Wang et al., 2011). AGF94 additionally inhibited growth of H2452 (malignant mesothelioma) cells *in vitro* and *in vivo* as tumor xenografts in severe-combined immunodeficient (SCID) mice (Cherian et al., 2013). Both drugs displayed potent GARFTase inhibition in R2/PCFT4 CHO cells (IC_{50}s of 0.69 nM for AGF94, 1.96 nM for AGF71) (Wang et al., 2011), as measured with an *in situ* metabolic assay which measured incorporation of [^{14}C]glycine into the GARFTase product formyl GAR. AGF71 and AGF94 displayed inhibition

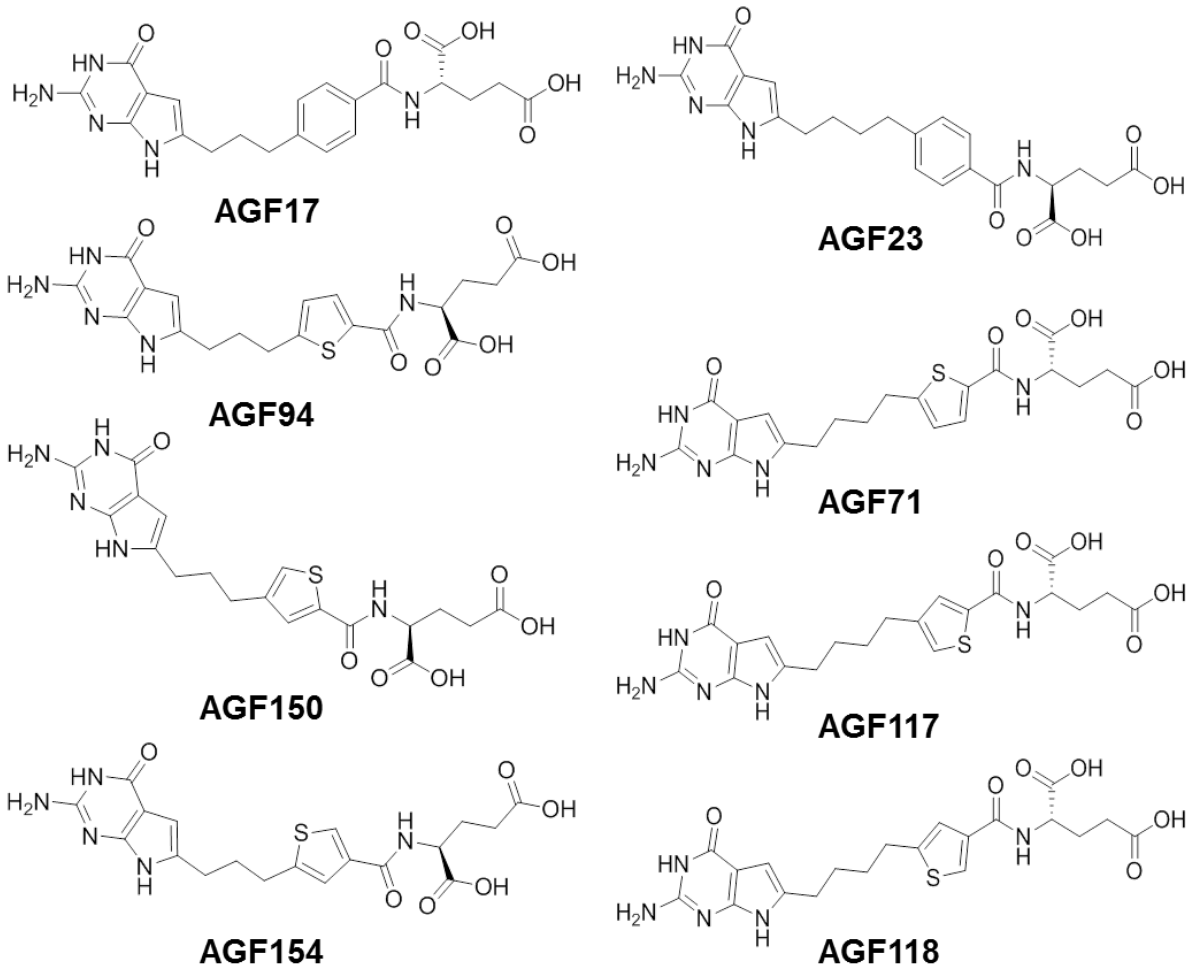

Figure 1.7 Structures of novel antifolates. Structures of novel tumor-targeted pyrollo[2,3-*d*]pyrimidines with specificity for PCFT over RFC. All compounds were synthesized by Dr. Aleem Gangjee of Duquesne University in collaboration with Dr. Larry Matherly. All drugs are discussed in Chapter 1.6.7.

of colony formation in PCFT-expressing CHO cells (derived from R2, CHO cells which lack RFC and PCFT expression) establishing cell killing, and both showed dose and time dependent killing (Wang et al., 2011). In HeLa cells, AGF94 and AGF71 were shown to be polyglutamylated at pH 6.8, while AGF94 revealed ~6 times greater polyglutamate accumulation compared to AGF71 (Desmoulin et al., 2012b). Compounds with longer carbon bridge regions displayed far less efficacy *in vitro* toward PCFT-expressing tumor cells (Wang et al., 2010; Wang et al., 2011).

A series of thieonyl regioisomers of AGF71 were synthesized, in which the position of the sulfur atom varies within the thiophene ring between molecules. Two of these novel compounds, AGF117 (thienoyl substitutions 3',5') and AGF118 (2',4') (Figure 1.7), were inactive towards RFC-expressing PC43-10 CHO cells but were very active towards PCFT-expressing R2/PCFT4 CHO cells (IC_{50}s of 63.82 for AGF117, 41.54 for AGF118) (Wang et al., 2012). AGF117 and AGF118 also displayed potent GARFTase inhibition in IGROV1 ovarian cancer cells (IC_{50}s of 2.03 nM for AGF117, 1.79 nM for AGF118). As with AGF17 and AGF23, AGF94, AGF71, AGF117 and AGF118 exhibited activity towards FR-expressing CHO cell lines (Wang et al., 2012; Wang et al., 2010; Wang et al., 2011).

A series of thieonyl regioisomers was also developed for AGF94. These include two potent PCFT-targeted compounds, AGF150 (thieonyl substitutions 2',4') and AGF154 (3',5') (Figure 1.7) (Wang et al., 2015) (also see Chapter 5). These drugs have very low IC_{50} values in R2/PCFT4 cells (5.39 nM for AGF150 and 6.51 nM for AGF154) (Wang et al., 2015). AGF150 and AGF154 were shown to be potent GARFTase inhibitors via a spectrophotometric assay with recombinant human GARFTase (formyltransferase domain) (K_i values of 13 nM for AGF150, 9.1 nM for AGF154 and 68 nM for AGF94), as well as parallel *in situ* GARFTase assays in KB

cells (IC_{50} values of 2.4 nM for AGF150, 2.6 nM for AGF154, and 3.5 nM for AGF94) (Wang et al., 2015). AGF150 and AGF154 also exhibited significant FR-binding affinities and *in vitro* efficacies in inhibiting proliferation of FR-expressing CHO cell lines (Wang et al., 2015). This characteristic of PCFT and FR dual-targeting may be a feature which could benefit the therapy of tumors that express FRs along with PCFT such as epithelial ovarian cancer (George and Matherly, unpublished) and a subset of NS-NSCLC (Wang et al., 2015) (also see Chapter 5). *In vivo*, AGF154 inhibited tumor growth of SKOV3 xenografts in SCID mice in a similar manner to AGF94, albeit at a lower dose (28 mg/kg for AGF94, 16 mg/kg for AGF154) (Wang et al., 2015). The development and characterization of tumor-targeted antifolates with PCFT selectivity and potent inhibition of *de novo* purine biosynthesis, typified by AGF17, 23, 71, 94, 117, 118, 150 and 154, provides a definitive proof-of-concept for tumor targeting via PCFT (with or without FR).

This dissertation will focus on both the characterization of important PCFT functional/structural determinants of drug transport, as well as the continued development and application of novel tumor targeted PCFT-selective antifolate compounds.

CHAPTER 2- PROTON-COUPLED FOLATE TRANSPORTER TRANSMEMBRANE DOMAIN 2-3 CONNECTING REGION FORMS REENTRANT LOOP STRUCTURE

2.1 Introduction

PCFT is predicted to have 12 TMDs with cytosolic N and C termini (Figure 1.4) (Unal et al., 2008; Zhao et al., 2010). This has been experimentally validated by indirect immunofluorescence staining of N- and C-terminal hemagglutinin (HA)-tagged human (h)PCFT and by SCAM involving Cys insertions into the TMD loop domains and reaction with MTSEA-biotin (Zhao et al., 2010). The extracellular location of the loop connecting TMDs 1 and 2 was further evidenced by the fact that two predicted N-linked glycosylation sites in that loop (Asn-58 and Asn-68) are glycosylated in human PCFT (Unal et al., 2008). Other aspects of hPCFT structure have been validated, including reactivity of membrane-impermeable methanethiosulfonate reagents with Phe157, Gly158, and Leu161 in TMD4 and with Ile188 in TMD5. Because methanethiosulfonate reactivity was protected by the hPCFT antifolate substrate PMX, these residues likely lie within or near the aqueous accessible substrate binding site (Shin et al., 2013; Zhao et al., 2012). Most recently, TMDs 1, 2, 7, and 11 have been shown to form an extracellular "gate" when PCFT is in the cytosol-facing conformation (Zhao et al., 2016). However, the contributions of other TMDs to the three-dimensional hPCFT structure have not been determined.

A number of specific amino acid residues were implicated as functionally important in hPCFT including Glu185 (TMD5; involved in proton coupling), His281 (TMD7; involved in substrate binding), and Arg376 (TMD10; impacts proton and substrate binding) (Figure 1.4) (Mahadeo et al., 2010; Unal et al., 2009a; Unal et al., 2009b). His247, localized to the loop

domain between TMDs 6 and 7, is predicted to interact with Ser172 at the cytoplasmic opening to control substrate access to the aqueous binding site (Unal et al., 2009a) (see Chapter 4).

The conserved loop domain linking TMD2 and TMD3 (residues 109–114) is of particular interest. This stretch is predicted to have a cytoplasmic orientation (Figure 1.4) and includes Asp109 and Arg113, both of which cannot be replaced by other amino acids regardless of charge or polarity (Lasry et al., 2008; Shin et al., 2010; Zhao et al., 2007). It was predicted that the loop region connecting TMD2 and TMD3 including Asp109 and Arg113 forms a β-turn structure involving the DSVG tetrapeptide and may be functionally important (Lasry et al., 2008; Subramanian et al., 2008). By homology modeling based on the GlpT template, Arg113 was predicted to protrude into a hydrophobic cavity composed of TMDs 1, 3, 4, and 6 (Lasry et al., 2008). However, experimental confirmation was not provided.

In this chapter we use SCAM with a cys-less (*cl*hPCFT^{HA}) hPCFT that exhibits functional characteristics virtually identical to wild-type (*wt*hPCFT^{HA}) hPCFT and MTSEA-biotin, combined with systematic site-directed mutagenesis, to directly explore the structural and functional significance of the TMD2-3 loop domain and TMD2 in hPCFT. Our results establish that the TMD2-3 domain forms a novel "reentrant loop" structure and suggest that amino acids at positions 93 and 94 in TMD2 may comprise part of a critical substrate binding domain with aqueous accessibilities (Yan and Luo, 2010). Our results are unprecedented and provide important new insights into key structural and functional determinants of hPCFT uptake. The work described in this chapter was previously published in the *Journal of Biological Chemistry* (Wilson et al., 2014).

2.2 Materials and Methods

2.2.1 Reagents

[3',5',7-^{3}H]MTX (20 Ci/mmol) was purchased from Moravek Biochemicals (Brea, CA). Unlabeled MTX was provided by the Drug Development Branch, NCI, National Institutes of Health (Bethesda, MD). Folic acid was purchased from Sigma. PMX (Alimta) was purchased from LC Laboratories (Woburn, MA). Tissue culture reagents and supplies were purchased from assorted vendors with the exception of fetal bovine serum (FBS), which was purchased from Hyclone Technologies (Logan, UT).

2.2.2 Generation of Cys-less hPCFT and Single-substitution Mutants

*cl*hPCFT^{HA}, including a HA epitope at the C terminus in pCDNA3, was prepared by PCR from the C-terminal HA-tagged *wt*hPCFT^{HA} (Hou et al., 2012) construct by mutagenizing individual Cys residues (Cys21, -66, -151, -229, -298, -328, and -397) to serine using the QuikChange^{TM} Multi Site-directed mutagenesis kit (Agilent Technologies, Santa Clara, CA) as described by the manufacturer. Single amino acid substitutions were generated using either *wt* or *cl*hPCFT^{HA} as a template and the QuikChange^{TM} site-directed mutagenesis kit (Agilent). Primers were developed using the QuikChange^{TM} Primer Design program (Agilent) and are available upon request. PCR conditions were 95 °C for 30s, 55°C for 1 min, and 68°C for 8 min for 16 cycles. All mutations were confirmed by DNA sequencing by Genewiz, Inc. (South Plainfield, NJ).

2.2.3 Cell Culture

The hPCFT-null R1-11 HeLa cell line was a gift of Dr. I. David Goldman (Bronx, NY) (Diop-Bove et al., 2009). Cells were grown in RPMI 1640 media supplemented with 10% FBS, 1% penicillin/streptomycin, and 2 mM *L*-glutamine. For transfections with hPCFT constructs, R1-11 cells were seeded in 60-mm culture dishes at a density of 0.8 million cells per plate in Dulbecco's modified Eagle's medium (DMEM) supplemented with 10% FBS and antibiotics.

After 24 h, the cells were transfected with hPCFT expression constructs (above) in pCDNA3 (1 μg/plate) using Lipofectamine 2000 (Invitrogen) (10 μl/plate) in Opti-MEM as described by the manufacturer (Invitrogen). After 4 h the transfection medium was replaced with DMEM containing 10% FBS.

2.2.4 Membrane Transport

Forty-eight hours post-transfection, cellular uptake of [^{3}H]MTX (0.5 μM) was measured over 2 min at 37 °C in 60-mm dishes in 2-(N-morpholino)ethanesulfonic acid (MES)-buffered saline (20 mM MES, 140 mM NaCl, 5 mM KCl, 2 mM MgCl2, and 5 mM glucose; pH 5.5), as previously described (Kugel Desmoulin et al., 2010). Cells were washed 3x with Dulbecco's phosphate-buffered saline (PBS), and the cells were solubilized in 0.5 N NaOH. Levels of intracellular radioactivity were calculated as pmol/mg of protein based on measurements of radioactivity and protein concentrations of the alkaline cell homogenates (Laemmli, 1970) (34). In some experiments cells were pretreated for 15 min at 37 °C with MTSEA-biotin (see below) before the transport assays with [^{3}H]MTX treatments. To measure MTX transport kinetics, cells were treated with concentrations of [^{3}H]MTX between 0.33 and 5 μM with results analyzed using Lineweaver-Burke plots for determinations of K_t and V_{max} values. For determining K_i values for nonradioactive substrates including folic acid and PMX, cells were treated with 0.5 μM [^{3}H]MTX and inhibitors at concentrations from 0.3 to 1.5 μM. Results were analyzed by Dixon plots to calculate K_i values. To compare the optimal pH for transport by *wt* and *cl*hPCFT^{HA}, transport assays were performed at pH values from 5.5 and 7.2. MES-buffered saline was used for pHs 5.5, 6.0 and 6.5, whereas HEPES-buffered saline (20 mM HEPES, 140 mM NaCl, 5 mM KCl, 2 mM MgCl2, and 5 mM glucose) was used for pH values 6.8 and 7.2.

2.2.5 Surface Biotinylation with MTSEA-biotin

Forty-eight hours post-transfection (above), cell surface proteins were surface-biotinylated with MTSEA-biotin (Biotium, Hayward, CA). MTSEA-biotin was freshly dissolved in DMSO at 2 mg/100 µl and then diluted 1:100 in PBS. Cells were washed with PBS twice and treated with MTSEA-biotin solution for 30 min at room temperature. The MTSEA-biotin was aspirated, and cells were treated with 14 mM β-mercaptoethanol in PBS for 5 min to quench the reactions, then washed twice with PBS. To collect crude membrane proteins, plates were placed in 4 °C and treated with 1.4 ml of hypotonic buffer (0.5 mM Na2 HPO4 , 0.1 mM EDTA, pH 7.0) containing a protease inhibitor mixture (Roche Applied Science). The cells were removed from the plates with a rubber policeman, followed by centrifugation at 16,000 rpm for 10 min at 4 °C. The supernatants were removed, and cell pellets were resuspended in 0.4 ml of lysis buffer (50 mM Tris base, 150 mM NaCl, 1% Nonidet P-40, 0.5% sodium deoxycholate, pH 7.4) by vortexing, then mixed on a rotisserie shaker for 1 h at 4°C. The samples were centrifuged at 16,000 x g for 15 min at 4 °C, leaving the detergent-solubilized membrane proteins in the supernatant. An aliquot (25 µl) of this fraction was used as a loading control, and the remaining 375 µl were added to 50 µl of streptavidin-agarose resin (Thermo Scientific, Waltham, MA) (prewashed 3x with lysis buffer). This mixture was mixed overnight at 4 °C in a rotisserie shaker. The following day the mixture was centrifuged at 16,000 x g for 1 min, and the supernatant was aspirated. The resin was washed 3 times with lysis buffer, followed by a wash with lysis buffer supplemented with 2% SDS. Bound proteins were released from the streptavidin resin by heating to 95 °C for 5 min in 2x Laemmli loading buffer that contained dithiothreitol (Laemmli, 1970). For some experiments protection from MTSEA-biotin biotinylation by the PCFT substrate, PMX, was tested. For these experiments, plates were treated with 2 ml of PBS containing 250 µM PMX

for 15 min immediately before MTSEA-biotin treatment. Results were compared with those for untreated controls, incubated in parallel.

2.2.6 Western Blotting

Procedures for SDS-polyacrylamide gel electrophoresis, and electrotransfer to polyvinylidene difluoride membranes (Pierce) were identical to previously reported methods (Hou et al., 2012). For standard Western blotting, membrane proteins were electrophoresed on 7.5% polyacrylamide gels in the presence of SDS (Laemmli, 1970) and electroblotted onto polyvinylidene difluoride membranes (Pierce) (Matsudaira, 1987). Blots were probed with anti-HA antibody (Covance, Princeton, NJ) and IRDye800-conjugated secondary antibody. Anti-β-actin antibody (Sigma) was used to probe for loading controls. Imaging and densitometry were performed with an Odyssey Infrared Imaging System (LI-COR, Lincoln, NE).

2.2.7 Statistical Analysis

Unpaired t tests were conducted using GraphPad 6.0 software.

2.3 Results

2.3.1 Alanine-scanning Mutagenesis of TMD2 and the TMD2-3 Loop Region of hPCFT

A previous study used progressive alanine substitution mutagenesis with stretches of alanines to disrupt the predicted TMD2-3 β-turn in hPCFT and found that transport activity was abolished due to impaired intracellular trafficking to the plasma membrane (Subramanian et al., 2008). As an extension of this work, we used a targeted alanine-scanning mutagenesis strategy with individual alanine substitutions across this stretch (including flanking regions) with *wt*hPCFT^{HA} as a template and extended this to include the entire TMD2 for a total of 33 mutants spanning positions 85–118 (Figure 1.4). Mutant hPCFT constructs were transfected into hPCFT-null R1-11 HeLa cells. Membrane transport of [^{3}H]MTX was measured at pH 5.5, the pH

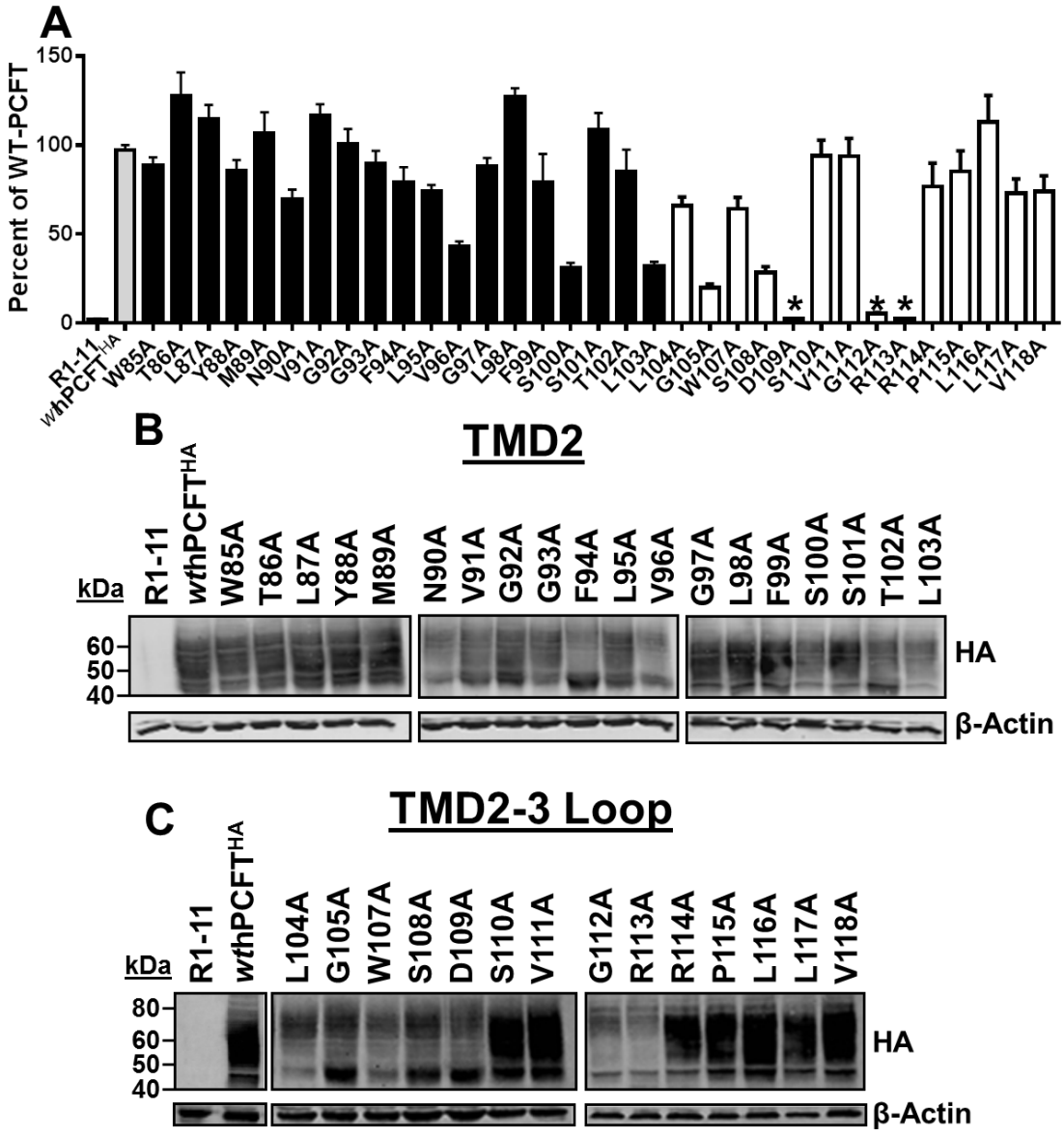

Figure 2.1 Impact of scanning alanine mutagenesis on hPCFT expression and transport. *Panel A*, *wt*hPCFT^{HA} and alanine mutants in TMD2 and the TMD2-3 loop domain were transiently transfected into R1-11 cells, and hPCFT activity was determined after 48 h by [^{3}H]MTX uptake assay at pH 5.5 over 2 min at 37 °C. Results are expressed as relative to *wt*hPCFT^{HA} and are reported as the mean values ± S.E. (*error bars*) from triplicate experiments. Results for D109A, G112A, and R113A were not significantly increased over those for R1-11 cells ($p < 0.05$, noted by *asterisks*). *wt*hPCFT^{HA} is indicated by the *gray bar*. TMD2 mutants are shown in *black*, and the TMD2-3 loop mutants are shown in *white*. *Panels B* and *C*, Western blots are shown for membrane proteins (10 g) from HA-tagged TMD2 (*Panel B*) and TMD2-3 loop (*Panel C*) alanine mutants isolated 48 h after transient transfections of R1-11 cells. Results are shown for membrane proteins probed with HA-specific antibody with equal loading confirmed with β-actin. Results are representative of at least two blots from independent experiments. Figure previously published in Wilson et. al. J Biol Chem. 2014.

optimum for PCFT, and HA-tagged hPCFT proteins in crude plasma membranes were assayed by Western blotting with HA-specific antibody. We found that all 33 hPCFT alanine mutants were expressed in crude membranes (Figure 2.1B) and that 30 of these were active for transport (25–115% of *wt*hPCFT^{HA}), including all of the mutants in TMD2 (Figure 2.1A). Conversely, for residues located in the TMD2-3 loop domain (i.e., positions 109, 112, and 113), Ala replacements abolished uptake ([^{3}H]MTX uptake values were not significantly different from those with R1-11 cells ($p < 0.05$)). Although most of the TMD2-3 loop mutants were detected at substantial levels on Western blots, for the Gly-112 and Arg-113 mutants, loss of transport activity was associated with substantially reduced hPCFT membrane expression (Figure 2.1C).

These results with Asp109 and Arg113 are consistent with previous reports that any amino acid replacement (including even conservative substitutions) at these positions was inactive (Lasry et al., 2008; Shin et al., 2010; Subramanian et al., 2008; Zhao et al., 2007) (9, 11, 17, 30). For Asp109, mutation disrupts the DSVG tetrad (109-112) and β-turn in the TMD2-3 loop domain. Similarly, mutation of Gly112 to Pro significantly reduced hPCFT expression on Western blots (Figure 2.2B) and caused a complete loss of transport activity (Figure 2.2A), further implying that disruption of the β-turn structure results in protein misfolding and protein degradation. By contrast, with Arg114, we found that mutation to increasingly non-conservative residues, including Lys, His, and Asp, preserved expression on Western blots (Figure 2.2B) while progressively decreasing transport without abolishing it altogether (Figure 2.2A).

2.3.2 Cys-scanning Mutagenesis and Cys Accessibilities to Biotinylation with MTSEA-biotin for TMD2 and the TMD2-3 Loop Region of hPCFT

Our goal was to further determine the structural and functional significance of TMD2 and the TMD2-3 loop domain in hPCFT using Cys-scanning mutagenesis and SCAM. hPCFT

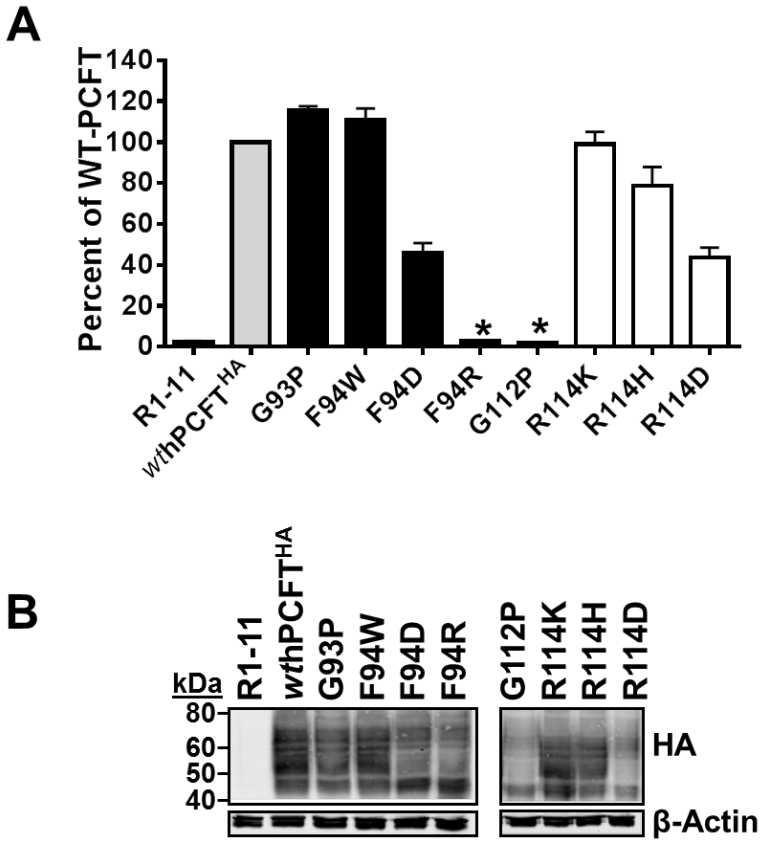

Figure 2.2 Characterization of hPCFT mutants. *Panel A*, TMD2 and TMD2-3 loop mutants were transiently transfected into R1-11 cells, and PCFT activity was determined 48 h later by [^{3}H]MTX uptake assay at 37 °C at pH 5.5 over 2 min. Results are expressed as relative to *wt*hPCFT^{HA} and are reported as the mean values S.E. (*error bars*) from triplicate experiments. Results for the F94R and G112P mutants were not significantly increased over the level in R1-11 cells (noted by the *asterisks*; $p > 0.05$). TMD2 mutants are shown in *black*, and TMD2-3 loop mutants are shown in *white*. *wt*hPCFT^{HA} is indicated by a *gray bar*. *Panel B*, Western blots of membrane proteins (10 μg) from HA-tagged TMD2 and TMD2-3 loop mutants 48 h after transient transfections of R1-11 cells. Results are representative of at least two independent experiments. Figure previously published in Wilson et. al. J Biol Chem. 2014.

includes 7 Cys residues (Figure 1.4), two (Cys66 and Cys298) of which form a disulfide linkage (Zhao et al., 2010). Because Cys residues in *wt*hPCFT^{HA} reacted with thiol-reactive MTSEA-biotin in pilot studies (not shown), we generated a "Cys-less" hPCFT construct (with a C-terminal HA epitope) by mutating the seven Cys residues to serine. When transiently expressed in hPCFT-null R1-11 HeLa cells, *cl*hPCFT^{HA} retained 77.5% (± 2.8%) of the transport activity of *wt*hPCFT^{HA}. The addition of 10 μM PMX completely blocked MTX transport levels for both *wt* and *cl*hPCFT^{HA} (Figure 2.3B). *cl*hPCFT^{HA} displayed a similar decrease in the level of membrane hPCFT protein on Western blots (70 ± 10%) of the *wt*hPCFT^{HA} level (Figure 2.3A). *cl*hPCFT^{HA} and *wt*hPCFT^{HA} showed nearly identical transport characteristics including K_t and V_{max} values for [^{3}H]MTX and K_i values for folic acid and PMX (Table 2.1). Furthermore, for both *cl*hPCFT^{HA} and *wt*hPCFT^{HA}, pH-dependent transport of [^{3}H]MTX was essentially identical with decreasing activity from the high level measured at pH 5.5 and the very low levels above pH 7 (Figure 2.3C). Collectively, these results establish that *wt* and *cl*hPCFT^{HA} are functionally equivalent.

To study the roles of the TMD2 and TMD2-3 loop regions in hPCFT structure and transport function, we used site-directed mutagenesis with *cl*hPCFT^{HA} as a template to introduce single Cys residues from positions 85 to 118 (Figure 1.4). The 33 individual Cys constructs were transiently transfected into R1-11 HeLa cells, followed by assays of [^{3}H]MTX uptake at pH 5.5 and of hPCFT protein levels on Western blots (Figure 2.4A-C). Cys substitutions at a number of positions were less tolerated than were the Ala substitutions (compare Figures 2.1A and 2.4A). Twenty-eight of the 33 Cys mutants were considered "active" based on statistically significant increases in [^{3}H]MTX uptake (2-fold; $p < 0.05$) over the very low residual level in R1-11 cells. These include Cys mutants of several residues (Asn90, Leu104, Gly105, Pro115) with modest

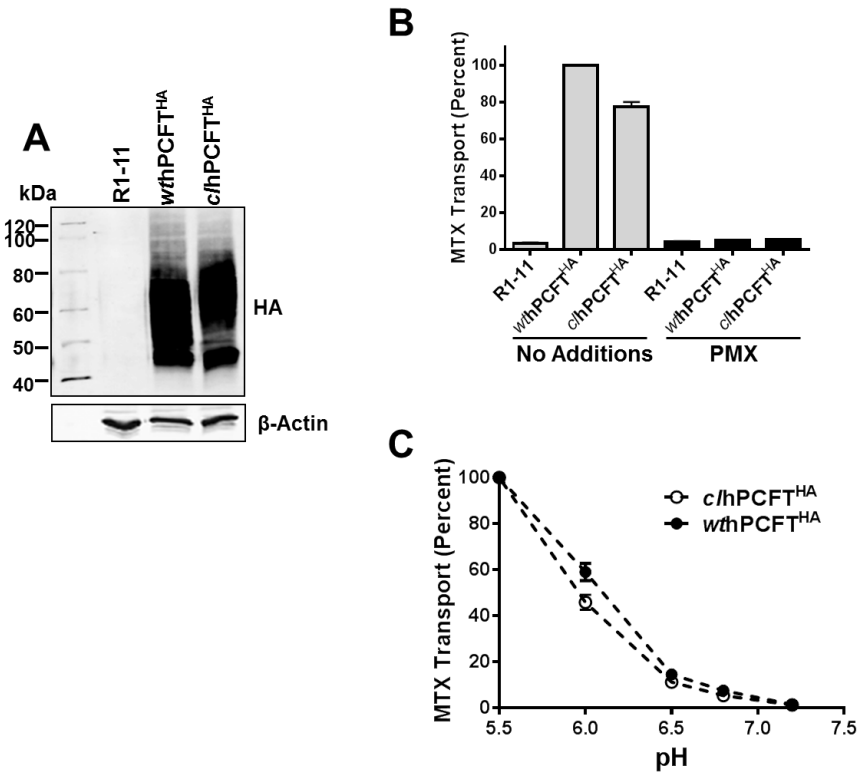

Figure 2.3 Characterization of Cys-less hPCFT. *Panel A*, *wt*hPCFT^{HA} and CL- PCFT were transiently transfected into R1-11 cells. A Western blot of membrane proteins (10 μg) prepared 48 h post-transfection for HA-tagged *wt*hPCFT^{HA} and *cl*hPCFT^{HA} is shown. β-Actin was used to confirm equal loading. Results are representative of three independent experiments. By densitometry, the hPCFT/ β-actin ratios of *cl*hPCFT^{HA} were 70% (± 10%) of the *wt*hPCFT^{HA} level. *Panel B*, hPCFT transport was measured 48 h later by [^{3}H]MTX uptake assay at pH 5.5 over 2 min, with (*black*) or without (*gray*) the addition of unlabeled 10 μM PMX. Data are presented as the mean values S.E. from three to seven independent experiments. For *cl*hPCFT^{HA}, transport was 77.5% (± 2.8%) that for *wt*hPCFT^{HA}. Transport was inhibited in the presence of 10 μM nonradioactive PMX. *Panel C*, the pH dependence for [^{3}H]MTX uptake over 2 min from pH 5.5 to 7.2 for transiently expressed *wt*hPCFT^{HA} and *cl*hPCFT^{HA} in R1-11 cells is shown. Results are presented as the mean values ± S.E. from triplicate experiments. Figure previously published in Wilson et. al. J Biol Chem. 2014.

TABLE 2.1

Kinetic Analysis of WT- and CL-PCFT.

Constant	Compounds	hPCFT Variants	
		WT-PCFT	**CL-PCFT**
K_t (μM)	MTX	0.44 ± 0.06	0.51 ± 0.03
V_{max} (pmol/mg/min)	MTX	276.8 ± 59.7	236.2 ± 27.5
K_i (μM)	Folic Acid	1.51 ± 0.18	1.49 ± 0.45
K_i (μM)	PMX	0.13 ± 0.04	0.13 ± 0.05

WT-PCFT and CL-PCFT were transiently transfected into R1-11 cells, and PCFT transport was measured 48 h later by [^{3}H]MTX uptake assay at pH 5.5 over 2 min. To determine K_t and V_{max} values, cells were treated with [^{3}H]MTX with concentrations between 0.33 μM and 5 μM, with results analyzed by Lineweaver-Burke plots. To determine K_i values, cells were incubated with 0.5 μM [^{3}H]MTX with folic acid or PMX as competitors from 0.3 μM to 1.5 μM, and results were analyzed by Dixon plots. Data are presented as mean values +/- standard errors from three independent experiments.

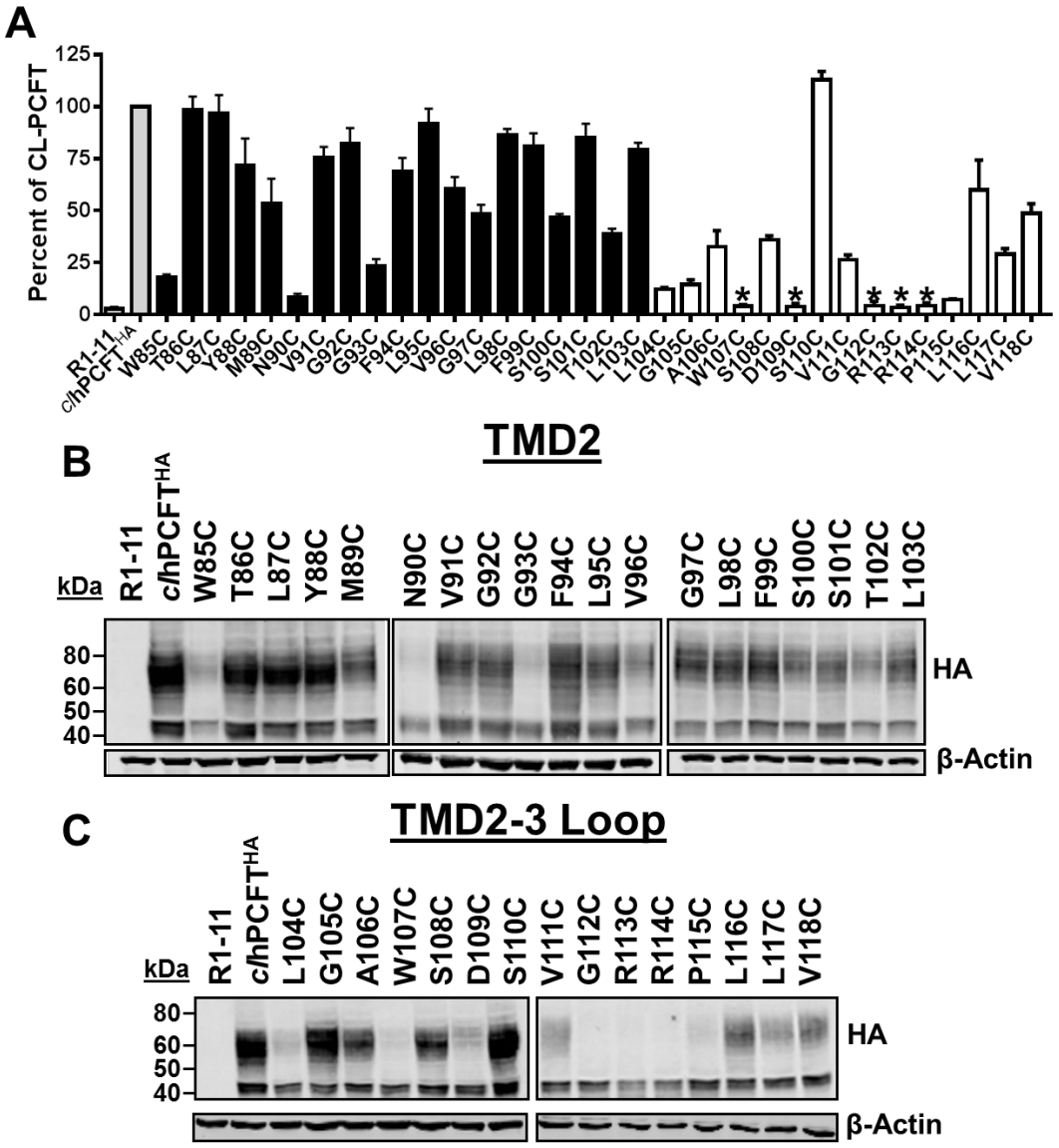

Figure 2.4 Characterization of hPCFT single-Cys mutants. *Panel A*, TMD2 and TMD2-3 loop single-Cys hPCFT mutants were transiently transfected into R1-11 cells, and PCFT activity was measured after 48 h by [^{3}H]MTX uptake assay at pH 5.5 over 2 min. Results are expressed as relative to those for *cl*hPCFT^{HA} and are reported as mean values ± S.E. (*error bars*) from triplicate experiments. Transport levels for W107C, D109C, G112C, R113C, and R114C mutants (noted with *asterisks*) were not significantly increased over the low level in R1-11 cells ($p > 0.05$), whereas transport for the other 28 samples was significantly increased over the transport level in R1-11 cells ($p < 0.05$). *cl*hPCFT^{HA} is indicated by the *gray bar*. The TMD2 mutants are shown in *black*, and the TMD2-3 loop mutants are shown in *white*. *Panels B* and *C*, Western blot analysis was performed on membrane proteins (10 μg) prepared from HA-tagged TMD2 (*Panel B*) and the TMD2-3 loop (*Panel C*) Cys mutants 48 h post-transfection. Results are shown for hPCFT proteins probed with HA-specific antibody, with equal loading confirmed with β-actin. Results are representative of at least two blots from independent experiments. Figure previously published in Wilson et. al. J Biol. Chem 2014.

levels of transport. Analogous to their Ala mutant counterparts, Cys replacements at Asp109, Gly112, and Arg113 were completely inert (Figure 2.4A). Whereas Ala replacements of Trp107 and Arg114 preserved substantial transport activity (Figure 2.1A), transport was abolished for Cys replacements at these positions (Figure 2.4A). For many of the Cys mutants, transport activity paralleled levels of hPCFT protein on Western blots (Figure 2.4B-C), suggesting that the substantial losses of transport for the inactive hPCFT Cys mutants were likely the result of mutant protein misfolding, resulting in impaired intracellular trafficking and protein degradation. However, for a few of the Cys mutants in the TMD2-3 loop domain (i.e. Cys105 and Cys108), transport was disproportionately low relative to the levels of PCFT protein (Figure 2.4A-C), suggesting functionally inactive protein.

For the 28 active Cys mutants spanning TMD2 and the TMD2-3 loop region, we used MTSEA-biotin to establish their aqueous accessibilities in forming an aqueous transmembrane pathway for anionic (anti)folate substrates. MTSEA-biotin is a membrane-impermeable, bifunctional reagent that includes thiol-reactive MTS and biotin moieties, thus permitting isolation of biotinylated hPCFT protein by precipitation with streptavidin beads for analysis on Western blots. R1-11 cells were transiently transfected with the active Cys hPCFT mutants, then treated with MTSEA-biotin, followed by pull-down with streptavidin beads. The biotinylated proteins were eluted and analyzed on Western blots with HA-specific antibody, and the results were compared with those for total hPCFT proteins in membrane fractions sampled before MTSEA-biotin treatments. The G207C hPCFT mutant mapping to the extracellular loop 3 domain (Figure 1.4) was used as a positive control for the pulldown experiments.

Cys mutants at positions 85-89 mapping to the exofacial segment of TMD2 (Figure 1.4) were extensively biotinylated, likely reflecting their extracellular accessibilities to the

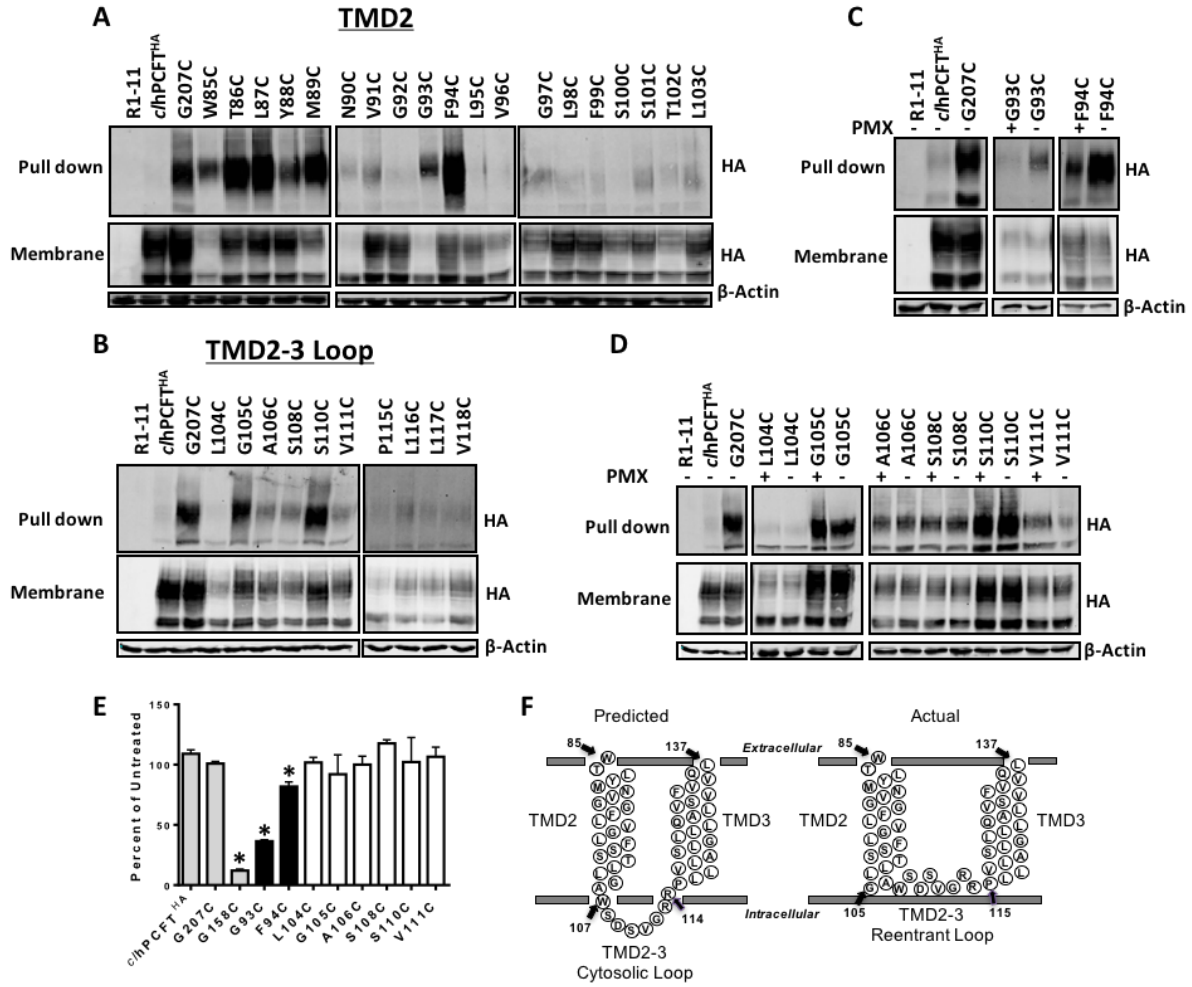

Figure 2.5 Biotinylation of single-Cys mutants in TMD2 and the TMD2-3 loop with MTSEA-biotin. *Panels A* and *B*, TMD2 (*Panel A*) and TMD2-3 loop (*Panel B*) single-Cys mutants were transiently transfected into R1-11 cells, and 48 h later cells were treated with MTSEA-biotin. Cells were harvested, and membranes prepared, solubilized, and incubated with streptavidin beads to pull down biotinylated proteins. The G207C mutant located in the extracellular loop 3 domain (Figure 1.4) was used as a positive control for the pulldown assays. Biotinylated proteins were eluted and analyzed by Western blotting using an anti-HA antibody (*Pull down*). An aliquot (25 µl) of the crude membrane fraction before MTSEA-biotin treatment was also analyzed by Western blotting as a control (*Membrane*). *Panels C* and *D*, transiently transfected R1-11 cells were treated with or without 250 µM PMX before treatment with MTSEA-biotin, streptavidin precipitation, and Western blotting as described for *Panels A* and *B*. *Panel E*, TMD2 and TMD2-3 loop single-Cys mutants were transiently transfected into R1-11 cells. After 48 h, cells were incubated with or without MTSEA-biotin followed by assay of PCFT transport with [^{3}H]MTX at pH 5.5 over 2 min. Results are expressed relative to the non-treated sample and are reported as the mean values ± S.E. for two (positions 104 –111) or three (R1-11, *cl*hPCFT^{HA}, and positions 207, 158, 93, and 94) independent experiments. For positions 158, 93, and 94, losses of transport activity by MTSEA-biotin treatment compared with untreated samples were statistically significant ($p < 0.05$; noted by asterisk). In the transport experiments, *cl*hPCFT^{HA} and G207C were negative controls, whereas MTSEA-biotin-reactive G158C was

used as a positive control (all shown in *gray*) (Shin et al., 2013). Results for the TMD2 mutants are shown in *black*, and TMD2-3 loop mutants are shown in *white*. *Panel F*, diagram of the TMD2-3 reentrant loop structure. Figure previously published in Wilson et. al. J Biol Chem. 2014.

hydrophilic MTSEA-biotin reagent (Figure 2.5A, upper panel). However, other positions in TMD2 also reacted with MTSEA-biotin, especially positions 93 and 94, predicted to lie in the mid-TMD2 region, although flanking positions were poorly or completely unreactive. For the G93C mutant, reaction with MTSEA-biotin is particularly notable given its modest levels in the total membrane fraction (Figure 2.5A, lower panel). For the TMD2-3 loop (positions 107-114) and flanking regions (104-106, 115-118), predicted to have a cytosolic orientation, we found that the G105C, A106C, S108C, S110C, and V111C *cl*hPCFT^{HA} mutants were uniquely reactive with MTSEA-biotin in comparison with other mutants (e.g. L104C and P115C) (Figure 2.5B). Thus, positions 93 and 94 in TMD2 and positions 105, 106, 108, 110, and 111 in the TMD2-3 loop region seem to be aqueous accessible despite their predicted membrane topologies.

2.3.3 Impact of hPCFT Substrate on Biotinylation and Transport Inhibition by Biotinylation

To examine whether the MTSEA-biotin-reactive positions in the TMD2 and the TMD2-3 loop regions (positions 93, 94, 105, 106, 108, 110, and 111) contribute to an aqueous binding domain for hydrophilic (anti)folate substrates, we preincubated transiently transfected R1-11 cells expressing the G93C, F94C, L104C, G105C, A106C, S108C, S110C, and V111C mutants with the PCFT substrate PMX (250 μM) before treatment with MTSEA-biotin. Controls were incubated in parallel without PMX. Biotinylated proteins were precipitated with streptavidin beads and analyzed on Western blots. PMX substantially decreased MTSEA-biotin reactivity with Cys residues at positions 93 and 94 (Figure 2.5C). However, the biotinylated TMD2-3 loop residues were unaffected by PMX treatment (Figure 2.5D). To determine whether biotinylation of these residues also inhibited transport activity, we incubated transiently transfected R1-11 cells expressing G93C, F94C, L104C, G105C, A106C, S108C, S110C, and V111C hPCFT mutants with [^{3}H]MTX (0.5 μM) for 15 min at 37 °C with or without a 15 min MTSEA-biotin

pretreatment. In this series of experiments, *cl*hPCFT^{HA} and G207C were negative controls, whereas MTSEA-biotin-reactive G158C was used as a positive control (Shin et al., 2013).

We found that of these residues, only for the G93C and F94C mutants was transport significantly inhibited by biotinylation (Figure 2.5E, 63.5 and 18.2%, respectively; $p < 0.05$). Collectively, these results are consistent with the notion of a direct interaction between positions 93 and 94 and substrate, although an indirect effect mediated by conformational changes resulting from more distal substrate binding cannot be excluded.

2.4 Discussion

In this chapter we studied the structural and mechanistic roles of TMD2 and the TMD2-3 loop region in hPCFT. Our results establish aqueous accessibilities of residues located in the TMD2-3 loop despite their predicted membrane topologies. These results are best interpreted as a reentrant loop structure (Figure 2.5F), similar to those reported for other MFS transporters (e.g. EAAT1) (Seal and Amara, 1998; Yan and Luo, 2010). These results support those of Subramanian et al., which establish that disruption of the TMD2-3 loop results in hPCFT protein misfolding and loss of surface expression and transport activity (Subramanian et al., 2008). In previous studies it was reported that Asp109 and Arg113 in this stretch cannot be replaced with even conservative substitutions (Lasry et al., 2009; Zhao et al., 2007). Our results show that this now extends to the G112P mutant as well, although substitutions (Lys, His, Asp) at Arg114 were tolerated. Finally, our results suggest that positions 93 and 94 in TMD2 may directly participate in forming the hPCFT substrate binding pocket/membrane translocation pathway. Determining the structural determinants of hPCFT membrane transport is requisite to understanding the molecular mechanisms of transport, including critical determinants of (anti)folate binding.

CHAPTER 3- TRANSMEMBRANE DOMAINS 3 AND 6 OF THE PROTON-COUPLED FOLATE TRANSPORTER FORM OLIGOMERIZATION INTERFACE

3.1 Introduction

Reflecting its biological and therapeutic importance, studies have begun to explore key structural determinants of hPCFT function (Hou et al., 2012; Hou and Matherly, 2014; Matherly et al., 2014). Thus, structurally and/or functionally important residues in hPCFT were identified, including Asp109, Arg113 , Asp156 , Gly158 , Leu161 , Ser172 , Glu185 , Ile188 , Gly189 , Gly192 , Glu232 , His247 , His281 , Ile304 , Arg376 and Pro425 (Lasry et al., 2008; Mahadeo et al., 2010; Matherly et al., 2014; Shin et al., 2011; Shin et al., 2010; Shin et al., 2013; Unal et al., 2009a; Unal et al., 2009b; Zhao and Goldman, 2007; Zhao et al., 2011b; Zhao et al., 2012), and stretches including TMDs 2, 4 and 5 were identified by SCAM as forming substrate-binding/membrane-translocation domains (Shin et al., 2013; Zhao et al., 2012) (also see Chapter 2). hPCFT is N-glycosylated at Asn58 and Asn68 (Unal et al., 2008). A unique β-turn structure in the TMD 2–3 loop region forms a novel reentrant loop structure and is essential for intracellular trafficking and high level transport (Lasry et al., 2008; Subramanian et al., 2008; Unal et al., 2008) (also see Chapter 2).

hPCFT forms homo-oligomers both in detergent solution and *in situ* with the hPCFT dimer as the dominant form (Hou et al., 2012). With ectopically expressed hPCFT, oligomerization was established by cross-linking with MTS-1-MTS, blue native gel electrophoresis, binding of co-expressed haemagglutinin (HA) and His10-tagged hPCFT monomers to nickel affinity columns and FRET between co-expressed YFP (YPet)- and enhanced cyan fluorescent protein (with K26R/N164H mutation; ECFP*)-tagged hPCFT monomers (Hou et al., 2012). Combined *wt* and inactive mutant P425R hPCFTs exhibited a distinctive ‘dominant-positive’ transport phenotype, implying positive co-operativity between

hPCFT monomers and functional 'rescue' of mutant hPCFT by *wt*hPCFT (Hou et al., 2012). hPCFT oligomers were also identified by Zhao et al. by homobifunctional cross-linking with MTS-1-MTS and a putative TMD6 interface between hPCFT monomers was implied from the finding that MTS-1-MTS treatment generated cross-links between Cys229 (located in TMD6) in individual PCFT monomers, but not when Cys229 was mutated to serine (Zhao et al., 2012). Based on these results, the experiments described in this chapter explore the roles of residues localized to TMDs 3 and 6 in forming critical structural interfaces between hPCFT monomers. The work described in this chapter was previously published in *Biochemical Journal* (Wilson et al., 2015)

3.2 Materials and Methods

3.2.1 Reagents

[3' ,5' ,7-^{3}H]MTX (20 Ci/mmol) was purchased from Moravek Biochemicals. Unlabelled Mtx was provided by the Drug Development Branch, National Cancer Institute, National Institutes of Health. Synthetic oligonucleotides were obtained from Invitrogen. Tissue culture reagents and supplies were purchased from assorted vendors with the exception of FBS, which was purchased from Hyclone Technologies. The cross-linking reagent 1,6-hexanediyl bismethanethiosulfonate (MTS-6-MTS) was purchased from Toronto Research Chemicals.

3.2.2 Cell Culture

The RFC- and hPCFT-null HeLa cell line, designated R1-11 (Diop-Bove et al., 2009), was a gift of Dr I. David Goldman (Bronx, NY). R1-11 cells were maintained in complete RPMI (Roswell Park Memorial Institute) 1640 medium containing 10% FBS, 2 mM *L*-glutamine, 100 units/ml penicillin and 100 μg/ml streptomycin (Hou et al., 2012).

3.2.3 hPCFT Plasmid Constructs and Transient Transfections

Cysteine-less (*cl*) hPCFT (see Chapter 2), including a HA epitope at the C-terminus (*cl*hPCFT^{HA}) in pCDNA3 was prepared by PCR from the hPCFT^{HA} construct (Diop-Bove et al., 2009), by mutagenizing Cys21 , Cys66 , Cys151 , Cys229 , Cys298 , Cys328 and Cys397 to serine, using the QuikChangeTM Multi Site-Directed Mutagenesis Kit (Agilent) (see Chapter 2) . Single cysteine replacements were generated using *cl*hPCFT^{HA} as template and the QuikChange^{TM} Site-Directed Mutagenesis Kit (Agilent). Primers were designed using the QuikChange^{TM} Primer Design program (Agilent) and are available upon request. All mutations were confirmed by DNA sequencing by Genewiz, Inc.

*wt*hPCFT^{HA} and mutant hPCFT constructs (see below) were transiently transfected into R1-11 HeLa cells with Lipofectamine-Plus reagent (Invitrogen), as previously described (Hou et al., 2005) (also see Chapter 2). With all transfections, cells were harvested after 48 h for transport and for preparing plasma membranes and Western blotting (see below). For experiments in which results for transfections with two plasmid constructs were directly compared with results for cells transfected with a single plasmid construct, constant DNA amounts were maintained by adding empty pCDNA3 (Invitrogen) to the single transfections.

3.2.4 Membrane Transport Experiments

Cellular uptake of [^{3}H]MTX (0.5 μM) was measured over 2 min at 37° C in 60-mm dishes in MES-buffered saline (20 mM MES, 140 mM NaCl, 5 mM KCl, 2 mM MgCl2 and 5 mM glucose) at pH 5.5 (Kugel Desmoulin et al., 2010) (see Chapter 2). Levels of intracellular radioactivity were expressed as pmol/mg protein, calculated from direct measurements of radioactivity and protein contents (Lowry et al., 1951) of the cell homogenates.

3.2.5 Membrane Preparations and Western Blot Analysis of Plasma Membrane hPCFT Proteins

Plasma membrane preparations, SDS/PAGE and electrotransfer to polyvinylene difluoride membranes (Pierce) were as reported previously (Hou et al., 2005) (see Chapter 2). Detection and quantification of immunoreactive proteins used anti-HA (Covance) or and IRDye800-conjugated secondary antibody with an Odyssey® infrared imaging system (LI-COR). β-Actin was used as a loading control (Sigma).

3.2.6 Cross-linking of Cysteine-substituted Mutants of hPCFT

Forty-eight hours post-transfection with hPCFT mutants, R1-11 cells (in 60-mm dishes) were washed twice with Dulbecco's PBS and then treated with MTS-6-MTS [freshly dissolved in DMSO at 7.2 mg/ml (30 mM) and then diluted in PBS 1:100 (0.072 mg/ml or 0.3 mM)] on ice for 1 h. The cells were washed twice with PBS, then treated with 1.4 ml of hypotonic buffer (0.5 mM Na2 HPO4 , 0.1 mM EDTA, pH 7.0) which contained a protease inhibitor cocktail (Roche) on ice for 30 min. The cells were scraped from the dishes with rubber policemen and then centrifuged at 16,000 x *g* at 4° C for 10 min. The cell pellets were solubilized in 0.4 ml of lysis buffer (50 mM Tris-base, 150 mM NaCl, 1% NP40 and 0.5% sodium deoxycholate, pH 7.4), then centrifuged (16,000 x *g*, 4° C) for 15 min to remove cell debris. The supernatant was frozen, protein contents determined [Bradford assay (BioRad)] and constant protein amounts were analysed by Western blotting using DTT-free 2× SDS/PAGE loading buffer.

3.2.7 Molecular Modeling

Using the crystal structure of GlpT (1PW4) as template (Huang et al., 2003), we did homology modelling of the hPCFT monomer with Robetta Server (http://robetta.bakerlab.org). The top five hPCFT homology models retrieved through Robetta were evaluated by superimposing them over crystal structures of LacY, obtained at various states (1PV6, 1PV7, 2CFP, 2CFQ, 2V8N and 2Y5Y) and of GlpT (1PW4), by Chimera MatchMaker

(http://www.cgl.ucsf.edu/chimera) with parameters optimized by superimposing GlpT (1PW4) over LacY (1PV6) that gave the lowest RMSD values over the longest Cα atoms. This was based on the notion that all crystal structures from three members (LacY, GlpT and EmrD) of the MFS of transporters have preserved both secondary and tertiary structure elements during evolution (Abramson et al., 2004). The hPCFT model (hPCFT_R5) showing the lowest RMSD values (above) was manually adjusted with COOT (http://lmb.bioch.ox.ac.uk/coot/) to reflect the TMD2-3 re-entrant loop (see Chapter 2), resulting in hPCFT_R5_2-3RL. The hPCFT_R5_2-3RL model was further validated by assigning known residues that line the potential substrate binding pocket of hPCFT. The validated hPCFT_R5_2-3RL homology model was used to build an hPCFT dimeric model using MDOCK server (Pierce et al., 2014), based on the notion that hPCFT forms oligomers with the dimer as dominant species (Hou et al., 2012). This modeling was performed by Zhanjun Hou (Karmanos Cancer Institute) and Jun Ye (Chinese Academy of Sciences).

3.2.8 Statistical Analysis

Statistical analyses were performed using GraphPad 6.0 software.

3.3 Results

3.3.1 TMDs 3 and 6 Form a Boundary Between Monomeric hPCFT

A role for Cys229 (in TMD6) in hPCFT oligomerization was previously implied from the finding that mutation of Cys229 to serine abolished cross-linking with MTS-1-MTS (Zhao et al., 2012). Using GlpT as a template (Huang et al., 2003) and based on published studies for hPCFT (Lasry et al., 2009; Lasry et al., 2008; Mahadeo et al., 2010; Shin et al., 2010; Shin et al., 2013; Unal et al., 2009a; Unal et al., 2009b; Zhao et al., 2011b; Zhao et al., 2012), we generated a 3D homology model for monomeric hPCFT in which TMDs 1, 2, 4, 5, 7, 8, 10 and 11 comprise an

aqueous transmembrane pathway, flanked by TMDs 3, 6, 9 and 12 (Figures 3.1A and B). With MDOCK modelling (Pierce et al., 2014) of this hPCFT monomer structure, a dimeric hPCFT structure was predicted (Figure 3.1C) with juxtaposed TMDs 2, 3, 4 and 6 as structural interfaces between hPCFT monomers, analogous to other oligomeric MFS proteins (Korkhov et al., 2004; Scholze et al., 2002; Sitte et al., 2004).

To begin to test this model and to extend the published results of Zhao et al. (Zhao et al., 2012), we inserted cysteine residues into a *cl*hPCFT^{HA} background (see Chapter 2) from positions 115–137 spanning TMD3 and from positions 213–236 spanning TMD6. Individual cysteine mutant constructs were transfected into R1-11 cells and after 48 h, transfected cells were assayed for hPCFT protein levels in crude membranes by SDS/PAGE and Western blotting (Figure 3.2A and B, lower panels) and for transport at pH 5.5 with [^{3}H]MTX (0.5μM) (Figure 3.2A and B, upper panels). Most of the cysteine-insertion mutants preserved substantial transport activity and only G123C, V130C, E232C and T233C were functionally inert (<2- fold increased over R1-11 cells; noted with asterisks in Figures 3.2A-B) ($p < 0.05$).

The active cysteine mutants in TMDs 3 and 6 were cross-linked with MTS-6-MTS cross-linker and analysed on Western blots. Cys229-hPCFT formed cross-links, as reflected in slowly

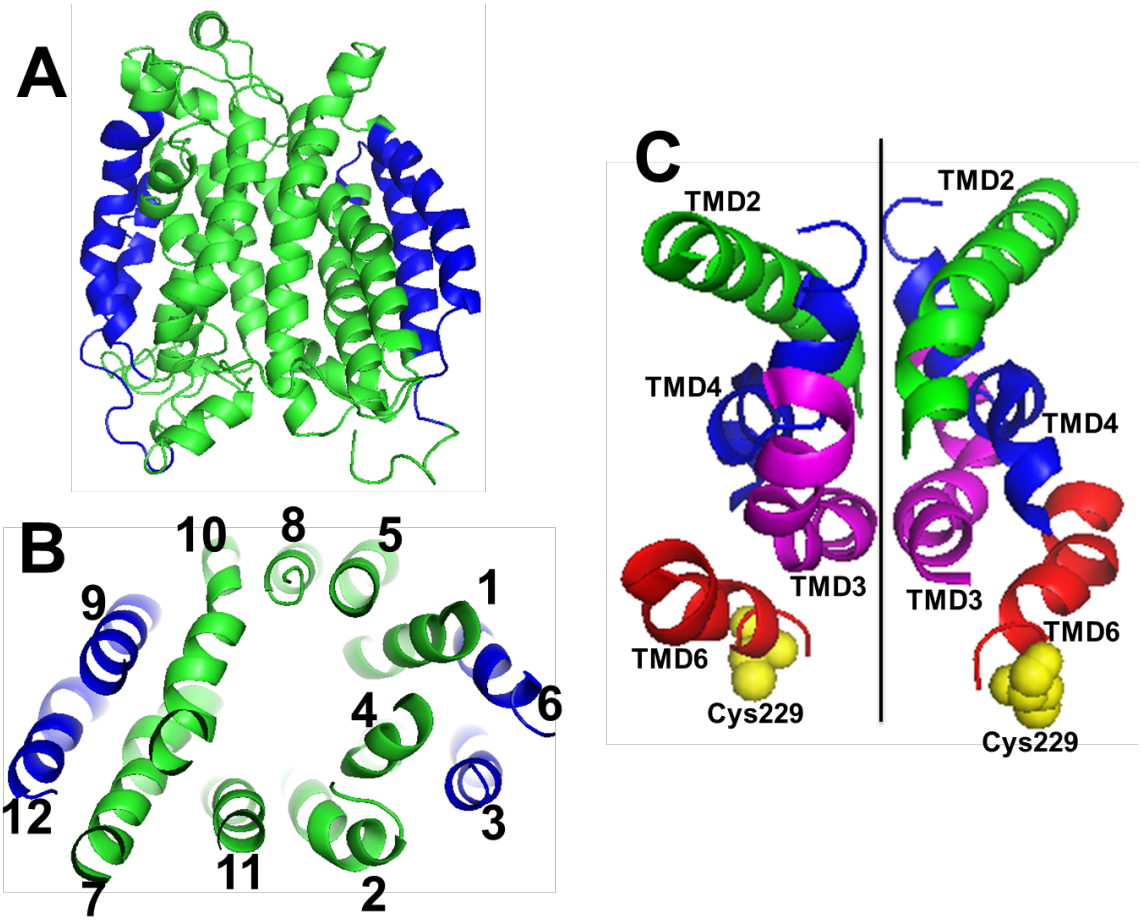

Figure 3.1 3D homology models for hPCFT. *Panels A and B,* Using Robetta as a modelling platform with GlpT as template (Huang et al., 2003) and based on experimental results and bibliographic data mining, we generated a 3D homology model for monomeric hPCFT in which TMDs 1, 2, 4, 5, 7, 8, 10 and 11 comprise an aqueous transmembrane pathway, flanked by TMDs 3, 6, 9 and 12. *Panel C,* A molecular model for dimeric hPCFT, predicted with MDOCK (Pierce et al., 2014) and based on experimental data in the present study, as described in the text. The model predicts that TMDs 2, 3, 4 and 6 in hPCFT form critical structural interfaces between hPCFT monomers. Modeling peroformed by Zhanjun Hou and Jun Ye. Figure previously published in Wilson et. al. Biochem J. 2015.

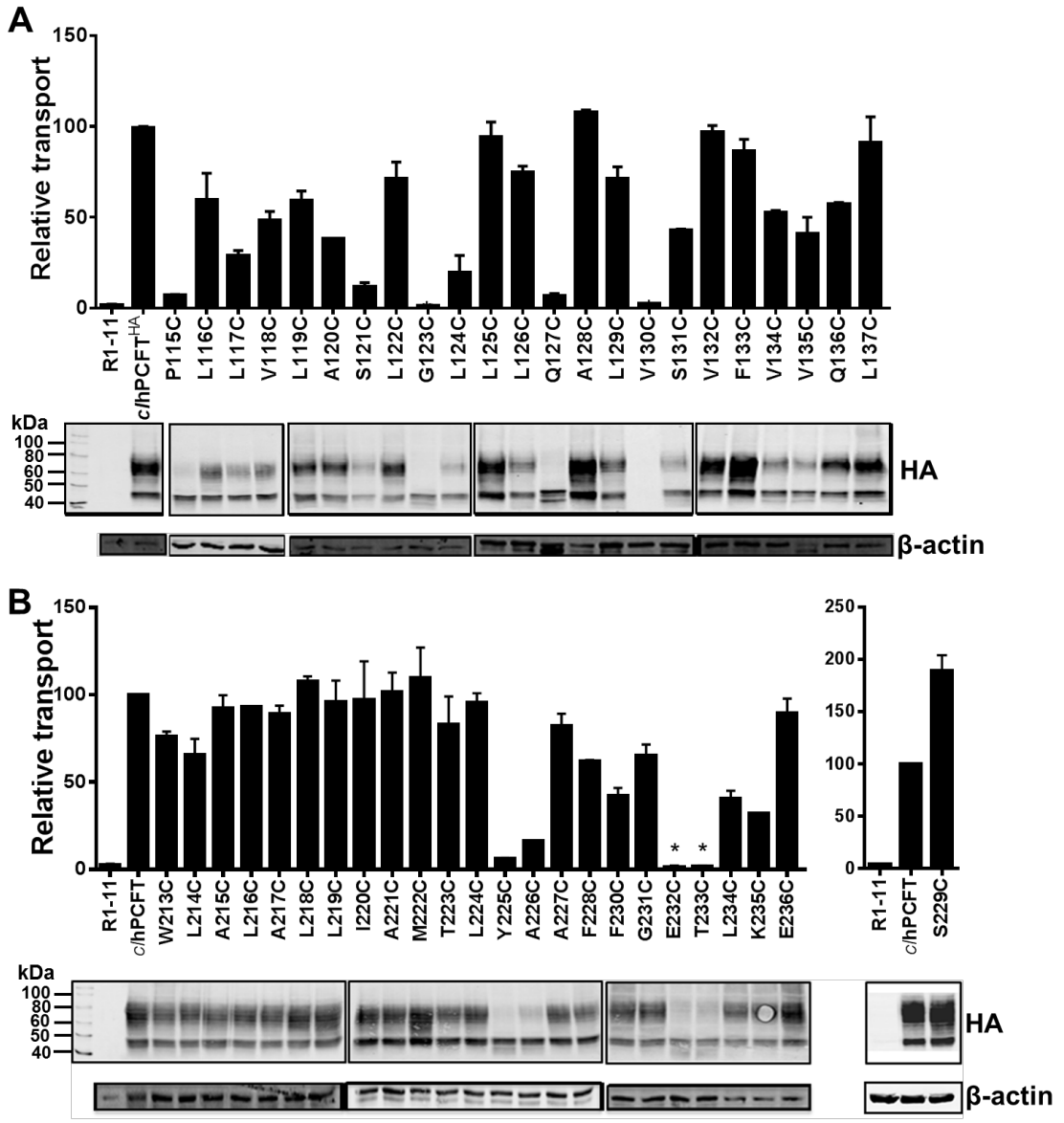

Figure 3.2 Cysteine scanning of TMD3 and TMD6 mutants in cysteine-less hPCFT^{HA}. *Panels A and B,* To characterize the transport function and protein expression of single-cysteine mutants of hPCFT, single-cysteine mutants of TMD3 (*Panel A*) and TMD6 (*Panel B*) were transiently transfected into hPCFT-null R1-11 cells. Transfected cells were assayed for transport at pH 5.5 with [^{3}H]MTX (0.5 μM) for 2 min at 37° C. hPCFT protein expression was measured in crude membranes by SDS/PAGE and Western blotting with HA-specific antibodies. β-Actin was used as a loading control. The molecular mass markers for SDS/PAGE are noted. Transport results are expressed relative to those for *cl*hPCFTHA and are reported as mean values ± standard errors from two independent experiments. Figure previously published in Wilson et. al. Biochem J. 2015.

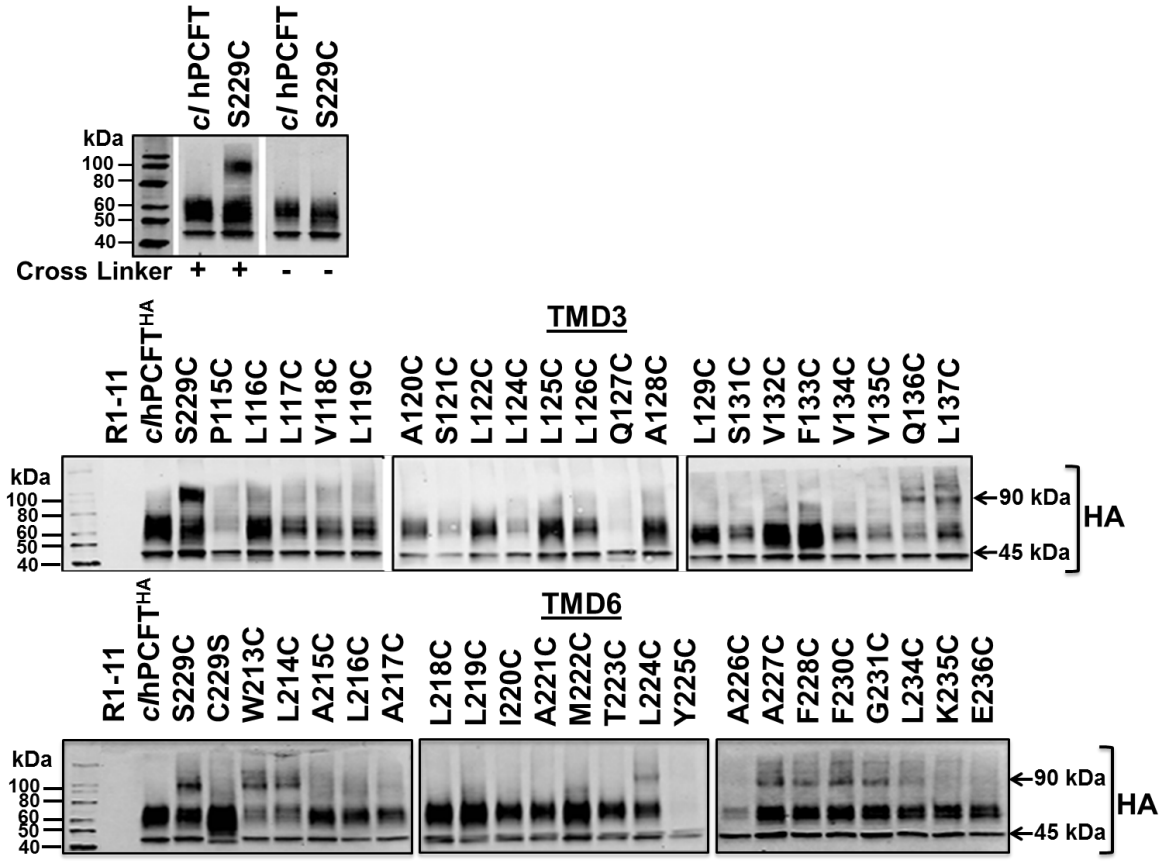

Figure 3.3 MTS-6-MTS cross-linking of TMD3 and TMD6 cysteine-insertion mutants in cysteine-less hPCFT^{HA}. Single cysteine mutants (HA-tagged) of TMD6 (from positions 213–236) and TMD3 (from positions 115–137) in a *cl*hPCFTHA background were transiently transfected into R1-11 cells and 48 h later cells were treated with the MTS-6-MTS cross-linker (0.3 mM for 1 h on ice). *cl*hPCFTHA and S229C hPCFTHA with and without cross-linker treatment were included as controls. Cells were harvested and membrane proteins were analysed on Westerns with anti-HA antibody. The hPCFT monomer migrates at ~45 kDa and cross-linked hPCFT migrates at ~90 kDa. The molecular mass markers for SDS/PAGE are noted. Figure previously published in Wilson et. al. Biochem J. 2015.

migrating high molecular mass (~90 kDa) hPCFT species not seen with *cl*hPCFTHA or non-cross-linked S229C (Figure 3.3, upper panel). Distinct cross-linked species were also formed for the Q136C and L137C mutants in TMD3 (Figure 3.3, middle panel) and for the W213C, L214C, L224C, A227C, F228C, F230C and G231C hPCFT mutants in TMD6 (Figure 3.3, lower panel). Again, no similar higher molecular mass species were detected in the absence of cross-linker (Figures 3.2A-B, lower panels).

These results establish the proximities between vicinal residues localized in the exofacial end of TMD3 and in the exofacial and cytosolic ends of TMD6, consistent with the notion that these stretches of amino acids form structural interfaces between hPCFT monomers, as suggested by the molecular model in Figure 3.1C.

3.4 Discussion

hPCFT forms homo-oligomers that are functionally important (Hou et al., 2012). In this chapter, we systematically interrogated potential structural determinants of hPCFT monomer associations in the formation of hPCFT oligomers. Previously published cross-linking results implied an important role for TMD6 in forming a critical interface between hPCFT monomers (Zhao et al., 2012).

Our cross-linking results implicated TMDs 3 and 6 as forming critical monomer interfaces in homo-oligomeric hPCFT since homobifunctional cross-linking of cysteine-insertion mutants across these stretches established the proximities between these individual TMDs. These results directly support molecular modelling results which predict that TMDs 2, 3, 4 and 6 form critical interfaces between hPCFT monomers. Based on these results, additional experiments are warranted to further define the minimal determinants for hPCFT oligomerization.

CHAPTER 4- FUNCTIONAL AND MECHANISTIC ROLES OF THE PROTON-COUPLED FOLATE TRANSPORTER TRANSMEMBRANE DOMAIN 6-7 LINKER

4.1 Introduction

PCFT contains a large loop domain connecting TMDs 6 and 7 (see Figure 1.4), which includes a stretch of 30 mostly non-conserved amino acids (positions 236-265) with the exception of a conserved stretch of amino acids (RLFXXRH) from positions 241-247, Leu254 and Arg264 (Figure 4.1). His247 was previously implicated as functionally important, as amino acid substitutions (Ala, Arg, Gln, or Glu) at this position were associated with decreased transport rates (decreased V_{max}) and increased substrate binding affinities (decreased K_t) compared to wild-type hPCFT (Unal et al., 2009a). By molecular modeling, His247 was predicted to reside at the cytoplasmic end of a solute pathway with hydrogen bonding to Ser172 where it restricts substrate access to the folate binding pocket (Unal et al., 2009a).

In this chapter, we systematically explore the functional and mechanistic importance of the hPCFT TMD6-7 connecting loop by site-directed, deletion, and insertion mutagenesis. Our findings suggest that the PCFT TMD6-7 connecting loop may serve a unique functional role by potentially restricting substrate access to the folate translocation pathway in a manner that depends principally on secondary structure rather than individual sequence elements. The work described in this chapter was previously published in *Biochemical Journal* (Wilson et al., 2016a).

4.2 Materials and Methods

4.2.1 Reagents

[3',5',7-^{3}H]MTX (20 Ci/mmol) was purchased from Moravek Biochemicals (Brea, CA). Unlabeled MTX was obtained from the Drug Development Branch, NCI, National Institutes of Health (Bethesda, MD). Folic acid, leucovorin (LCV) [(6R,S)5-formyl tetrahydrofolate] and FBS

were purchased from Sigma Chemical Co. (St. Louis, MO). Other tissue culture supplies were purchased from various vendors.

4.2.2 hPCFT Mutagenesis.

Wild-type hPCFT constructs with various epitope tags, including *wt*hPCFT^{HA} and *wt*^{FLAG}hPCFT$^{Myc\text{-}His10}$, and *cl*hPCFT^{HA} were previously described and used as templates for site-directed, deletion, and insertion mutagenesis (Hou et al., 2012) (see Chapter 2). Mutations were generated with the QuikChange^{TM} Site-Directed Mutagenesis Kit (Agilent, Santa Clara, CA). (i) Twenty-nine individual alanine insertions from positions 236 to 266 were introduced using *wt*hPCFT^{HA} in the pCDNA3 vector as a template. (ii) Eleven Cys residues were introduced from positions 241-251 using *cl*hPCFT^{HA} in pCDNA3 as a template. (iii) Additional mutants of His247 and His248, including amino acid replacements (Ala, Arg, Gln, Glu) or deletions [ΔH247 (deletion of His247), ΔH247/ΔH248 (deletions of both His247 and His248), and ΔH247/H248A (His247 deletion, Ala248 replacement)], were generated using *wt*hPCFT^{HA} as a template. (iv) *wt*hPCFT^{HA} was used as a template for PCR to remove the TMD6-7 loop including amino acids 236 to 265, generating *dl*hPCFT^{HA}. With *dl*hPCFT^{HA} as a template, we reintroduced 30 amino acids (positions 236 to 265) from hPCFT (designated *pp*hPCFT^{HA}; as a control) or from SLC19A2 (ThTr1; positions 250 to 279) (designated *tt*hPCFT^{HA}), or we replaced hPCFT sequence in 15 amino acid segments (positions 236 to 250 or positions 251 to 265) with ThTr1 sequence (positions 250 to 264 or positions 265 to 279, respectively, from ThTr1), generating *tp*hPCFT^{HA} and *pt*hPCFT^{HA}, respectively. (v) Additional mutagenesis generated several new replacements at position 247 (Glu, Arg, Ala, His) or position 247 deletions, using *tp*hPCFT^{HA}, *pt*hPCFT^{HA}, and *tt*hPCFT^{HA} as templates.

To generate the hPCFT-TMD1-6^{HA} half-molecule construct, we used PCR to introduce a HA tag, followed by a stop codon after amino acid 251 of *wt*hPCFT^{HA} in pcDNA3. To create ^{FLAG}hPCFT-TMD7-12$^{Myc\text{-}His10}$, we introduced EcoR1 cleavage sites following amino acids 24 and 249 in full length *wt*^{FLAG}hPCFT$^{Myc\text{-}His10}$ by PCR. The mutant construct was digested with EcoR1 (New England Biolabs; Ipswich, MA) and the linearized fragment was gel-purified from a 1% agarose gel with a QIAquick Gel Extraction Kit (Qiagen, Hilden, Germany). The fragment was religated (Promega, Fitchburg, WI) to reassemble ^{FLAG}hPCFT-TMD7-12$^{Myc\text{-}His10}$ in pCDNA3, which contained a FLAG epitope following Met1, followed by amino acids 2-24 and 252-459 from wild-type hPCFT sequence. We used additional mutagenesis to remove the TMD6-7 loop residues from the PCFT half-molecules, generating hPCFT-TMD1-6^{HA}236-251Δ (residues 1-235) and ^{FLAG}hPCFT-TMD7-12$^{Myc\text{-}His10}$252-265Δ (residues 1-24 and 266-459).

In all cases, mutagenesis primers were designed with the QuikChange^{TM} Primer Design program and are available upon request. PCR conditions were 95° C for 30 s, 55° C for 1 min, and 68° C for 8 min for 16 cycles. All hPCFT mutant constructs were confirmed by DNA sequencing (Genewiz, Inc., South Plainfield, NJ).

4.2.3 Cell Culture

The human RFC and hPCFT-null R1-11 HeLa cell line was a gift from Dr. I. David Goldman (Bronx, NY) (Zhao et al., 2008). R1-11 cells were grown in RPMI 1640 media supplemented with 10% FBS, 2 mM *L*-glutamine, 100 units/ml penicillin/100 μg/ml streptomycin, and 600 μg/ml G418 and 500 nM MTX. For transfections with the hPCFT constructs, R1-11 cells were seeded in DMEM) supplemented with 10% FBS in 60 mm culture dishes at a density of 0.8 million cells per dish. After 24 hours, R1-11 cells were transiently transfected with hPCFT constructs (in pCDNA3) (above) at 1 μg DNA/plate using

Lipofectamine 2000 (10 μL/plate) in Opti-MEM, per the manufacturer's instructions (Life Technologies, Carlsbad, CA). The transfection medium was replaced with DMEM, containing 10% FBS, 4 hours after transfection.

4.2.4 Membrane Transport

Forty-eight hours after transfection of R1-11 cells, cellular uptake of [^{3}H]MTX (0.5 μM) was measured at 37° C over 2 min. Uptake assays were performed in 60 mm dishes using MES-buffered saline (20 mM MES, 140 mM NaCl, 5 mM KCl, 2 mM $MgCl_2$, and 5 mM glucose; pH 5.5), as previously described (Hou et al., 2012). Dishes were washed three times with PBS and cells were solubilized in 0.5 N NaOH. Intracellular radioactivity was calculated in units of pmol/mg protein, based on measurements of radioactivity and protein concentrations of the alkaline cell homogenates (Lowry et al., 1951). To measure MTX transport kinetics for R1-11 cells transfected with *wt*hPCFT^{HA} and hPCFT mutant constructs, [^{3}H]MTX uptake was measured over 2 min at 37° C from 0.33 μM to 5 μM [^{3}H]MTX, and results were analyzed using Lineweaver-Burke plots to calculate K_t and V_{max} values. To determine K_i values for non-radioactive substrates (folic acid, LCV), transfected cells were incubated with 0.5 μM [^{3}H]MTX and unlabeled inhibitors from 0.3 μM to 1.5 μM, with results compared to those without inhibitors. K_i values were calculated from Dixon plots. To compare transport pH dependences for *wt*hPCFT^{HA} and hPCFT mutants, transport assays were conducted at pHs from 7.2 to 5.5. HEPES-buffered saline (20 mM HEPES, 140 mM NaCl, 5 mM KCl, 2 mM $MgCl_2$, and 5 mM glucose) was used for pHs 7.2 and 6.8, and MES-buffered saline (20 mM MES, 140 mM NaCl, 5 mM KCl, 2 mM $MgCl_2$, and 5 mM glucose) was used for pHs 6.5, 6.0, 5.8 and 5.5.

4.2.5 Surface Biotinylation with MTSEA-Biotin

Forty-eight hours after transfection of R1-11 cells with hPCFT Cys mutants in *cl*hPCFT^{HA} (above), cells were treated with MTSEA-biotin (Biotium, Hayward, CA) to biotinylate aqueous accessible Cys residues exactly as previously described (see Chapter 2).

4.2.6 Surface Protein Biotinylation with Sulfo-NHS (N-hydroxysuccinimide)-SS-Biotin

We used the Cell Surface Labeling Accessory Pack (Thermo Scientific) to biotinylate and isolate surface membrane proteins. Forty-eight hours after transfection of R1-11 cells with the hPCFT constructs, the cells were treated with 0.25 mg/ml sulfo-NHS-SS-biotin in PBS at 4° C for 30 min. The cells were treated with lysis buffer, followed by sonication and centrifugation to remove the insoluble fraction. The supernatants were incubated with immobilized NeutrAvidin^{TM} gel slurry for 1 h at room temperature, and the beads were washed five times with wash buffer. Proteins were eluted with 1× Laemmli sample buffer (Lowry et al., 1951) containing 50 mM dithiotheitol and analyzed by SDS/polyacrylamide gel electrophoresis (PAGE)/Western blotting (see below). All buffers (i.e., lysis, washing, elution) were supplemented with a protease inhibitor mixture (Roche Applied Science).

4.2.7 Western Blotting

Protocols for plasma membrane preparation, SDS-PAGE, and electrotransfer to polyvinylidene difluoride membranes (Pierce; Rockford, IL) were identical to those previously described (Hou et al., 2012; Matherly et al., 1991). For fractionation of crude membrane fractions, 10% SDS/PAGE gels were used. For fractionation of biotinylated surface membrane proteins, Novex^{TM} 4-20% Tris-Glycine mini protein gels were used. Anti-HA antibody (Covance; Princeton, NJ), anti-Myc antibody (Covance) and IRDye800-conjugated secondary antibody were used with an Odyssey Infrared Imaging System (LI-COR, Lincoln, NE) to

identify HA- and Myc-tagged hPCFT proteins. Anti-β-actin (Sigma) or anti-Na^+/K^+ ATPase (Novus Biologicals, Littleton, CO) antibodies were used to establish equal protein loading. Densitometry values were calculated using the Odyssey Infrared Imaging System and software package.

4.2.8 Confocal Microscopy

R1-11 cells were seeded in Lab-Tek II Chamber Slides (Nalge Nunc International, Naperville, IL) at a density of 6.9×10^4 cells/well. After 24 hours, cells were transfected with hPCFT constructs in pCDNA3, as described above, using 88.7 ng of DNA and 0.86 µl of Lipofectamine 2000 per sample. Forty eight hours post-transfection, cells were fixed with 3.3% paraformaldehyde (in PBS) and permeabilized with 0.1% Triton X-100 (in PBS). Chamber slides were stained with primary antibodies, followed by incubation with secondary antibodies. The primary antibodies used were goat anti-HA polyclonal antibodies (Abcam, Cambridge, MA) and mouse anti-FLAG antibody (Sigma). Fluorescent secondary antibodies included Alexa Fluor® 568 donkey anti-goat IgG (H+L) and Alexa Fluor® 488 donkey anti-mouse IgG (H+L) (Life Technologies). Slides were viewed with a Zeiss LSM-510 META NLO microscope, using a 63× water immersion lens and the same parameters for all samples. Confocal microscopy was performed in the Microscopy, Imaging, and Cytometry Resources Core at Wayne State University School of Medicine.

4.2.9 Molecular Modeling

We used the crystal structures of members of MFS transporters GlpT (1PW4; for *pp*hPCFT) (Huang et al., 2003) and YajR (3WDO; for *pt*, *tp* and *tt*hPCFT) (Jiang et al., 2013) as templates for homology modeling of hPCFT monomers containing varied 6-7 loop sequence replacements with Robetta Server (http://robetta.bakerlab.org). Modeling was based on the

notion that all crystal structures from members of MFS members have preserved tertiary structural elements during evolution, thus enabling published structures to extrapolate to other MFS members (Abramson et al., 2004; Lemieux, 2007; Vardy et al., 2004). The top hPCFT homology model retrieved through Robetta for each hPCFT form was superimposed by the SALIGN server (http://modbase.compbio.ucsf.edu/salign/). Structures were visualized with PyMol. The secondary structure of the 6-7 loop from each form was predicted with GOR4 (Garnier et al., 1996). This modeling was performed by Zhanjun Hou (Karmanos Cancer Institute) and Jun Ye (Chinese Academy of Sciences).

4.2.10 Statistical Analysis

GraphPad v.6.0 software was used for plotting and data analysis including descriptive statistics.

4.3 Results

4.3.1 Homology Analysis and Cysteine Accessibilities of Positions 241-251 in the hPCFT TMD6-7 Loop Region

Based on computer-predicted hydropathy models (Matherly et al., 2014; Zhao et al., 2010), hPCFT contains twelve TMDs with cytosolic-oriented C- and N- termini and segments comprised of TMDs 1-6 and TMDs 7-12, connected by a long *cytosolic*-facing loop domain (30 amino acids) between TMDs 6 and 7 (positions 236-265) (Figure 1.4). Portions of this topology structure have been confirmed experimentally (Zhao et al., 2010) (also see Chapter 2). We compared the amino acid sequences across the TMD6-7 loop in PCFTs from five species from *Xenopus* to humans. Of the 30 amino acids, seven residues were completely conserved among all five species, including Arg241, Leu242, Phe243, Arg246, His247, Leu254, and Arg264 (numbering corresponds to hPCFT; Figure 4.1). His247 was previously implicated from site-

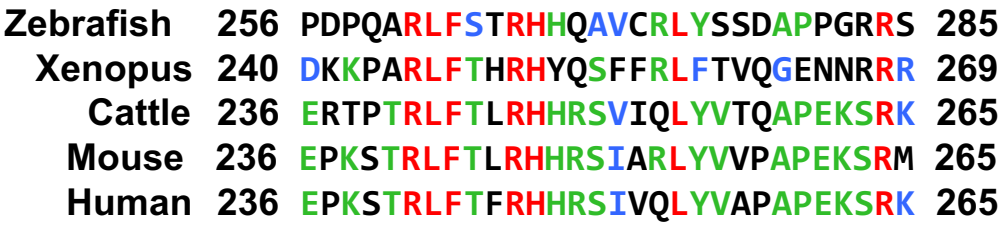

Figure 4.1 Sequence alignment of the PCFT TMD6-7 connecting loop across five species including zebrafish, xenopus, cattle, mouse, and human. The color codes are as follows: red, residues are conserved across all species; green, residues are conserved across three or four species; blue, residues are similar across species; and black, residues are not similar. Figure previously published in Wilson et. al. Biochem J. 2016.

directed mutagenesis and molecular homology modeling to be important in hPCFT transport by virtue of its location at the putative cytoplasmic opening to the membrane translocation pathway (Unal et al., 2009a).

Previous studies used SCAM and MTSEA-biotin reactivity with Cys insertions at Thr240 and Glu261 in the TMD6-7 loop of *cl*hPCFT^{HA} to establish the likely cytosolic orientations at these positions (Zhao et al., 2010). To further establish the aqueous accessibilities (i.e., membrane topology) of amino acids comprising the TMD6-7 loop, particularly the *conserved stretch from positions 241 to 247*, we generated 11 Cys replacements from positions 241-251, using *cl*hPCFT^{HA} as a template for site-directed mutagenesis. As we previously reported, *cl*hPCFT^{HA} exhibits functional characteristics virtually identical to those for *wt*hPCFT^{HA} (see Chapter 2). The Cys mutant constructs were transfected into hPCFT-null R1-11 cells and were assayed for [^{3}H]MTX transport at pH 5.5 and 37^{o}C (Figure 4.2A) and for hPCFT protein expression on Western blots (Figures 4.2B-C). Results were compared to those for *cl*hPCFT^{HA} transfected cells and for untransfected R1-11 cells. We found that all hPCFT Cys mutants were expressed in crude membrane fractions (as broadly banding glycosylated proteins on 10% gels) (~21% to ~54% of *cl*hPCFT^{HA} levels by densitometry; Figure 4.2B) and that most mutants were active for [^{3}H]MTX transport [~55%-100% of *cl*hPCFT^{HA} transport (Figure 4.2A); all uptakes were significantly greater than for R1-11 cells], although activities for two Cys mutants, L242C and H247C, were notably decreased (18.3% and 12.4%, respectively, of *cl*hPCFT^{HA} uptake; $p < 0.0002$). These decreases were accompanied by reduced surface protein expression relative to *cl*hPCFT (28% for L242C, 29% for H247C) (Figure 4.2C).

To establish aqueous accessibilities, we treated the 11 Cys mutants with membrane impermeable MTSEA-biotin, using G207C in the TMD5-6 external loop and S110C in the

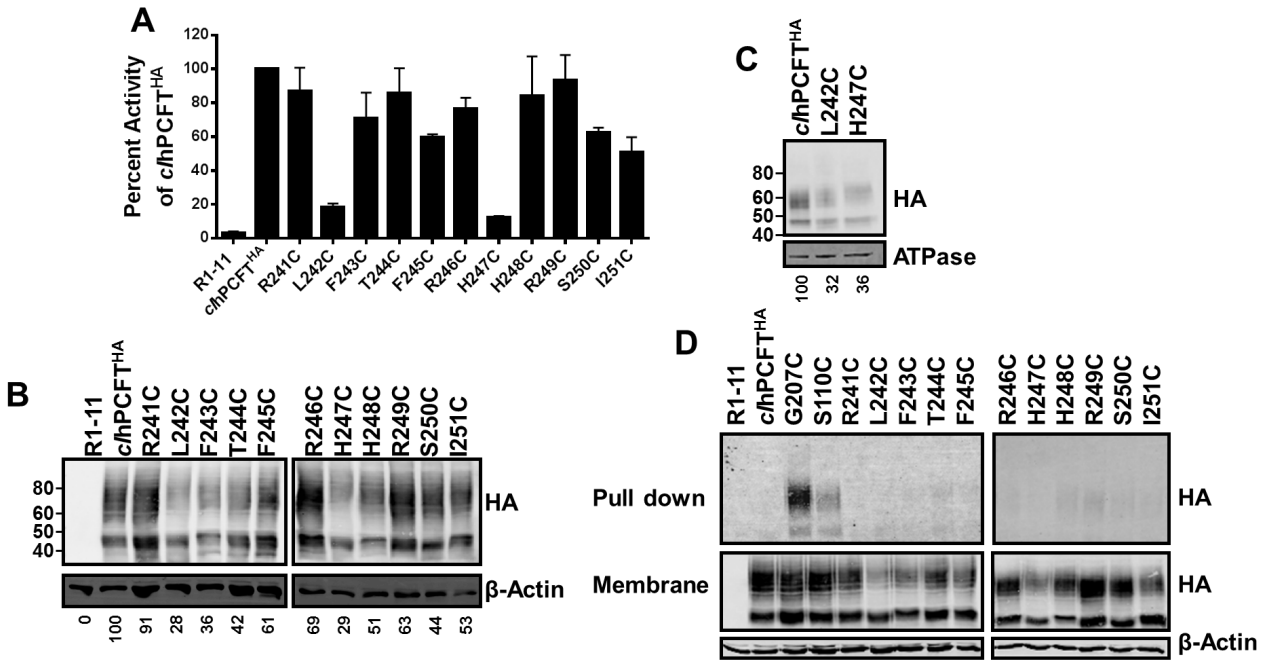

Figure 4.2 Scanning Cys-insertion mutagenesis for positions 241-251 in the TMD6-7 connecting loop. *Panel A*, hPCFT single-Cys mutants from positions 241-251 in a *cl*hPCFT^{HA} background were transiently transfected into hPCFT-null R1-11 cells. Transport activity was measured after 48 h with [^{3}H]MTX (0.5 μM) over 2 min at pH 5.5 and at 37^{o}C. Results expressed as a percentage of *cl*hPCFT^{HA} activity and reported as mean values ± S.E. (error bars) from triplicate experiments. All single-Cys mutants were significantly more active than the non-transfected R1-11 control ($p<0.05$). *Panel B*, Western blots are shown for membrane proteins (10 μg) from HA-tagged hPCFT Cys mutants, compared *cl*hPCFT^{HA} transfected and untransfected R1-11 cells. Densitometry (as relative percentages, noted below each lane) is representative of duplicate experiments and was normalized to β-actin expression. Migrations of molecular mass standard proteins (in kDa) are shown. *Panel C*, HA-tagged hPCFT surface membrane proteins (40 μg) were labeled with sulfo-NHS-SS-biotin (0.25 mg/ml) and isolated on immobilized NeutrAvidin^{TM} gel. Biotinylated proteins were analyzed by SDS/PAGE and Western blotting. Relative densitometry is representative of duplicate experiments and is normalized to Na^+/K^+ ATPase expression. Migrations of molecular mass standard proteins (in kDa) are shown. *Panel D*, Substituted Cys accessibility analysis for positions 241-251 in the TMD6-7 connecting loop. TMD6-7 loop single-Cys mutants were transiently transfected into R1-11 cells. Cells were treated with MTSEA-biotin (0.2 mg/mL) 48 h later. After 30 min, cells were harvested, and membranes prepared, solubilized and incubated with streptavidin beads in order to pull-down biotinylated proteins. Biotinylated proteins were eluted and analyzed by Western blotting using an anti-HA antibody (labeled "Pull-down"). A 25 μl aliquot of the crude membrane fraction prior to exposure to streptavidin beads was also analyzed by Western blotting as a control (labeled "Membrane"). The S110C and G207C mutants (located in the 1st intracellular (reentrant) loop and 3rd extracellular loop, respectively) were used as positive controls and *cl*hPCFT^{HA} was a negative control. Figure previously published in Wilson et. al. Biochem J. 2016.

TMD2-3 reentrant loop as positive controls (see Chapter 2). Following MTSEA-biotin treatments, biotinylated proteins were "pulled down" with streptavidin beads and analyzed on Western blots with HA-specific antibody. Whereas G207C and S110C were biotinylated, *none* of the 11 Cys mutants from positions 241-251 were biotinylated (Figure 4.2D). These results suggest that residues in the TMD6-7 loop are not accessible to the extracellular aqueous milieu, and that the TMD6-7 loop does indeed have a cytosolic orientation, as predicted by the hPCFT hydropathy model (Matherly et al., 2014), analogous to other MFS proteins such as RFC (Liu and Matherly, 2002).

4.3.2 Scanning Alanine Mutagenesis Across the hPCFT TMD6-7 Loop Region

To explore the functional importance of the TMD6-7 loop region in hPCFT membrane transport, we used scanning alanine mutagenesis with *wt*hPCFT^{HA} in pCDNA3 to generate alanine replacement mutants from positions 236 to 266 (positions 257 and 259 are already alanines). Each of the 29 alanine mutant constructs was transfected into R1-11 Hela cells, and after 48 hours the transfectants were assayed for [^{3}H]MTX transport (Figure 4.3A), and for hPCFT membrane protein expression (Figure 4.3B), compared to *wt*hPCFT^{HA}. All of the hPCFT mutants were expressed, although there were some variations (measured by densitometry), ranging from ~28% (for S250A) to ~128% (for P260A) of the *wt*hPCFT^{HA} level. Twenty-six of the alanine mutants showed high levels of transport (~60-110% of *wt*hPCFT^{HA}). Although three mutants (H247A, S250A, I251A) were notably less active (13%, 15%, and 13%, respectively, of *wt*hPCFT^{HA}; $p < 0.0001$), they were nonetheless significantly more active than the non-transfected negative control (R1-11; $p < 0.01$) (Figure 4.3A). In each case, loss of transport activity and hPCFT expression in crude membranes was related to loss in surface membrane

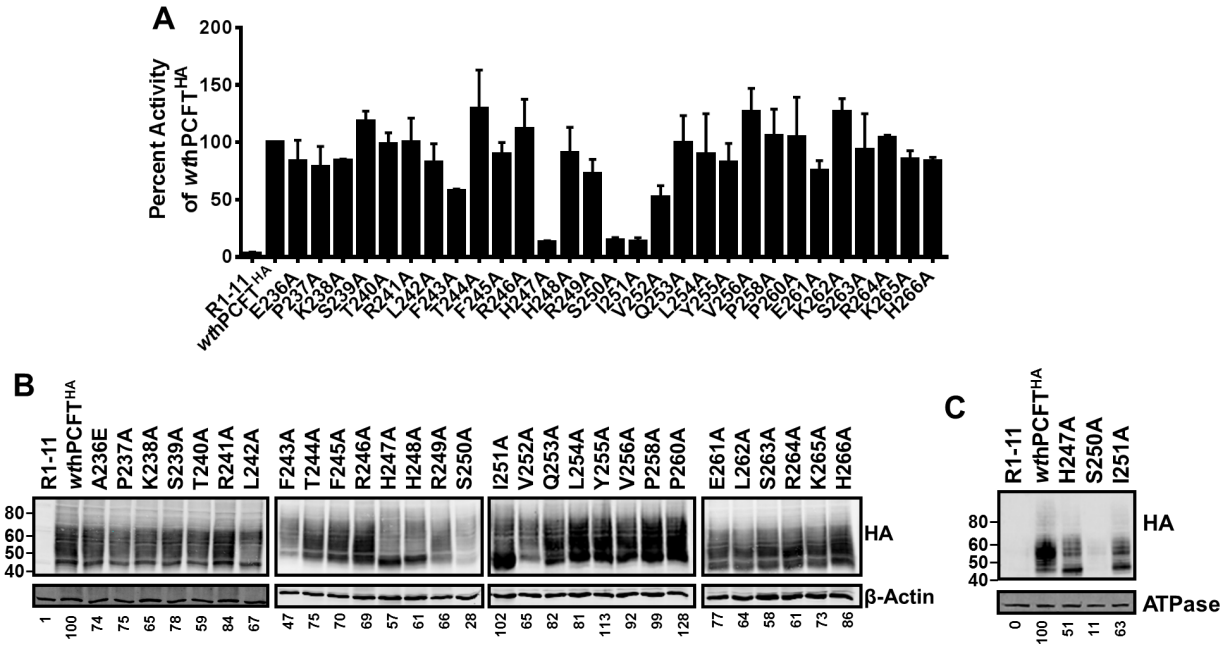

Figure 4.3 Alanine-scanning mutagenesis of residues 236-266 in the TMD6-7connecting loop. *Panel A*, Alanine mutants were generated in *wt*hPCFT^{HA} from positions 236-266 spanning the TMD6-7 connecting loop and transfected into hPCFT-null R1-11 cells. Transport activity was measured after 48 h with [^{3}H]MTX over 2 min at pH 5.5 and at 37^{o}C. Results are expressed as a percentage of *wt*hPCFT^{HA} activity and are reported as mean values ± standard errors (error bars) from triplicate experiments. All the alanine mutants were significantly more active than the non-transfected control, R1-11 ($p<0.05$). *Panel B*, Western blots are shown for membrane proteins (10 μg) from HA-tagged hPCFT alanine mutants. Densitometry (as relative percentages, noted below each lane) is representative of duplicate experiments and was normalized to β-actin expression. Migrations of molecular mass standard proteins (in kDa) are shown. *Panel C*, HA-tagged hPCFT surface membrane proteins (40 μg) were labeled with sulfo-NHS-SS-biotin (0.25 mg/ml) and isolated on immobilized NeutrAvidin^{TM} gel. Biotinylated proteins were analyzed by SDS/PAGE and Western blotting. Relative densitometry is representative of duplicate experiments and is normalized to Na^+/K^+ ATPase expression. Migrations of molecular mass standard proteins (in kDa) are shown. Figure previously published in Wilson et. al. Biochem J. 2016.

expression (Figure 4.3C; relative surface expression by densitometry of 51% for H247A, 11% for S250A, and 63% for I251A, compared to the *wt*hPCFT level).

Taken with the results of the Cys-scanning mutagenesis (Figure 4.2), these results imply that most of the residues comprising the hPCFT TMD6-7 loop region are *not essential* for transport. When comparing results for Cys and alanine substitutions across the TMD6-7 loop, His247 in the conserved RLFXXRH motif (positions 241-247; Figure 4.1) was the *only* amino acid for which its replacement consistently caused a significant loss of transport activity.

4.3.3 Co-expression of hPCFT TMD1-6 and TMD7-12 Half-Molecules

To further investigate the functional and structural roles of the hPCFT TMD6-7 connecting loop, we generated hPCFT "half-molecule" constructs. These include hPCFT-TMD1-6^{HA}, comprised of amino acids 1-251 (TMDs 1-6) with a C-terminal HA epitope, and ^{FLAG}hPCFT-TMD7-$12^{Myc\text{-}His10}$, comprised of amino acids 252-459 (TMDs 7-12) and an N-terminal FLAG epitope just after Met1, followed by 23 N-terminal amino acids (residues 2-24) and a C-terminal Myc-His_{10} (see schematic in Figure 4.4A).

The hPCFT half-molecule constructs were expressed in R1-11 HeLa cells both individually and together, which were then assayed for restoration of [^{3}H]MTX transport and protein expression. Results were compared to those for *wt*hPCFT^{HA} and *wt*^{FLAG}hPCFT$^{Myc\text{-}His10}$ transfectants, and for untransfected R1-11 cells. When transfected separately, individual half-molecules were detected on Westerns (Figure 4.4D) but were unable to restore transport activity above the low residual level in R1-11 cells (Figure 4.4B). The HA signal on the Westerns for hPCFT-TMD1-6^{HA} was notably decreased (48%) compared to that for *wt*hPCFT^{HA} (Figure 4.4D, left panel); the Myc signal for ^{FLAG}hPCFT-TMD7-$12^{Myc\text{-}His10}$ was ~12% compared to *wt*^{FLAG}hPCFT$^{Myc\text{-}His10}$ (Figure 4.4D, right panel). Cotransfection of hPCFT-TMD1-6^{HA} with

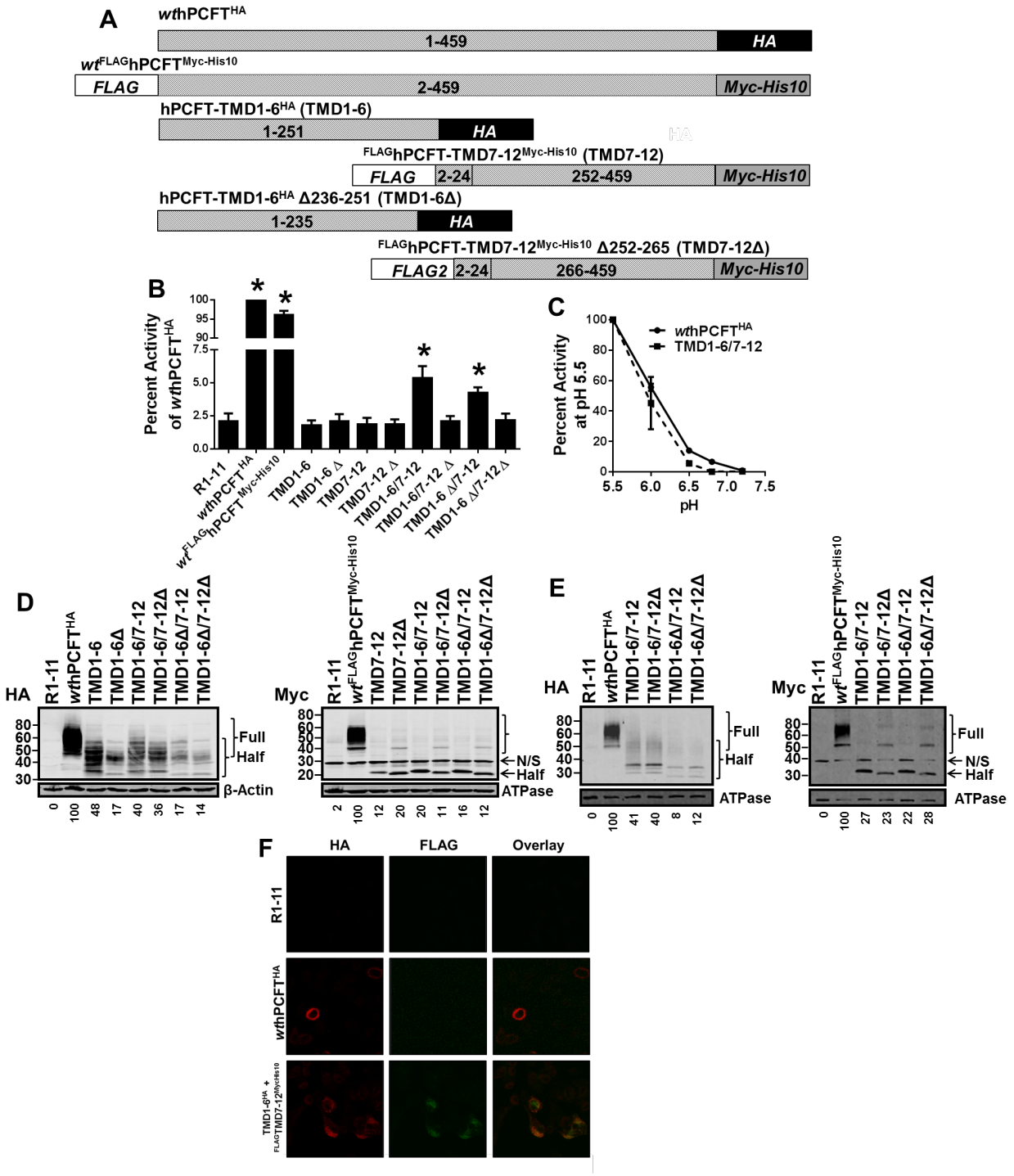

Figure 4.4 Expression of TMD1-6 and TMD7-12 hPCFT half-molecules. *Panel A*, A schematic is shown of all half-molecule constructs/proteins. *Panel B*, Half-molecule constructs were transiently transfected into R1-11 cells both individually and together. Transport activity was measured after 48 h by [^{3}H]MTX uptake assays over 2 min at pH 5.5 and at 37^{o}C. Results are expressed as a percentage of *wt*hPCFT^{HA} activity and are reported as mean values ± standard errors (error bars) from triplicate experiments. Transport by the individual hPCFT-TMD1-6^{HA}

and ^{FLAG}hPCFT-TMD7-12$^{Myc\text{-}His10}$ transfectants was not significantly greater than for negative control R1-11 cells ($p > 0.05$). However, when transfected together, hPCFT-TMD1-6^{HA} and ^{FLAG}hPCFT-TMD7-12$^{Myc\text{-}His10}$ showed significantly increased transport activity, exceeding that for R1-11 cells. hPCFT-TMD1-6^{HA}/ ^{FLAG}hPCFT-TMD7-12$^{Myc\text{-}His10}$Δ252-265 cotransfection also restored transport activity over R1-11 cells ($p < 0.05$) which was not statistically different from that for the hPCFT-TMD1-6^{HA}/^{FLAG}hPCFT-TMD7-12$^{Myc\text{-}His10}$ cotransfected cells ($p > 0.05$) (* indicates an increased level of transport over R1-11; $p < 0.05$). *Panel C*, [^{3}H]MTX transport activity of *wt*hPCFT^{HA} and hPCFT-TMD1-6^{HA}/^{FLAG}hPCFT-TMD7-12$^{Myc\text{-}His10}$ transfectants at pHs from 5.5 to 7.2 is shown. Uptake for each transfectant (*wt*hPCFT^{HA} and hPCFT-TMD1-6^{HA}/ ^{FLAG}hPCFT-TMD7-12$^{Myc\text{-}His10}$) was normalized to its own uptake at pH 5.5. *Panel D*, Western blots are shown for membrane proteins (10 μg) from HA-tagged or Myc-tagged hPCFT half-molecules. Densitometry (as relative percentages, noted below each lane) is representative of duplicate experiments and was normalized to β-actin. Migrations of molecular mass standard proteins (in kDa) are shown. *Panel E*, HA- and Myc-tagged hPCFT surface membrane proteins (40 μg) were labeled with sulfo-NHS-SS-biotin (0.25 mg/ml) and isolated on immobilized NeutrAvidin^{TM} gel. Proteins were analyzed by SDS/PAGE and Western blotting. Relative densitometry (as relative percentages, noted below each lane) is representative of duplicate experiments and was normalized to Na^+/K^+ ATPase expression. Migrations of molecular mass standard proteins (in kDa) are shown. *Panel F*, Confocal microscopy of hPCFT TMD1-6 and TMD7-12 half-molecules. Results are shown for HeLa R1-11 cells transfected with *wt*hPCFT^{HA} or co-transfected with hPCFT-TMD1-6^{HA} and ^{FLAG}hPCFT-TMD7-12$^{Myc\text{-}His10}$ constructs. Transfected cells were fixed with 3.3% paraformaldehyde, permeabilized with 0.1% Triton X-100, and stained with Alexa Fluor® 488-conjugated (for FLAG-tagged PCFT; *green*) or Alexa Fluor® 568-conjugated (for HA-tagged hPCFT; *red*) secondary antibodies. Images were obtained using a Zeiss LSM-510 META NLO using a 63x water immersion lens. Staining is shown for the individual fluors and as a merged image. Figure previously published in Wilson et. al. Biochem J. 2016.

^{FLAG}hPCFT-TMD7-12$^{Myc-His10}$ resulted in an increased level of ^{FLAG}hPCFT-TMD7-12$^{Myc-His10}$ over the individual transfectant, accompanying a modest restoration of transport activity (5.3% of *wt*hPCFT^{HA}) that was significantly higher than for the non-transfected R1-11 cells ($p < 0.05$) (Figure 4.4B). By confocal microscopy, hPCFT-TMD1-6^{HA} and ^{FLAG}hPCFT-TMD7-12$^{Myc-His10}$ were co-expressed and at least a portion co-localized to the cell surface, although significant intracellular fluorescence for both hPCFT-TMD1-6^{HA} and ^{FLAG}hPCFT-TMD7-12$^{Myc-His10}$ was detected (Figure 4.4F). Surface expression of co-expressed hPCFT-TMD1-6^{HA} and ^{FLAG}hPCFT-TMD7-12$^{Myc-His10}$ was confirmed by surface biotinylation (Figure 4.4E). Transport activity for the hPCFT-TMD1-6^{HA} and ^{FLAG}hPCFT-TMD7-12$^{Myc-His10}$ co-transfected cells showed the characteristic pH dependence for PCFT transport that was essentially identical to that for *wt*hPCFT^{HA} (Figure 4.4C).

Since hPCFT-TMD1-6^{HA} and ^{FLAG}hPCFT-TMD7-12$^{Myc-His10}$ included TMD6-7 loop sequence (residues 236-251 and 252-265, respectively), we created and expressed two variant half-molecule constructs in which segments of the TMD6-7 loop were deleted. These constructs are hPCFT-TMD1-6Δ236-251^{HA} (TMD1-6Δ), comprised of PCFT amino acids 1-235, and ^{FLAG}hPCFT-TMD7-12Δ252-265$^{Myc-His10}$ (TMD7-12Δ), comprised of PCFT amino acids 1-24 and 266-459 (Figure 4.4A). Low levels of hPCFT-TMD1-6Δ236-251^{HA} and ^{FLAG}hPCFT-TMD7-12Δ252-265$^{Myc-His10}$ were detected on Westerns when transfected both singly and in combination (Figure 4.4D). Surface biotinylation confirmed surface expression of the co-expressed half-molecules (Figure 4.4E), paralleling patterns seen in crude membrane fractions (Figure 4.4D). Deletion of the residual loop sequence from *both* half-molecule constructs (hPCFT-TMD1-6Δ236-251^{HA} and ^{FLAG}hPCFT-TMD7-12Δ252-265$^{Myc-His10}$) abolished the modest transport activity recorded for combined hPCFT-TMD1-6Δ236-251^{HA} with ^{FLAG}hPCFT-TMD7-12$^{Myc-His10}$

(Figure 4.4B). Whereas hPCFT-TMD1-6^{HA} (including amino acids 236-251) combined with ^{FLAG}hPCFT-TMD7-12Δ252-265$^{Myc\text{-}His10}$ failed to restore transport above that for R1-11 cells, co-transfection of hPCFT-TMD1-6Δ236-251^{HA} with ^{FLAG}hPCFT-TMD7-12$^{Myc\text{-}His10}$ (including amino acids 252-265) restored low level transport activity (4.2% of *wt*hPCFT^{HA}), greater than for R1-11 cells ($p < 0.05$) and equivalent to that for combined hPCFT-TMD1-6^{HA} and ^{FLAG}hPCFT-TMD7-12$^{Myc\text{-}His10}$.

Collectively, these results demonstrate that transport function can be partly restored by expressing hPCFT as separate TMD1-6 and TMD7-12 half-molecules and suggest that the 252-265 loop segment (but not amino acids 236-251) is essential for this restored transport activity.

4.3.4 Expression of hPCFT-ThTr1 TMD6-7 Loop Chimeric Transporters

The thiamine transporter ThTr1 (SLC19A2) is less than 20% homologous to hPCFT at the amino acid level and there is an almost complete loss of amino acid identity across the TMD6-7 loop domains for hPCFT and ThTr1 (Figure 4.5A). To further examine the primary sequence requirement for the hPCFT TMD6-7 loop (amino acids 236-265), we replaced this stretch in hPCFT with *structurally analogous but non-homologous* sequence from the TMD6-7 loop of ThTr1 (amino acids 250-279) (Figure 4.5A).

To achieve this, we first removed the nucleotide sequence encoding amino acids 236-265 from *wt*hPCFT^{HA} by PCR, generating *dl*hPCFT^{HA} (Figure 4.5A). Using *dl*hPCFT^{HA} as a template, we then reintroduced hPCFT 236-265 sequence (designated *pp*hPCFT^{HA}; as a control) or ThTr1 250-279 sequence (*tt*hPCFT^{HA}). Two additional mutant constructs were generated with *partial* (15 amino acids) TMD6-7 loop replacements. These include *pt*hPCFT^{HA}, with amino acids 236-250 from hPCFT, followed by amino acids 265-279 from ThTr1, and *tp*hPCFT^{HA}, with amino acids 250-264 from ThTr1, followed by amino acids 251-265 from hPCFT (Figure

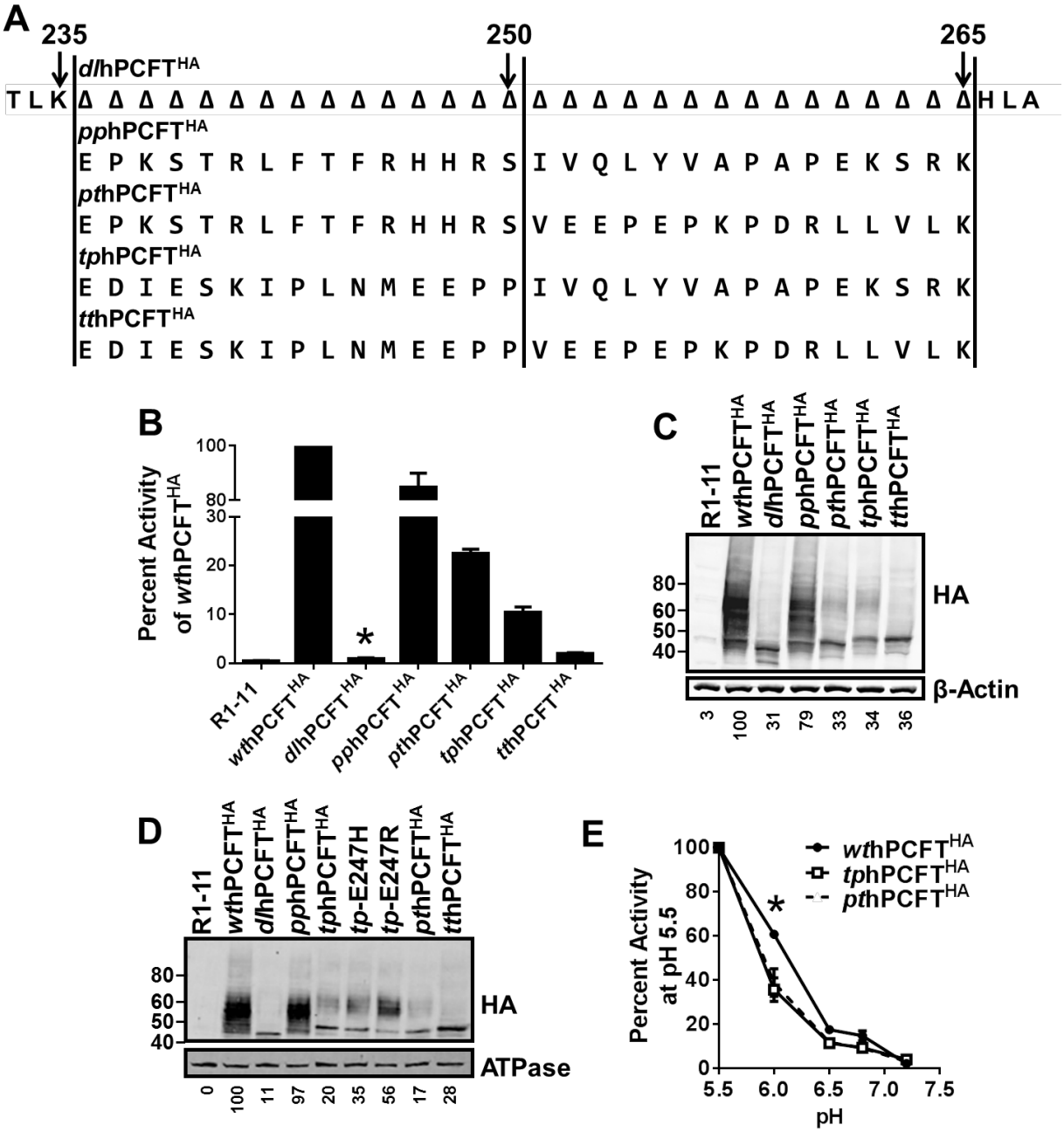

Figure 4.5 Expression of hPCFT-ThTr1 chimeric transporters with replacement of the hPCFT TMD6-7 loop with ThTr1 sequence. *Panel A*, A schematic is shown of the ThTr1 sequence replacements for *pp*hPCFT^{HA}, *pt*hPCFT^{HA}, *tp*hPCFT^{HA}, and *tt*hPCFT^{HA}. Mutants were generated first by removing amino acid residues 236-265 through PCR mutagenesis (*dl*hPCFT^{HA}) and then inserting new sequence. *pp*hPCFT^{HA} serves as a positive control and contains an exact replacement of the hPCFT residues 236-265. *tt*hPCFT^{HA} contains ThTr1 residues 250-279 in place of hPCFT residues 236-265. The TMD6-7 loop of *pt*hPCFT^{HA} contains hPCFT residues 236-250, followed by ThTr1 residues 265-279. The TMD6-7 loop of *tp*hPCFT^{HA} contains ThTr1 residues 250-264, followed by hPCFT residues 251-265. *Panels B*, hPCFT/ThTr1 chimera mutants were transiently transfected into R1-11 cells. Transport activity

was measured after 48 h by [^{3}H]MTX uptake assays over 2 min at pH 5.5 and at 37^o C. Results are expressed as a percentage of *wt*hPCFT^{HA} activity and are reported as mean values ± standard errors (error bars) from triplicate experiments. All hPCFT-ThTr1 chimera proteins were significantly more active than for the non-transfected control, R1-11. Transport for *dl*hPCFT^{HA} and *tt*hPCFT^{HA}-E247H was insignificantly different from that for R1-11 cells (* indicates that transport activity is *not* significantly different than R1-11; $p > 0.05$). *Panel C*, Western blots are shown for membrane proteins (10 μg) from HA-tagged hPCFT chimera mutants. Densitometry (as relative percentages, noted below each lane) is representative of duplicate experiments and was normalized to β-actin levels. Migrations of molecular mass standard proteins (in kDa) are shown. *Panel D*, HA-tagged hPCFT surface membrane proteins (40 μg) were labeled with sulfo-NHS-SS-biotin (0.25 mg/ml) and isolated on immobilized NeutrAvidin^{TM} gel. Biotinylated proteins were analyzed by SDS/PAGE and Western blotting. Relative densitometry (as relative percentages, noted below each lane) is representative of duplicate experiments and was normalized to Na^+/K^+ ATPase expression. Migrations of molecular mass standard proteins (in kDa) are shown. *Panel E*, R1-11 cells expressing hPCFT/ThTr1 chimera mutant proteins were tested for [^{3}H]MTX transport activity as in panel B, using MES- and HEPES-buffered saline, as appropriate, at different pHs. Uptake for each mutant at the individual pHs was normalized to uptake at pH 5.5 (* indicates that mutant PCFT transport showed a greater decrease from pH 5.5 to pH 6.0 than *wt*hPCFT; $p < 0.05$). Figure previously published in Wilson et. al. Biochem J. 2016.

4.5A). All hPCFT mutant constructs were transiently expressed in R1-11 HeLa cells and were assayed for hPCFT levels on Westerns and for [^{3}H]MTX uptake compared to *wt*hPCFT^{HA} (Figures 4.5B and C).

The *re-engineered* full-length hPCFT (*pp*hPCFT^{HA}) showed a modest decrease in transport activity (~85% of *wt*hPCFT^{HA}; Figure 4.5B), accompanying slightly decreased hPCFT protein expression (Figures 4.5C), including surface hPCFT (Figure 4.5D). Complete removal of the hPCFT TMD6-7 loop sequence (residues 236-265) in *dl*hPCFT^{HA} abolished [^{3}H]MTX transport (< 2% of *wt*hPCFT^{HA}), reflecting a significant loss of membrane (Figure 4.5C) and surface (Figure 4.5D) hPCFT protein. Complete replacement of the 236-265 hPCFT sequence with amino acids 265-279 from ThTr1 (*tt*hPCFT^{HA}) likewise resulted in low expression and activity (~2% of *wt*hPCFT^{HA}, although this was significantly higher than R1-11 transport; $p < 0.0001$) (Figures 4.5B-D). Replacement of either the C-terminal TMD6-7 loop fragment (amino acids 251-265) in *pt*hPCFT^{HA} or the N-terminal fragment (amino acids 236-250) in *tp*hPCFT^{HA} with ThTr1 sequence preserved significant transport (23% and 11%, respectively; Figure 4.5B). Compared to *wt*hPCFT^{HA}, *pt*hPCFT^{HA} and *tp*hPCFT^{HA} showed insignificant differences in binding affinities for assorted transport substrates (as reflected in K_t and K_i values; Table 4.1) and only minor differences in pH dependence for transport (Figure 4.5E). The reduced transport activity relative to *wt*hPCFT^{HA} appeared to be entirely due to decreased V_{max} values (measured with [^{3}H]MTX; Table 4.1) and was reflected in levels of membrane (Figure 4.5C) and surface (Figure 4.5D) hPCFT^{HA} proteins on Western blots.

To better understand functional differences between wild-type hPCFT and the hPCFT-ThTr1 chimeric transporters with various TMD6-7 loop sequence replacements in relation to structure, we used molecular homology modeling. Superimposition of structural models for the

Table 4.1

Kinetic Analysis of *wt*hPCFT^{HA}, His247 hPCFT Substitution and Deletion Mutants, and hPCFT/ThTr1 Chimera Proteins.

Constant	K_t (μM)	V_{max} (pmol/mg/min)	V_{max}/K_t	K_i (μM)	K_i (μM)
hPCFT variant	MTX			FA	LCV
*wt*hPCFT^{HA}	0.75 ± 0.10	261.5 ± 28.3	414.3 ± 80.1	0.59 ± 0.08	0.38 ± 0.08
wt-H247A	0.18 ± 0.01*	10.8 ± 1.06*	60.8 ± 10.7*	0.12 ± 0.03*	0.13 ± 0.02
wt-ΔH247	0.54 ± 0.05	67.6 ± 12.2*	122.8 ± 24.8	0.27 ± 0.07	0.25 ± 0.06
wt-ΔH247/ΔH248	0.82 ± 0.07	101.6 ± 7.7*	125.8 ± 15.3	0.46 ± 0.12	0.46 ± 0.13
*tp*hPCFT	0.99 ± 0.21	63.0 ± 10.1*	73.6 ± 20.9*	0.71 ± 0.16	0.29 ± 0.06
tp-E247H	1.00 ± 0.10	141.6 ± 20.0*$^{\#}$	150.2 ± 31.1	0.47 ± 0.06	0.72 ± 0.11$^{\#}$
tp-E247R	1.50 ± 0.17*	276.8 ± 30.5$^{\#}$	194.5 ± 30.1$^{\#}$	0.60 ± 0.12	0.53 ± 0.18
*pt*hPCFT	0.77 ± 0.07	68.0 ± 10.9*	92.0 ± 20.0*	0.55 ± 0.13	0.17 ± 0.06

*wt*hPCFT^{HA} and hPCFT^{HA} mutants were transiently transfected into R1-11 cells, and 48 h later, [^{3}H]MTX uptake was assayed at pH 5.5 over 2 min at 37^{o}C. To determine K_t and V_{max} values, cells were treated with [^{3}H]MTX with concentrations between 0.33 μM and 5 μM, and results were analyzed by Lineweaver-Burke plots. To determine K_i values, cells were incubated with 0.5 μM [^{3}H]MTX with folic acid (FA) and LCV as competitors from 0.3 μM to 1.5 μM, with results analyzed by Dixon plots. Data are presented as mean values ± standard errors from four independent experiments. Values significantly different from those for *wt*hPCFT^{HA} ($p < 0.05$) are marked with *. Values significantly different from *tp*hPCFT^{HA} ($p < 0.05$) are marked with $^{\#}$ (only *tp*-E247H and *tp*-E247R were compared to *tp*hPCFT). Table previously published in Wilson et. al. Biochem J. 2016.

wt-, *pt*-, *tp*-, and *tt*hPCFT proteins gave a composite RMSD value of 1.2 Å for 234 Cα atoms from 10 transmembrane helices (TMDs 1-10), implying that the overall structures of these various hPCFT forms were almost identical (Figure 4.6A). This suggests that the sequence composition of the TMD6-7 loop has minimal impact on *overall* folding of the hPCFT protein. We also considered isolated conformational changes involving the TMD6-7 loop domain that may impact transport activity for the individual hPCFT insertion mutants compared to wild-type PCFT. We explored the secondary structure changes in the hPCFT TMD6-7 loop domain for the hPCFT-ThTr1 chimeric proteins, using the secondary structure prediction tool GOR4 (Garnier et al., 1996). Whereas wild-type hPCFT showed significant α-helix (16.7%) for this region, this was lost for the insertion mutants (*tp*hPCFT^{HA}, *pt*hPCFT^{HA}, and *tt*hPCFT^{HA}). This loss of α-helical structure for the TMD6-7 mutant proteins was accompanied by progressively increased random coil structures, as reflected in major conformational changes (Figure 4.6B), from 60% for *wt*PCFT to 70% for *pt*hPCFT, 80% for *tp*hPCFT and 87% for *tt*hPCFT. Thus, there is an inverse relationship between the extent of random coil for the TMD6-7 loop region and hPCFT transport activity.

These results establish that the TMD6-7 loop is important for hPCFT transport activity. However, this functional role likely depends on preservation of secondary structure rather than particular sequence motifs.

4.3.5 Characterization of His247 Substitution and Deletion Mutants in Wild-Type hPCFT and hPCFT-ThTr1 Chimera Transporters

While the above studies imply a relative independence of the TMD6-7 loop primary sequence for transport activity, scanning alanine and cysteine mutagenesis (Figures 4.2 and 4.3)

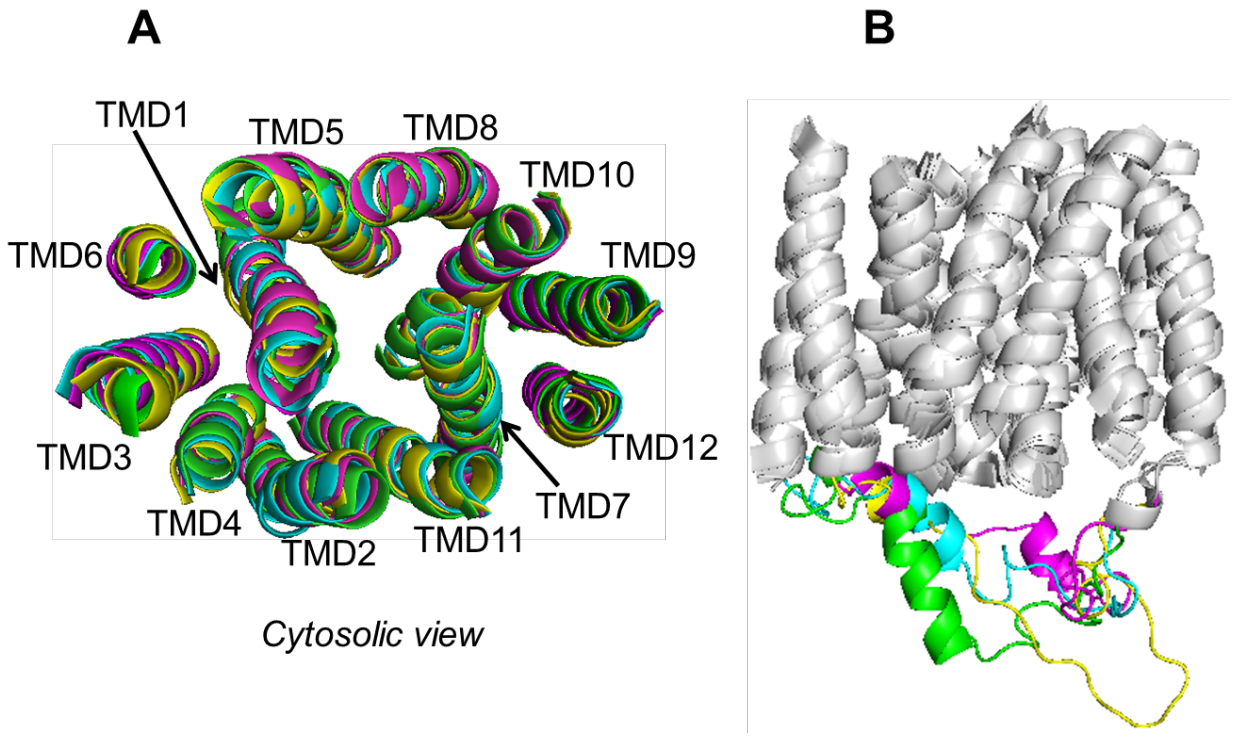

Figure 4.6 Protein modeling of PCFT/ThTr1 chimera mutants. *Panels A and B*, hPCFT protein modeling using Robetta and SALIGN software, as described in Materials and Methods. hPCFT TMDs 1-12 only, (including TMDs 1, 2, 4 5, 7, 8, 10, and 11, predicted to form the transmembrane translocation pathway), as a composite structure from *pp*hPCFT^{HA} (green), *pt*hPCFT^{HA} (pink), *tp*hPCFT^{HA} (cyan), and *tt*hPCFT^{HA} (yellow). In Panel B, the TMD6-7 loop is highlighted and can be distinguished from TMDs1-12 (grey) including *pp*hPCFT^{HA} (green), *pt*hPCFT^{HA} (pink), *tp*hPCFT^{HA} (cyan), and *tt*hPCFT^{HA} (yellow). Modeling done in collaboration with Zhanjun Hou and Jun Ye. Figure previously published in Wilson et. al. Biochem J. 2016.

nonetheless identified His247 as a residue for which its replacement consistently caused a significant loss of transport activity. Unal *et al*. previously showed that amino acid substitutions (Ala, Arg, Gln, Glu) at position 247 had various effects on hPCFT transport activity (Unal et al., 2009a). All of these mutants were expressed (Figure 4.7B) and relative to wild-type hPCFT (*wt*hPCFT^{HA}), activity ranged from ~5% for *wt*-H247R to ~13% for *wt*-H247A, and ~26% and ~28% for *wt*-H247E and *wt*-H247Q, respectively (Figure 4.7A).

Interestingly, the impact of position 247 replacements was much different for the hPCFT-ThTr1 chimeric transporters. For the partially active *tp*hPCFT^{HA} mutant with a glutamate at position 247, substitution with alanine (*tp*-E247A) resulted in decreased transport (3% of *wt*hPCFT), while re-introduction of histidine (*tp*-E247H) or replacement with glutamine (*tp*-E247Q) subtly increased transport over *tp*hPCFT^{HA} (~19% and ~22.4% of *wt*hPCFT, respectively) (Figure 4.7A). Arginine insertion at position 247 of *tp*hPCFT restored transport activity at ~50% of the *wt*hPCFT level. These effects on activity for *tp*-E247H and *tp*-E247R were accompanied by disproportionately elevated V_{max} values compared to *tp*hPCFT (Table 4.1), even when normalized to surface expression levels on Western blots (Figure 4.5D). While the K_i for LCV was increased for *tp*-E247H compared to *tp*hPCFT, for both *tp*-E247H and *tp*-E247R, there were minor differences in pH dependences for transport compared to *tp*hPCFT (Figure 4.7F).

For *pt*hPCFT, the effects of alanine, arginine, glutamine and glutamic acid substitutions for His247 on transport activity (Figure 4.7A) and expression (Figure 4.7B) were nominal. Histidine insertion at position 247 in *tt*hPCFT resulted in a subtle but significant decrease in activity (from 2% of *wt*hPCFT^{HA} for *tt*hPCFT to 1% for *tt*-E247H) ($p < 0.05$) (Figure 4.7A).

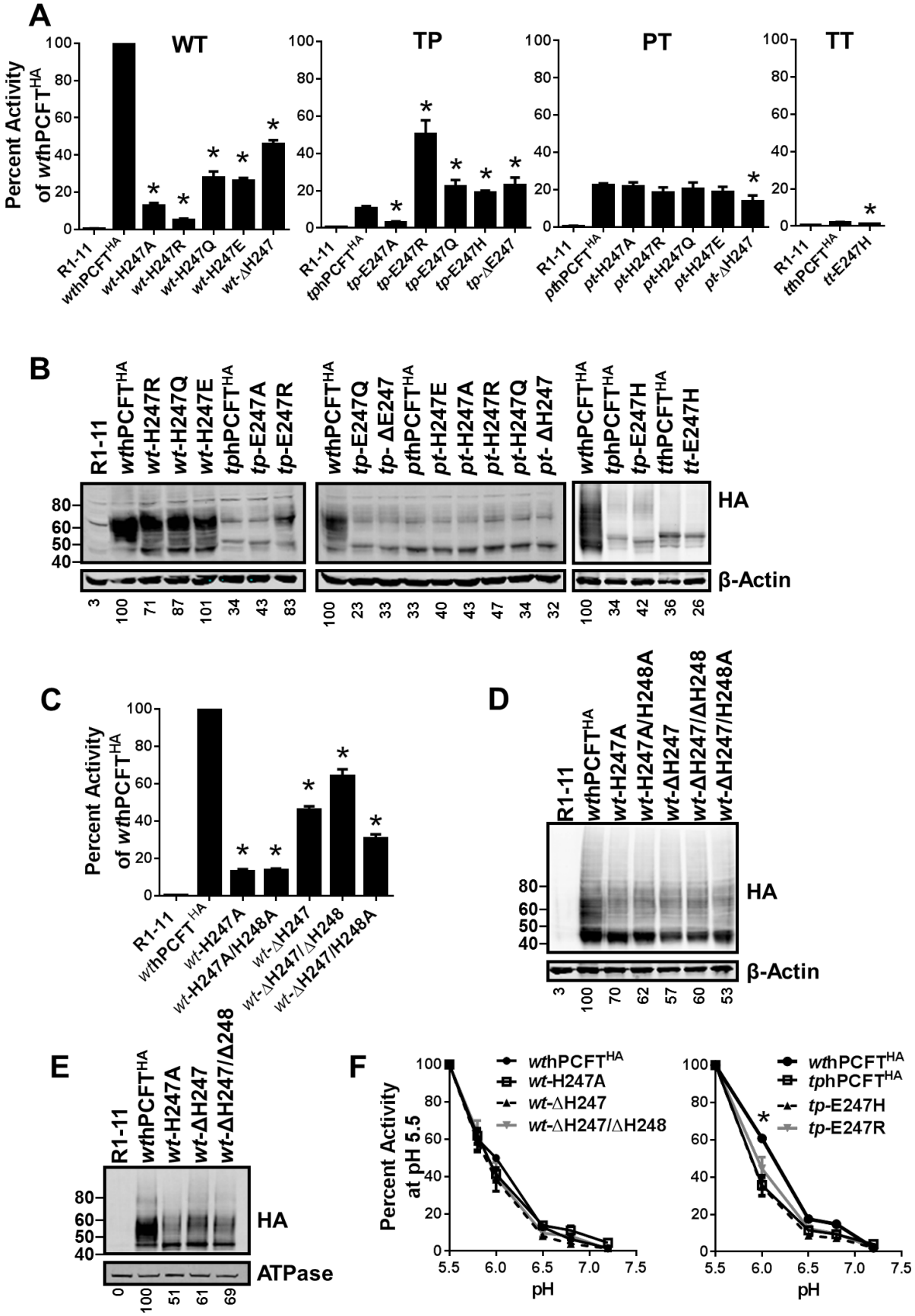
A
WT
TP
PT
TT
Percent Activity of wthPCFT^HA
R1-11
wthPCFT^HA
wt-H247A
wt-H247R
wt-H247Q
wt-H247E
wt-ΔH247
tphPCFT^HA
tp-E247A
tp-E247R
tp-E247Q
tp-E247H
tp-ΔE247
pthPCFT^HA
pt-H247A
pt-H247R
pt-H247Q
pt-H247E
pt-ΔH247
tthPCFT^HA
tt-E247H
B
tp-E247Q
tp- ΔE247
pthPCFT^HA
pt-H247E
pt-H247A
pt-H247R
pt-H247Q
pt- ΔH247
tt-E247H
HA
β-Actin
3 100 71 87 101 34 43 83
100 23 33 33 40 43 47 34 32
100 34 42 36 26
C
wt-H247A/H248A
wt-ΔH247
wt-ΔH247/ΔH248
wt-ΔH247/H248A
D
wt-H247A/H248A
wt-ΔH247
wt-ΔH247/ΔH248
wt-ΔH247/H248A
3 100 70 62 57 60 53
E
wt-ΔH247/Δ248
ATPase
0 100 51 61 69
F
Percent Activity at pH 5.5
wt-ΔH247/ΔH248
pH

Figure 4.7 Analysis of 247/248 substitution and deletion mutants. *Panels A and C*, Amino acid substitution and deletion mutants were generated from *wt*hPCFT^{HA}, *pt*hPCFT^{HA} , *tp*hPCFT^{HA} , and *tt*hPCFT^{HA}, as described in the text, and were transfected into R1-11 cells. Transport activity was measured after 48 h with [^{3}H]MTX (0.5 μM) over 2 min at pH 5.5 and at 37^{o}C. Results are expressed as a percentage of *wt*hPCFT^{HA} activity and are reported as mean values ± standard errors (error bars) from triplicate experiments. With the exception of *tt*-E247H, all mutants were significantly more active than the non-transfected control, R1-11 ($p<0.05$) [* indicates where transport activity is significantly different from parent *wt*-, *pt*-, *tp*-, or *tt*hPCFT^{HA}, as appropriate; $p < 0.05$]. *Panels B and D*, Western blots are shown for membrane proteins (10 μg) from HA-tagged hPCFT 247/248 substitution and deletion mutants. Densitometry (as relative percentages, noted below each lane) is representative of duplicate experiments and was normalized to β-actin expression. Migrations of molecular mass standard proteins (in kDa) are shown. *Panel E*, HA-tagged hPCFT surface membrane proteins (40 μg) were labeled with sulfo-NHS-SS-biotin (0.25 mg/ml) and isolated on immobilized NeutrAvidin^{TM} gel. Biotinylated proteins were analyzed by SDS/PAGE and Western blotting. Relative densitometry (as relative percentages, noted below each lane) is representative of duplicate experiments and results for hPCFT were normalized to Na^+/K^+ ATPase expression. Migrations of molecular mass standard proteins (in kDa) are shown. *Panel F*, R1-11 cells expressing hPCFT His247 mutant proteins were tested for [^{3}H]MTX transport activity as in panel A, using MES- and HEPES- buffered saline, as appropriate, at various pHs. Uptake for each mutant at the individual pHs was normalized to uptake at pH 5.5 (* indicates that mutant PCFT transport showed a greater decrease from pH 5.5 to pH 6.0 than *wt*hPCFT; $p < 0.05$). Figure previously published in Wilson et. al. Biochem J. 2016.

To further characterize the functional importance of His247 to hPCFT transport, we deleted this residue entirely, using *wt*hPCFT^{HA} as a template, generating *wt*-ΔH247. Since His247 in hPCFT is followed by His248 (thus, effectively replacing His247 in the *wt*-ΔH247 mutant), we also created three additional mutants in the *wt*hPCFT^{HA} background. These include *wt*-H247A/H248A, in which both His247 and His248 are mutated to alanine, *wt*-ΔH247/ΔH248, in which both histidines are deleted, and *wt*-ΔH247/H248A, in which His247 is deleted and His248 is replaced by alanine. ΔH247 and ΔE247 deletion mutants were also prepared for *pt*hPCFT^{HA} and *tp*hPCFT^{HA}, respectively.

All of the wild-type hPCFT His deletion mutants showed similar, albeit slightly decreased, levels of PCFT^{HA} protein from that for *wt*hPCFT^{HA} (Figure 4.7D). Interestingly, for *wt*-ΔH247, *wt*-ΔH247/ΔH248 and *wt*-ΔH247/H248A, transport activity was significantly increased over that for *wt*-H247A ($p < 0.05$) (Figure 4.7C); for *wt*-ΔH247 and *wt*-ΔH247/ΔH248 transport approximated ~46% and ~64%, respectively, of *wt*hPCFT^{HA} levels. Increased activity for *wt*-ΔH247 and *wt*-ΔH247/ΔH248 compared to *wt*-H247A hPCFT was accompanied by slightly increased surface protein (Figure 4.7E). When transport was normalized to *surface* hPCFT levels, this gave ~75% and ~93% of that of *wt*hPCFT^{HA} for *wt*-ΔH247 and *wt*-ΔH247/ΔH248, respectively. While position 247 deletion in *tp*hPCFT (*tp*-ΔE247) also increased transport activity compared to *tp*E247A (23% of *wt*hPCFT), position 247 deletion in *pt*hPCFT (*pt*-ΔH247) resulted in a subtle decrease in transport activity (14% of *wt*hPCFT^{HA} for *pt*-ΔH247 compared to 23% for *pt*hPCFT) ($p < 0.05$) (Figure 4.7A).

We examined transport characteristics for the restored transport activity of the *wt*-ΔH247, and *wt*-ΔH247/ΔH248 mutants compared to H247A and *wt*hPCFT^{HA}, including pH dependences and transport kinetics. There were no differences in the pH profiles between mutant and wild-

type PCFTs, as maximal transport activity was measured at pH 5.5 and decreased with increasing pH (Figure 4.7F). By kinetic analysis, *wt*-H247A showed decreases in both K_t (4.2-fold) and V_{max} (26.7-fold) for MTX compared to *wt*hPCFT^{HA} (Table 4.1), similar to published results by Unal *et al* (Unal et al., 2009a). Interestingly, for the deletion mutants (*wt*-ΔH247 and *wt*-ΔH247/ΔH248), the MTX K_ts were restored to approximate the wild-type values, accompanying increased V_{max} values, compared to H247A (Table 4.1). The latter reflect increased surface hPCFT, as noted above (Figure 4.7E). Analogous patterns were seen in the K_is for both folic acid and LCV for the *wt*-H247A, *wt*-ΔH247, and *wt*-ΔH247/ΔH248 mutants, determined by Dixon analysis from the inhibition of [^{3}H]MTX uptake.

Overall, our results suggest that neither His247 nor His248 is absolutely essential for hPCFT transport. Whereas *wt*-H247A resulted in increased affinity for transport substrates, His247 deletion had no impact on substrate binding (as reflected in the K_t and K_i values for various substrates). The decreased V_{max} values for *wt*-H247A, *wt*-ΔH247, and *wt*-ΔH247/ΔH248 mutants were all accompanied by reduced surface hPCFT levels, suggesting decreased stability (and intracellular trafficking) for these mutant transporters compared to wild-type hPCFT.

4.4 Discussion

hPCFT is predicted to be formed from distinct TMD1-6 and TMD7-12 segments, with the longest of its 11 connecting loop domains linking TMDs 6 and 7 comprised of amino acids 236-265. In this chapter, we explored the structure and transport function of the TMD6-7 connecting loop using a range of complementary approaches.

(i) Ala and Cys substitutions mutagenesis across the TMD6-7 loop identified His247 as the only amino acid residue in this stretch for which its replacement consistently and substantially suppressed transport activity. However, deletion of His247 significantly restored

transport activity compared to *wt*-H247A. This implies that His247 is not in itself essential to high levels of transport. (ii) Further studies established that large (15 amino acid) segments of the hPCFT TMD6-7 loop including His247 could be replaced with non-homologous sequence from ThTr1 (in *pt*hPCFT^{HA} and *tp*hPCFT^{HA}), resulting in significant preservation of transport, although complete deletion of the loop (in *dl*hPCFT^{HA}) or its replacement with non-homologous sequence from ThTr1 (in *tt*hPCFT^{HA}) abolished transport activity. These differences in transport activity between the *pt*hPCFT^{HA} and *tp*hPCFT^{HA} compared to *wt*hPCFT^{HA} were independent of substrate binding but were associated with a pronounced impact on transport V_{max}, likely due to impaired trafficking to the cell surface and loss of stability, resulting in decreased hPCFT protein expression. (iii) While His247 replacements with Ala, Arg, Gln and Glu in *wt*hPCFT replicated previous findings of Unal *et al*. (Unal et al., 2009a), substitutions of Glu247 in *tp*hPCFT followed a distinctly different pattern. The same His247 replacements in *pt*hPCFT showed no obvious impact on transport activity. Analogous results were obtained for the His247 deletion mutants (*wt*-ΔH247 and *tp*-ΔE247 versus *pt*-ΔH247). Thus, the impact of position 247 alterations is *context-dependent* and varies with flanking sequence and secondary structure. Indeed, the role of the TMD6-7 loop domain in hPCFT function appears to be largely unrelated to specific primary sequence elements, as long as sufficient secondary structure is preserved and proper spacing between the TMD1-6 and TMD7-12 segments is ensured to facilitate optimal membrane transport. (iv) Consistent with the latter notion, hPCFT could be expressed as TMD1-6 and TMD7-12 half-molecules to restore transport activity, albeit in low levels.

Collectively, our results demonstrate that the TMD6-7 loop structure is critical to intracellular trafficking and protein stability essential to transport function. Our biochemical and molecular modeling results further suggest that while absolute primary sequence elements of the

TMD6-7 loop is not essential to transport function, as long as sufficient secondary structure is preserved, the loop may nonetheless serve a unique functional role, even possibly restricting substrate access to the folate binding site and membrane translocation pathway, as previously suggested (Unal et al., 2009a). While our results imply that His247 can play a role in hPCFT transport, this is subtle, as loss of His247 can be compensated by other primary sequence elements as indicated by our results with *pt*hPCFT His-replacement muttants. Characterization of key structural features of hPCFT is important for understanding the transport mechanism, including identifying critical determinants of substrate binding and membrane translocation.

CHAPTER 5- TARGETING NON-SQUAMOUS NON-SMALL CELL LUNG CANCER VIA PCFT-MEDIATED UPTAKE OF 6-SUBSTITUTED PYRROLO[2,3-*d*]PYRIMIDINE THEINOYL ANTIFOLATES

5.1 Introduction

NSCLC is the leading cause of cancer-related deaths in the United States, accounting for 85% of all diagnosed lung cancers and resulting in over 100,000 deaths per year (American Cancer Society, 2015). PMX is a 5-substituted pyrrolo[2,3-*d*]pyrimidine antifolate (Figure 1.2) (Chattopadhyay et al., 2007) and is an important first-line and maintenance therapy in the treatment of nonsquamous (NS)-NSCLC, although patient responses are variable (Esteban et al., 2009; Genova et al., 2013; Gerber and Schiller, 2013; Tomasini et al., 2013). Cellular uptake of folates and classic antifolates is primarily via the facilitative folate transporters, RFC and PCFT (Matherly et al., 2014). FRα is expressed in some malignancies including NSCLC (Christoph et al., 2013; Nunez et al., 2012; O'Shannessy et al., 2012) and is being exploited for targeted drug delivery (Assaraf et al., 2014; Xia and Low, 2010). However, FRα levels in NS-NSCLC can be variable (Christoph et al., 2013; Nunez et al., 2012; O'Shannessy et al., 2012), at least in part reflecting epidermal growth factor receptor (EGFR) mutation status (Nunez et al., 2012) or stage of disease (O'Shannessy et al., 2012), with the highest levels in a subset of specimens. RFC is a ubiquitously expressed folate/anion antiporter, and is widely considered to be the major tissue transporter of folate cofactors and antifolates such as MTX and PMX (Matherly et al., 2007). PCFT was identified in 2006 as a folate/proton symporter with an acidic pH optimum and was localized to the upper gastrointestinal tract where it transports dietary folates across the apical brush border of the small intestine (Qiu et al., 2006). Although other tissues such as liver and kidney also express PCFT (Desmoulin et al., 2012a), in these tissues its biologic role is less certain since the neutral pH microenvironment is not conducive to high levels of PCFT transport

(Zhao et al., 2009a). PCFT is commonly expressed in human tumor cells including NS-NSCLC cell lines (Kugel Desmoulin et al., 2011), and likely facilitates PMX uptake and contributes to antitumor efficacy with this disease since the acidic microenvironment of tumors greatly favors transport by PCFT over RFC (Desmoulin et al., 2012a; Zhao and Goldman, 2007).

Once internalized, PMX is metabolized to polyglutamates by FPGS, resulting in drug forms with enhanced cellular retention over nonpolyglutamyl PMX and increased binding affinities for intracellular enzyme targets (Chattopadhyay et al., 2007). TS is the primary intracellular enzyme target for PMX (Chattopadhyay et al., 2007) and TS levels have been implicated in some studies as an important determinant of PMX clinical response, such that tumors with highly elevated TS would be expected to show PMX resistance (Christoph et al., 2013; Liu et al., 2013). At least some of the variable responses to PMX seen clinically may reflect an impact of coadministering dexamethasone with PMX to alleviate possible side effects since dexamethasone attenuates PMX cytotoxicity in NS-NSCLC cells by reversibly blocking cell cycle progression, secondary to the presence of high levels of the glucocorticoid receptor a (Patki et al., 2014). Interestingly, dexamethasone treatment of NS-NSCLC cells in vitro also resulted in reduced expression of RFC and PCFT (Patki et al., 2014). PMX can inhibit folate-dependent enzymes other than TS, including GARFTase and AICARFTase in *de novo* purine nucleotide biosynthesis (Racanelli et al., 2009).

Given variable patient responses to PMX, another promising strategy is to develop analogs with increased selectivity for membrane transport by PCFT over RFC, thus increasing specificity toward tumors, while decreasing toxicity toward normal tissues (Desmoulin et al., 2012a). Ideally, these agents would target intracellular enzymes other than TS, thus potentially circumventing PMX resistance due to TS alterations.

The synthesis and biologic activities of a novel series of 2',4' and 2',5' thienoyl 6-substituted pyrrolo[2,3-d]pyrimidine antifolates, typified by AGF94 and AGF154 (Figure 1.2), have been previously described (Cherian et al., 2013; Desmoulin et al., 2012b; Wang et al., 2011; Wang et al., 2015). AGF94 and AGF154 exhibit transport specificity for PCFT over RFC and deplete purine nucleotides due to inhibition of *de novo* biosynthesis at GARFTase, the first folate-dependent step. Although GARFTase inhibitors have been previously described (i.e., LMX, AG2034) (Boritzki et al., 1996; Mendelsohn et al., 1999a) and have shown potent antitumor effects, this was accompanied by unacceptable levels of toxicity in patients, possibly reflecting significant RFC-driven transport of these compounds (Budman et al., 2001; Ray et al., 1993). This problem may be overcome by combining GARFTase targeting and PCFT transport selectivity, which characterizes antifolates such as AGF94 and AGF154. In this chapter, we explore the therapeutic potential of these novel tumor-targeted 6-substituted pyrrolo[2,3-d]pyrimidine antifolates with selective membrane transport by PCFT over RFC in NS-NSCLC. The work described in this chapter was previously published in *Molecular Pharmacology* (Wilson et al., 2016b).

5.2 Materials and Methods

5.2.1 Reagents

The 6-substituted pyrrolo[2,3-*d*]pyrimidine antifolates AGF94 [(S)-2-((5-[3-(2-amino-4-oxo-4,7-dihydro-3H-pyrrolo[2,3-*d*]pyrimidin-6-yl)-propyl]-thiophene-2-carbonyl)-amino)-pentanedioic acid] and AGF154 [(S)-2-((5-[3-(2-amino-4-oxo-4,7-dihydro-3H-pyrrolo[2,3-d]-pyrimidin-6-yl)-propyl]-thiophene-3-carbonyl)-amino)-pentanedioic acid] were synthesized as previously described (Wang et al., 2011; Wang et al., 2015). PMX [N-(4-[2-(2-amino-3,4-dihydro-4-oxo-7H-pyrrolo[2,3-d]pyrimidin-5-yl)ethyl]benzoyl)-*L*-glutamic acid] (Alimta) was

obtained from Eli Lilly and Co. (Indianapolis, IN). PT523 [Na-(4-amino-4-deoxypteroyl)-Nd-hemiphthaloyl-L-ornithine) (Rosowsky et al., 1994) was a gift of Dr. A. Rosowsky (Boston, MA). LCV was obtained from the Drug Development Branch, National Cancer Institute, Bethesda, MD. [^{3}H]PMX (87 Ci/mmol), [^{3}H]AGF154 (12.3 Ci/mmol), and [^{14}C(U)]glycine (87mCi/mmol) were purchased from Moravek Biochemicals (Brea, CA). Other chemicals were obtained from commercial sources in the highest available purity.

5.2.2 Real-Time Reverse-Transcription Polymerase Chain Reaction (RT-PCR) Analysis of Folate-Related Transcripts

Patient cDNAs were purchased from Origene (Rockville, MD), including 26 NS-NSCLC specimens (8, stage I; 5, stage II; 7, stage III; and 6, stage IV) and eight unmatched normal lung specimens. RNAs were isolated from the NS-NSCLC cell lines using TRIzol reagent (Invitrogen, Carlsbad, CA). cDNAs were synthesized with random hexamers and MuLV reverse transcriptase (including RNase inhibitor) (Applied Biosystems, Waltham, MA) and were purified using a QIAquick PCR Purification Kit (QIAGEN, Valen- cia, CA). Quantitative real-time RT-PCR was performed using a Roche LightCycler 480 (Roche Diagnostics, Indianapolis, IN) with gene-specific primers and FastStart DNA Master SYBR Green I Reaction Mix (Roche Diagnostics). Primer sequences are available upon request. Transcript levels were normalized to transcript levels of β-actin.

5.2.3 Immunohistochemistry (IHC)

The tissue microarray (BC041115b) and IHC services were purchased from US Biomax, Inc. (Rockville, MD). The array included 61 NS-NSCLC specimens (25, stage I; 19, stage II; 16, stage III; and 1, stage IV) and 10 unmatched normal lung tissues. The tissues were formalin-fixed and paraffin-embedded. The tissue microarrays were deparafinized, rinsed, microwaved, and incubated with polyclonal antibody to human PCFT raised in rabbits (Hou et al., 2012). The

serum was purified using a peptide affinity column synthesized from Affi-Gel 10 (BioRad, Richmond, CA). The slides were developed with ImmPRESS anti-Rabbit IgG (peroxidase) (Vector Laboratories, Burlingam, CA) and peroxidase substrate 3,3'-diaminobenzidine tetrahydrochloride, and then rinsed, counterstained with Hematoxylin QS (Vector Laboratories), cleared, and mounted with permanent mounting medium (C0487; Sigma-Aldrich, St. Louis, MO). The slides were manually scored by two independent pathologists with the intensities scored as negative (0), weak (11), moderate (21), or strong (31), and then scanned by an Aperio Image Scanner (Aperio Technologies, Inc., Vista, CA) for microarray image scanning. The total positive cell numbers and intensity of antibody staining of each tissue core were computed.

5.2.4 Cell Culture Conditions

NS-NSCLC cell lines, including A549, H1437, H460, H1299, H1650, and H2030, were obtained from the American Type Culture Collection (Manassas, VA). The identities of the NS-NSCLC cell lines were verified by Genetica DNA Laboratories (Burlington, NC). HeLa cells were gifts from Dr. I. David Goldman (Bronx, NY). Prior to experiments, all cell lines were grown in folate-free RPMI 1640 supplemented with 10% dialyzed FBS (Sigma- Aldrich), 1% penicillin/streptomycin, 2 mM *L*-glutamine, and 25 nM LCV for at least 2 weeks.

For growth inhibition assays, the NS-NSCLC cell lines were plated in 96-well culture dishes (1500–4000 cells/well; 200 ml/well) in the aforementioned medium with drug concentrations from 1 to 1000 nM PMX, AGF94, or AGF154. Cells were incubated from 96 to 120 hours (depending on the cell line) at 37° C in a CO_2 incubator. Cell viabilities were measured with a fluorescence-based viability assay (CellTiter Blue; Promega, Madison, WI) and a fluorescence plate reader (emission at 590 nm; excitation at 560 nm) to determine drug concentrations that inhibit growth by 50% (IC_{50}). To confirm the targeted pathways and enzymes,

proliferation assays were performed with H460 cells treated with PMX, AGF94, or AGF154 in the presence of adenosine (60 mM), thymidine (10 mM), or AICA (320 mM) (Wang et al., 2011, 2015).

For colony-forming assays, H460 cells (100–150 cells) in log phase were plated into 60-mm dishes in folate-free RPMI 1640 medium (pH 7.2), supplemented with 25 nM LCV, 10% dialyzed fetal bovine serum, 1% penicillin/streptomycin, and 2 mM *L*-glutamine, and then allowed to adhere for 24 hours. Cells were then treated with drugs in the aforementioned media at pH 6.8 or 7.2. For treatments at pH 6.8, 25 mM 1,4-piperazinediethanesulfonic acid/25 mM HEPES was added (Kugel Desmoulin et al., 2011). After 24 hours, cells were rinsed with PBS, and then incubated in drug-free, folate-free RPMI 1640 medium (pH 7.2) plus dialyzed fetal bovine serum and antibiotics, supplemented with 25 nM LCV. After 9 days, the dishes were washed with PBS, 5% trichloroacetic acid, and then with borate buffer (10 mM, pH 8.8), followed by 1% methylene blue (in borate buffer). Dishes were again rinsed with borate buffer, and colonies were counted in order to calculate the percent colony formation relative to the vehicle (e.g., dimethylsulfoxide) control.

5.2.5 Development of H460 PCFT Knockdown (KD) Cell Line

H460 cells were seeded at $2x10^5$ cells per well in 24-well plates containing RPMI 1640 (pH 7.2), supplemented with 10% fetal bovine serum, 1% penicillin/streptomycin, and 2 mM *L*-glutamine, with the addition of 4 mg/ml polybrene and 105 transducing units of MISSION Lentiviral particles (Sigma-Aldrich) containing shRNA targeting PCFT or a nontargeted control (NTC) shRNA sequence. After 24 hours, fresh medium including 2 mg/ml puromycin as a selection marker was added. Confluent cultures were trypsinized and passaged 3 to 4 times in the presence of 2 mg/ml puromycin, and then plated in 60-mm dishes in complete medium with 2

mg/ml puromycin at a density of 100 cells/dish to isolate single clones. Clones were picked and expanded and RNAs were isolated to determine the extent of PCFT knockdown by real-time RT-PCR (described previously). Two PCFT KD clones were isolated, designated as KD-3 and KD- 4. Altogether, five shRNAs were tested, of which only one (TRCN0000437092) gave .50% knockdown for PCFT.

5.2.6 Gel Electrophoresis and Western Blotting

The NS-NSCLC cell lines were cultured, as described previously. The cells were disrupted by sonication, cell debris was removed by centrifugation (1800 rpm, 5 minutes), and a particulate membrane fraction was prepared by centrifugation at 37,000g. The membrane pellet was solubilized with 1% SDS in 10 mM Tris-HCl (pH 7), containing protease inhibitors (Roche Diagnostics). Membrane proteins (30 mg) were electrophoresed on 7.5% polyacrylamide gels with SDS (Laemmli, 1970) and transferred to polyvinylidene difluoride membranes (Thermo Fisher Scientific, Waltham, MA) (Matsudaira, 1987). To detect PCFT, human PCFT-specific polyclonal antibody raised in rabbits to a carboxyl termini peptide (Hou et al., 2012) was used, with IRDye800CW-conjugated goat anti-rabbit IgG secondary antibody (LICOR Biosciences, Omaha, NE). Membranes were scanned and densitometry was performed with an Odyssey infrared imaging system (LICOR Biosciences). Protein loading was normalized to levels of β -actin using anti-β-actin mouse antibody (Sigma-Aldrich).

5.2.7 Antifolate Transport Assays

Transport assays were performed essentially as described previously (Desmoulin et al., 2012b; Kugel Desmoulin et al., 2011; Kugel Desmoulin et al., 2010). For transport assays, the NS-NSCLC cell lines were plated at 30%–40% confluence into 60-mm dishes containing complete folate-free RPMI 1640 supplemented with 25 nM LCV. After 48 hours, cellular

uptakes of [^{3}H]PMX and [^{3}H]AGF154 (both at 0.5 mM) were measured over 5 minutes (NS-NSCLC cell lines) or 2 minutes (PCFT KD cell lines) at 37°C in 60-mm dishes in MES-buffered saline (20 mM MES, 140 mM NaCl, 5 mM KCl, 2 mM MgCl2, and 5 mM glucose; pH 5.5). The dishes were washed three times with PBS and cells were solubilized in 0.5 N NaOH. Intracellular radioactivity was calculated as pmol/mg of protein, based on measurements of radioactivity and protein concentrations of the alkaline cell homogenates. To confirm PCFT-mediated transport activity, 10 μM nonradioactive AGF94 was added to the transport incubations to block uptake.

5.2.8 *In Situ* GARFTase Enzyme Inhibition Assay

Incorporation of [^{14}C(U)]glycine into [^{14}C]formyl glycinamide ribonucleotide, as an *in situ* measure of intracellular GARFTase activity in folate-depleted H460 cells at pH 6.8, was performed exactly as previously described (Kugel Desmoulin et al., 2010; Wang et al., 2011). For these experiments, H460 cells were plated in folate-free RPMI 1640 plus 25 nM LCV, 10% dFBS, 2 mM *L*-glutamine, and penicillin-streptomycin in 60 mm dishes at 20% confluency. After 48 h, the media was replaced folate-free, *L*-glutamine-free RPMI 1640 plus penicillin/streptomycin, 10% dFBS, 0.46 g/L NaHCO3 and 1.21 g/L NaCl medium, which had been adjusted to pH 6.8, with antifolates at various concentrations (or DMSO). After 15h, cells were washed twice with DPBS and the pH 6.8 media was replaced, containing antifolates and 4 μM azaserine and incubated for 30 min. Then, 2 mM *L*-glutamine and 0.1 mCi/L [^{14}C]glycine were added, followed by an 8h incubation at 37°C, after which cells were trypsinized and washed twice with ice-cold DPBS. Cell pellets were treated with 2 ml of 5% trichloroacetic acid at 0°C for 10 min. Cell debris was removed by centrifugation, and cell debris pellets were solubilized in 0.5 N NaOH and protein concentrations were determined (Lowry et al., 1951). To

remove trichloroacetic acid from supernatants, ice-cold ether was used to extract trichloroacetic acid. The aqueous layer passed through a 1-cm column of AG1x8 (chloride form), 100 to 200 mesh (Bio-Rad Laboratories) washed twice with 0.5 N formic acid and then twice with 4 N formic acid, and eluted as eight 1-mL fractions with 1 N HCl. Fractions were used to determine radioactivity. Results were expressed as pmol/mg protein. Drug-treated samples were normalized to untreated controls to calculate the IC_{50} values.

5.2.9 *In Vivo* Antitumor Efficacy of AGF94 Toward H460 Xenografts in SCID Mice

Cultured H460 cells were implanted subcutaneously (10^7 cells/flank) into female ICR SCID mice (National Institutes of Health DCT/DTP Animal Production Program, Frederick, MD) to develop a solid tumor xenograft model (passage 0). Mice were supplied water and food ad libitum. Study mice were maintained on a folate-deficient diet (TD.00434; Harlan Teklad, Madison, WI) starting 14 days prior to tumor implant to ensure that serum folate levels approximated those of humans before the start of therapy (Cherian et al., 2013; Wang et al., 2010; Wang et al., 2011). Serum folate assays (Varela-Moreiras and Selhub, 1992) were performed just prior to tumor engraftment and were repeated at the conclusion of the drug treatments. This design is analogous to those previously published (Alati et al., 1996; Gibbs et al., 2005).

To test drug efficacy, experimental mice were pooled, divided into groups (five mice/group), and bilaterally implanted subcutaneously with 30–60 mg H460 tumor fragments, using a 12-gauge trocar (day 0). Chemotherapy began on day 1 after tumor implantation, when the number of cells was between 107 and 108 cells (below the limit of palpation). Organic solvent (ethanol, 5% v/v), carrier (Tween 80, 1% v/v), and sodium bicarbonate (0.5% v/v) were used to effect solubilization of AGF94, while cisplatin and gemcitabine were dissolved in sterile

saline. All drugs were administered intravenously using an injection volume of 0.2 ml. Mice were weighed daily and tumor measurements were determined using a caliper two-to-three times weekly. Mice were sacrificed when their individual tumor burdens reached 1500 mg (asymptomatic). Mice were necropsied and tissue was harvested to evaluate potential organ-related toxicities (by H&E staining).

Methods for protocol design, drug treatments, toxicity evaluation, and data analysis were previously described (Corbett et al., 1998; Corbett et al., 1997; Polin et al., 2011; Polin et al., 1997). Experimental parameters as qualitative and quantitative end points to assess antitumor activities include: T/C (as a percentage) and T–C (tumor growth delay) [where T is the median time (days) required for the treatment group tumors to reach a predetermined size (e.g., 1000 mg) and C is the median time (days) for the control tumors to reach the same size; tumor-free survivors are excluded from these calculations]; and tumor cell kill [$\log_{10}$ cell kill total (gross) 5 (T–C)/(3.32)(T_d), where (T–C) is the tumor growth delay, as described previously, and T_d is the tumor volume doubling time (days), estimated from the best-fit straight line from a log-linear growth plot of control group tumors in exponential growth (100–800 mg)]. For comparisons of antitumor activities with standard agents or between tumors, $\log_{10}$ kill values were converted to an arbitrary activity rating (Corbett et al., 1997). With the exception of the H460 xenograft cell line and the drugs used in treatment, these methods are identical to those described previously (Cherian et al., 2013; Wang et al., 2010; Wang et al., 2011; Wang et al., 2015).

5.2.10 Statistical Analysis

Descriptive statistical tests (e.g., t tests) were conducted using GraphPad 6.0 software (La Jolla, CA).

5.3 Results

5.3.1 Expression Profiles for Folate Transport and Metabolism Genes in NS-NSCLC Patient Specimens

To begin to identify key determinants of antitumor efficacy of the 2',4', and 2',5' thienoyl pyrrolo[2,3-d]pyrimidine antifolates AGF94 and AGF154 (Figure 1.2) toward NS-NSCLC, we measured PCFT transcripts (by real-time RT-PCR) and proteins (by IHC) in NS-NSCLC and unmatched (i.e., from different patients) normal lung specimens (Figure 5.1). Clinical specimens were obtained from different commercial sources such that PCFT gene expression and protein levels could not be directly compared for individual samples.

PCFT transcripts were similarly expressed (based on median values) in 26 NS-NSCLC and 8 normal lung specimens, although the range was much broader in the former (16- versus 3-fold, respectively) (Figure 5.1A). By IHC, PCFT proteins were substantially increased (3.8-fold) in NS-NSCLC specimens ($n = 61$) over normal lung ($n = 10$) ($P < 0.001$) and again showed a broad expression pattern (~150-fold for NS- NSCLC and ~4-fold for normal lung, respectively) (Figure 5.1G-H). Representative IHC sections for NS-NSCLC specimens expressing low, intermediate, and high PCFT levels are shown in Figure 5.2C. For both RT-PCR and IHC analyses, there were no significant changes in PCFT levels with tumor stage.

Transcript levels for other genes relevant to antitumor efficacy of this series of compounds were also measured in the clinical specimens, including folate transporters (RFC, FRα) and metabolism enzymes (TS, GARFTase, and FPGS) (Figure 5.1B-F). Transcripts for all these genes were detected. Transcript levels were increased in NS-NSCLC ($n = 26$) compared with normal lung ($n = 8$) for TS (median 2.25-fold increased; $P < 0.015$) and GARFTase (median ~2-fold increased; $P < 0.0001$). Slightly decreased median RFC transcript levels (2.64-fold; $P < 0.016$) were measured in the NS-NSCLC specimens. Although median FRα and FPGS levels

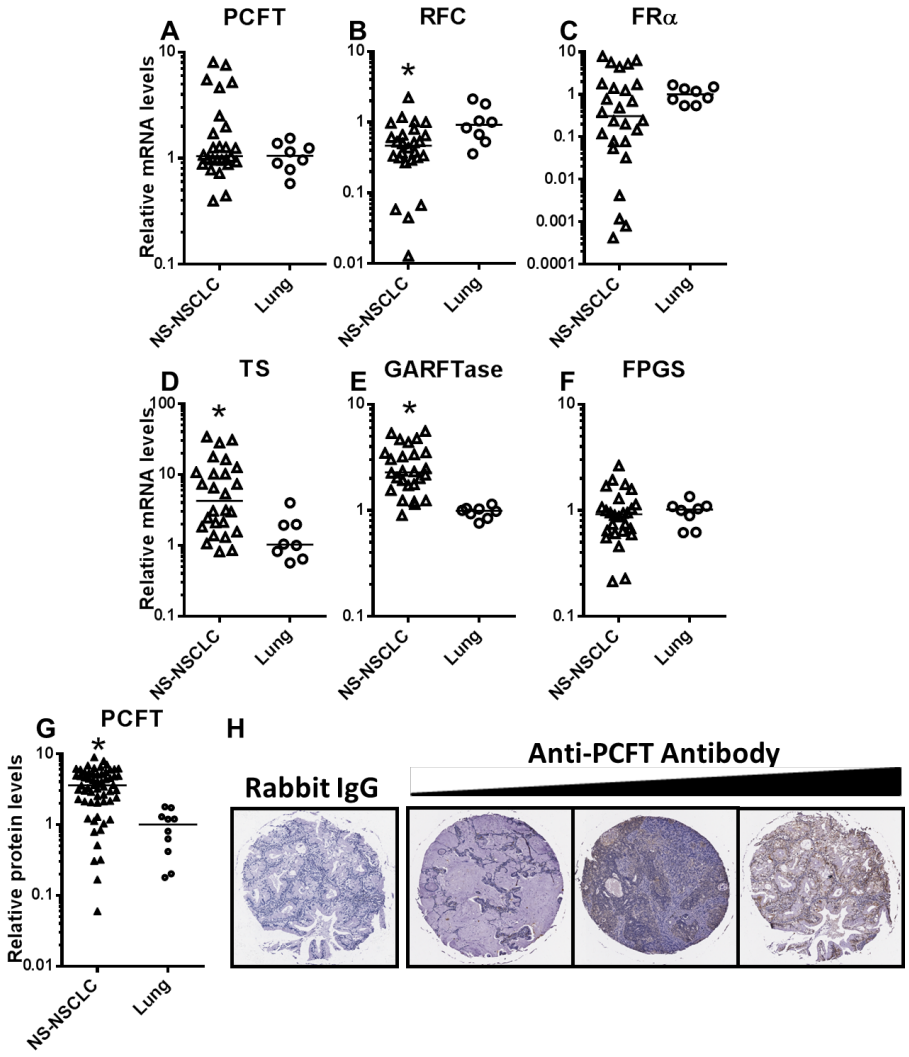

Figure 5.1 PCFT expression in primary NS-NSCLC and normal lung specimens. *Panels A-F,* Results for quantitative real-time RT-PCR are shown for 26 NS-NSCLC and 8 normal lung specimens (Origene). Gene transcript levels were normalized to transcript levels for β-actin. The median value for the normal lung specimens was assigned a value of 1. *Panels G and H,* IHC results are shown for 61 NS-NSCLC and 10 normal lung tissues from a tissue microarray (TMA) (US Biomax, Inc.). The TMA was incubated with affinity-purified PCFT-specific antibody or rabbit IgG, and the slides were developed, counterstained, and mounted, as described in Materials and Methods. Representative images are shown in (*Panel H*) for IgG and for three NS-NSCLC specimens with low-, intermediate-, and high-level staining (left to right). The slides were scanned by an Aperio Image Scanner (Aperio Technologies, Inc.) for microarray image scanning. The total positive cell numbers and intensity of antibody staining of each tissue core were computed and are shown in *Panel G*. The median value for the normal lung specimens was assigned a value of 1. Statistical significance between the groups was analyzed by the student's t test. An asterisk indicates a statistically significant difference between the median NS-NSCLC value and the median value for the normal lung specimens ($p < 0.001$). Figure previously published in Wilson et. al. Mol Pharmacol. 2016.

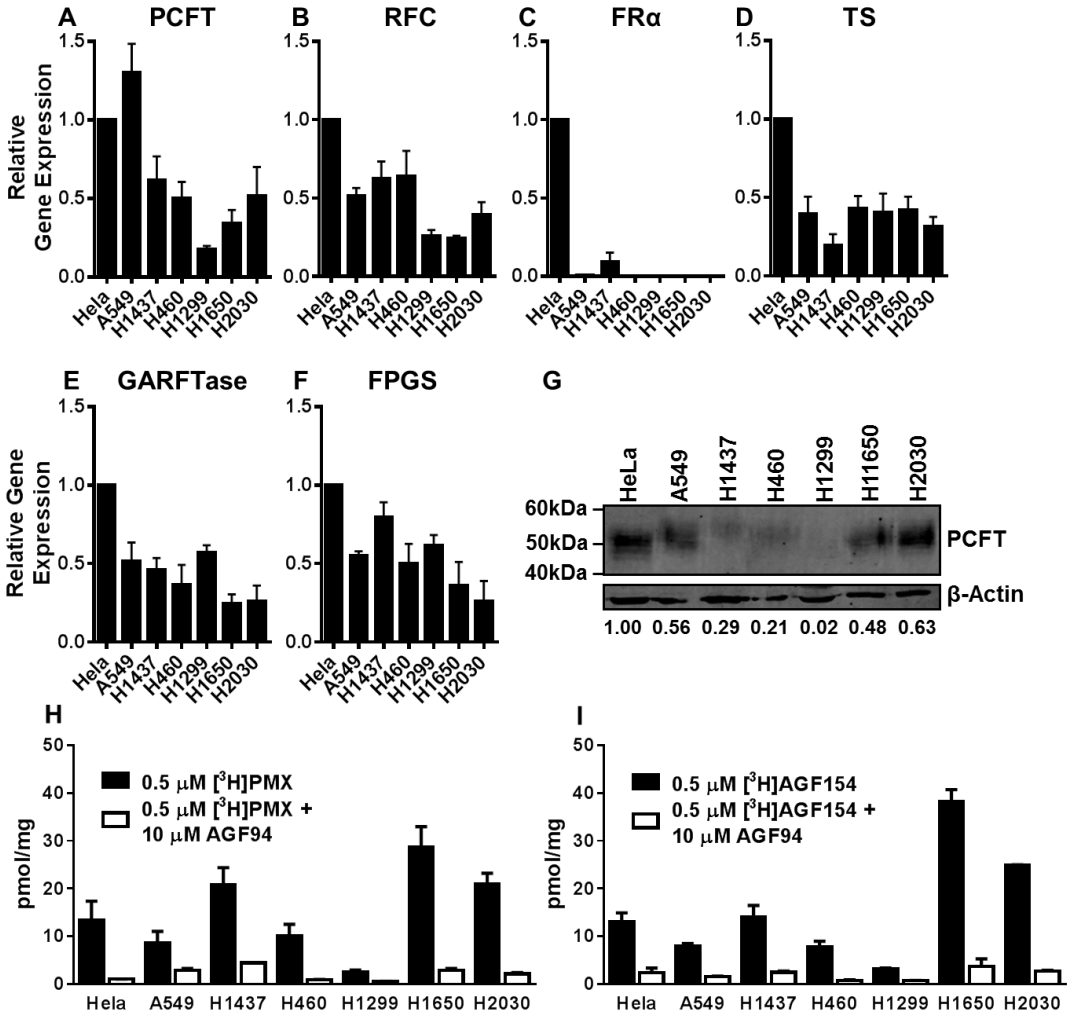

Figure 5.2 PCFT expression and function in NS-NSCLC cell lines. *Panels A-F,* Results are shown for gene transcript levels measured by real-time RT-PCR in NS- NSCLC cell lines (A549, H1437, H460, H1299, H1650, and H2030). Gene transcript levels were normalized to transcript levels for β-actin. The gene transcript level for the HeLa cell line was assigned a value of 1. Results are shown as mean ± S.E. values from triplicate experiments. *Panel G,* Particulate membrane fractions were prepared as described in Materials and Methods. Membrane proteins (30 mg) from human tumor cell lines were electrophoresed on a 7.5% polyacrylamide gel and immunoblotted with human PCFT polyclonal antibody. β-actin levels were used as loading controls. Densitometry was performed using Odyssey software, and PCFT protein expression was normalized to β-actin. Normalized densitometry results (as an average from three experiments) are shown. *Panels H and G,* NS-NSCLC cells (in 60-mm dishes) were treated with 0.5 mM [^{3}H]PMX or [^{3}H]AGF154 at pH 5.5 and 37°C for 5 minutes (black bars). Nonradioactive AGF94 (10 mM) was added to competitively block PCFT-mediated uptake as a negative control for PCFT transport (white bars). Internalized pmol values of [^{3}H]PMX or [^{3}H]AGF154 were normalized to total cell proteins and expressed as pmol/mg. Histograms show mean 6 S.E. values from triplicate experiments. Figure previously published in Wilson et. al. Mol Pharmacol. 2016.

were unchanged between NS-NSCLC and normal lung specimens, the range was much broader for the tumors (from 13-fold for FPGS and ~2000-fold for FRα, compared with 2- to 3-fold for normal lung for both FPGS and FRα). Collectively, these results establish high-level expression of PCFT in NS-NSCLC, along with appreciable expression of other folate-related genes. Although FRα is expressed in NS-NSCLC, its levels were highly variable.

5.3.2 Expression Profiles for Folate Transport and Metabolism Genes in NS-NSCLC Cell Lines

We extended our gene expression analysis to NS-NSCLC cell lines, including A549, H1437, H460, H1299, H1650, and H2030. For these experiments, HeLa cells were used as a positive control since HeLa cells express abundant RFC and PCFT accompanying low levels of FRα (Kugel Desmoulin et al., 2011). PCFT was expressed in the six NS-NSCLC cell lines over a ~13-fold range, with the highest transcript levels in A549 cells and a very low level in H1299 cells (Figure 5.2A). Correlations between levels of PCFT transcripts by real-time RT-PCR and PCFT proteins on western blots probed with PCFT antibody (Figure 5.2G) were inexact. For H1299 cells, PCFT protein was undetectable. FRα was undetectable in five out of six of the NS-NSCLC cell lines, the only exception being the H1437 cell line (expresses ~9% of the FRα levels in HeLa cells) (Figure 5.3A). RFC, TS, GARFTase and FPGS transcripts were expressed at similar levels among the various NS-NSCLC cell lines (Figure 5.2B-F).

5.3.3 PMX and AGF154 Transport by PCFT in NS-NSCLC Cell Lines

The 5-substituted pyrrolo[2,3-d]pyrimidine antifolate PMX is a transport substrate for both RFC and PCFT (Matherly et al., 2014). Unlike PMX, the 6-pyrrolo[2,3-d] pyrimidine thienoyl analogs AGF94 and AGF154 are highly selective transport substrates for PCFT over

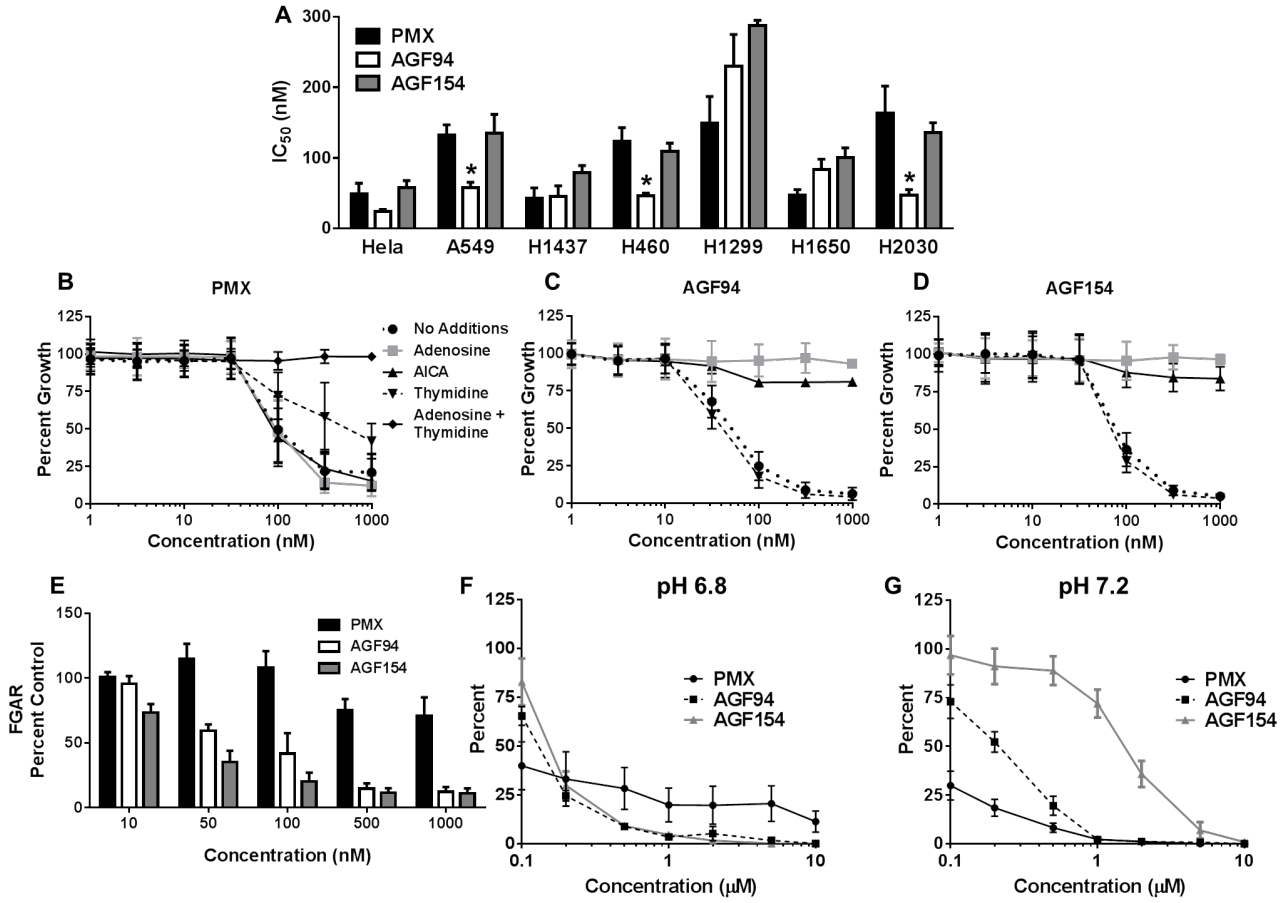

Figure 5.3 *In vitro* characterization of PMX, AGF94 and AGF154 of NS-NSCLC cell lines. *Panel A,* NS-NSCLC cells were seeded in 96-well plates at 1500–4000 cells/ well in complete folate-free RPMI 1640 (pH ~7.2), 10% dialyzed fetal bovine serum, and 25 nM LCV. Cells were incubated with varying concentrations of PMX, AGF94, or AGF154 from 1 to 1000 nM for 4 to 5 days, depending on the cell line. Cell viabilities were determined with a fluorescence-based assay (Cell Titer Blue). Mean IC50 6 S.E. values from triplicate experiments were determined graphically for each drug. Asterisks designate statistically greater sensi- tivity for AGF94 compared with PMX (P , 0.01). *Panels B-D,* H460 cells were seeded in the presence of 0-1000 nM PMX, **C1** or **C2**, with or without additions of 60 μM adenosine, 320 μM 5-aminoimidazole-4-carboxamide (AICA), 10 μM thymidine, or adenosine plus thymidine. Cell viabilities were determined with a fluorescence-based assay (Cell Titer Blue™). *Panel E,* Incorporation of [^{14}C(U)]glycine into [^{14}C]formyl glycinamide ribonucleotide (GAR) as an *in situ* measure of endogenous GARFTase was determined. For the GARFTase assays, IC_{50} values were 78.9 nM and 27.1 nM for **C1** and **C2**, respectively. For PMX, the IC_{50} value was >1000 nM. Experimental details are described in Materials and Methods. For *Panels A-E*, the plots show mean values ± standard errors and represent triplicate experiments. *Panels F and G,* H460 cells (100–150 cells) were plated in 60-mm dishes in complete folate-free RPMI 1640 (pH 7.2), 10% dialyzed fetal bovine serum, and 25 nM LCV. After 24 hours, cells were then treated with PMX, AGF94, or AGF154 at varying concentrations in complete folate-free RPMI 1640 (at pH 7.2 or 6.8) supplemented with 25 nM LCV. After an additional 24 hours, cells were rinsed with PBS, and then incubated in complete folate-free RPMI 1640 supplemented with 25 nM LCV (pH 7.2) for 9

days. Colonies were stained with methylene blue and counted, and colony numbers were normalized to the controls. Plots show mean ± S.E. values, representative of triplicate experiments. Figure previously published in Wilson et. al. Mol Pharmacol. 2016.

RFC, although both are also FRα substrates (Cherian et al., 2013; Desmoulin et al., 2012b; Wang et al., 2011; Wang et al., 2015). To demonstrate that the PCFT proteins detected on western blots in A549, H1437, H460, H1650, and H2030 NS-NSCLC cell lines could transport [^{3}H] PMX and [^{3}H]AGF154, we measured cellular uptake of these compounds (both at 0.5 μM; 5 minutes; 37°C) at pH 5.5, the PCFT pH optimum. An excess (10 μM) of unlabeled AGF94 was added as a competitive inhibitor of PCFT to confirm the PCFT- specific uptake component.

The NS-NSCLC cell lines accumulated [^{3}H]PMX and [^{3}H]AGF154 over 5 minutes to generally similar extents (Figure 5.2H-I), but only partially reflected levels of PCFT proteins (Figure 5.2G). For instance, PCFT proteins were generally proportional to transport of both [^{3}H]PMX and [^{3}H]AGF154 for the H1437, H460, H1299, H1650, and H2030 cell lines; however, transport was disproportionately low for A549 cells. For both [^{3}H]PMX and [^{3}H]AGF154, uptake was blocked (~80%–95%) by nonradioactive AGF94. For PCFT-selective [^{3}H]AGF154, uptake for five of the NS-NSCLC cell lines far exceeded the low residual level measured in the H1299 cells ($P < 0.05$).

5.3.4 Antiproliferative and Cytotoxic Activities of AGF94 and AGF154 Toward NS-NSCLC Sublines Reflect Inhibition of GARFTase in De Novo Purine Nucleotide Biosynthesis

To evaluate the antiproliferative potencies of the 6-substituted pyrrolo[2,3-d]pyrimidine thienoyl antifolates AGF94 and AGF154 compared with PMX toward the NS-NSCLC cell lines, we performed cell outgrowth assays. Cells were treated in the presence of the drugs for 4 to 5 days and cell proliferation was assayed with a fluorescence-based assay (i.e., CellTiter Blue) to calculate the IC_{50} values corresponding to drug concentrations that inhibit growth by 50%. Under these conditions, the pH of the culture medium decreased to ~pH 6.7–6.8 (Kugel Desmoulin et al., 2010). The NS-NSCLC cell lines were sensitive to AGF94 and AGF154 (Figure 5.3A), with AGF94 IC_{50} values ranging from 45 nM (H1437) to 230 nM (H1299), and AGF154 IC_{50}s

ranging from 79 nM (H1437) to 288 nM (H1299). The PMX IC_{50} values ranged from 43 nM (H1437) to 163 nM (H2030). Interestingly, the A549, H460, and H2030 cell lines were all more sensitive to AGF94 than to PMX ($p < 0.05$). Resistance of the H1299 cell line to AGF94 and AGF154 likely reflects the lack of detectable PCFT protein (Figure 5.2G) and limited PCFT transport (Figure 5.2H-I). Although [^{3}H]PMX uptake by PCFT was also low in H1299 cells (Figure 5.2H), this was not manifested as PMX resistance (Figure 5.3A), likely reflecting RFC transport of PMX (Matherly et al., 2014).

For additional experiments, we used H460 NS-NSCLC cells, reflecting their moderate and proportional level of PCFT protein and transport (Figure 5.2G-I). In H460 cells, AGF94 and AGF154 inhibited *de novo* purine nucleotide biosynthesis at the step catalyzed by GARFTase, as reflected in protection from growth inhibition by adenosine (60 μM) and AICA (320 μM), but not by thymidine (10 μM) (Figure 5.3C-D). GARFTase inhibition in H460 cells was confirmed with a cell-based *in situ* assay that measures [^{14}C(U)]glycine incorporation into the GARFTase product, [^{14}C]formyl glycinamide ribonucleotide (Figure 5.3E) (Kugel Desmoulin et al., 2010; Wang et al., 2011; Wang et al., 2015). IC_{50} values for in situ GARFTase inhibition of 78.9 and 27.1 nM were measured for AGF94 and AGF154, respectively. AGF94 and AGF154 have been previously described as GARFTase inhibitors in other tumor models (Wang et al., 2011; Wang et al., 2015). By *in vitro* assays with isolated GARFTase, K_i values of 68 nM for AGF94 and 11 nM for AGF154 have been previously reported (Wang et al., 2015), paralleling IC_{50} values from the *in situ* GARFTase assays in H460 cells.

We assessed cytotoxicity resulting from exposure of H460 cells to AGF94, AGF154, or PMX, following treatment with drugs (0.1–10 μM) for 24 hours at pH 6.8 or 7.2 (approximating the microenvironment pH of many solid tumors and normal tissues, respectively) (Gallagher et

al., 2008; Gillies et al., 2002; Webb et al., 2011). Cells were then washed with PBS and incubated in drug-free medium for 9 days (at neutral pH), at which time colonies were stained with methylene blue and counted. Both AGF94 and AGF154 showed a steep concentration-dependent decrease in colony formation following drug treatments at pH 6.8, with a complete loss of clonogenicity at 10 μM (Figure 5.3F). Conversely, while PMX was more active than AGF94 or AGF154 at 0.1 μM, the dose-response relationship for PMX at pH 6.8 was shallow and incomplete (~10%), even at 10 μM drug. However, following treatment at pH 7.2, PMX showed a dramatically enhanced dose-responsive decrease in colony formation, whereas AGF94 and AGF154 showed progressively impaired responses (Figure 5.3G). These results demonstrate selective antitumor efficacy of the novel 6-substituted pyrrolo [2,3-d]pyrimidine antifolates AGF94 and AGF154 compared with PMX at a pH characterizing the tumor microenvironment versus neutral pH typical of most normal tissues. Collectively, these studies establish that AGF94 and AGF154 are cytotoxic toward H460 NS-NSCLC cells associated with inhibition of GARFTase and de novo purine nucleotide biosynthesis.

5.3.5 Impact of Knockdown of PCFT on PMX and AGF154 Transport and Antitumor Drug Efficacy

The results shown in Figure 5.2H and I demonstrate that both [^{3}H]PMX and [^{3}H]AGF154 are transported by PCFT into the NS-NSCLC cell lines. However, PMX (unlike AGF154) is also transported by RFC (Matherly et al., 2014). To directly examine the impact of this apparent transport redundancy by PCFT and RFC on PMX cellular uptake and antitumor efficacy compared with AGF94 and AGF154, we tested five lentiviral shRNAs for knockdown of PCFT in H460 NS-NSCLC cells. For the shRNA construct with the greatest knockdown, two clonal PCFT KD cell lines, KD-3 and KD-4, were developed, both of which showed significant loss of

PCFT gene expression (~2.7- and ~3.3-fold decreases, respectively), compared with NTC cells or wild-type (i.e., nontransduced) H460 cells (Figure 5.4A). PCFT protein levels were also reduced in KD-3 and KD-4 sublines (29% and 19% of the NTC level by densitometry) (Figure 5.4B). There were no significant differences in transcript levels for RFC, TS, GARFTase, and FPGS between KD and NTC cells (data not shown), suggesting no significant off-target effects. Furthermore, there were no significant differences in rates of cell proliferation between KD and NTC cells (data not shown).

We also measured PCFT-specific transport activity for KD-3 and KD-4 cells with [^{3}H]PMX and [^{3}H]AGF154 (both at 0.5 mM) over 2 minutes at 37°C and pH 5.5 in the presence and absence of 10 mM nonradioactive AGF94 (Figure 5.4C and D, respectively). PCFT-selective uptake for both substrates decreased in KD-3 and KD-4 cells compared with the NTC (~70% and ~80% for [^{3}H] AGF154 and [^{3}H]PMX, respectively, calculated from the difference with and without AGF94 competitor), paralleling changes in PCFT transcripts and proteins.

To extend these studies to analyses of drug sensitivities, we assessed *in vitro* antitumor efficacies of PMX, AGF94, and AGF154 toward KD-3 and KD-4, compared with NTC and wild-type H460 cells. Results were compared with those for PT523, a RFC-selective antifolate

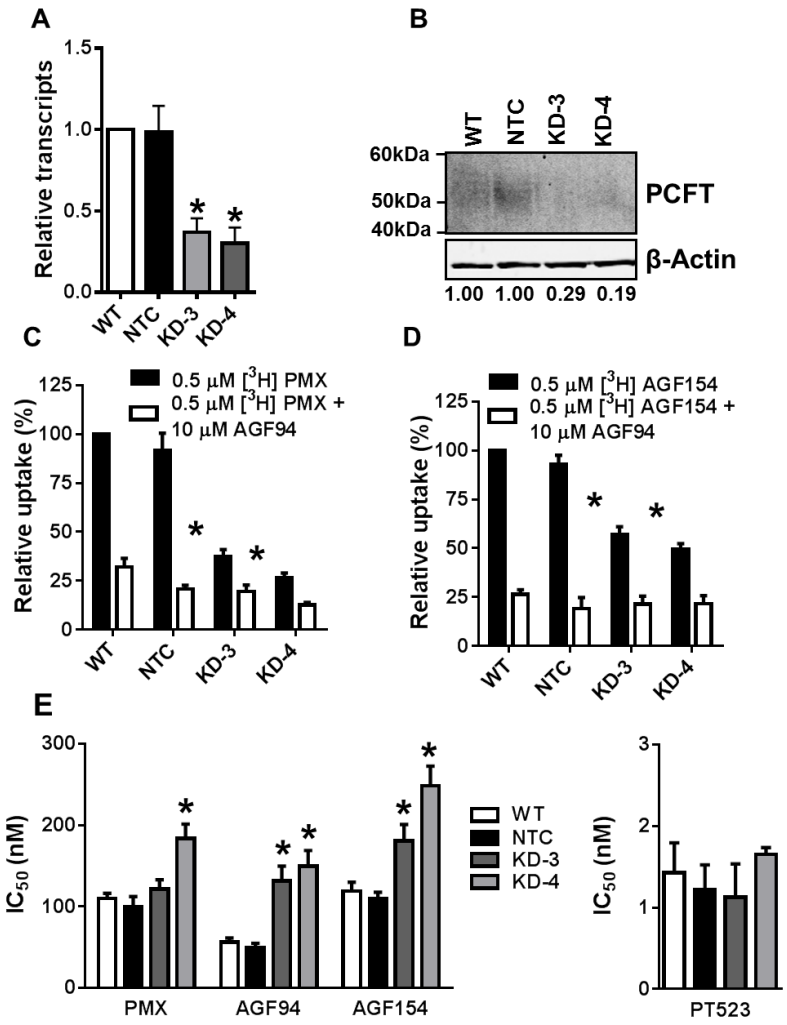

Figure 5.4 Characterization of H460 PCFT KD cells. *Panel A,* Real-time RT-PCR was used to measure transcript levels for PCFT in H460 wild-type (WT), NTC, KD-3, and KD4 cells. Transcript levels were normalized to β-actin and results are presented relative to those for WT H460 cells (assigned a value of 1). Results are expressed as mean ± S.E. values and represent triplicate experiments. The asterisks indicate a statistically significant difference between the PCFT KD gene expression and that for the NTC cells ($p < 0.05$). *Panel B,* H460 particulate membrane fractions were isolated as described in Materials and Methods. Membrane proteins (30 mg) from WT, NTC, KD-3, and KD4 H460 cell lines were electrophoresed on a 7.5% polyacrylamide gel and immunoblotted with PCFT antibody. β-actin protein levels were used as loading controls. Densitometry was measured using Odyssey software, and PCFT protein expression was normalized to β-actin. Normalized densitometry results (average from four experiments) are noted below each lane. *Panels C and D,* WT, NTC, KD-3, and KD-4 H460 cells (in 60-mm dishes) were incubated with 0.5 mM [^{3}H]PMX and [^{3}H]AGF154 at pH 5.5 and 37°C, with or without 10 mM nonradioactive AGF94 for 2 minutes. Internalized [^{3}H]PMX or [^{3}H]AGF154 was normalized to total cell protein and results calculated as pmol/mg. Uptake results are presented as relative uptake with WT H460 cells assigned a value of 100%. Results are expressed as mean ± S.E. values, representative of triplicate experiments. The asterisks indicate a statistically significant difference between the PCFT transport activity in the KD (KD-

3 and KD-4) cells and that of the NTC cells ($p < 0.05$). *Panel E,* The H460 sublines including WT, NTC, KD-3, and KD-4 H460 cells were cultured in complete folate-free RPMI 1640 with 25 nM LCV in 96-well plates at 1500 cells/well with varying concentrations of PMX, AGF94, AGF154 (left panel), or PT523 (right panel) for 4 days. Viable cells were measured by a fluorescence-based assay (Cell Titer Blue) and IC_{50} values were determined graphically. Results are expressed as mean IC_{50} ± S.E. values from triplicate experiments (the asterisk indicates where IC_{50} values for PCFT KD cells are significantly greater than for NTC; $p < 0.05$). Figure previously published in Wilson et. al. Mol Pharmacol. 2016.

with no PCFT transport activity (Rosowsky et al., 1994; Wang et al., 2010). Both KD and NTC cells were highly sensitive to the growth inhibitory effects of PT523 (Figure 5.4E, right panel). In contrast, the IC_{50} values in the KD cells were significantly increased for both AGF94 (2.7- and 3.0-fold increases for KD-3 and KC-4, respectively) and AGF154 (1.7- and 2.3-fold increases for KD-3 and KC-4, respectively) (Figure 5.4, left panel). This further establishes the reliance on PCFT membrane transport for AGF94 and AGF154 drug efficacy. For PMX, a similar, albeit lesser, impact on drug sensitivity was observed for KD-3 and KD-4 cells (1.2- and 1.8-fold decreases, respectively) (Figure 5.4E, left panel), suggesting a reduced dependence on PCFT transport for PMX antitumor efficacy, likely reflecting its RFC substrate activity.

5.3.6 Effects of AGF94 on NS-NSCLC Tumor Growth *In Vivo*

To assess antitumor effects of AGF94 in the context of NS-NSCLC *in vivo*, we performed antitumor efficacy studies with 8-week-old female ICR SCID mice implanted subcutaneously with H460 tumor fragments. Mice were maintained *ad libitum* on a folate-deficient diet in order to decrease serum folates to levels approximating those seen in humans (Alati et al., 1996; Wang et al., 2010; Wang et al., 2011; Wang et al., 2015). Control and drug treatment groups were nonselectively randomized (five mice/group), and AGF94 (32 mg/kg), gemcitabine (125 mg/kg), or cisplatin (2.4 mg/kg) was administered intravenously on days 1, 5, 9, and 13 after tumor implantation. Treatment regimens were based on the efficacious dose range for each of the drugs (i.e., the highest nontoxic total dose range), as tolerated by SCID mice on an every fourth day for four times schedule [the in-house highest nontoxic total dose ranges were as follows: AGF94 (96–160 mg/kg); gemcitabine (450–750 mg/kg), and cisplatin (8–12 mg/kg)]. Mice were observed and weighed daily; tumors were measured two-to-three times per week.

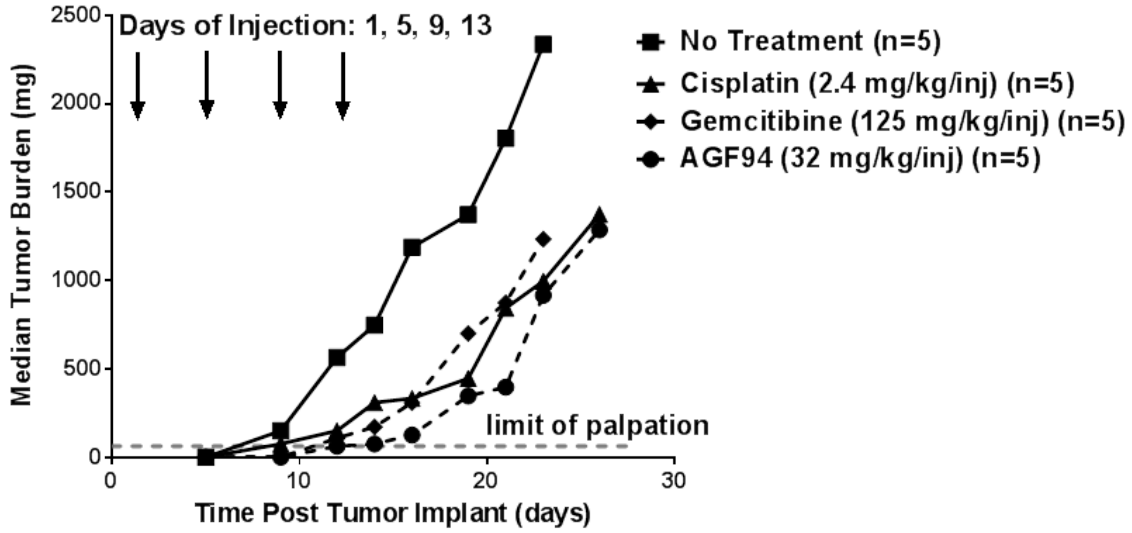

Figure 5.5 Analysis of *in vivo* efficacy of AGF94. An *in vivo* efficacy trial of AGF94 in H460 xenografts was performed. Female ICR SCID mice were maintained on a folate-deficient diet *ad libitum*. Human H460 tumors were implanted bilaterally and subcutaneously, and mice were nonselectively randomized into five mice per group. AGF94 [32 mg/kg injection, dissolved in 5% ethanol (v/v), 1% Tween 80 (v/v), and 0.5% NaHCO3], gemcitabine (125 mg/kg injection, dissolved in 0.9% saline), and cisplatin (2.4 mg/kg injection, dissolved in 0.9% saline) were administered on a schedule of every 4 days for four intravenous treatments on days 1, 5, 9, and 13 (indicated by arrows). Mice were observed and weighed daily; tumors were measured 2 to 3 times per week. On day 16, T/C values equaled 11%, 26%, and 28% for AGF94, gemcitabine, and cisplatin, respectively. Antitumor activities were recorded for AGF94 (T–C = 9 days; 1.9 gross $\log_{10}$ kill), gemcitabine (T–C = 7 days; 1.5 gross $\log_{10}$ kill), and cisplatin (T–C = 8 days, 1.7 gross $\log_{10}$ kill). Data are shown for the median tumor burdens of each treatment group. Figure previously published in Wilson et. al. Mol Pharmacol. 2016.

AGF94 showed greater efficacy toward H460 xenografts (T/C 5 11%; T–C 5 9 days; 1.9 gross log_{10} kill) than either cisplatin (T/C 5 28%; T–C 5 8 days; 1.7 gross log_{10} kill) or gemcitabine (T/C 5 26%; T–C 5 7 days; 1.5 gross log_{10} kill) (Figure 5.5). The drugs appeared to be well tolerated and there was no drug-related lethality. Minimal adverse toxicities occurred and there was no evidence of organ-related toxicities. The only dose-limiting symptom was weight loss. For cisplatin and gemcitabine, mice sustained weight losses of 19.8% with a nadir on days 20–22, and 5.9% with a nadir on day 15, respectively. Full recovery did not occur prior to sacrifice due to the mice reaching the tumor burden limit [94% weight recovery for cisplatin within 4 days postnadir (day 26) and 99% weight recovery for gemcitabine 9 days postnadir (day 24)]. For AGF94, 14% maximal weight loss was measured on day 7 post-treatment, with full weight recovery by day 16. These results demonstrate potent in vivo efficacy of AGF94 toward H460 lung cancer xenografts.

5.4 Discussion

The potential utility of the 2',4', and 2',5' thienoyl pyrrolo [2,3-d]pyrimidine antifolates, AGF94 and AGF154, for selective targeting of ovarian cancer and malignant mesothelioma via FRα and/or PCFT over RFC, has been previously reported (Cherian et al., 2013; Wang et al., 2011; Wang et al., 2015). In this chapter, we extended this work to NS-NSCLC, a disease for which PMX is heavily used in both first-line and maintenance therapies (Genova et al., 2013; Gerber and Schiller, 2013; Tomasini et al., 2013). However, only about one-third of patients with NS-NSCLC respond to PMX, such that the median progression-free survival is only ~6 months in the front-line setting, when combined with platinum, and ~4 months as a single agent in patients with recurrent NS-NSCLC (Esteban et al., 2009).

Our investigation of NS-NSCLC clinical specimens and cell lines established that PCFT transcripts and proteins are significantly expressed in NS-NSCLC, along with RFC and FRα. PCFT protein levels were increased in primary NS-NSCLC over normal lung specimens, although there was no association of PCFT levels with tumor stage. In our analysis, FRα transcripts were variably expressed in primary NS-NSCLC, and FRα was detected in only one of the NS-NSCLC cell lines (H1437). A wide range of FRα expression in NSCLC has been previously reported (Christoph et al., 2013; Nunez et al., 2012; O'Shannessy et al., 2012) suggesting that a subset of these patients might be amenable to FR-targeted therapies (Assaraf et al., 2014; Vergote and Leamon, 2015), whereas patients with lower FRα levels might be better treated with other therapies.

We demonstrated high levels of PCFT transport in five out of six NS-NSCLC cell lines, using radiolabeled PMX and AGF154 as surrogate substrates, accompanying detection of PCFT transcripts and proteins. Correlations between levels of PCFT transcripts and proteins, or between PCFT proteins and transport activity, were inconsistent for the NS-NSCLC cell lines, suggesting involvement of post-transcriptional and post-translational regulatory mechanisms. Similar results were previously reported for PCFT (Kugel Desmoulin et al., 2011) in a disparate panel of human tumor cell lines, implying a post-translational regulation of PCFT. For H1299 NS-NSCLC cells, a lack of detectable PCFT protein was accompanied by very low levels of transport activity. PCFT transport of PMX and AGF154 in H460 cells was further confirmed by PCFT knockdowns. Although *in vitro* AGF94 and AGF154 antitumor efficacies were significantly decreased in the PCFT KD cells, this effect was reduced for PMX, likely reflecting transport promiscuity for PMX with both PCFT and RFC.

PCFT transport of AGF94 and AGF154 into H460 cells was accompanied by inhibition of cellular GARFTase in *de novo* purine nucleotide biosynthesis, and resulted in inhibition of cell proliferation, even at comparatively neutral pH levels. Growth inhibition, as reflected in IC_{50} values, was generally on par with that for PMX, although increased sensitivity was measured for AGF94 toward A549, H460, and H2030 NS-NSCLC cells. The basis for this is unclear. *In vivo* AGF94 efficacy against an H460 tumor xenograft was also demonstrated, with T/C, T–C, and log_{10} cell kill values modestly superior to those for cisplatin and gemcitabine. These results provide proof-of-principle validation of our *in vitro* findings that antitumor effects of targeted AGF94 may be equally potent, if not more potent, than standard chemotherapies used to treat NS-NSCLC. Unfortunately, direct *in vivo* comparisons of AGF94 efficacy with PMX were not possible due to elevated serum thymidine in mice, which circumvents antitumor efficacy of TS inhibitors in the presence of thymidine kinase (van der Wilt et al., 2001).

The results of colony-forming assays with H460 cells treated with AGF94 and AGF154 at pH 6.8, conditions that approximate the pH of the tumor microenvironment (Gallagher et al., 2008; Gillies et al., 2002; Webb et al., 2011)and favor PCFT over RFC transport, were of particular interest. At pH 6.8, cytotoxicity for the 6-pyrrolo[2,3-d]pyrimidines AGF94 and AGF154 was clearly evident, whereas for PMX cytotoxicity was modest and incomplete up to 10 mM drug. Conversely, PMX treatment at pH 7.2 potently inhibited clonogenicity, with progressively reduced effects for AGF94, followed by AGF154. Thus, our results document selective antitumor efficacies of the novel 6-substituted pyrrolo [2,3-d]pyrimidine antifolates AGF94 and AGF154 compared with PMX at a pH characterizing the tumor microenvironment versus a neutral pH characteristic of most normal tissues. Accordingly, transport specificities of AGF94 and AGF154 for PCFT over RFC should confer selectivity for tumors including NS-

NSCLC cells that express PCFT, which would be augmented by increased transport activity in the acidic microenvironment typical of many tumors. By this reasoning, PMX might be expected to show greater cytotoxicity than AGF94 or AGF154 toward normal tissues, where RFC transport prevails over PCFT and neutral pH favors RFC transport. As previously noted, since a subset of NS-NSCLC specimens also express significant FRα (Christoph et al., 2013; Nunez et al., 2012; O'Shannessy et al., 2012), increased tumor targeting of AGF94 and AGF154 via FRα in addition to PCFT (Wang et al., 2015; Webb et al., 2011) may also occur. The net effect of these targeted therapies would be increased killing of tumors, while decreasing toxicity toward normal tissues.

CHAPTER 6- EFFECTS OF FLUORINATION ON ANTI-TUMOR EFFICACY OF NOVEL 6-SUBSTITUTED PYRROLO[2,3-*d*]PYRIMIDINE ANTIFOLATES

6.1 Introduction

In recent years, there has been in interest in treating ovarian cancer with folate receptor-targeted agents (see Chapter 1.6.6) (Lorusso et al., 2012; Naumann et al., 2013; Siegel et al., 2003). FRα has been shown to be overexpressed in ovarian cancers, with the expression level correlating with histological grade (Buist et al., 1995; Garin-Chesa et al., 1993; Siu et al., 2012; Toffoli et al., 1997; Veggian et al., 1989). Ovarian cancer is the most lethal of gynecological cancers, with an estimated 22,280 new cases and 14,240 deaths resulting from ovarian cancer in the United States in 2016 (Siegel et al., 2016). The 5-year survival rate is only 10-25% for epithelial ovarian cancer patients, and this disease often recurs after initial treatment (Siegel et al., 2016). Beyond platinum-based therapies, against which many tumors can develop resistance, clinicians have few treatment options at their disposal (Temkin et al., 2016).

Recently, there has been an interest in the development of FRα-targeted therapies for the treatment of ovarian cancer (see Chapter 1.6.6). FRα shows an increased expression in a subset of ovarian cancer patients (Elnakat and Ratnam, 2004; Leamon et al., 2013; Toffoli et al., 1997; Vergote et al., 2015). While FRα is only expressed on the apical membrane of normal ovarian epithelial cells, in ovarian tumor cells FRα is exposed to the circulation, creating an opportunity for tumor targeting via FRα uptake (Assaraf et al., 2014; Vergote et al., 2015). Additionally, our laboratory recently described a substantial expression of PCFT protein in ovarian cancer patients (Z. Hou and L. H. Matherly, manuscript submitted), suggesting a potential for PCFT-targeted therapies for ovarian cancer.

Progress has been made in the development of tumor-targeted antifolate molecules based on their selective transport by FRs and PCFT over RFC. Previously, we described the 6-

substituted pyrrolo[2,3-*d*]pyrimidine benzoyl *L*-glutamate antifolates AGF17 and AGF23 (Figure 6.1) as GARFTase inhibitors which are transported by PCFT and FRα more favorably than RFC (see Chapter 1.6.7) (Deng et al., 2008; Gangjee et al., 2005; Gangjee et al., 2004; Kugel Desmoulin et al., 2010). Replacements of the side-chain benzoyl group with a thiophene resulted in novel compounds AGF150 and AGF117, respectively (Figure 6.1) (Wang et al., 2012; Wang et al., 2015), related to our lead compound AGF94 (see Chapter 5), while replacement of the benzoyl moiety of AGF23 by a pyridine resulted in AGF107 (Figure 6.1) (C. George and L. H. Matherly, unpublished). We previously described potent antitumor efficacy by our lead compound AGF94 (see Chapter 5) toward ovarian cancer cell lines *in vitro* as well as *in vivo* (Wang et al., 2011; Wang et al., 2015) (Z. Hou and L. H. Matherly, manuscript submitted). AGF117, AGF150, and AGF107, like AGF17, AGF23, and AGF94 are all selective for PCFT and FR cellular uptake over RFC.

In this chapter, we describe further modifications to these novel antifolate compounds through the addition of fluorine to the side-chain benzoyl and thionyl groups. Fluorine modifications of drugs have ample precedent and can improve potency and impact selectivity of drugs by altering pKa, lipophilicity and hydrophobic interactions, modifying conformation, or any combination of these possibilities (Gillis et al., 2015). Additionally, fluorine-labeled antifolates have potential clinical applications as theranostic agents, as PET imaging using ^{18}F-labeled drugs can provide valuable tumor imaging data, as well as providing a measurement of drug uptake for individual patients (Basu and Alavi, 2016). In this chapter, we describe five novel antifolates containing fluorine ring substitutions and studies of their specificities for RFC,

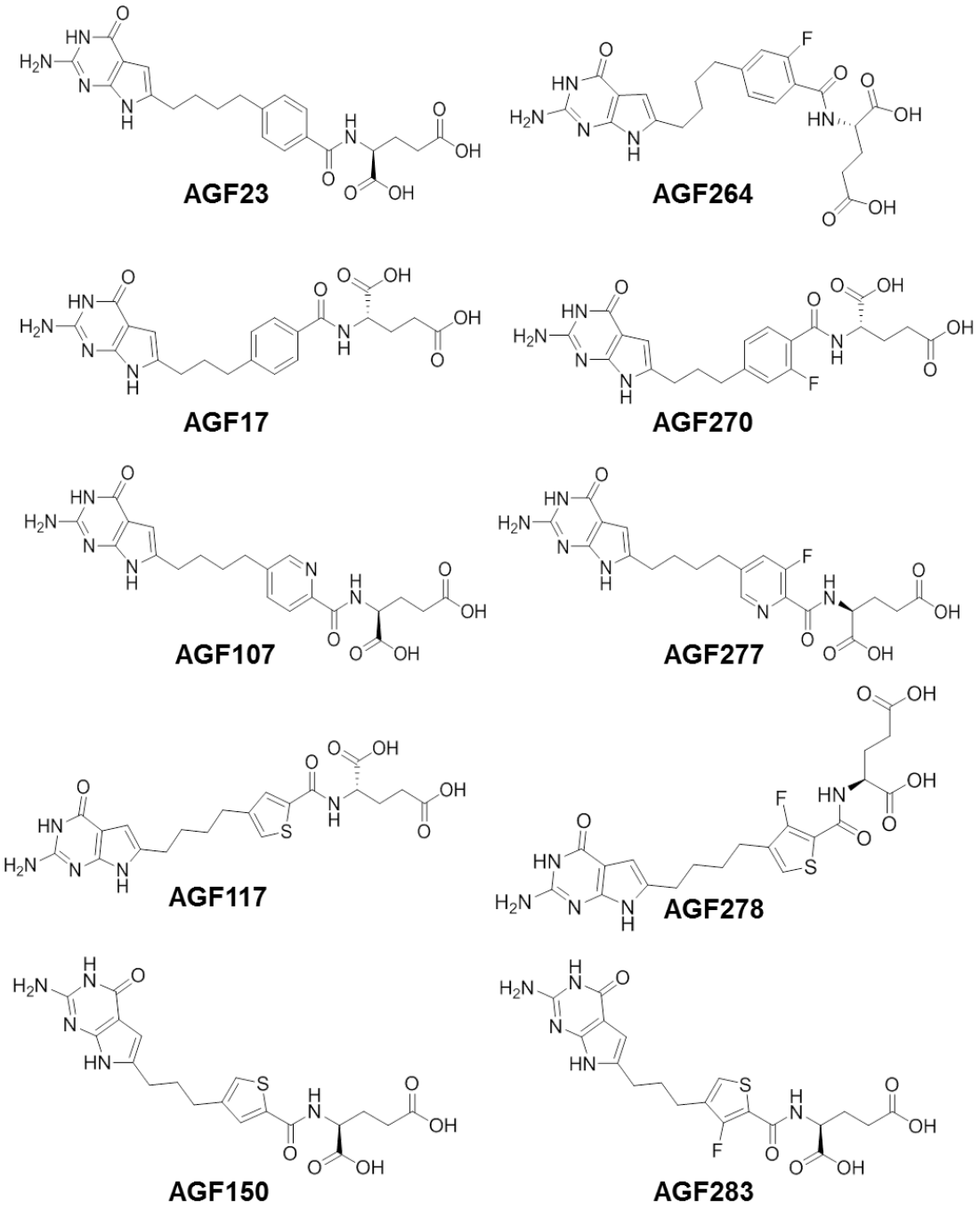

Figure 6.1 Structures of novel fluorinated antifolates. Structures are shown for both previously established parent compounds (AGF17, AGF23, AGF107, AGF117 and AGF150) and novel fluorinated compounds (AGF264, AGF270, AGF277, AGF278, AGF283). All compounds were synthesized by Dr. Aleem Gangjee of Duquesne University in collaboration with Dr. Larry Matherly.

PCFT and FRα/β targeting compared to the corresponding parent compounds AGF17, AGF23, AGF107, AGF117 and AGF150 (Figure 6.1). Among the new molecules, AGF278 emerged as an antifolate with high potency and great specificity for PCFT and FRα activity over RFC. This compound may prove to be an effective treatment for ovarian cancer patients, reflecting its potency and dual targeting via FRα and PCFT.

6.2 Materials and Methods

6.2.1 Reagents

[3',5',7-^{3}H]MTX (20 Ci/mmol) [3', 5', 7, 9-^{3}H], folic acid (25 Ci/mmol), and [^{14}C(U)]-glycine (87 mCi/mmol) were purchased from Moravek Biochemicals (Brea, CA). Unlabeled folic acid was purchased from Sigma-Aldrich (St. Louis, MO). LCV [(6R,S)5-formyl tetrahydrofolate] was provided by the Drug Development Branch, National Cancer Institute (Bethesda, MD). MTX was supplied by the Drug Development Branch, National Cancer Institute. PMX [N-[4-[2-(2-amino-3,4-dihydro-4-oxo-7H-pyrrolo[2,3-d]pyrimidin-5-yl)ethyl]benzoyl]-*L*-glutamic acid] (Alimta) was provided by Eli Lilly and Co. (Indianapolis, IN). PT523 [N(alpha)-(4-amino-4-deoxypteroyl)-N(delta)-hemiphthaloyl-L-ornithine] was a gift from A. Rosowsky (Boston, MA). The 6-substituted pyrrolo[2,3-*d*]pyrimidine antifolates, including AGF17, AGF23, AGF94, AGF107, AGF117, AGF150, AGF264, AGF270, AGF277, AGF278 and AGF283, were all synthesized by Dr. Aleem Gangjee and colleagues at Duquesne University (Pittsburgh, PA) (Figure 6.1). Other chemicals were obtained from commercial sources in the highest available purities.

6.2.2 Cell Lines

The engineered CHO sublines including RFC-, PCFT- and FRα-null MTXRIIOua^{R}2-4 (R2), and RFC- (pC43-10), PCFT- (R2/PCFT4), or FRα- (RT16) and FRβ- (D4) expressing

CHO sublines were previously described (Deng et al., 2008; Deng et al., 2009; Flintoff et al., 1976; Flintoff and Nagainis, 1983; Wong et al., 1995). The CHO cells were grown in α-minimal essential medium (MEM) supplemented with 10% bovine calf serum (Invitrogen, Carlsbad, CA), *L*-glutamine (2 mM), penicillin (1000 U/ml), and streptomycin (1000 μg/ml) at 37° C with 5% CO_2. R2 transfected cells (PC43-10, RT16, R2/hPCFT4) were cultured in complete α-MEM media plus G418 (1 mg/ml). Prior to the proliferation assays, RT16 and D4 cells were cultured in complete folate-free RPMI 1640 (without added folate), plus 10% dialyzed fetal bovine serum (FBS) (Sigma-Aldrich) and penicillin/streptomycin for 3 days. HeLa R1-11-FR2 and R1-11-PCFT4 cells were derived from RFC- and PCFT-null R1-11 cells by stable transfection with FRα-pcDNA3.1 and pZeoSV2(+)-PCFT constructs, respectively (Zhao et al., 2009b; Zhao et al., 2008). These HeLa sublines, along with R1-11 cells, were gifts from Dr. I. David Goldman (Albert Einstein School of Medicine, Bronx, NY). The R1-11-RFC2 cell line was developed in our laboratory by transfection with the pZeoSV2-RFC vector and clonal selection, as previously described (Wang et al., 2015). R1-11-RFC2, -PCFT4 and -FR2 sublines were routinely cultured in folate-free RPMI 1640 medium, supplemented with 10% FBS (Sigma-Aldrich), *L*-glutamine, penicillin-streptomycin solution, and 100 μg/ml Zeocin.

IGROV1 (Benard et al., 1985) and A2780 (Johnson et al., 1994) ovarian carcinoma cells were a gift of Dr. Manohar Ratnam (Karmanos Cancer Institute) and Dr. Thomas Hamilton (Fox Chase Cancer Center). SKOV3 (Morimoto et al., 1993) cells were purchased from the American Type Culture Collection (Manassas, VA). IGROV1, SKOV3 and A2780 cells were routinely cultured in folate-free RPMI 1640 medium, supplemented with 10% FBS (Sigma-Aldrich), *L*-glutamine, and penicillin-streptomycin solution. IGROV1 NTC and FRα knockdown cells (#4, #10) were developed using MISSION® Lentiviral particles (Sigma-Aldrich) containing shRNA

targeting FRα or a non-targeted control (NTC) shRNA sequence as previously described (Z. Hou and L. H. Matherly, manuscript submitted).

6.2.3 Cell Proliferation Assays

For growth inhibition studies, cells (CHO, R1-11 and ovarian cancer cell lines) were plated in 96 well dishes (~2000 cells/well, total volume of 200 μl) and treated with a range of antifolate concentrations (0-1000 nM) in folate-free RPMI 1640 medium with 10% dialyzed FBS, *L*-glutamine and penicillin/streptomycin, and supplemented with 2 nM (RT16, D4 CHO cells) or 25 nM (all others) LCV, as previously described (Wang et al., 2015). To confirm FR-mediated drug uptake, 200 nM folic acid was added to parallel incubations for RT16 and D4 cells. After 96 h, viable cells were assayed with Cell-Titer Blue^{TM} reagent (Promega, Madison, WI), with fluorescence measured with a fluorescence plate reader. Fluorescence measurements were used for calculations of IC_{50}s, corresponding to the drug concentrations at which cells showed 50% loss of proliferation (Wang et al., 2011; Wang et al., 2015).

To confirm the targeted pathway/enzyme target, *in vitro* growth inhibition of IGROV1 tumor cells was measured in the presence of thymidine (10 μM) or adenosine (60 μM). For *de novo* purine biosynthesis, additional protection experiments used AICA (320 μM) to distinguish inhibitory effects at GARFTase from those at AICARFTase. Folic acid (200 nM) was used as an inhibitor of FR-mediated anti-proliferative effects, as previously described (Deng et al., 2008; Wang et al., 2011; Wang et al., 2015) (also see Chapter 5).

6.2.4 Folate Receptor Binding Assay

To determine antifolate relative binding affinities, RT16 and D4 CHO cells were plated in 60 mm dishes at $7.5x10^5$ cell/plate and grown for two days (~80% confluency) (Wang et al., 2015). Cells were sequentially washed with Dulbecco's phosphate-buffered saline (PBS) at 4° C

(3x), followed by acidic buffer (10 mM sodium acetate, 150 mM NaCl, pH 3.5) (2x) to remove FR-bound folates, and finally HEPES-buffered saline (20 mM HEPES, 140 mM NaCl, 5 mM KCl, 2 mM $MgCl_2$, 5 mM glucose, pH7.4) (HBS). Cells were treated with [^{3}H]folic acid (50 nM, specific activity, 0.5 Ci/mmol) in HBS in the presence and absence of unlabeled folic acid, MTX (negative control), or the 6-substituted pyrrolo[2,3-*d*]pyrimidine antifolates (10 nM to 1000 nM) for 15 min at 4° C. Dishes were washed with HBS at 4°C (3x), cells were solubilized with 0.5 N NaOH (3 h, 37°C), and aliquots were measured for radioactivity and protein contents. Protein concentrations were measured using Folin-phenol reagent (Lowry et al., 1951). FR-bound [^{3}H]folic acid was calculated as pmol/mg protein, and binding affinities were calculated as the inverse molar ratios of unlabeled ligands required to inhibit [^{3}H]folic acid binding by 50%. The relative binding affinity of unlabeled folic acid was assigned a value of 1 (Deng et al., 2008; Deng et al., 2009; Wang et al., 2012; Wang et al., 2010; Wang et al., 2011; Wang et al., 2015).

6.2.5 Transport Assays

R2 and R2/hPCFT4 CHO sublines and R1-11 and R1-11-RFC2 HeLa sublines were grown in suspension as spinner cultures at densities of 2-5 x 10^5 cells/mL (Kugel Desmoulin et al., 2010; Wang et al., 2015). Cells were isolated by centrifugation, washed with PBS (3x), and the cell pellets (~1 x 10^7 cells) were suspended in transport buffer (2 ml) for cellular uptake assays (Wang et al., 2015). PCFT-dependent uptake of 0.5 μM [^{3}H]MTX was assayed in cell suspension over 2 min at 37° C in MES-buffered saline (20 mM MES, 140 mM NaCl, 5 mM KCl, 2 mM $MgCl_2$, and 5 mM glucose) at pH 5.5 or in HBS at pH 6.8 in the presence or 1 or 10 μM inhibitor, while RFC-dependent uptake was measured over 2 min at 37° C in pH 7.2 HBS. Transport was quenched with ice-cold PBS after 2 min and cells were washed three times with ice-cold PBS. Cellular proteins were solubilized with 0.5 N NaOH (3 h, 37° C). Transport levels

were expressed as pmol/mg protein, calculated using direct measurements of radioactivity and protein contents of the cell homogenates. Protein concentrations were measured using Folin-phenol reagent (Lowry et al., 1951). Transport levels were normalized to levels in untreated (R2/PCFT4 or R1-11-RFC2) controls. To determine K_i values for 6-pyrrolo[2,3-*d*]pyrimidine antifolates, transport was measured over 2 min with 0.5 μM [^{3}H]MTX and 0.05-1 μM of unlabeled antifolate (Kugel Desmoulin et al., 2010). Dixon plots were used to analyze data.

6.2.6 *In Situ* GARFTase Inhibition Assay

In situ measure of intracellular GARFTase activity, via incorporation of [^{14}C(U)]glycine into [^{14}C]formyl glycinamide ribonucleotide, in IGROV1 cells at pH 6.8, was performed exactly as previously described (Kugel Desmoulin et al., 2010; Wang et al., 2011) (also see Chapter 5). Antifolates were used over a concentration range of 0.3 nM to 100 nM. Results were normalized to cell proteins. To calculate the IC_{50} values, drug-treated samples were normalized to untreated controls.

6.2.7 Statistical Analysis

Descriptive statistical tests (e.g., t tests) were conducted using GraphPad 6.0 software (La Jolla, CA).

6.3 Results

6.3.1 Cytotoxic Activity in Engineered Models

In this chapter, our goal was to explore the antiproliferative effects of novel fluorinated 6-substituted pyrrolo[2,3-*d*]pyrimidines (Figure 6.1) on tumor cells, and identify whether these modifications to previously established antifolates may enhance potency or transporter specificity. In order to determine the selectivity of each compound between RFC, PCFT, and FRs, we utilized isogenic CHO sublines that were engineered to express RFC (PC43-10), PCFT

(R2/hPCFT4), FRα (RT16), or FRβ (D4), all derived from the transporter-null CHO cell line MTXRIIOua^{R}2-4 (R2) (Deng et al., 2008; Deng et al., 2009; Flintoff et al., 1976; Flintoff and Nagainis, 1983; Wong et al., 1995). Cells were continuously treated with the novel 6-substituted pyrrolo[2,3-d]pyrimidine antifolates for 4 days and proliferation measured with a fluorescence-based assay. IC_{50} values were determined for each drug in each cell line, and the novel fluorinated antifolates were directly compared to their corresponding parent compounds. AGF264 and AGF270 displayed an enhanced inhibition of proliferation toward R2/hPCFT4 cells compared to parent compounds AGF23 and AGF17 (~3.5-fold and ~2.9-fold decrease in IC_{50}, respectively) (Table 6.1). Conversely, AGF277 had a decreased anti-proliferative effect on R2/hPCFT4 cells relative to the parent AGF107 (~2.2-fold increase in IC_{50}) (Table 6.1). AGF278, in comparison to parent AGF117, had dramatically increased (~6.9-fold) *in vitro* efficacy in RT16 cells (Table 6.1). AGF283, structurally homologous to AGF278 but with 3 rather than 4 bridge carbons, also displayed significantly enhanced *in vitro* efficacy in PC43, R2/hPCFT4 and RT16 cells compared to its parent compound AGF150, although this increased activity was accompanied by a dramatically increased non-specific activity in R2 cells (20.5 nM for AGF283 compared to 271 nM for AGF150). This suggests a high affinity for another transporter other than RFC, PCFT or FRα/β. Collectively, these results suggest that fluorination of antifolate compounds can have dramatic effects on anti-proliferative efficacy towards cells which express a single folate uptake protein.

In order to extend the analysis from the CHO cell line models, we performed additional ploriferation assays in engineered human cancer cells. We tested the drug efficacies toward several HeLa sublines which were engineered from the RFC- PCFT- and FR-null R1-11 HeLa cell line, including the R1-11-RFC2 (expresses RFC), R1-11-PCFT4 (PCFT) and R1-11-FR2

Table 6.1

IC_{50} Values (nM) for Inhibition of CHO Sublines

	R2 (null)	PC43-10 (RFC)	R2/hPCFT4 (PCFT)	RT16 (FRα)	D4 (FRβ)
PMX	138(13)	26.2(5.5)	8.3(2.7)	42(9)	60(8)
AGF94	249(25)	106(17)	3.3(0.5)	0.31(0.15)	0.16(0.02)
AGF23	>1000	>1000	83.1(20.1)	0.84(0.07)	2.0(0.3)
AGF264	>1000	>1000	23.5(1.5)	0.49(0.18)	1.6(0.44)
AGF17	>1000	424(116)	10.9(1.9)	0.68(0.22)	0.41(0.08)
AGF270	140(27)	61.6(11.5)*	3.8(0.3)*	1.1(0.4)	3.9(0.1)*
AGF107	>1000	>1000	30.4(10.7)	1.3(0.1)	0.52(0.09)
AGF277	>1000	467(142)	66.9(25.0)	0.69(0.39)	0.44(0.13)
AGF117	>1000	>1000	32.0(11.6)	2.5(0.5)	0.43(0.14)
AGF278	>1000	>1000	6.0(0.9)	0.36(0.12)*	0.75(0.42)
AGF150	271(52)	157(36)	9.7(1.8)	0.71(0.20)	0.32(0.03)
AGF283	20.5(1.6)*	20.1(6.1)*	1.5(0.4)*	0.14(0.03)*	0.19(0.02)*

Growth inhibition assays were performed using CHO sublines derived from RFC- PCFT-and FR-null MTXRIIOua^{R}2-4 CHO cells (R2) and engineered to overexpress human RFC (PC43-10), PCFT (R2/hPCFT4), FRα (RT16) or FRβ (D4). Results are shown as a mean of five experiments (± standard error in parentheses) and are described as calculated IC_{50} values representing the concentration at which growth of 50% of cells was inhibited relative to untreated cells. Fluorinated compounds which displayed statistically different IC_{50} values from parent compounds (directly above) within each cell line are marked with * ($p < 0.05$).

Table 6.2

IC_{50} Values (nM) for Inhibition of HeLa R1-11 Sublines

	R1-11-RFC2	R1-11-PCFT4	R1-11-FR2
PMX	23.8(1.5)	66.8(4.8)	863(81)
AGF94	444(5)	53.1(15.5)	30.2(5.6)
AGF23	>1000	5.21(1.33)	11.6(2.7)
AGF264	>1000	21.6(17.1)	7.78(1.89)
AGF17	>1000	9.71(2.78)	12.2(4.4)
AGF270	507(76)	5.54(3.35)	5.22(1.32)
AGF107	634(43.9)	8.98(3.64)	6.54(1.29)
AGF277	>1000	37.6(16.3)	21.7(3.9)*
AGF117	>1000	72.6(18.1)	35.3(6.2)
AGF278	213(9)	5.01(2.12)*	2.84(0.67)*
AGF150	62.9(3.8)	40.0(9.8)	7.57(1.16)
AGF283	66.2(6.2)	20.4(4.7)	3.11(0.69)*

Growth inhibition assays were performed using HeLa sublines derived from R1-11 RFC- and PCFT-null cells and engineered to overexpress human RFC (R1-11-RFC2), PCFT (R1-11-PCFT4), or FRα (R1-11-FR2). Results are shown as a mean of five experiments (± standard error in parentheses) and are described as calculated IC_{50} values representing the concentration at which growth of 50% of cells was inhibited relative to untreated cells. Fluorinated compounds which displayed statistically different IC_{50} values from parent compounds (directly above) within each cell line are marked with * ($p < 0.05$).

(FRα) cell lines (Wang et al., 2015; Zhao et al., 2009b; Zhao et al., 2008). Results generally reflected growth inhibitions seen in the CHO cell lines (i.e., compare results in Table 6.1 with those in Table 6.2). Notably, in this conext, AGF278 displayed a significantly enhanced efficacy toward both R1-11-PCFT4 and R1-11-FR2 cells compared to AGF117, suggesting an increased activity for both PCFT and FRα uptake (~14.5-fold and ~12.4-fold decrease in IC_{50}, respectively) (Table 6.2). AGF283 displayed an increased efficacy for R1-11-FR2 cells compared to AGF150 (~2.4-fold increase in IC50), as seen with RT16 CHO cells. However, unlike RT16 CHO cells, AGF277 was significantly less potent than AGF107 in these cells (~3.3-fold decrease in IC_{50}) (Table 6.2). While AGF264 and AGF270 were selective toward PCFT4-expressing R1-11-PCFT4 over the R1-11-RFC2 HeLa cells, this was not significantly enhanced compared to respective parent compounds AGF23 and AGF17 (Table 6.2).

In order to more specifically describe the PCFT and FRα selectivies of these compounds, RFC/PCFT and RFC/FR IC_{50} ratios were calculated (Table 6.3). For these selectivity ratios, a larger number is indicative of increased selectivity for tumor specific (FR and/or PCFT) transporters compared to ubiquitously expressed RFC. In this case, PMX, widely considered to be an excellent substrate for both PCFT an RFC, displayed only a RFC/PCFT selectivity ratio of only 0.36 (Table 6.3), a clear reflection of limited transporter selectivity. AGF94, considered to be among the best PCFT substrates (Cherian et al., 2013; Desmoulin et al., 2012b; Wang et al., 2011) (also see Chapter 5), showed an RFC2/PCFT4 IC_{50} ratio of 8.36 (~23.2-fold increase over PMX) while also displaying an RFC2/FR2 IC_{50} ratio of 14.7 (~490-fold increase over PMX) (Table 6.3). AGF283, as expected, did not display a high level of specificity for PCFT (3.25 RFC2/PCFT4 IC_{50} ratio), although there was substantial FRα selectivity (21.3 RFC2/FR2 IC_{50} ratio) (Table 6.3). We did observe over 90-fold specificity for PCFT (91.5 RFC2/PCFT4 IC_{50}

Table 6.3

Ratios of Transporter Selectivity over RFC

	$\frac{\text{RFC2 } IC_{50}}{\text{PCFT4 } IC_{50}}$	$\frac{\text{RFC2 } IC_{50}}{\text{FR2 } IC_{50}}$
PMX	0.36	0.03
AGF94	8.36	14.7
AGF270	91.5	97.1
AGF278	42.5	75
AGF283	3.25	21.3

Selectivity ratios determined by IC_{50} values in R1-11-RFC2, R1-11-PCFT4 and R1-11-FR2 cell lines (Table 6.2). By this metric, higher values represent an increased selectivity for PCFT or FRα-mediated uptake compared to RFC. Compounds with >1000 nM IC_{50} values in the R1-11-RFC2 cell line were excluded from comparison.

ratio) and FRα (97.1 RFC2/FR2 IC_{50} ratio) for AGF270, somewhat greater than the specificity seen for AGF278 with PCFT (42.5 RFC2/PCFT4 IC_{50} ratio) and FRα (75.0 RFC2/FR2 IC_{50} ratio) (Table 6.3). The levels of specificity for AGF270 and AGF278 are unprecedented, as these selectivity ratios are much higher than that of our previous lead compound AGF94. Compared to AGF94, AGF278 has a ~5-fold increase in selectivity for both PCFT and FRα over RFC, while AGF270 had an ~11-fold increase for PCFT selectivity and a ~6-fold increase for FRα selectivity, establishing AGF270 and AGF278 as the most selective PCFT- and FRα-targeted antifolates to date (Table 6.3), establishing AGF270 and AGF278 as the most selective PCFT- and FRα-targeted antifolates to date (Table 6.3).

6.3.2 Transport Binding Specificity of 6-Substituted Pyrrolo[2,3-d]pyrimidine Antifolates for the Major Folate Transporters

In order to further examine the level of specificity for each compound in the context of RFC and PCFT uptake, we determined the binding affinity for each compound as a competitor to [^{3}H]MTX. To determine the binding specificity of each antifolate for PCFT, we tested the capability of each compound to inhibit 0.5 μM [^{3}H]MTX uptake in PCFT-expressing R2/PCFT4 CHO cells at pH 5.5. All inhibitors were tested at 1 μM and 10 μM, and results were normalized to those for the non-treated control R2/PCFT4 cells. PCFT-null R2 cells were used as a negative control for membrane transport, while the RFC-specific antifolate PT523 was used as a negative control for PCFT inhibition and PMX was used as a positive control for inhibition. All compounds displayed some level of transport inhibition at both 1 μM and 10 μM. For AGF264, inhibition was significantly greater than parent AGF23 at both 1 μM (80% compared to 66% inhibition, respectively) and 10 μM (92% compared to 95%, respectively), suggesting an enhanced PCFT selectivity (Figure 6.2A). AGF270 also displayed significantly greater inhibition

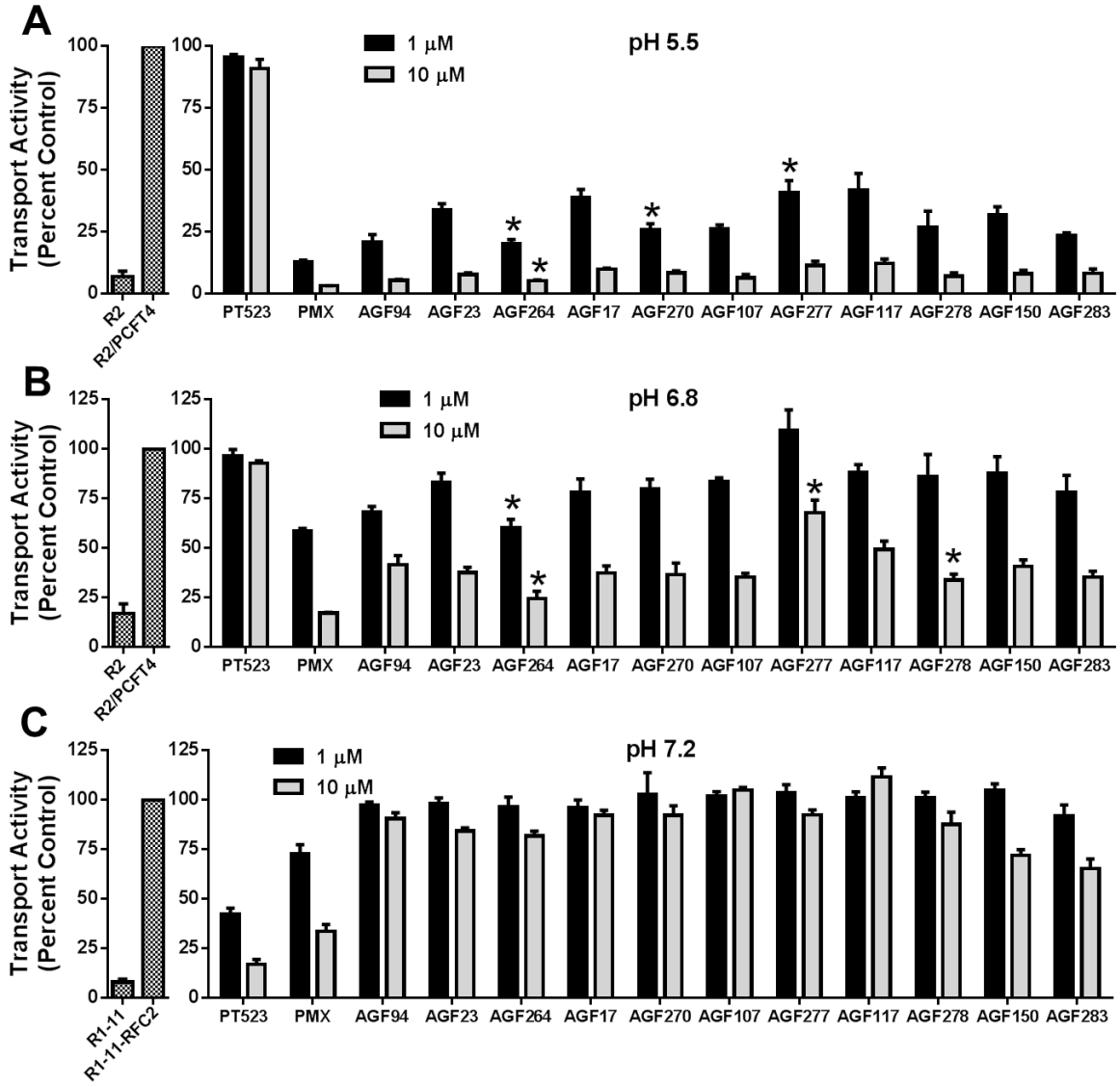

Figure 6.2 PCFT and RFC transport inhibition by the fluorinated antifolates compared to parent compounds. *Panels A and B,* Inhibition of PCFT [^{3}H] MTX transport by unlabeled 6-substituted pyrrolo[2,3-d]pyrimidine analogues in R2/PCFT4 CHO cells. Relative PCFT inhibition for assorted antifolate substrates were measured at pH 5.5 (*A)* and pH 6.8 (*B)* over 2 min in the presence [^{3}H] MTX (0.5 μM), with 1 or 10 μM of inhibitor. Results are presented as mean values ± standard errors for three experiments. Results are normalized to transport in the absence of any additions. *Panel C,* Inhibition of RFC [^{3}H] MTX transport by unlabeled 6-substituted pyrrolo[2,3-d]pyrimidine analogues in R1-11-RFC2 cells. Experiments were performed as in *A* at pH 7.2. For all experiments, bars noted with asterisks were statistically different from the corresponding parent compound (to the right) at the same concentration ($p < 0.05$) by paired t-test analysis.

than parent AGF17 at 1 μM (74% compared to 61%, respectively), while AGF277 displayed poorer inhibition than parent AGF107 at 1 μM (59% compared to 74%, respectively) (Figure 6.2A). These experiments were repeated at pH 6.8 and results were largely the same, albeit with reduced transport inhibition (Figure 6.2B). While the results for AGF278 were similar at pH 5.5 and pH 6.8, at pH 6.8 with 10 μM AGF278, transport inhibition was significantly increased over that for the parent AGF117 at 10 μM (51% compared to 66%, respectively). In order to determine, K_i values, a quantititative measure of substrate binding affinities, for PCFT, we used a range of inhibitor concentrations (0.05 μM to 1 μM) with a constant (1 μM) concentration of [^{3}H]MTX. K_is were calculated using Dixon analysis. Based on this parameter, all novel fluorinated antifolates displayed differential PCFT specificities compared to parent antifolates which were statistically significant. With the exception of AGF277, which had a higher K_i value than parent AGF107 (~1.9-fold increase), all fluorinated antifolates had decreased K_is compared to parent antifolates, suggesting an increased PCFT transport capability (Table 6.4). Notably, AGF283 showed a ~4-fold decrease in K_i compared to parent AGF150.

Analogous experiments were performed to assess binding to RFC. For these experiments, we measured [^{3}H]MTX uptake (at 0.5 μM) in RFC-expressing R1-11-RFC2 HeLa cells at pH 7.2 in the presence of 1 μM and 10 μM inhibitor. Transporter-null R1-11 cells were used as a negative control. Although some minor inhibition of RFC transport was observed at 10 μM inhibitor, particularly for AGF150 and AGF283, these levels were modest and above 30% inhibition (Figure 6.2C). In all cases, RFC inhibition by fluorinated antifolates was not significantly different from the corresponding parent antifolate (Figure 6.2C). Together, these data suggest that all 6-substituted pyrrolopyrimidines are potent PCFT inhibitors and poor RFC

Table 6.4
Kinetic Inhibition Analysis of Antifolates Competing with MTX in R2/PCFT4 cells.

	K_i
PMX	0.12 (0.03)
AGF94	0.14 (0.02)
AGF23	0.46 (0.05)
AGF264	0.17 (0.01)*
AGF17	0.63 (0.13)
AGF270	0.26 (0.01)*
AGF107	0.24 (0.02)
AGF277	0.46 (0.06)*
AGF117	0.36 (0.03)
AGF278	0.25 (0.01)*
AGF150	0.28 (0.07)
AGF283	0.07 (0.04)*

[^{3}H]MTX uptake was assayed at using R2/PCFT4 cells at pH 5.5 over 2 min at 37^{o}C. To determine K_i values, cells were incubated with 0.5 μM [^{3}H]MTX with antifolates as competitors from 0.05 μM to 0.5 μM, with results analyzed by Dixon plots. Data are presented as mean values ± standard errors from four independent experiments. For fluorinated antifolates, values significantly different from those of parent antifolate ($p < 0.05$) are marked with *.

inhibitors, paralleling inhibitions of proliferation (Table 6.2). Fluorination of compounds appeared to enhance PCFT binding in several cases.

6.3.3 Folate Receptor Binding Affinity of 6-Substituted Pyrrolo[2,3-*d*]pyrimidine Antifolates

As suggested by the antiproliferative effects in RT16, D4, and R1-11-FR2 cells, the fluorinated 6-substituted pyrrolo[2,3-d]pyrimidine antifolates appeared to target FRs although there were somewhat divergent specificities for FRα-expressing cells over FRβ-expressing cells. As a direct metric for FR specificity, we measured the binding of each compound in competition with 50 nM [^{3}H]folic acid. A range of concentrations (10 nM to 1000 nM) was used to determine IC_{50} values, corresponding to the concentration that inhibited [^{3}H]folic acid binding. IC_{50} values for the antifolate inhibitors were further normalized to that for non-radioactive folic acid, giving a measure of relative binding affinities. Both RT16 (FRα) and D4 (FRβ) CHO cells were used in order to test for relative affinity to both FR isoforms. Generally, results observed in D4 cells were reflective of results in RT16, although binding affinities for FRβ tended to be lower, suggesting an increased targeting for FRα over FRβ (assuming that the affinity for folic acid in each isoform is equal). An exceptional difference was observed with AGF283, which appeared to have a much stronger binding affinity for FRα (binding affinity 0.83) than for FRβ (binding affinity 0.12), a ~7-fold difference in binding affinity. This difference was not observed between RT16 and D4 anti-proliferative effects, likely due to the non-specific uptake of AGF283 (as reflected by the low IC_{50} in R2 cells) (Table 6.1).

For both FRα and FRβ, the fluorinated antifolate AGF278 appeared to have an enhanced specificity for FRs in comparison to its parent compound AGF117 (Figure 6.3A-B). Particularly for FRα, AGF278 displayed a binding affinity approximating that of folic acid (1.0 binding

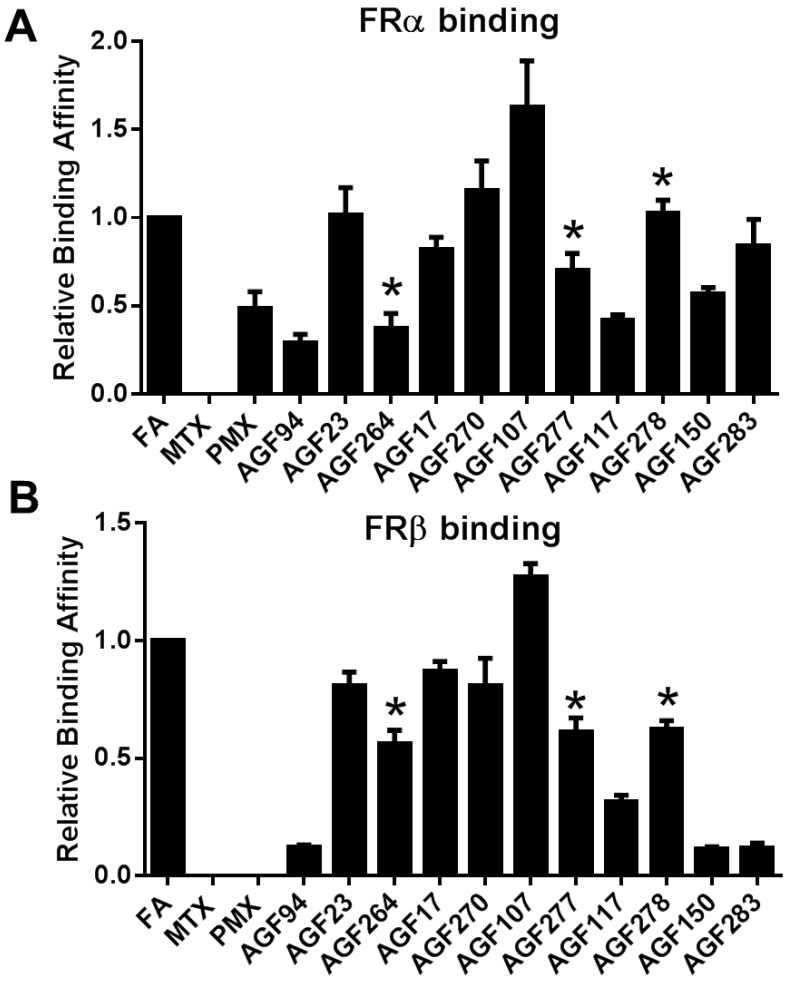

Figure 6.3 FRα and FRβ binding affinities. *Panels A and B,* Binding of 6-substituted pyrrolo[2,3-d]pyrimidine analogues to FRα (*A*) in RT16 cells and FRβ (*B*) in D4 relative to FA. Relative binding affinities for assorted folate/antifolate substrates were determined over a range of ligand concentrations from 10nM to 1000 nM and were calculated as the inverse molar ratios of unlabeled compounds required to inhibit [^{3}H] folic acid binding by 50% (the relative affinity of folic acid being 1). Results are presented as mean values ± standard errors from three experiments. The bars noted with asterisks were statistically different from the corresponding parent compound (to the right) ($p < 0.05$) by paired t-test analysis.

affinity for AGF278 compared to 0.42 for AGF117) (Figure 6.3A). While fluorinated analogs AGF270 and AGF283 appeared to have no change in binding affinities compared to their respective parent compounds AGF17 and AGF150, AGF264 and AGF277 showed lower binding affinities than respective parent compounds AGF23 and AGF107, respectively. For AGF270, a FRα binding affinity comparable to that for folic acid was measured, establishing potent FRα binding. Thus, in general, fluorination of the targeted antifolates did not enhance antifolate binding affinities to FR, as only AGF278 of the five novel fluorinated compounds displayed significantly enhanced FR binding affinity compared to the parent compound AGF117.

6.3.4 Cytotoxicity of of 6-Substituted Pyrrolo[2,3-d]pyrimidine Antifolates in Ovarian Cancer Cell Lines

We extended our studies of these novel fluorinated pyrrolopyrimine antifolates to clinically relevant ovarian cancer cells. We determined the antiproliferative efficacies toward IGROV1, SKOV3, and A2780 cells. These three cell lines were previously shown to express both PCFT and FRα transcripts, and while IGROV1 displayed the highest levels of FRα transcripts and binding (~4-fold increase in binding over SKOV3, ~11-fold increase over A2780), PCFT transcripts and binding were nearly identical between all three cell lines (<2-fold difference) (Wang et al., 2015) (Z. Hou and L. H. Matherly, submitted). In two of three cell lines, A2780 and IGROV1, we observed significant increases in *in vitro* efficacies for both AGF278 and AGF283 (from 2-fold to 29-fold increases), in comparison to respective parent compounds AGF117 and AGF150 (Table 6.5). Furthermore, AGF278 and AGF283 were significantly more potent than AGF94 toward both IGROV1 and A2780 cells ($p < 0.02$). These results suggest that compounds with increased specificity for PCFT and FRα may also be more potent inhibitors of proliferation in some ovarian cancer cell lines.

Table 6.5

IC_{50} Values (nM) for Inhibition of Ovarian Cancer Cell Lines and FRα Knockdown Sublines

			IGROV1			
	SKOV3	A2780	WT	NTC	FR KD-4	FR KD-10
PMX	24.1(2.1)	39.4(9.2)	104(11)	71.0(8.5)	46.6(10.4)	22.2(6.6)
AGF94	38.7(4.9)	27.4(3.4)	16.7(3.4)	10.1(1.5)	190(99)	74.6(33.9)
AGF23	868(32)	14.2(3.6)	4.37(0.95)	5.21(1.59)	>1000	>1000
AGF264	224(75)*	13.6(4.2)	5.44(0.81)	6.89(1.13)	>1000	>1000
AGF17	273(47)	2.72(0.53)	2.01(0.14)	1.97(0.69)	453(262)	190(48)
AGF270	27.9(2.5)*	2.14(0.18)	1.67(0.30)	1.14(0.25)	41.0(12.7)	19.2(4.3)*
AGF107	90.5(16.4)	5.42(1.39)	1.87(0.19)	1.55(0.18)	64.1(6.5)	30.5(0.5)
AGF277	59.2(12.4)	15.7(3.6)*	6.36(1.04)*	5.17(1.34)*	>1000	>1000
AGF117	114(34)	28.8(1.4)	54.3(4.8)	40.7(5.8)	>1000	>1000
AGF278	37.8(10.1)	3.11(0.14)*	1.90(0.15)*	1.79(0.19)*	138(6.8)	66.9(28.3)
AGF150	25.1(2.6)	21.7(1.5)	12.1(1.6)	12.8(1.4)	80.5(24.2)	30.3(2.1)
AGF283	30.2(7.1)	7.6(1.0)*	6.92(1.03)*	5.61(1.20)*	85.6(3.9)	42.2(11.2)

Growth inhibition assays were performed using ovarian cancer cell lines SKOV3, A780 and IGROV1, as well as FRα-knockdown sublines (KD-4, KD-10) derived from IGROV1 as well as non-targeted control (NTC) as previously described. Results are shown as a mean of five experiments (± standard error in parentheses) and are described as calculated IC_{50} values representing the concentration at which growth of 50% of cells was inhibited relative to untreated cells. Fluorinated compounds which displayed statistically different IC_{50} values from parent compounds (directly above) within each cell line are marked with * ($p < 0.05$).

Interestingly, in the SKOV3 cells, we observed a significant increase in efficacy for AGF264 (224 nM IC_{50}) in comparison to AGF23 (868 nM IC_{50}), and an increased efficacy for AGF270 (27.9 nM IC_{50}) compared to AGF17 (273 nM IC_{50}). Differences between AGF278 (37.8 nM IC_{50}) and AGF117 (114 nM IC_{50}) also suggested an increased efficacy, although this difference was not statistically significant (Table 6.5). However, contradictory to the enhanced efficacy observed in IGROV1 and A2780, AGF278 and AGF283 did not have IC_{50} values in SKOV3 which were significantly lower than AGF94 ($p > 0.05$). Because SKOV3 has roughly equivalent PCFT expression to both IGROV1 and A2780, with FRα expression higher than A2780 but lower than IGROV1 (Hou and Matherly, manuscript submitted), the differential effects observed in the SKOV3 cell line are likely due to factors other than antifolate uptake.

Additionally, we tested the antiproliferative effects of the novel compounds in IGROV1 FRα knockdowns (KD-4, KD-10) and non-targeted control (NTC) (Hou and Matherly, manuscript submitted). These knockdown cell lines each display >90% knockdown of FRα, as reflected in gene expression (measured by real-time RT-PCFT) and levels of FRα protein (measured by direct binding of [^{3}H]folic acid). Knockdown of FRα was accompanied by modest decreases in PCFT gene and protein expression (decreases of 28% for KD-4 and 40% for KD-10 compared to NTC) and PCFT membrane transport. Under these conditions, PMX efficacy was increased ~2-fold by FRα knockdown, suggesting that decreased FR-driven LCV uptake (and a reduction of folate pools) had a greater impact on PMX efficacy than on the decreased FR-driven PMX uptake, as FRα-mediated uptake of PMX into solid tumor cell lines has been shown to be of minor importance (Chattopadhyay et al., 2004). However, for other 6-substituted pyrollo[2,3-*d*]pyrimidine antifolates, FR knockdown in IGROV1 cells greatly reduced drug efficacy. The fold change in efficacy with FR knockdown varied between drugs. For instance, for some

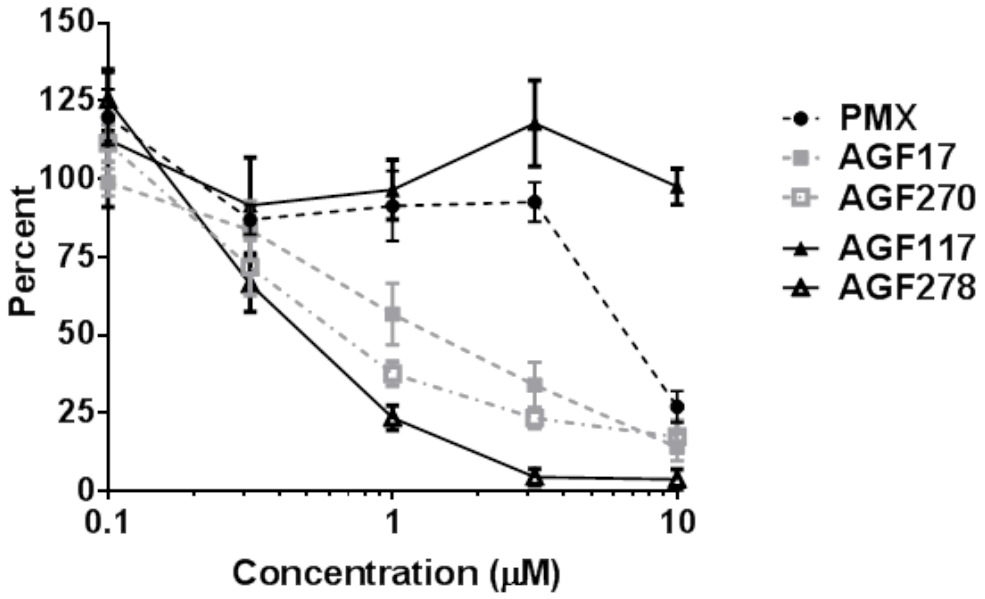

Figure 6.4 Cytotoxicity via colony formation assay. IGROV1 cells (400 cells) were plated in 6-well plates in complete folate-free RPMI 1640 (pH 7.2), 10% dialyzed fetal bovine serum, and 25 nM LCV. After 24 hours, cells were then treated with PMX, AGF17, AGF270, AGF117 or AGF278 at varying concentrations (0.1 to 10 μM) in complete folate-free RPMI 1640 adjusted to pH 6.8 and supplemented with 25 nM LCV. After an additional 24 hours, cells were rinsed with PBS, and then incubated in complete folate-free RPMI 1640 supplemented with 25 nM LCV (pH 7.2) for 9 days. Colonies were stained with methylene blue and counted, and colony numbers were normalized to the controls. Plots show mean ± S.E. values, representative of triplicate experiments. IC_{50} (mean and S.E.) values (μM) were as follows PMX: 7.4 (1.0); AGF17: 1.7 (0.5); AGF270: 0.7 (0.1); AGF117: >10 (0); AGF278: 0.5 (0.1).

compounds, including AGF283, we saw a subtle increase in IC_{50} (~11-fold,) compared to NTC, while other drugs, such as AGF278, we saw a dramatic increase in drug efficacy (~57-fold increase in IC_{50}), likely reflecting differences in the specificities for PCFT and FRα over RFC (Table 6.3). Some drugs, such as AGF264 and AGF277, were completely ineffective in IGROV1 FR knockdowns, possibly reflecting the decreased PCFT expression in these cells in conjunction with FR knockdown.

As an additional method to evaluate antitumor efficacy *in vitro* using IGROV1 cells, we used a colony formation assay to measure cytotoxicity under conditions more representative of those characterizing the tumor microenvironment (i.e., pH 6.8) (see Chapter 5). Cells were seeded in 6-well plates at a density of 400 cells/well, and one day later were treated with drugs for 24 hours in pH 6.8 media, followed by nine days of growth in the absence of drug. Here, we observed that AGF17, AGF270 and AGF278 were all significantly more potent than PMX (IC_{50} values of 1.7, 0.7, 0.5 and 7.4 μM, respectively) (Figure 6.4), paralleling the PCFT-specificity observed in engineered models (Tables 6.1-6.3, Figure 6.2). Interestingly, AGF117 was completely ineffective in clonogenic assays, and the potency of AGF278 far exceeded that for AGF117 at 1 μM and above ($p < 0.05$) (Figure 6.4). These experiments establish that these drugs are cytotoxic rather than simply cytostatic.

6.3.5 Metabolic Activity of of 6-Substituted Pyrrolo[2,3-d]pyrimidine Antifolates

We next determined the metabolic target for each compound. It has been well established that AGF17, AGF23, AGF117 and AGF150 are all potent inhibitors of GARFTase, the first folate dependent reaction in *de novo* purine nucleotide biosynthesis (Figure 1.6), with little to no activity towards TS, DHFR, or AICARFTase (Deng et al., 2008; Deng et al., 2009; Wang et al., 2012; Wang et al., 2015) (also see Chapter 5). By testing growth inhibition in the presence of

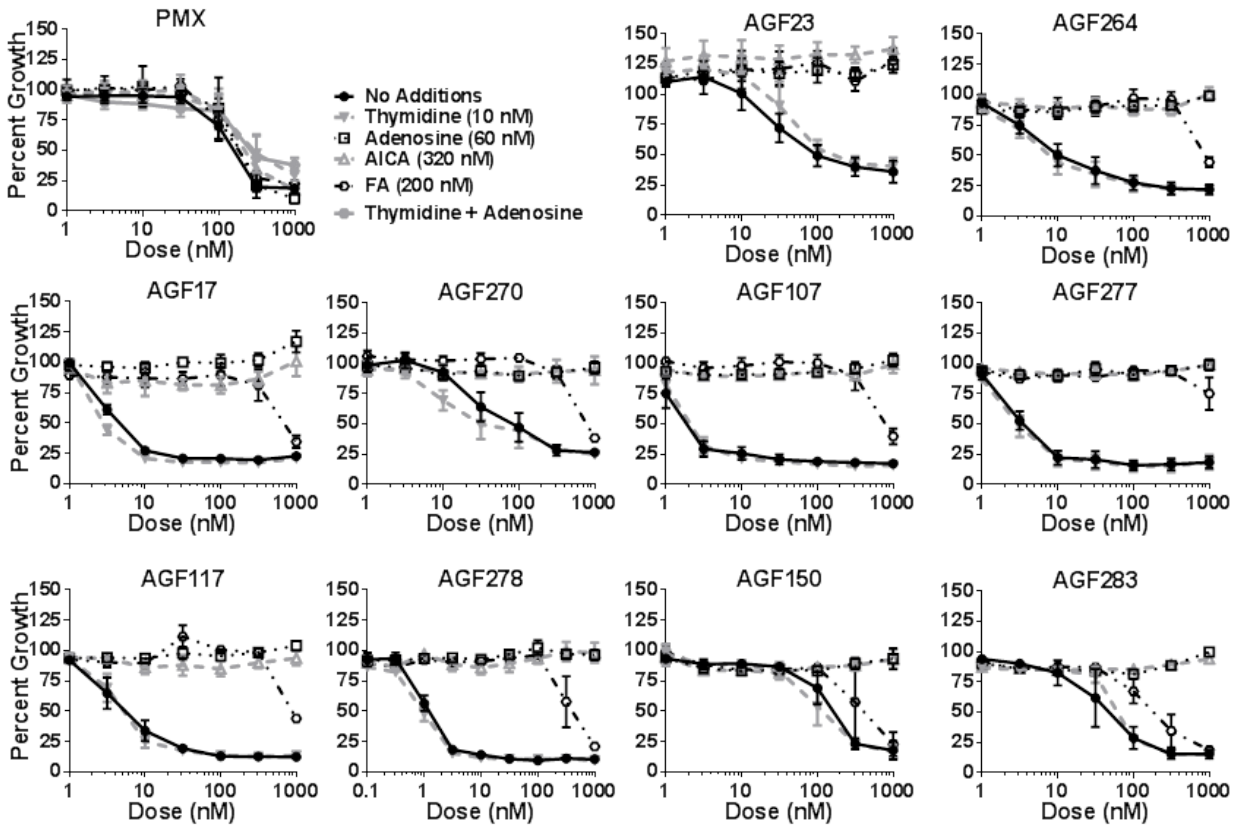

Figure 6.5 Protection assay in IGROV1 cells. Growth inhibition of IGROV1 cells and protection by excess folic acid, nucleosides, AICA. IGROV1 cells were plated (2000 cells/well) in folate-free RPMI 1640 medium with 10% FBS, antibiotics, *L*-glutamine, and 25 nM LCV with a range of concentrations antifolates in the presence of folic acid (200 nM), adenosine (60 μM), and/or thymidine (10 μM) or AICA (320 μM). Cell proliferation was assayed with Cell Titer Blue using a fluorescence plate reader. Data are representative of at least triplicate experiments. Error bars represent standard error for each replicate. IC_{50} values for IGROV1 cells without additions are detailed in Table 6.4.

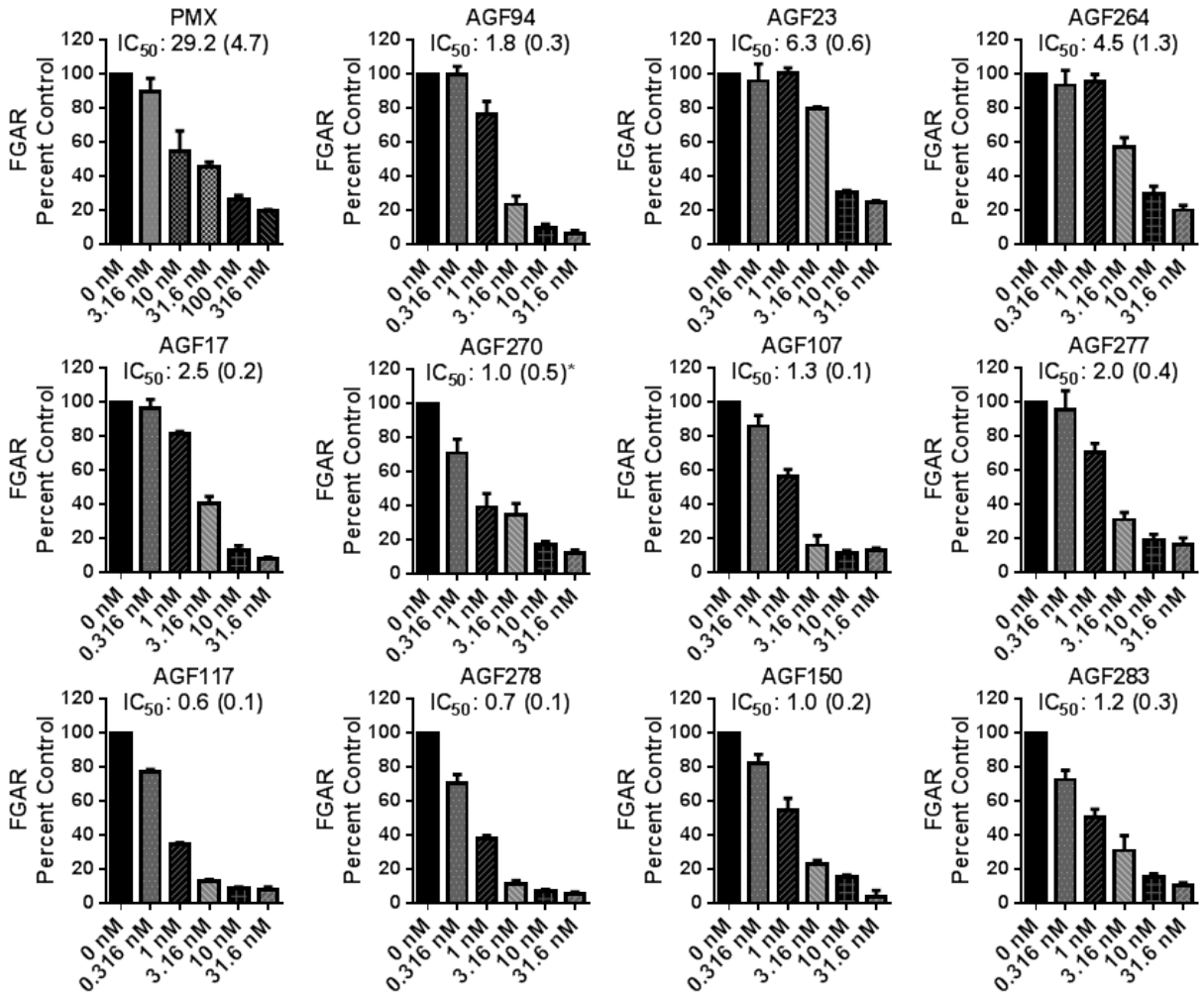

Figure 6.6 *In situ* GARFTase activity by the fluorinated antifolates compared to parent compounds. Incorporation of [^{14}C(U)]glycine into [^{14}C]formyl glycinamide ribonucleotide (GAR) as an *in situ* measure of endogenous GARFTase activity in IGROV1 cells. Cells were treated with a range of concentrations of antifolates in media which was adjusted to pH 6.8 IC_{50} values (nM) are listed with S.E. values. Data are representative of triplicate experiments. IC_{50} values for fluorinated antifolates which are statistically different from parent antifolates are marked with * ($p < 0.05$).

thymidine (10 nM), adenosine (60 nM) or AICA (320 nM) in IGROV1 cells, we determined that antiproliferative activities of these compounds were completely protected by the addition of either adenosine or AICA, suggesting *de novo* purine nucleotide biosynthesis as the targeted pathway with inhibition of GARFTase as the principal cellular target (Figure 6.5). Compounds were also tested in the presence of 200 nM folic acid, and we observed that some compounds displayed incomplete protection under this condition, particularly AGF278, AGF150 and AGF283, suggesting an alternative uptake mechanism to folate receptor, most likely PCFT, consistant with the results observed in the PCFT-expressing CHO and HeLa sublines (Tables 6.1-6.3).

In order to determine the potency of GARFTase inhibition, we utilized an *in situ* GARFTase assay to measure the accumulation of [^{14}C]formyl GAR (the GARFTase product in *de novo* purine biosynthesis) in IGROV1 cells. Cells were treated with [^{14}C]glycine, which allowed for incorporation of [^{14}C] into formyl GAR, and azaserine, which allowed for formyl-GAR accumulation, in the presence of absence of the targeted antifolates. PMX was included as a negative control, as it displays weak GARFTase activity (Racanelli et al., 2009), while AGF94, an established potent GARFTase inhibitor, was included as a positive control (Wang et al., 2011). In this case, we observed that all the 6-substituted pyrrolo[2,3-*d*]pyrimidine compounds were potent GARFTase inhibitors, with nearly all IC_{50} values below 3 nM (Figure 6.6), a paralleling the range at which these compounds inhibit IGROV1 cell proliferation (Table 6.5). However, in most cases, GARFTase activity of the fluorinated antifolates was not significantly different than for parent antifolates (Figure 6.6). The exception to this is AGF270, which displayed a significantly lower IC_{50} value than AGF17 (1.0 nM compared to 2.5 nM, respectively), suggesting an increased GARFTase inhibition ($p < 0.05$) (Figure 6.5).

6.4 Discussion

Our previous studies have demonstrated the potential therapeutic utility of novel 6-substituted pyrollo[2,3-*d*]pyrimidine antifolates for the targeted treatment of ovarian cancer, lung cancer, and malignant mesothelioma (Cherian et al., 2013; Wang et al., 2012; Wang et al., 2015) (Z. Hou and L. H. Matherly, manuscript submitted) (also see Chapter 5). In this chapter, we expanded our studies to include several novel fluorinated antifolate molecules (Figure 6.1) derived from previously studied PCFT- and FR-targeted inhibitors with established patterns of transporter specificity and limited transport by the ubiquitous RFC (Wang et al., 2012; Wang et al., 2010; Wang et al., 2011; Wang et al., 2015). Fluorination of drugs is a common strategy to enhance efficacy and specificity of small molecule therapeutics (Gillis et al., 2015). In this case, fluorination of antifolates played a substantial albeit variable role in drug efficacy via changes to transporter specificity.

We observed that AGF278 in particular displayed enhanced PCFT transport, as well as increased FR-binding, which led to increased efficacy toward PCFT- and FR- expressing CHO and HeLa cells, in comparison to parent drug AGF117. In engineered CHO cells, AGF278 displayed inhibition toward transporter-null (R2) and RFC-expressing cells (PC43-10) up to 1000 nM, while showing very potent in PCFT- (R2/PCFT4) and FR-expressing (RT16/D4) cells (Table 6.1). In engineered HeLa cells, AGF278 also displayed a high level of PCFT and FRα specificity (Table 6.3). Similarly, AGF278 showed an increased potency toward ovarian cancer cell lines with both high (IGROV1) and low (A2780) FRα expression, accompanied by similar levels of PCFT, and this potency was dramatically reduced by FR knockdown in IGROV1 cells (Table 6.4). AGF278 was specifically targeted to both PCFT and FRα (Table 6.3) and showed enhanced potency toward certain ovarian cancer cells lines (Table 6.4) than the previous lead

compound AGF94 (Wang et al., 2011). Finally, AGF278 was a highly effective inhibitor of IGROV1 colony formation, while parent compound AGF117 failed to inhibit colony formation in conditions representing the acidic tumor microenvironment (Figure 6.4). These results establish that AGF278 is cytotoxic rather than cytostatic.

The notion of PCFT- and FRα-targeted treatments for cancer is not unprescedented. PMX, an excellent PCFT substrate, is used for the treatment of several cancer types (e.g., non-small cell lung cancer, malignant pleural mesothelioma), while several novel therapeutics have been developed to target ovarian cancer using FRα as the primary mechanism of delivery. Here, we describe compounds which display high affinities for both FRs and PCFT, with minimal off-target (RFC) uptake, typified by AGF278. Additionally, these compounds may have an additional therapeutic applications, as the addition of fluorine could allow these molecules to be used as PET imaging agents. As a theranostic tool, ^{18}F-labeled antifolates could used to detect tumors and to measure drug uptake in patients to directly determine tumor targeting. Certainly, these novel antifolates will be the subject of future studies.

CHAPTER 7- CONCLUSIONS

The goal of this dissertation work was to characterize key domains of PCFT protein structure, as well as to characterize novel PCFT-targeted antifolate compounds. Using SCAM, a reentrant loop structure was identified in the TMD2-3 loop domain via accessibility of single-cysteine mutants in this region to the membrane-impermeable MTSEA-biotin (Chapter 2). The interface for PCFT oligomerization was characterized using cysteine-scanning and MTS-6-MTS crosslinking (Chapter 3). Through the development of PCFT half molecules and PCFT/ThTr1 chimera proteins, the functional significance of the TMD6-7 loop region of PCFT was determined (Chapter 4). In a continuation of the ongoing effort to identify novel PCFT-targeted antifolate drugs, AGF94 and AGF154 were characterized in the context of NS-NSCLC and their increased specificity under conditions approximating those in the acidic tumor microenvironment was demonstrated (Chapter 5). Previously established PCFT- and FRα-targeted antifolates were modified through fluorine substitution, resulting in very targeted compounds including AGF278 (Chapter 6).

Structural information about PCFT will contribute to our understanding of both nutrition and HFM, given the important role that PCFT plays in the uptake of dietary folates. These studies will provide insights into future crystal structures of PCFT when they become available. Additionally, the work presented here is significant in its contribution toward the development of novel cancer therapies. As protein modeling technologies become increasingly advanced, PCFT structural information will become increasingly important in the development of PCFT-targeted antifolates. Likewise, the continued characterization of antifolate molecules will lead to the development of structure/activity relationships for PCFT, allowing for comprehensive data analysis of each antifolate compound and its relationship to PCFT structural elements.

The development of PCFT-targeted antifolates will provide a useful tool for clinicians in a wide variety of tumor types, reflecting broad expression of PCFT in tumors and high level activity under conditions approximating those in the tumor microenvironment. As previously described (see Chapter 1), classical antifolate molecules are used to treat a wide variety of tumor types, despite off-target effects. PCFT-targeted antifolates may provide a method by which chemotherapy can become more targeted. As tumor profiling becomes cheaper and more universal, PCFT may be a useful biomarker for clinicians to use to identify proper treatments for patients. Accordingly, PCFT-targeted antifolate molecules may become an increasingly valuable tool to clinicians as the field of oncology moves away from conventional chemotherapy in favor of more targeted treatments.

APPENDIX- Copyrights

REFERENCES

Abramson J, Kaback HR and Iwata S (2004) Structural comparison of lactose permease and the glycerol-3-phosphate antiporter: members of the major facilitator superfamily. *Curr Opin Struct Biol* **14**(4): 413-419.

Abramson J, Smirnova I, Kasho V, Verner G, Kaback HR and Iwata S (2003) Structure and mechanism of the lactose permease of Escherichia coli. *Science* **301**(5633): 610-615.

Alati T, Worzalla JF, Shih C, Bewley JR, Lewis S, Moran RG and Grindey GB (1996) Augmentation of the therapeutic activity of lometrexol -(6-R)5,10-dideazatetrahydrofolate- by oral folic acid. *Cancer Res* **56**(10): 2331-2335.

Albrecht AM, Biedler JL and Hutchison DJ (1972) Two different species of dihydrofolate reductase in mammalian cells differentially resistant to amethopterin and methasquin. *Cancer Res* **32**(7): 1539-1546.

Allegra CJ, Chabner BA, Drake JC, Lutz R, Rodbard D and Jolivet J (1985) Enhanced inhibition of thymidylate synthase by methotrexate polyglutamates. *J Biol Chem* **260**(17): 9720-9726.

Allegra CJ, Hoang K, Yeh GC, Drake JC and Baram J (1987) Evidence for direct inhibition of de novo purine synthesis in human MCF-7 breast cells as a principal mode of metabolic inhibition by methotrexate. *J Biol Chem* **262**(28): 13520-13526.

Almassy RJ, Janson CA, Kan CC and Hostomska Z (1992) Structures of apo and complexed Escherichia coli glycinamide ribonucleotide transformylase. *Proceedings of the National Academy of Sciences of the United States of America* **89**(13): 6114-6118.

Alt FW, Kellems RE, Bertino JR and Schimke RT (1978) Selective multiplication of dihydrofolate reductase genes in methotrexate-resistant variants of cultured murine cells. *J Biol Chem* **253**(5): 1357-1370.

American Cancer Society A (2015) What are the key statistics about lung cancer?

Anderson CM, Grenade DS, Boll M, Foltz M, Wake KA, Kennedy DJ, Munck LK, Miyauchi S, Taylor PM, Campbell FC, Munck BG, Daniel H, Ganapathy V and Thwaites DT (2004) H+/amino acid transporter 1 (PAT1) is the imino acid carrier: An intestinal nutrient/drug transporter in human and rat. *Gastroenterology* **127**(5): 1410-1422.

Anderson CM, Jevons M, Thangaraju M, Edwards N, Conlon NJ, Woods S, Ganapathy V and Thwaites DT (2010) Transport of the photodynamic therapy agent 5-aminolevulinic acid by distinct H+-coupled nutrient carriers coexpressed in the small intestine. *J Pharmacol Exp Ther* **332**(1): 220-228.

Anderson CM and Thwaites DT (2010) Hijacking solute carriers for proton-coupled drug transport. *Physiology (Bethesda, Md)* **25**(6): 364-377.

Ardizzoni A, Tiseo M, Boni L, Vincent AD, Passalacqua R, Buti S, Amoroso D, Camerini A, Labianca R, Genestreti G, Boni C, Ciuffreda L, Di Costanzo F, de Marinis F, Crino L, Santo A, Pazzola A, Barbieri F, Zilembo N, Colantonio I, Tibaldi C, Mattioli R, Cafferata MA, Camisa R and Smit EF (2012) Pemetrexed versus pemetrexed and carboplatin as second-line chemotherapy in advanced non-small-cell lung cancer: results of the GOIRC 02-2006 randomized phase II study and pooled analysis with the NVALT7 trial. *Journal of clinical oncology : official journal of the American Society of Clinical Oncology* **30**(36): 4501-4507.

Assaraf YG (2006) The role of multidrug resistance efflux transporters in antifolate resistance and folate homeostasis. *Drug resistance updates : reviews and commentaries in antimicrobial and anticancer chemotherapy* **9**(4-5): 227-246.

Assaraf YG (2007) Molecular basis of antifolate resistance. *Cancer Metastasis Rev* **26**(1): 153-181.

Assaraf YG, Babani S and Goldman ID (1998) Increased activity of a novel low pH folate transporter associated with lipophilic antifolate resistance in chinese hamster ovary cells. *J Biol Chem* **273**(14): 8106-8111.

Assaraf YG, Leamon CP and Reddy JA (2014) The folate receptor as a rational therapeutic target for personalized cancer treatment. *Drug resistance updates : reviews and commentaries in antimicrobial and anticancer chemotherapy* **17**(4-6): 89-95.

Atabay B, Turker M, Ozer EA, Mahadeo K, Diop-Bove N and Goldman ID (2010) Mutation of the proton-coupled folate transporter gene (PCFT-SLC46A1) in Turkish siblings with hereditary folate malabsorption. *Pediatr Hematol Oncol* **27**(8): 614-619.

Azzoli CG, Krug LM, Gomez J, Miller VA, Kris MG, Ginsberg MS, Henry R, Jones J, Tyson L, Dunne M, Pizzo B, Farmer A, Venkatraman E, Steffen R and Sirotnak FM (2007) A phase 1 study of pralatrexate in combination with paclitaxel or docetaxel in patients with advanced solid tumors. *Clin Cancer Res* **13**(9): 2692-2698.

Badagnani I, Castro RA, Taylor TR, Brett CM, Huang CC, Stryke D, Kawamoto M, Johns SJ, Ferrin TE, Carlson EJ, Burchard EG and Giacomini KM (2006) Interaction of methotrexate with organic-anion transporting polypeptide 1A2 and its genetic variants. *J Pharmacol Exp Ther* **318**(2): 521-529.

Baggott JE, Vaughn WH and Hudson BB (1986) Inhibition of 5-aminoimidazole-4-carboxamide ribotide transformylase, adenosine deaminase and 5'-adenylate deaminase by polyglutamates of methotrexate and oxidized folates and by 5-aminoimidazole-4-carboxamide riboside and ribotide. *Biochem J* **236**(1): 193-200.

Baldwin SW, Tse A, Gossett LS, Taylor EC, Rosowsky A, Shih C and Moran RG (1991) Structural features of 5,10-dideaza-5,6,7,8-tetrahydrofolate that determine inhibition of mammalian glycinamide ribonucleotide formyltransferase. *Biochemistry* **30**(7): 1997-2006.

Bareford MD, Park MA, Yacoub A, Hamed HA, Tang Y, Cruickshanks N, Eulitt P, Hubbard N, Tye G, Burow ME, Fisher PB, Moran RG, Nephew KP, Grant S and Dent P (2011) Sorafenib enhances pemetrexed cytotoxicity through an autophagy-dependent mechanism in cancer cells. *Cancer Res* **71**(14): 4955-4967.

Barlowe CK and Appling DR (1988) In vitro evidence for the involvement of mitochondrial folate metabolism in the supply of cytoplasmic one-carbon units. *BioFactors (Oxford, England)* **1**(2): 171-176.

Barlowe CK and Appling DR (1990) Molecular genetic analysis of Saccharomyces cerevisiae C1-tetrahydrofolate synthase mutants reveals a noncatalytic function of the ADE3 gene product and an additional folate-dependent enzyme. *Mol Cell Biol* **10**(11): 5679-5687.

Basu S and Alavi A (2016) PET-Based Personalized Management in Clinical Oncology: An Unavoidable Path for the Foreseeable Future. *PET Clin* **11**(3): 203-207.

Baugh CM, Krumdieck CL and Nair MG (1973) Polygammaglutamyl metabolites of methotrexate. *Biochem Biophys Res Commun* **52**(1): 27-34.

Beardsley GP, Moroson BA, Taylor EC and Moran RG (1989) A new folate antimetabolite, 5,10-dideaza-5,6,7,8-tetrahydrofolate is a potent inhibitor of de novo purine synthesis. *J Biol Chem* **264**(1): 328-333.

Belkov VM, Krynetski EY, Schuetz JD, Yanishevski Y, Masson E, Mathew S, Raimondi S, Pui CH, Relling MV and Evans WE (1999) Reduced folate carrier expression in acute lymphoblastic leukemia: a mechanism for ploidy but not lineage differences in methotrexate accumulation. *Blood* **93**(5): 1643-1650.

Benard J, Da Silva J, De Blois MC, Boyer P, Duvillard P, Chiric E and Riou G (1985) Characterization of a human ovarian adenocarcinoma line, IGROV1, in tissue culture and in nude mice. *Cancer Res* **45**(10): 4970-4979.

Bissett D, McLeod HL, Sheedy B, Collier M, Pithavala Y, Paradiso L, Pitsiladis M and Cassidy J (2001) Phase I dose-escalation and pharmacokinetic study of a novel folate analogue AG2034. *Br J Cancer* **84**(3): 308-312.

Bolusani S, Young BA, Cole NA, Tibbetts AS, Momb J, Bryant JD, Solmonson A and Appling DR (2011) Mammalian MTHFD2L encodes a mitochondrial methylenetetrahydrofolate dehydrogenase isozyme expressed in adult tissues. *J Biol Chem* **286**(7): 5166-5174.

Boritzki TJ, Barlett CA, Zhang C and Howland EF (1996) AG2034: a novel inhibitor of glycinamide ribonucleotide formyltransferase. *Investigational new drugs* **14**(3): 295-303.

Borzutzky A, Crompton B, Bergmann AK, Giliani S, Baxi S, Martin M, Neufeld EJ and Notarangelo LD (2009) Reversible severe combined immunodeficiency phenotype secondary to a mutation of the proton-coupled folate transporter. *Clin Immunol* **133**(3): 287-294.

Bronder JL and Moran RG (2003) A defect in the p53 response pathway induced by de novo purine synthesis inhibition. *J Biol Chem* **278**(49): 48861-48871.

Budman DR, Johnson R, Barile B, Bowsher RR, Vinciguerra V, Allen SL, Kolitz J, Ernest CS, 2nd, Kreis W, Zervos P and Walling J (2001) Phase I and pharmacokinetic study of LY309887: a specific inhibitor of purine biosynthesis. *Cancer Chemother Pharmacol* **47**(6): 525-531.

Bueno R, Appasani K, Mercer H, Lester S and Sugarbaker D (2001) The alpha folate receptor is highly activated in malignant pleural mesothelioma. *J Thorac Cardiovasc Surg* **121**(2): 225-233.

Buist MR, Molthoff CF, Kenemans P and Meijer CJ (1995) Distribution of OV-TL 3 and MOv18 in normal and malignant ovarian tissue. *Journal of clinical pathology* **48**(7): 631-636.

Busco G, Cardone RA, Greco MR, Bellizzi A, Colella M, Antelmi E, Mancini MT, Dell'Aquila ME, Casavola V, Paradiso A and Reshkin SJ (2010) NHE1 promotes invadopodial ECM proteolysis through acidification of the peri-invadopodial space. *FASEB J* **24**(10): 3903-3915.

Campbell IG, Jones TA, Foulkes WD and Trowsdale J (1991) Folate-binding protein is a marker for ovarian cancer. *Cancer Res* **51**(19): 5329-5338.

Cao W and Matherly LH (2003) Characterization of a cysteine-less human reduced folate carrier: localization of a substrate-binding domain by cysteine-scanning mutagenesis and cysteine accessibility methods. *Biochem J* **374**(Pt 1): 27-36.

Cao W and Matherly LH (2004) Analysis of the membrane topology for transmembrane domains 7-12 of the human reduced folate carrier by scanning cysteine accessibility methods. *Biochem J* **378**(Pt 1): 201-206.

Chancy CD, Kekuda R, Huang W, Prasad PD, Kuhnel JM, Sirotnak FM, Roon P, Ganapathy V and Smith SB (2000) Expression and differential polarization of the reduced-folate transporter-1 and the folate receptor alpha in mammalian retinal pigment epithelium. *J Biol Chem* **275**(27): 20676-20684.

Chattopadhyay S, Moran RG and Goldman ID (2007) Pemetrexed: biochemical and cellular pharmacology, mechanisms, and clinical applications. *Mol Cancer Ther* **6**(2): 404-417.

Chattopadhyay S, Wang Y, Zhao R and Goldman ID (2004) Lack of Impact of the Loss of Constitutive Folate Receptor {alpha} Expression, Achieved by RNA Interference, on the Activity of the New Generation Antifolate Pemetrexed in HeLa Cells. *Clin Cancer Res* **10**(23): 7986-7993.

Chattopadhyay S, Zhao R, Krupenko SA, Krupenko N and Goldman ID (2006) The inverse relationship between reduced folate carrier function and pemetrexed activity in a human colon cancer cell line. *Mol Cancer Ther* **5**(2): 438-449.

Chello PL, Sirotnak FM, Wong E, Kisliuk RL, Gaumont Y and Combepine G (1982) Further studies stereospecificity at carbon 6 for membrane transport of tetrahydrofolates. Diastereoisomers of 5-methyltetrahydrofolates as competitive inhibitors of transport of methotrexate in L1210 cells. *Biochem Pharmacol* **31**(8): 1527-1530.

Cherian C, Kugel Desmoulin S, Wang L, Polin L, White K, Kushner J, Stout M, Hou Z, Gangjee A and Matherly LH (2013) Therapeutic targeting malignant mesothelioma with a novel

6-substituted pyrrolo[2,3-d]pyrimidine thienoyl antifolate via its selective uptake by the proton-coupled folate transporter. *Cancer Chemother Pharmacol* **71**(4): 999-1011.

Chiang Y, Chou CY, Hsu KF, Huang YF and Shen MR (2008) EGF upregulates Na+/H+ exchanger NHE1 by post-translational regulation that is important for cervical cancer cell invasiveness. *Journal of cellular physiology* **214**(3): 810-819.

Chiche J, Le Fur Y, Vilmen C, Frassineti F, Daniel L, Halestrap AP, Cozzone PJ, Pouyssegur J and Lutz NW (2012) In vivo pH in metabolic-defective Ras-transformed fibroblast tumors: key role of the monocarboxylate transporter, MCT4, for inducing an alkaline intracellular pH. *Int J Cancer* **130**(7): 1511-1520.

Chladek J, Martinkova J, Simkova M, Vaneckova J, Koudelkova V and Nozickova M (1998) Pharmacokinetics of low doses of methotrexate in patients with psoriasis over the early period of treatment. *European journal of clinical pharmacology* **53**(6): 437-444.

Christoph DC, Asuncion BR, Hassan B, Tran C, Maltzman JD, O'Shannessy DJ, Wynes MW, Gauler TC, Wohlschlaeger J, Hoiczyk M, Schuler M, Eberhardt WE and Hirsch FR (2013) Significance of folate receptor alpha and thymidylate synthase protein expression in patients with non-small-cell lung cancer treated with pemetrexed. *Journal of thoracic oncology : official publication of the International Association for the Study of Lung Cancer* **8**(1): 19-30.

Christopherson RI, Lyons SD and Wilson PK (2002) Inhibitors of de novo nucleotide biosynthesis as drugs. *Accounts of chemical research* **35**(11): 961-971.

Chu E, Callender MA, Farrell MP and Schmitz JC (2003) Thymidylate synthase inhibitors as anticancer agents: from bench to bedside. *Cancer Chemother Pharmacol* **52 Suppl 1**: S80-89.

Ciuleanu T, Brodowicz T, Zielinski C, Kim JH, Krzakowski M, Laack E, Wu YL, Bover I, Begbie S, Tzekova V, Cucevic B, Pereira JR, Yang SH, Madhavan J, Sugarman KP, Peterson P, John WJ, Krejcy K and Belani CP (2009) Maintenance pemetrexed plus best supportive care versus placebo plus best supportive care for non-small-cell lung cancer: a randomised, double-blind, phase 3 study. *Lancet* **374**(9699): 1432-1440.

Ciuleanu T, Diculescu M, Hoepffner NM, Trojan J, Sailer V, Zalupski M, Herrmann T, Roth A, Chick J, Brock K, Albert D and Philip PA (2007) A randomised phase II study of OSI-7904L versus 5-fluorouracil (FU)/leucovorin (LV) as first-line treatment in patients with advanced biliary cancers. *Investigational new drugs* **25**(4): 385-390.

Cohen MH, Cortazar P, Justice R and Pazdur R (2010) Approval summary: pemetrexed maintenance therapy of advanced/metastatic nonsquamous, non-small cell lung cancer (NSCLC). *Oncologist* **15**(12): 1352-1358.

Cohen MH, Justice R and Pazdur R (2009) Approval summary: pemetrexed in the initial treatment of advanced/metastatic non-small cell lung cancer. *Oncologist* **14**(9): 930-935.

Cole PD, Drachtman RA, Masterson M, Smith AK, Glod J, Zebala JA, Lisi S, Drapala DA and Kamen BA (2008) Phase 2B trial of aminopterin in multiagent therapy for children with newly diagnosed acute lymphoblastic leukemia. *Cancer Chemother Pharmacol* **62**(1): 65-75.

Corbett TH, LoRusso P, Demchick L, Simpson C, Pugh S, White K, Kushner J, Polin L, Meyer J, Czarnecki J, Heilbrun L, Horwitz JP, Gross JL, Behrens CH, Harrison BA, McRipley RJ and Trainor G (1998) Preclinical antitumor efficacy of analogs of XK469: sodium-(2-[4-(7-chloro-2-quinoxalinyloxy)phenoxy]propionate. *Investigational new drugs* **16**(2): 129-139.

Corbett TH, Valeriote FA, Demchik L, Lowichik N, Polin L, Panchapor C, Pugh S, White K, Kushner J, Rake J, Wentland M, Golakoti T, Hetzel C, Ogino J, Patterson G and Moore R (1997) Discovery of cryptophycin-1 and BCN-183577: examples of strategies and problems in the detection of antitumor activity in mice. *Investigational new drugs* **15**(3): 207-218.

Davis SR, Stacpoole PW, Williamson J, Kick LS, Quinlivan EP, Coats BS, Shane B, Bailey LB and Gregory JF, 3rd (2004) Tracer-derived total and folate-dependent homocysteine remethylation and synthesis rates in humans indicate that serine is the main one-carbon donor. *American journal of physiology Endocrinology and metabolism* **286**(2): E272-279.

DeGraw JI, Colwell WT, Piper JR and Sirotnak FM (1993) Synthesis and antitumor activity of 10-propargyl-10-deazaaminopterin. *J Med Chem* **36**(15): 2228-2231.

Deng Y, Wang Y, Cherian C, Hou Z, Buck SA, Matherly LH and Gangjee A (2008) Synthesis and discovery of high affinity folate receptor-specific glycinamide ribonucleotide formyltransferase inhibitors with antitumor activity. *J Med Chem* **51**(16): 5052-5063.

Deng Y, Zhou X, Kugel Desmoulin S, Wu J, Cherian C, Hou Z, Matherly LH and Gangjee A (2009) Synthesis and biological activity of a novel series of 6-substituted thieno[2,3-d]pyrimidine antifolate inhibitors of purine biosynthesis with selectivity for high affinity folate receptors over the reduced folate carrier and proton-coupled folate transporter for cellular entry. *J Med Chem* **52**(9): 2940-2951.

Denkert C, Budczies J, Weichert W, Wohlgemuth G, Scholz M, Kind T, Niesporek S, Noske A, Buckendahl A, Dietel M and Fiehn O (2008) Metabolite profiling of human colon carcinoma--deregulation of TCA cycle and amino acid turnover. *Molecular cancer* **7**: 72.

Desmoulin SK, Hou Z, Gangjee A and Matherly LH (2012a) The human proton-coupled folate transporter: Biology and therapeutic applications to cancer. *Cancer biology & therapy* **13**(14): 1355-1373.

Desmoulin SK, Wang L, Polin L, White K, Kushner J, Stout M, Hou Z, Cherian C, Gangjee A and Matherly LH (2012b) Functional loss of the reduced folate carrier enhances the antitumor activities of novel antifolates with selective uptake by the proton-coupled folate transporter. *Mol Pharmacol* **82**(4): 591-600.

Ding BC, Witt TL, Hukku B, Heng H, Zhang L and Matherly LH (2001) Association of deletions and translocation of the reduced folate carrier gene with profound loss of gene expression in methotrexate-resistant K562 human erythroleukemia cells. *Biochem Pharmacol* **61**(6): 665-675.

Diop-Bove NK, Wu J, Zhao R, Locker J and Goldman ID (2009) Hypermethylation of the human proton-coupled folate transporter (SLC46A1) minimal transcriptional regulatory region in an antifolate-resistant HeLa cell line. *Mol Cancer Ther* **8**(8): 2424-2431.

Dixon KH, Lanpher BC, Chiu J, Kelley K and Cowan KH (1994) A novel cDNA restores reduced folate carrier activity and methotrexate sensitivity to transport deficient cells. *J Biol Chem* **269**(1): 17-20.

Dolnick BJ, Berenson RJ, Bertino JR, Kaufman RJ, Nunberg JH and Schimke RT (1979) Correlation of dihydrofolate reductase elevation with gene amplification in a homogeneously staining chromosomal region in L5178Y cells. *The Journal of cell biology* **83**(2 Pt 1): 394-402.

Drake JC, Allegra CJ, Moran RG and Johnston PG (1996) Resistance to tomudex (ZD1694): multifactorial in human breast and colon carcinoma cell lines. *Biochem Pharmacol* **51**(10): 1349-1355.

Duan P, Wu J and You G (2011) Mutational analysis of the role of GXXXG motif in the function of human organic anion transporter 1 (hOAT1). *International journal of biochemistry and molecular biology* **2**(1): 1-7.

Duch DS, Banks S, Dev IK, Dickerson SH, Ferone R, Heath LS, Humphreys J, Knick V, Pendergast W, Singer S and et al. (1993) Biochemical and cellular pharmacology of 1843U89, a novel benzoquinazoline inhibitor of thymidylate synthase. *Cancer Res* **53**(4): 810-818.

Edelman MJ, Harb WA, Pal SE, Boccia RV, Kraut MJ, Bonomi P, Conley BA, Rogers JS, Messmann RA and Garon EB (2012) Multicenter trial of EC145 in advanced, folate-receptor positive adenocarcinoma of the lung. *Journal of thoracic oncology : official publication of the International Association for the Study of Lung Cancer* **7**(10): 1618-1621.

Elnakat H and Ratnam M (2004) Distribution, functionality and gene regulation of folate receptor isoforms: implications in targeted therapy. *Adv Drug Deliv Rev* **56**(8): 1067-1084.

Elwood PC (1989) Molecular cloning and characterization of the human folate-binding protein cDNA from placenta and malignant tissue culture (KB) cells. *J Biol Chem* **264**(25): 14893-14901.

Esteban E, Casillas M and Cassinello A (2009) Pemetrexed in first-line treatment of non-small cell lung cancer. *Cancer treatment reviews* **35**(4): 364-373.

Evans CO, Young AN, Brown MR, Brat DJ, Parks JS, Neish AS and Oyesiku NM (2001) Novel patterns of gene expression in pituitary adenomas identified by complementary deoxyribonucleic acid microarrays and quantitative reverse transcription-polymerase chain reaction. *The Journal of clinical endocrinology and metabolism* **86**(7): 3097-3107.

Fairbanks LD, Bofill M, Ruckemann K and Simmonds HA (1995) Importance of ribonucleotide availability to proliferating T-lymphocytes from healthy humans. Disproportionate expansion of pyrimidine pools and contrasting effects of de novo synthesis inhibitors. *J Biol Chem* **270**(50): 29682-29689.

Falk S, Anthoney A, Eatock M, Van Cutsem E, Chick J, Glen H, Valle JW, Drolet DW, Albert D, Ferry D and Ajani J (2006) Multicentre phase II pharmacokinetic and pharmacodynamic study of OSI-7904L in previously untreated patients with advanced gastric or gastroesophageal junction adenocarcinoma. *Br J Cancer* **95**(4): 450-456.

Farber S (1949) Some observations on the effect of folic acid antagonists on acute leukemia and other forms of incurable cancer. *Blood* **4**(2): 160-167.

Farber S, Cutler EC, Hawkins JW, Harrison JH, Peirce EC, 2nd and Lenz GG (1947) The Action of Pteroylglutamic Conjugates on Man. *Science* **106**(2764): 619-621.

Farber S and Diamond LK (1948) Temporary remissions in acute leukemia in children produced by folic acid antagonist, 4-aminopteroyl-glutamic acid. *N Engl J Med* **238**(23): 787-793.

Feagan BG, Rochon J, Fedorak RN, Irvine EJ, Wild G, Sutherland L, Steinhart AH, Greenberg GR, Gillies R, Hopkins M and et al. (1995) Methotrexate for the treatment of Crohn's disease. The North American Crohn's Study Group Investigators. *N Engl J Med* **332**(5): 292-297.

Ferguson PL and Flintoff WF (1999) Topological and functional analysis of the human reduced folate carrier by hemagglutinin epitope insertion. *J Biol Chem* **274**(23): 16269-16278.

Ferreri AJ, Dell'Oro S, Capello D, Ponzoni M, Iuzzolino P, Rossi D, Pasini F, Ambrosetti A, Orvieto E, Ferrarese F, Arrigoni G, Foppoli M, Reni M and Gaidano G (2004) Aberrant methylation in the promoter region of the reduced folate carrier gene is a potential mechanism of resistance to methotrexate in primary central nervous system lymphomas. *British journal of haematology* **126**(5): 657-664.

Flintoff WF, Davidson SV and Siminovitch L (1976) Isolation and partial characterization of three methotrexate-resistant phenotypes from Chinese hamster ovary cells. *Somatic Cell Genet* **2**(3): 245-261.

Flintoff WF and Essani K (1980) Methotrexate-resistant Chinese hamster ovary cells contain a dihydrofolate reductase with an altered affinity for methotrexate. *Biochemistry* **19**(18): 4321-4327.

Flintoff WF and Nagainis CR (1983) Transport of methotrexate in Chinese hamster ovary cells: a mutant defective in methotrexate uptake and cell binding. *Arch Biochem Biophys* **223**(2): 433-440.

Freemantle SJ, Jackman AL, Kelland LR, Calvert AH and Lunec J (1995) Molecular characterisation of two cell lines selected for resistance to the folate-based thymidylate synthase inhibitor, ZD1694. *Br J Cancer* **71**(5): 925-930.

Friedkin M and Roberts D (1956) Conversion of uracil deoxyriboside to thymidine of deoxyribonucleic acid. *J Biol Chem* **220**(2): 653-660.

Gallagher FA, Kettunen MI, Day SE, Hu DE, Ardenkjaer-Larsen JH, Zandt R, Jensen PR, Karlsson M, Golman K, Lerche MH and Brindle KM (2008) Magnetic resonance

imaging of pH in vivo using hyperpolarized 13C-labelled bicarbonate. *Nature* **453**(7197): 940-943.

Gangjee A, Zeng Y, McGuire JJ and Kisliuk RL (2005) Synthesis of classical, four-carbon bridged 5-substituted furo[2,3-d]pyrimidine and 6-substituted pyrrolo[2,3-d]pyrimidine analogues as antifolates. *J Med Chem* **48**(16): 5329-5336.

Gangjee A, Zeng Y, McGuire JJ, Mehraein F and Kisliuk RL (2004) Synthesis of classical, three-carbon-bridged 5-substituted furo[2,3-d]pyrimidine and 6-substituted pyrrolo[2,3-d]pyrimidine analogues as antifolates. *J Med Chem* **47**(27): 6893-6901.

Garcia-Martinez LF and Appling DR (1993) Characterization of the folate-dependent mitochondrial oxidation of carbon 3 of serine. *Biochemistry* **32**(17): 4671-4676.

Garin-Chesa P, Campbell I, Saigo PE, Lewis JL, Jr., Old LJ and Rettig WJ (1993) Trophoblast and ovarian cancer antigen LK26. Sensitivity and specificity in immunopathology and molecular identification as a folate-binding protein. *The American journal of pathology* **142**(2): 557-567.

Garnier J, Gibrat JF and Robson B (1996) GOR method for predicting protein secondary structure from amino acid sequence. *Methods Enzymol* **266**: 540-553.

Ge H, Ni S, Wang X, Xu N, Liu Y, Wang X, Wang L, Song D, Song Y and Bai C (2012) Dexamethasone reduces sensitivity to cisplatin by blunting p53-dependent cellular senescence in non-small cell lung cancer. *PloS one* **7**(12): e51821.

Geller J, Kronn D, Jayabose S and Sandoval C (2002) Hereditary folate malabsorption: family report and review of the literature. *Medicine (Baltimore)* **81**(1): 51-68.

Genova C, Rijavec E, Truini A, Coco S, Sini C, Barletta G, Dal Bello MG, Alama A, Savarino G, Pronzato P, Boccardo F and Grossi F (2013) Pemetrexed for the treatment of non-small cell lung cancer. *Expert opinion on pharmacotherapy* **14**(11): 1545-1558.

Gerber D and Shai Y (2001) In vivo detection of hetero-association of glycophorin-A and its mutants within the membrane. *J Biol Chem* **276**(33): 31229-31232.

Gerber DE and Schiller JH (2013) Maintenance chemotherapy for advanced non-small-cell lung cancer: new life for an old idea. *Journal of clinical oncology : official journal of the American Society of Clinical Oncology* **31**(8): 1009-1020.

Gibbs DD, Theti DS, Wood N, Green M, Raynaud F, Valenti M, Forster MD, Mitchell F, Bavetsias V, Henderson E and Jackman AL (2005) BGC 945, a novel tumor-selective thymidylate synthase inhibitor targeted to alpha-folate receptor-overexpressing tumors. *Cancer Res* **65**(24): 11721-11728.

Gillies RJ, Raghunand N, Karczmar GS and Bhujwalla ZM (2002) MRI of the tumor microenvironment. *Journal of magnetic resonance imaging : JMRI* **16**(4): 430-450.

Gillis EP, Eastman KJ, Hill MD, Donnelly DJ and Meanwell NA (2015) Applications of Fluorine in Medicinal Chemistry. *J Med Chem* **58**(21): 8315-8359.

Gokhale M, Thakur A and Rinaldi F (2013) Degradation of BMS-753493, a novel epothilone folate conjugate anticancer agent. *Drug development and industrial pharmacy* **39**(9): 1315-1327.

Golani LK, George C, Zhao S, Raghavan S, Orr S, Wallace A, Wilson MR, Hou Z, Matherly LH and Gangjee A (2014) Structure-activity profiles of novel 6-substituted pyrrolo[2,3-d]pyrimidine thienoyl antifolates with modified amino acids for cellular uptake by folate

receptors alpha and beta and the proton-coupled folate transporter. *J Med Chem* **57**(19): 8152-8166.

Goldie JH, Krystal G, Hartley D, Gudauskas G and Dedhar S (1980) A methotrexate insensitive variant of folate reductase present in two lines of methotrexate-resistant L5178Y cells. *Eur J Cancer* **16**(12): 1539-1546.

Goldin A, Venditti JM, Humphreys SR, Dennis D, Mantel N and Greenhouse SW (1955) A quantitative comparison of the antileukemic effectiveness of two folic acid antagonists in mice. *Journal of the National Cancer Institute* **15**(6): 1657-1664.

Goldman ID (1969) Transport energetics of the folic acid analogue, methotrexate, in L1210 leukemia cells. Enhanced accumulation by metabolic inhibitors. *J Biol Chem* **244**(14): 3779-3785.

Goldman ID (1971) The characteristics of the membrane transport of amethopterin and the naturally occurring folates. *Annals of the New York Academy of Sciences* **186**: 400-422.

Goldman ID, Lichtenstein NS and Oliverio VT (1968) Carrier-mediated transport of the folic acid analogue, methotrexate, in the L1210 leukemia cell. *J Biol Chem* **243**(19): 5007-5017.

Gonen N and Assaraf YG (2012) Antifolates in cancer therapy: structure, activity and mechanisms of drug resistance. *Drug resistance updates : reviews and commentaries in antimicrobial and anticancer chemotherapy* **15**(4): 183-210.

Gonen N, Bram EE and Assaraf YG (2008) PCFT/SLC46A1 promoter methylation and restoration of gene expression in human leukemia cells. *Biochem Biophys Res Commun* **376**(4): 787-792.

Gorlick R, Goker E, Trippett T, Steinherz P, Elisseyeff Y, Mazumdar M, Flintoff WF and Bertino JR (1997) Defective transport is a common mechanism of acquired methotrexate resistance in acute lymphocytic leukemia and is associated with decreased reduced folate carrier expression. *Blood* **89**(3): 1013-1018.

Gregory JF, 3rd, Cuskelly GJ, Shane B, Toth JP, Baumgartner TG and Stacpoole PW (2000) Primed, constant infusion with [2H3]serine allows in vivo kinetic measurement of serine turnover, homocysteine remethylation, and transsulfuration processes in human one-carbon metabolism. *The American journal of clinical nutrition* **72**(6): 1535-1541.

Guo W, Healey JH, Meyers PA, Ladanyi M, Huvos AG, Bertino JR and Gorlick R (1999) Mechanisms of methotrexate resistance in osteosarcoma. *Clin Cancer Res* **5**(3): 621-627.

Gwinn DM, Shackelford DB, Egan DF, Mihaylova MM, Mery A, Vasquez DS, Turk BE and Shaw RJ (2008) AMPK phosphorylation of raptor mediates a metabolic checkpoint. *Molecular cell* **30**(2): 214-226.

Haber DA, Beverley SM, Kiely ML and Schimke RT (1981) Properties of an altered dihydrofolate reductase encoded by amplified genes in cultured mouse fibroblasts. *J Biol Chem* **256**(18): 9501-9510.

Hainsworth J, Vergote I and Janssens J (2003) A review of phase II studies of ZD9331 treatment for relapsed or refractory solid tumours. *Anti-cancer drugs* **14 Suppl 1**: S13-19.

Hanlon MH and Ferone R (1996) In vitro uptake, anabolism, and cellular retention of 1843U89 and other benzoquinazoline inhibitors of thymidylate synthase. *Cancer Res* **56**(14): 3301-3306.

Hanna N, Juhasz E, C. Cainap OG, Ramlau R, Juan-Vidal O, JS RL, Perex W, Nguyen B and Harb W (2014) Target: A randomixed, phase II trial comparing vintafolide plus

docetaxel, versus docetaxel alone in second line treatment of folate-receptor-positive non-small cell lung cancer (NSCLC) *Annals of Oncology* **1-41**.

Hanna N, Shepherd FA, Fossella FV, Pereira JR, De Marinis F, von Pawel J, Gatzemeier U, Tsao TC, Pless M, Muller T, Lim HL, Desch C, Szondy K, Gervais R, Shaharyar, Manegold C, Paul S, Paoletti P, Einhorn L and Bunn PA, Jr. (2004) Randomized phase III trial of pemetrexed versus docetaxel in patients with non-small-cell lung cancer previously treated with chemotherapy. *Journal of clinical oncology : official journal of the American Society of Clinical Oncology* **22**(9): 1589-1597.

Hartman SC and Buchanan JM (1959a) The biosynthesis of the purines. *Ergebnisse der Physiologie, biologischen Chemie und experimentellen Pharmakologie* **50**: 75-121.

Hartman SC and Buchanan JM (1959b) Biosynthesis of the purines. XXVI. The identification of the formyl donors of the transformylation reactions. *J Biol Chem* **234**(7): 1812-1816.

Hatch FT, Larrabee AR, Cathou RE and Buchanan JM (1961) Enzymatic synthesis of the methyl group of methionine. I. Identification of the enzymes and cofactors involved in the system isolated from Escherichia coli. *J Biol Chem* **236**: 1095-1101.

Hazarika M, White RM, Jr., Booth BP, Wang YC, Ham DY, Liang CY, Rahman A, Gobburu JV, Li N, Sridhara R, Morse DE, Lostritto R, Garvey P, Johnson JR and Pazdur R (2005) Pemetrexed in malignant pleural mesothelioma. *Clin Cancer Res* **11**(3): 982-992.

Henderson GB and Strauss BP (1990) Characteristics of a novel transport system for folate compounds in wild-type and methotrexate-resistant L1210 cells. *Cancer Res* **50**(6): 1709-1714.

Herbig K, Chiang EP, Lee LR, Hills J, Shane B and Stover PJ (2002) Cytoplasmic serine hydroxymethyltransferase mediates competition between folate-dependent

deoxyribonucleotide and S-adenosylmethionine biosyntheses. *J Biol Chem* **277**(41): 38381-38389.

Hill BT, Bailey BD, White JC and Goldman ID (1979) Characteristics of transport of 4-amino antifolates and folate compounds by two lines of L5178Y lymphoblasts, one with impaired transport of methotrexate. *Cancer Res* **39**(7 Pt 1): 2440-2446.

Hinton A, Sennoune SR, Bond S, Fang M, Reuveni M, Sahagian GG, Jay D, Martinez-Zaguilan R and Forgac M (2009) Function of a subunit isoforms of the V-ATPase in pH homeostasis and in vitro invasion of MDA-MB231 human breast cancer cells. *J Biol Chem* **284**(24): 16400-16408.

Horns RC, Jr., Dower WJ and Schimke RT (1984) Gene amplification in a leukemic patient treated with methotrexate. *Journal of clinical oncology : official journal of the American Society of Clinical Oncology* **2**(1): 2-7.

Hou Z, Kugel Desmoulin S, Etnyre E, Olive M, Hsiung B, Cherian C, Wloszczynski PA, Moin K and Matherly LH (2012) Identification and functional impact of homo-oligomers of the human proton-coupled folate transporter. *J Biol Chem* **287**(7): 4982-4995.

Hou Z and Matherly LH (2009) Oligomeric structure of the human reduced folate carrier: identification of homo-oligomers and dominant-negative effects on carrier expression and function. *J Biol Chem* **284**(5): 3285-3293.

Hou Z and Matherly LH (2014) Biology of the major facilitative folate transporters SLC19A1 and SLC46A1. *Current topics in membranes* **73**: 175-204.

Hou Z, Stapels SE, Haska CL and Matherly LH (2005) Localization of a substrate binding domain of the human reduced folate carrier to transmembrane domain 11 by radioaffinity

labeling and cysteine-substituted accessibility methods. *J Biol Chem* **280**(43): 36206-36213.

Hou Z, Wu J, Ye J, Cherian C and Matherly LH (2010) Substrate-specific binding and conformational changes involving Ser313 and transmembrane domain 8 of the human reduced folate carrier, as determined by site-directed mutagenesis and protein cross-linking. *Biochem J* **430**(2): 265-274.

Hou Z, Ye J, Haska CL and Matherly LH (2006) Transmembrane domains 4, 5, 7, 8, and 10 of the human reduced folate carrier are important structural or functional components of the transmembrane channel for folate substrates. *J Biol Chem* **281**(44): 33588-33596.

Hovi T, Smyth JF, Allison AC and Williams SC (1976) Role of adenosine deaminase in lymphocyte proliferation. *Clinical and experimental immunology* **23**(3): 395-403.

Howell SB, Mansfield SJ and Taetle R (1981) Thymidine and hypoxanthine requirements of normal and malignant human cells for protection against methotrexate cytotoxicity. *Cancer Res* **41**(3): 945-950.

Huang Y, Lemieux MJ, Song J, Auer M and Wang DN (2003) Structure and mechanism of the glycerol-3-phosphate transporter from Escherichia coli. *Science* **301**(5633): 616-620.

Hughes LR, Stephens TC, Boyle FT and Jackman AL (1999) Raltitrexed (Tomudex), a Highly Polyglutamatable Antifolate Thymidylate Synthase Inhibitor, in *Anticancer Drug Development Guide: Antifolate Drugs in Cancer Therapy* (Jackman AL ed) pp 147-165, Humana Press, Inc., Totowa, NJ.

Hum DW, Bell AW, Rozen R and MacKenzie RE (1988) Primary structure of a human trifunctional enzyme. Isolation of a cDNA encoding methylenetetrahydrofolate

dehydrogenase-methenyltetrahydrofolate cyclohydrolase-formyltetrahydrofolate synthetase. *J Biol Chem* **263**(31): 15946-15950.

Humphreys GK and Greenberg DM (1958) Studies on the conversion of deoxyuridylic acid to thymidylic acid by a soluble extract from rat thymus. *Archives of biochemistry and biophysics* **78**(2): 275-287.

Ifergan I, Meller I, Issakov J and Assaraf YG (2003) Reduced folate carrier protein expression in osteosarcoma: implications for the prediction of tumor chemosensitivity. *Cancer* **98**(9): 1958-1966.

Inoki K, Zhu T and Guan KL (2003) TSC2 mediates cellular energy response to control cell growth and survival. *Cell* **115**(5): 577-590.

Inoue K, Nakai Y, Ueda S, Kamigaso S, Ohta KY, Hatakeyama M, Hayashi Y, Otagiri M and Yuasa H (2008) Functional characterization of PCFT/HCP1 as the molecular entity of the carrier-mediated intestinal folate transport system in the rat model. *Am J Physiol Gastrointest Liver Physiol* **294**(3): G660-668.

Jackman AL (1999) Past and Future Perspectives, in *Anticancer Drug Development Guide: Antifolate Drugs in Cancer Therapy* (Jackman AL ed) pp 1-12, Humana Press Inc., Totowa, NJ.

Jackman AL, Boyle FT and Harrap KR (1996) Tomudex (ZD1694): from concept to care, a programme in rational drug discovery. *Investigational new drugs* **14**(3): 305-316.

Jackman AL and Calvert AH (1995) Folate-based thymidylate synthase inhibitors as anticancer drugs. *Annals of oncology : official journal of the European Society for Medical Oncology / ESMO* **6**(9): 871-881.

Jackman AL, Kimbell R, Aherne GW, Brunton L, Jansen G, Stephens TC, Smith MN, Wardleworth JM and Boyle FT (1997) Cellular pharmacology and in vivo activity of a new anticancer agent, ZD9331: a water-soluble, nonpolyglutamatable, quinazoline-based inhibitor of thymidylate synthase. *Clin Cancer Res* **3**(6): 911-921.

Jackman AL, Marsham PR, Moran RG, Kimbell R, O'Connor BM, Hughes LR and Calvert AH (1991a) Thymidylate synthase inhibitors: the in vitro activity of a series of heterocyclic benzoyl ring modified 2-desamino-2-methyl-N10-substituted-5,8-dideazafolates. *Advances in enzyme regulation* **31**: 13-27.

Jackman AL, Taylor GA, Gibson W, Kimbell R, Brown M, Calvert AH, Judson IR and Hughes LR (1991b) ICI D1694, a quinazoline antifolate thymidylate synthase inhibitor that is a potent inhibitor of L1210 tumor cell growth in vitro and in vivo: a new agent for clinical study. *Cancer Res* **51**(20): 5579-5586.

Jackson RC and Harkrader RJ (1981) The contributions of de-novo and salvage pathways of nucleotide biosynthesis in normal and malignant cells, in *Nucleosides and Cancer Treatment* (Tattersall MHN and Fox RM eds) pp 18-31, Academic Press, Sydney.

Jackson RC and Harrap KR (1973) Studies with a mathematical model of folate metabolism. *Arch Biochem Biophys* **158**(2): 827-841.

Jackson RC, Hart LI and Harrap KR (1976) Intrinsic resistance to methotrexate of cultured mammalian cells in relation to the inhibition kinetics of their dihydrololate reductases. *Cancer Res* **36**(6): 1991-1997.

Jacques PF, Selhub J, Bostom AG, Wilson PW and Rosenberg IH (1999) The effect of folic acid fortification on plasma folate and total homocysteine concentrations. *N Engl J Med* **340**(19): 1449-1454.

Jansen G (1999) Receptor- and carrier- mediated transport system for folates and antifolates, in *Anticancer Drug Development Guide: Antifolate Drugs in Cancer Therapy* (Jackman AL ed) p 293, Humana Press Inc., Totowa, NJ.

Jiang D, Zhao Y, Wang X, Fan J, Heng J, Liu X, Feng W, Kang X, Huang B, Liu J and Zhang XC (2013) Structure of the YajR transporter suggests a transport mechanism based on the conserved motif A. *Proceedings of the National Academy of Sciences of the United States of America* **110**(36): 14664-14669.

Johnson SW, Swiggard PA, Handel LM, Brennan JM, Godwin AK, Ozols RF and Hamilton TC (1994) Relationship between platinum-DNA adduct formation and removal and cisplatin cytotoxicity in cisplatin-sensitive and -resistant human ovarian cancer cells. *Cancer Res* **54**(22): 5911-5916.

Jolivet J, Cowan KH, Curt GA, Clendeninn NJ and Chabner BA (1983) The pharmacology and clinical use of methotrexate. *N Engl J Med* **309**(18): 1094-1104.

Kamen BA, Wang MT, Streckfuss AJ, Peryea X and Anderson RG (1988) Delivery of folates to the cytoplasm of MA104 cells is mediated by a surface membrane receptor that recycles. *J Biol Chem* **263**(27): 13602-13609.

Kastanos EK, Woldman YY and Appling DR (1997) Role of mitochondrial and cytoplasmic serine hydroxymethyltransferase isozymes in de novo purine synthesis in Saccharomyces cerevisiae. *Biochemistry* **36**(48): 14956-14964.

Kennedy KM and Dewhirst MW (2010) Tumor metabolism of lactate: the influence and therapeutic potential for MCT and CD147 regulation. *Future Oncol* **6**(1): 127-148.

King ME, Honeysett JM and Howell SB (1983) Regulation of de novo purine synthesis in human bone marrow mononuclear cells by hypoxanthine. *J Clin Invest* **72**(3): 965-970.

Kisliuk RL (2003) Deaza analogs of folic acid as antitumor agents. *Current pharmaceutical design* **9**(31): 2615-2625.

Kitchens ME, Forsthoefel AM, Barbour KW, Spencer HT and Berger FG (1999) Mechanisms of acquired resistance to thymidylate synthase inhibitors: the role of enzyme stability. *Mol Pharmacol* **56**(5): 1063-1070.

Kondo M, Yamaoka T, Honda S, Miwa Y, Katashima R, Moritani M, Yoshimoto K, Hayashi Y and Itakura M (2000) The rate of cell growth is regulated by purine biosynthesis via ATP production and G(1) to S phase transition. *Journal of biochemistry* **128**(1): 57-64.

Korkhov VM, Farhan H, Freissmuth M and Sitte HH (2004) Oligomerization of the {gamma}-aminobutyric acid transporter-1 is driven by an interplay of polar and hydrophobic interactions in transmembrane helix II. *J Biol Chem* **279**(53): 55728-55736.

Krug LM, Azzoli CG, Kris MG, Miller VA, Khokhar NZ, Tong W, Ginsberg MS, Venkatraman E, Tyson L, Pizzo B, Baez V, Ng KK and Sirotnak FM (2003) 10-propargyl-10-deazaaminopterin: an antifolate with activity in patients with previously treated non-small cell lung cancer. *Clin Cancer Res* **9**(6): 2072-2078.

Kugel Desmoulin S, Wang L, Hales E, Polin L, White K, Kushner J, Stout M, Hou Z, Cherian C, Gangjee A and Matherly LH (2011) Therapeutic targeting of a novel 6-substituted pyrrolo [2,3-d]pyrimidine thienoyl antifolate to human solid tumors based on selective uptake by the proton-coupled folate transporter. *Mol Pharmacol* **80**(6): 1096-1107.

Kugel Desmoulin S, Wang Y, Wu J, Stout M, Hou Z, Fulterer A, Chang MH, Romero MF, Cherian C, Gangjee A and Matherly LH (2010) Targeting the proton-coupled folate transporter for selective delivery of 6-substituted pyrrolo[2,3-d]pyrimidine antifolate

inhibitors of de novo purine biosynthesis in the chemotherapy of solid tumors. *Mol Pharmacol* **78**(4): 577-587.

Kuhnel JM, Chiao JH and Sirotnak FM (2000) Contrasting effects of oncogene expression on two carrier-mediated systems internalizing folate compounds in Fisher rat 3T3 cells. *Journal of cellular physiology* **184**(3): 364-372.

Kumar AP, Quake AL, Chang MK, Zhou T, Lim KS, Singh R, Hewitt RE, Salto-Tellez M, Pervaiz S and Clement MV (2009) Repression of NHE1 expression by PPARgamma activation is a potential new approach for specific inhibition of the growth of tumor cells in vitro and in vivo. *Cancer Res* **69**(22): 8636-8644.

Lacey SW, Sanders JM, Rothberg KG, Anderson RG and Kamen BA (1989) Complementary DNA for the folate binding protein correctly predicts anchoring to the membrane by glycosyl-phosphatidylinositol. *J Clin Invest* **84**(2): 715-720.

Laemmli UK (1970) Cleavage of structural proteins during the assembly of the head of bacteriophage T4. *Nature* **227**(5259): 680-685.

Lasry I, Berman B, Glaser F, Jansen G and Assaraf YG (2009) Hereditary folate malabsorption: a positively charged amino acid at position 113 of the proton-coupled folate transporter (PCFT/SLC46A1) is required for folic acid binding. *Biochem Biophys Res Commun* **386**(3): 426-431.

Lasry I, Berman B, Straussberg R, Sofer Y, Bessler H, Sharkia M, Glaser F, Jansen G, Drori S and Assaraf YG (2008) A novel loss-of-function mutation in the proton-coupled folate transporter from a patient with hereditary folate malabsorption reveals that Arg 113 is crucial for function. *Blood* **112**(5): 2055-2061.

Leamon CP, Lovejoy CD and Nguyen B (2013) Patient selection and targeted treatment in the management of platinum-resistant ovarian cancer. *Pharmgenomics Pers Med* **6**: 113-125.

Leamon CP and Low PS (1991) Delivery of macromolecules into living cells: a method that exploits folate receptor endocytosis. *Proceedings of the National Academy of Sciences of the United States of America* **88**(13): 5572-5576.

Leamon CP and Low PS (2001) Folate-mediated targeting: from diagnostics to drug and gene delivery. *Drug Discov Today* **6**(1): 44-51.

Leamon CP, Parker MA, Vlahov IR, Xu LC, Reddy JA, Vetzel M and Douglas N (2002) Synthesis and biological evaluation of EC20: a new folate-derived, (99m)Tc-based radiopharmaceutical. *Bioconjugate chemistry* **13**(6): 1200-1210.

Leamon CP, Reddy JA, Klein PJ, Vlahov IR, Dorton R, Bloomfield A, Nelson M, Westrick E, Parker N, Bruna K, Vetzel M, Gehrke M, Nicoson JS, Messmann RA, LoRusso PM and Sausville EA (2011) Reducing undesirable hepatic clearance of a tumor-targeted vinca alkaloid via novel saccharopeptidic modifications. *J Pharmacol Exp Ther* **336**(2): 336-343.

Lebovka NI, Khrapatiy S, Melnyk R and Vygornitskii M (2014) Effects of hydrodynamic retardation and interparticle interactions on the self-assembly in a drying droplet containing suspended solid particles. *Physical review E, Statistical, nonlinear, and soft matter physics* **89**(5): 052307.

Lee JW, Lu JY, Low PS and Fuchs PL (2002) Synthesis and evaluation of taxol-folic acid conjugates as targeted antineoplastics. *Bioorganic & medicinal chemistry* **10**(7): 2397-2414.

LeLeiko NS, Bronstein AD, Baliga BS and Munro HN (1983) De novo purine nucleotide synthesis in the rat small and large intestine: effect of dietary protein and purines. *Journal of pediatric gastroenterology and nutrition* **2**(2): 313-319.

Lemieux MJ (2007) Eukaryotic major facilitator superfamily transporter modeling based on the prokaryotic GlpT crystal structure. *Molecular membrane biology* **24**(5-6): 333-341.

Leuthold S, Hagenbuch B, Mohebbi N, Wagner CA, Meier PJ and Stieger B (2009) Mechanisms of pH-gradient driven transport mediated by organic anion polypeptide transporters. *Am J Physiol Cell Physiol* **296**(3): C570-582.

Levy AS, Sather HN, Steinherz PG, Sowers R, La M, Moscow JA, Gaynon PS, Uckun FM, Bertino JR and Gorlick R (2003) Reduced folate carrier and dihydrofolate reductase expression in acute lymphocytic leukemia may predict outcome: a Children's Cancer Group Study. *Journal of pediatric hematology/oncology* **25**(9): 688-695.

Li WW, Lin JT, Schweitzer BI, Tong WP, Niedzwiecki D and Bertino JR (1992) Intrinsic resistance to methotrexate in human soft tissue sarcoma cell lines. *Cancer Res* **52**(14): 3908-3913.

Liani E, Rothem L, Bunni MA, Smith CA, Jansen G and Assaraf YG (2003) Loss of folylpoly-gamma-glutamate synthetase activity is a dominant mechanism of resistance to polyglutamylation-dependent novel antifolates in multiple human leukemia sublines. *Int J Cancer* **103**(5): 587-599.

Lima CR, SV O, J G, GM M, A D, JA Q, C A, ML R, GS C and G B (2006) A phase I study of talotrexin (PT-523) in patients with relapsed or refractory non-small cell lung cancer (NSCLC). *J Med Chem* **24**(18S): 7142.

Liu M, Ge Y, Cabelof DC, Aboukameel A, Heydari AR, Mohammad R and Matherly LH (2005) Structure and regulation of the murine reduced folate carrier gene: identification of four noncoding exons and promoters and regulation by dietary folates. *J Biol Chem* **280**(7): 5588-5597.

Liu M, Whetstine JR, Payton SG, Ge Y, Flatley RM and Matherly LH (2004) Roles of USF, Ikaros and Sp proteins in the transcriptional regulation of the human reduced folate carrier B promoter. *Biochem J* **383**(Pt 2): 249-257.

Liu XY and Matherly LH (2001) Functional interactions between arginine-133 and aspartate-88 in the human reduced folate carrier: evidence for a charge-pair association. *Biochem J* **358**(Pt 2): 511-516.

Liu XY and Matherly LH (2002) Analysis of membrane topology of the human reduced folate carrier protein by hemagglutinin epitope insertion and scanning glycosylation insertion mutagenesis. *Biochim Biophys Acta* **1564**(2): 333-342.

Liu XY, Witt TL and Matherly LH (2003) Restoration of high-level transport activity by human reduced folate carrier/ThTr1 thiamine transporter chimaeras: role of the transmembrane domain 6/7 linker region in reduced folate carrier function. *Biochem J* **369**(Pt 1): 31-37.

Liu Y, Yin TJ, Zhou R, Zhou S, Fan L and Zhang RG (2013) Expression of thymidylate synthase predicts clinical outcomes of pemetrexed-containing chemotherapy for non-small-cell lung cancer: a systemic review and meta-analysis. *Cancer Chemother Pharmacol* **72**(5): 1125-1132.

Lorusso PM, Edelman MJ, Bever SL, Forman KM, Pilat M, Quinn MF, Li J, Heath EI, Malburg LM, Klein PJ, Leamon CP, Messmann RA and Sausville EA (2012) Phase I study of folate conjugate EC145 (Vintafolide) in patients with refractory solid tumors. *Journal of*

clinical oncology : official journal of the American Society of Clinical Oncology **30**(32): 4011-4016.

Louvet C, Andre T, Gamelin E, Garcia ML, Saavedra A, Lenaers G, de Gramont A, Mery-Mignard D and Kalla S (2004) A phase I-II, dose-escalating trial of ZD9331 in combination with irinotecan (CPT11) in previously pretreated metastatic colorectal cancer patients. *Bulletin du cancer* **91**(12): 279-284.

Lowry OH, Rosebrough NJ, Farr AL and Randall RJ (1951) Protein measurement with the Folin phenol reagent. *J Biol Chem* **193**(1): 265-275.

Lu SC (2000) S-Adenosylmethionine. *The international journal of biochemistry & cell biology* **32**(4): 391-395.

Lu YS, Lien HC, Yeh PY, Kuo SH, Chang WC, Kuo ML and Cheng AL (2006) Glucocorticoid receptor expression in advanced non-small cell lung cancer: clinicopathological correlation and in vitro effect of glucocorticoid on cell growth and chemosensitivity. *Lung Cancer* **53**(3): 303-310.

Lunt SY and Vander Heiden MG (2011) Aerobic glycolysis: meeting the metabolic requirements of cell proliferation. *Annual review of cell and developmental biology* **27**: 441-464.

Mackinnon AM and Deller DJ (1973) Purine nucleotide biosynthesis in gastrointestinal mucosa. *Biochimica et Biophysica Acta (BBA) - Nucleic Acids and Protein Synthesis* **319**(1): 1-4.

Mahadeo K, Diop-Bove N, Shin D, Unal ES, Teo J, Zhao R, Chang MH, Fulterer A, Romero MF and Goldman ID (2010) Properties of the Arg376 residue of the proton-coupled folate transporter (PCFT-SLC46A1) and a glutamine mutant causing hereditary folate malabsorption. *Am J Physiol Cell Physiol* **299**(5): C1153-1161.

Mahadeo KM, Diop-Bove N, Ramirez SI, Cadilla CL, Rivera E, Martin M, Lerner NB, DiAntonio L, Duva S, Santiago-Borrero PJ and Goldman ID (2011) Prevalence of a loss-of-function mutation in the proton-coupled folate transporter gene (PCFT-SLC46A1) causing hereditary folate malabsorption in Puerto Rico. *J Pediatr* **159**(4): 623-627 e621.

Mangelsdorf DJ, Thummel C, Beato M, Herrlich P, Schutz G, Umesono K, Blumberg B, Kastner P, Mark M, Chambon P and Evans RM (1995) The nuclear receptor superfamily: the second decade. *Cell* **83**(6): 835-839.

Marchi E, Mangone M, Zullo K and O'Connor OA (2013) Pralatrexate pharmacology and clinical development. *Clin Cancer Res* **19**(24): 6657-6661.

Marchi E, Paoluzzi L, Scotto L, Seshan VE, Zain JM, Zinzani PL and O'Connor OA (2010) Pralatrexate is synergistic with the proteasome inhibitor bortezomib in in vitro and in vivo models of T-cell lymphoid malignancies. *Clin Cancer Res* **16**(14): 3648-3658.

Martinez-Zaguilan R, Lynch RM, Martinez GM and Gillies RJ (1993) Vacuolar-type H(+)-ATPases are functionally expressed in plasma membranes of human tumor cells. *The American journal of physiology* **265**(4 Pt 1): C1015-1029.

Matherly LH, Angeles SM and McGuire JJ (1993) Determinants of the disparate antitumor activities of (6R)-5,10-dideaza-5,6,7,8-tetrahydrofolate and methotrexate toward human lymphoblastic leukemia cells, characterized by severely impaired antifolate membrane transport. *Biochem Pharmacol* **46**(12): 2185-2195.

Matherly LH, Barlowe CK, Phillips VM and Goldman ID (1987) The effects on 4-aminoantifolates on 5-formyltetrahydrofolate metabolism in L1210 cells. A biochemical basis of the selectivity of leucovorin rescue. *J Biol Chem* **262**(2): 710-717.

Matherly LH, Czajkowski CA and Angeles SM (1991) Identification of a highly glycosylated methotrexate membrane carrier in K562 human erythroleukemia cells up-regulated for tetrahydrofolate cofactor and methotrexate transport. *Cancer Res* **51**(13): 3420-3426.

Matherly LH and Gangjee A (2011) Discovery of Novel Antifolate Inhibitors of De Novo Purine Nucleotide Biosynthesis with Selectivity for High Affinity Folate Receptors and the Proton-coupled Folate Transporter Over the Reduced Folate Carrier for Cellular Entry in *Targeted Drug Strategies for Cancer and Inflammation* (Jackman AL and Leamon CP eds) pp 119-134, Springer Science+Buisness Media, New York.

Matherly LH and Goldman DI (2003) Membrane transport of folates. *Vitam Horm* **66**: 403-456.

Matherly LH and Hou Z (2008) Structure and function of the reduced folate carrier a paradigm of a major facilitator superfamily mammalian nutrient transporter. *Vitam Horm* **79**: 145-184.

Matherly LH, Hou Z and Deng Y (2007) Human reduced folate carrier: translation of basic biology to cancer etiology and therapy. *Cancer Metastasis Rev* **26**(1): 111-128.

Matherly LH, Voss MK, Anderson LA, Fry DW and Goldman ID (1985) Enhanced polyglutamylation of aminopterin relative to methotrexate in the Ehrlich ascites tumor cell in vitro. *Cancer Res* **45**(3): 1073-1078.

Matherly LH, Wilson MR and Hou Z (2014) The Major Facilitative Folate Transporters Solute Carrier 19A1 and Solute Carrier 46A1: Biology and Role in Antifolate Chemotherapy of Cancer. *Drug metabolism and disposition: the biological fate of chemicals* **42**(4): 632-649.

Matsudaira P (1987) Sequence from picomole quantities of proteins electroblotted onto polyvinylidene difluoride membranes. *J Biol Chem* **262**(21): 10035-10038.

Matsui SI, Arredondo MA, Wrzosek C and Rustum YM (1996) DNA damage and p53 induction do not cause ZD1694-induced cell cycle arrest in human colon carcinoma cells. *Cancer Res* **56**(20): 4715-4723.

Mauritz R, Peters GJ, Priest DG, Assaraf YG, Drori S, Kathmann I, Noordhuis P, Bunni MA, Rosowsky A, Schornagel JH, Pinedo HM and Jansen G (2002) Multiple mechanisms of resistance to methotrexate and novel antifolates in human CCRF-CEM leukemia cells and their implications for folate homeostasis. *Biochem Pharmacol* **63**(2): 105-115.

McBurney MW and Whitmore GF (1974) Isolation and biochemical characterization of folate deficient mutants of Chinese hamster cells. *Cell* **2**(3): 173-182.

McClain MS, Iwamoto H, Cao P, Vinion-Dubiel AD, Li Y, Szabo G, Shao Z and Cover TL (2003) Essential role of a GXXXG motif for membrane channel formation by Helicobacter pylori vacuolating toxin. *J Biol Chem* **278**(14): 12101-12108.

McCloskey DE, McGuire JJ, Russell CA, Rowan BG, Bertino JR, Pizzorno G and Mini E (1991) Decreased folylpolyglutamate synthetase activity as a mechanism of methotrexate resistance in CCRF-CEM human leukemia sublines. *J Biol Chem* **266**(10): 6181-6187.

McDougall BM and Blakley R (1960) Mechanism of the action of thymidylate synthetase. *Nature* **188**: 944.

McGuire JJ, Russell CA and Balinska M (2000) Human cytosolic and mitochondrial folylpolyglutamate synthetase are electrophoretically distinct. Expression in antifolate-sensitive and -resistant human cell lines. *J Biol Chem* **275**(17): 13012-13016.

McIvor RS and Simonsen CC (1990) Isolation and characterization of a variant dihydrofolate reductase cDNA from methotrexate-resistant murine L5178Y cells. *Nucleic acids research* **18**(23): 7025-7032.

McLean LA, Roscoe J, Jorgensen NK, Gorin FA and Cala PM (2000) Malignant gliomas display altered pH regulation by NHE1 compared with nontransformed astrocytes. *Am J Physiol Cell Physiol* **278**(4): C676-688.

Mejia NR and MacKenzie RE (1985) NAD-dependent methylenetetrahydrofolate dehydrogenase is expressed by immortal cells. *J Biol Chem* **260**(27): 14616-14620.

Melera PW, Davide JP, Hession CA and Scotto KW (1984) Phenotypic expression in Escherichia coli and nucleotide sequence of two Chinese hamster lung cell cDNAs encoding different dihydrofolate reductases. *Mol Cell Biol* **4**(1): 38-48.

Melera PW, Davide JP and Oen H (1988) Antifolate-resistant Chinese hamster cells. Molecular basis for the biochemical and structural heterogeneity among dihydrofolate reductases produced by drug-sensitive and drug-resistant cell lines. *J Biol Chem* **263**(4): 1978-1990.

Melnyk RA, Partridge AW and Deber CM (2002) Transmembrane domain mediated self-assembly of major coat protein subunits from Ff bacteriophage. *J Mol Biol* **315**(1): 63-72.

Mendelsohn LG, Gates SB, Habeck LL, Shackelford KA, Worzalla J, Shih C and Grindey GB (1996) The role of dietary folate in modulation of folate receptor expression, folylpolyglutamate synthetase activity and the efficacy and toxicity of lometrexol. *Advances in enzyme regulation* **36**: 365-381.

Mendelsohn LG, Shih C, Chen VJ, Habeck LL, Gates SB and Shackelford KA (1999a) Enzyme inhibition, polyglutamation, and the effect of LY231514 (MTA) on purine biosynthesis. *Semin Oncol* **26**(2 Suppl 6): 42-47.

Mendelsohn LG, Worzalla JF and Walling JM (1999b) Preclinical and Clinical Evaluation of the Glycinamide Ribonucleotide Formyltransferase Inhibitors Lometrexol and LY309887, in

Anticancer Drug Development Guide: Antifolate Drugs in Cancer Therapy (Jackman AL ed) pp 261-280, Humana Press, Inc., Totowa, NJ.

Mendrola JM, Berger MB, King MC and Lemmon MA (2002) The single transmembrane domains of ErbB receptors self-associate in cell membranes. *J Biol Chem* **277**(7): 4704-4712.

Menter A, Thrash B, Cherian C, Matherly LH, Wang L, Gangjee A, Morgan JR, Maeda DY, Schuler AD, Kahn SJ and Zebala JA (2012) Intestinal transport of aminopterin enantiomers in dogs and humans with psoriasis is stereoselective: evidence for a mechanism involving the proton-coupled folate transporter. *J Pharmacol Exp Ther* **342**(3): 696-708.

Merck (2014) Press Release

.

Meyer E, Kurian MA, Pasha S, Trembath RC, Cole T and Maher ER (2010) A novel PCFT gene mutation (p.Cys66LeufsX99) causing hereditary folate malabsorption. *Mol Genet Metab* **99**(3): 325-328.

Mihaylova MM and Shaw RJ (2011) The AMPK signalling pathway coordinates cell growth, autophagy and metabolism. *Nat Cell Biol* **13**(9): 1016-1023.

Min SH, Oh SY, Karp GI, Poncz M, Zhao R and Goldman ID (2008) The clinical course and genetic defect in the PCFT gene in a 27-year-old woman with hereditary folate malabsorption. *J Pediatr* **153**(3): 435-437.

Mini E, Srimatkandada S, Medina WD, Moroson BA, Carman MD and Bertino JR (1985) Molecular and karyological analysis of methotrexate-resistant and -sensitive human leukemic CCRF-CEM cells. *Cancer Res* **45**(1): 317-324.

Miraglia E, Viarisio D, Riganti C, Costamagna C, Ghigo D and Bosia A (2005) Na+/H+ exchanger activity is increased in doxorubicin-resistant human colon cancer cells and its modulation modifies the sensitivity of the cells to doxorubicin. *Int J Cancer* **115**(6): 924-929.

Mitchell-Ryan S, Wang Y, Raghavan S, Ravindra MP, Hales E, Orr S, Cherian C, Hou Z, Matherly LH and Gangjee A (2013) Discovery of 5-substituted pyrrolo[2,3-d]pyrimidine antifolates as dual-acting inhibitors of glycinamide ribonucleotide formyltransferase and 5-aminoimidazole-4-carboxamide ribonucleotide formyltransferase in de novo purine nucleotide biosynthesis: implications of inhibiting 5-aminoimidazole-4-carboxamide ribonucleotide formyltransferase to ampk activation and antitumor activity. *J Med Chem* **56**(24): 10016-10032.

Miyachi H, Takemura Y, Kobayashi H and Ando Y (1995) Expression of variant dihydrofolate reductase with decreased binding affinity to antifolates in MOLT-3 human leukemia cell lines resistant to trimetrexate. *Cancer letters* **88**(1): 93-99.

Monahan BPA, C.J. (2001) Antifolates in *Cancer Chemotherapy and Biotherapy* (D.L. CBAL ed) pp 109-148, Lippincott-Raven, Philadelphia.

Moran RG (1999) Roles of folylpoly-gamma-glutamate synthetase in therapeutics with tetrahydrofolate antimetabolites: an overview. *Semin Oncol* **26**(2 Suppl 6): 24-32.

Moran RG, Baldwin SW, Taylor EC and Shih C (1989) The 6S- and 6R-diastereomers of 5, 10-dideaza-5, 6, 7, 8-tetrahydrofolate are equiactive inhibitors of de novo purine synthesis. *J Biol Chem* **264**(35): 21047-21051.

Moran RG, Werkheiser WC and Zakrzewski SF (1976) Folate metabolism in mammalian cells in culture. I Partial characterization of the folate derivatives present in L1210 mouse leukemia cells. *J Biol Chem* **251**(12): 3569-3575.

Morimoto H, Yonehara S and Bonavida B (1993) Overcoming tumor necrosis factor and drug resistance of human tumor cell lines by combination treatment with anti-Fas antibody and drugs or toxins. *Cancer Res* **53**(11): 2591-2596.

Moscow JA, Gong M, He R, Sgagias MK, Dixon KH, Anzick SL, Meltzer PS and Cowan KH (1995) Isolation of a gene encoding a human reduced folate carrier (RFC1) and analysis of its expression in transport-deficient, methotrexate-resistant human breast cancer cells. *Cancer Res* **55**(17): 3790-3794.

Mueller BK, Subramaniam S and Senes A (2014) A frequent, GxxxG-mediated, transmembrane association motif is optimized for the formation of interhelical Calpha-H hydrogen bonds. *Proceedings of the National Academy of Sciences of the United States of America* **111**(10): E888-895.

Murray AW (1971) The biological significance of purine salvage. *Annual review of biochemistry* **40**: 811-826.

Nakai Y, Inoue K, Abe N, Hatakeyama M, Ohta KY, Otagiri M, Hayashi Y and Yuasa H (2007) Functional characterization of human proton-coupled folate transporter/heme carrier protein 1 heterologously expressed in mammalian cells as a folate transporter. *J Pharmacol Exp Ther* **322**(2): 469-476.

Nakanishi T, Tamai I, Takaki A and Tsuji A (2000) Cancer cell-targeted drug delivery utilizing oligopeptide transport activity. *Int J Cancer* **88**(2): 274-280.

Nakashima-Matsushita N, Homma T, Yu S, Matsuda T, Sunahara N, Nakamura T, Tsukano M, Ratnam M and Matsuyama T (1999) Selective expression of folate receptor beta and its possible role in methotrexate transport in synovial macrophages from patients with rheumatoid arthritis. *Arthritis and rheumatism* **42**(8): 1609-1616.

Naumann RW, Coleman RL, Burger RA, Sausville EA, Kutarska E, Ghamande SA, Gabrail NY, Depasquale SE, Nowara E, Gilbert L, Gersh RH, Teneriello MG, Harb WA, Konstantinopoulos PA, Penson RT, Symanowski JT, Lovejoy CD, Leamon CP, Morgenstern DE and Messmann RA (2013) PRECEDENT: a randomized phase II trial comparing vintafolide (EC145) and pegylated liposomal doxorubicin (PLD) in combination versus PLD alone in patients with platinum-resistant ovarian cancer. *Journal of clinical oncology : official journal of the American Society of Clinical Oncology* **31**(35): 4400-4406.

Niethammer D and Jackson RC (1975) Changes of molecular properties associated with the development of resistance against methotrexate in human lymphoblastoid cells. *Eur J Cancer* **11**(12): 845-854.

Nozawa T, Imai K, Nezu J, Tsuji A and Tamai I (2004) Functional characterization of pH-sensitive organic anion transporting polypeptide OATP-B in human. *J Pharmacol Exp Ther* **308**(2): 438-445.

Nunberg JH, Kaufman RJ, Schimke RT, Urlaub G and Chasin LA (1978) Amplified dihydrofolate reductase genes are localized to a homogeneously staining region of a single chromosome in a methotrexate-resistant Chinese hamster ovary cell line. *Proceedings of the National Academy of Sciences of the United States of America* **75**(11): 5553-5556.

Nunez MI, Behrens C, Woods DM, Lin H, Suraokar M, Kadara H, Hofstetter W, Kalhor N, Lee JJ, Franklin W, Stewart DJ and Wistuba, II (2012) High expression of folate receptor alpha in lung cancer correlates with adenocarcinoma histology and EGFR [corrected] mutation. *Journal of thoracic oncology : official publication of the International Association for the Study of Lung Cancer* **7**(5): 833-840.

O'Connor BM, Jackman AL, Crossley PH, Freemantle SE, Lunec J and Calvert AH (1992) Human lymphoblastoid cells with acquired resistance to C2-desamino-C2-methyl-N10-propargyl-5,8-dideazafolic acid: a novel folate-based thymidylate synthase inhibitor. *Cancer Res* **52**(5): 1137-1143.

O'Connor OA, Horwitz S, Hamlin P, Portlock C, Moskowitz CH, Sarasohn D, Neylon E, Mastrella J, Hamelers R, Macgregor-Cortelli B, Patterson M, Seshan VE, Sirotnak F, Fleisher M, Mould DR, Saunders M and Zelenetz AD (2009) Phase II-I-II study of two different doses and schedules of pralatrexate, a high-affinity substrate for the reduced folate carrier, in patients with relapsed or refractory lymphoma reveals marked activity in T-cell malignancies. *Journal of clinical oncology : official journal of the American Society of Clinical Oncology* **27**(26): 4357-4364.

O'Shannessy DJ, Yu G, Smale R, Fu YS, Singhal S, Thiel RP, Somers EB and Vachani A (2012) Folate receptor alpha expression in lung cancer: diagnostic and prognostic significance. *Oncotarget* **3**(4): 414-425.

Overton MC, Chinault SL and Blumer KJ (2003) Oligomerization, biogenesis, and signaling is promoted by a glycophorin A-like dimerization motif in transmembrane domain 1 of a yeast G protein-coupled receptor. *J Biol Chem* **278**(49): 49369-49377.

Pan XQ, Zheng X, Shi G, Wang H, Ratnam M and Lee RJ (2002) Strategy for the treatment of acute myelogenous leukemia based on folate receptor beta-targeted liposomal doxorubicin combined with receptor induction using all-trans retinoic acid. *Blood* **100**(2): 594-602.

Pasternack LB, Laude DA, Jr. and Appling DR (1994) 13C NMR analysis of intercompartmental flow of one-carbon units into choline and purines in Saccharomyces cerevisiae. *Biochemistry* **33**(1): 74-82.

Pasternack LB, Littlepage LE, Laude DA, Jr. and Appling DR (1996) 13C NMR analysis of the use of alternative donors to the tetrahydrofolate-dependent one-carbon pools in Saccharomyces cerevisiae. *Arch Biochem Biophys* **326**(1): 158-165.

Patel JD, Krug LM, Azzoli CG, Gomez J, Kris MG and Miller VA (2003) Targeting lethal minimal residual disease in small cell lung cancer. *Semin Oncol* **30**(1): 79-85.

Patki M, Gadgeel S, Huang Y, McFall T, Shields AF, Matherly LH, Bepler G and Ratnam M (2014) Glucocorticoid receptor status is a principal determinant of variability in the sensitivity of non-small-cell lung cancer cells to pemetrexed. *Journal of thoracic oncology : official publication of the International Association for the Study of Lung Cancer* **9**(4): 519-526.

Paukert JL, Williams GR and Rabinowitz JC (1977) Formyl-methenyl-methylenetetrahydrofolate synthetase (combined); correlation of enzymic activities with limited proteolytic degradation of the protein from yeast. *Biochem Biophys Res Commun* **77**(1): 147-154.

Payton SG, Liu M, Ge Y and Matherly LH (2005a) Transcriptional regulation of the human reduced folate carrier A1/A2 promoter: Identification of critical roles for the USF and GATA families of transcription factors. *Biochim Biophys Acta* **1731**(2): 115-124.

Payton SG, Whetstine JR, Ge Y and Matherly LH (2005b) Transcriptional regulation of the human reduced folate carrier promoter C: synergistic transactivation by Sp1 and C/EBP beta and identification of a downstream repressor. *Biochim Biophys Acta* **1727**(1): 45-57.

Peethambaram PP, Hartmann LC, Jonker DJ, de Jonge M, Plummer ER, Martin L, Konner J, Marshall J, Goss GD, Teslenko V, Clemens PL, Cohen LJ, Ahlers CM and Alland L (2015) A phase I pharmacokinetic and safety analysis of epothilone folate (BMS-753493), a folate receptor targeted chemotherapeutic agent in humans with advanced solid tumors. *Investigational new drugs* **33**(2): 321-331.

Phear EA and Greenberg DM (1957) The Methylation of Deoxyuridine1. *Journal of the American Chemical Society* **79**(14): 3737-3741.

Pierce BG, Wiehe K, Hwang H, Kim BH, Vreven T and Weng Z (2014) ZDOCK server: interactive docking prediction of protein-protein complexes and symmetric multimers. *Bioinformatics* **30**(12): 1771-1773.

Pinheiro C, Longatto-Filho A, Ferreira L, Pereira SM, Etlinger D, Moreira MA, Jube LF, Queiroz GS, Schmitt F and Baltazar F (2008a) Increasing expression of monocarboxylate transporters 1 and 4 along progression to invasive cervical carcinoma. *International journal of gynecological pathology : official journal of the International Society of Gynecological Pathologists* **27**(4): 568-574.

Pinheiro C, Longatto-Filho A, Scapulatempo C, Ferreira L, Martins S, Pellerin L, Rodrigues M, Alves VA, Schmitt F and Baltazar F (2008b) Increased expression of monocarboxylate

transporters 1, 2, and 4 in colorectal carcinomas. *Virchows Archiv : an international journal of pathology* **452**(2): 139-146.

Pinheiro C, Reis RM, Ricardo S, Longatto-Filho A, Schmitt F and Baltazar F (2010) Expression of monocarboxylate transporters 1, 2, and 4 in human tumours and their association with CD147 and CD44. *Journal of biomedicine & biotechnology* **2010**: 427694.

Pizzorno G, Chang YM, McGuire JJ and Bertino JR (1989) Inherent resistance of human squamous carcinoma cell lines to methotrexate as a result of decreased polyglutamylation of this drug. *Cancer Res* **49**(19): 5275-5280.

Pizzorno G, Mini E, Coronnello M, McGuire JJ, Moroson BA, Cashmore AR, Dreyer RN, Lin JT, Mazzei T, Periti P and et al. (1988) Impaired polyglutamylation of methotrexate as a cause of resistance in CCRF-CEM cells after short-term, high-dose treatment with this drug. *Cancer Res* **48**(8): 2149-2155.

Pizzorno G, Moroson BA, Cashmore AR, Russello O, Mayer JR, Galivan J, Bunni MA, Priest DG and Beardsley GP (1995) Multifactorial resistance to 5,10-dideazatetrahydrofolic acid in cell lines derived from human lymphoblastic leukemia CCRF-CEM. *Cancer Res* **55**(3): 566-573.

Pohland RC, Alati T, Lantz RJ and Grindey GB (1994) Whole-body autoradiographic disposition and plasma pharmacokinetics of 5,10-dideazatetrahydrofolic acid in mice fed folic acid-deficient or regular diets. *J Pharm Sci* **83**(10): 1396-1399.

Polgar O, Robey RW, Morisaki K, Dean M, Michejda C, Sauna ZE, Ambudkar SV, Tarasova N and Bates SE (2004) Mutational analysis of ABCG2: role of the GXXXG motif. *Biochemistry* **43**(29): 9448-9456.

Polin L, Corbett TH, Roberts BJ, Lawson AJ, Leopold WR, White K, Kushner J, Hazeldine S, Moore R, Rake J and Horwitz JP (2011) Transplantable Syngeneic Rodent Tumors: Solid Tumors in Mice

Tumor Models in Cancer Research, (Teicher BA ed) pp 43-78, Humana Press.

Polin L, Valeriote F, White K, Panchapor C, Pugh S, Knight J, LoRusso P, Hussain M, Liversidge E, Peltier N, Golakoti T, Patterson G, Moore R and Corbett TH (1997) Treatment of human prostate tumors PC-3 and TSU-PR1 with standard and investigational agents in SCID mice. *Investigational new drugs* **15**(2): 99-108.

Prasad PD, Ramamoorthy S, Leibach FH and Ganapathy V (1995) Molecular cloning of the human placental folate transporter. *Biochem Biophys Res Commun* **206**(2): 681-687.

Prasannan P, Pike S, Peng K, Shane B and Appling DR (2003) Human mitochondrial C1-tetrahydrofolate synthase: gene structure, tissue distribution of the mRNA, and immunolocalization in Chinese hamster ovary calls. *J Biol Chem* **278**(44): 43178-43187.

Pui CH and Evans WE (2006) Treatment of acute lymphoblastic leukemia. *N Engl J Med* **354**(2): 166-178.

Qiu A, Jansen M, Sakaris A, Min SH, Chattopadhyay S, Tsai E, Sandoval C, Zhao R, Akabas MH and Goldman ID (2006) Identification of an intestinal folate transporter and the molecular basis for hereditary folate malabsorption. *Cell* **127**(5): 917-928.

Qiu A, Min SH, Jansen M, Malhotra U, Tsai E, Cabelof DC, Matherly LH, Zhao R, Akabas MH and Goldman ID (2007) Rodent intestinal folate transporters (SLC46A1): secondary structure, functional properties, and response to dietary folate restriction. *Am J Physiol Cell Physiol* **293**(5): C1669-1678.

Quinlivan EP, Davis SR, Shelnutt KP, Henderson GN, Ghandour H, Shane B, Selhub J, Bailey LB, Stacpoole PW and Gregory JF, 3rd (2005) Methylenetetrahydrofolate reductase 677C->T polymorphism and folate status affect one-carbon incorporation into human DNA deoxynucleosides. *J Nutr* **135**(3): 389-396.

Racanelli AC, Rothbart SB, Heyer CL and Moran RG (2009) Therapeutics by cytotoxic metabolite accumulation: pemetrexed causes ZMP accumulation, AMPK activation, and mammalian target of rapamycin inhibition. *Cancer Res* **69**(13): 5467-5474.

Rader JS, Clarke-Pearson D, Moore M, Carson L, Holloway R, Kao MS, Wiznitzer I and Douglass EC (2003) A phase II study to determine the efficacy and tolerability of intravenous ZD9331 in heavily pretreated patients with ovarian cancer. *Gynecologic oncology* **91**(2): 318-325.

Ratnam M, Marquardt H, Duhring JL and Freisheim JH (1989) Homologous membrane folate binding proteins in human placenta: cloning and sequence of a cDNA. *Biochemistry* **28**(20): 8249-8254.

Ray MS, Muggia FM, Leichman CG, Grunberg SM, Nelson RL, Dyke RW and Moran RG (1993) Phase I study of (6R)-5,10-dideazatetrahydrofolate: a folate antimetabolite inhibitory to de novo purine synthesis. *Journal of the National Cancer Institute* **85**(14): 1154-1159.

Reddy JA, Dorton R, Dawson A, Vetzel M, Parker N, Nicoson JS, Westrick E, Klein PJ, Wang Y, Vlahov IR and Leamon CP (2009) In vivo structural activity and optimization studies of folate-tubulysin conjugates. *Molecular pharmaceutics* **6**(5): 1518-1525.

Reddy JA, Haneline LS, Srour EF, Antony AC, Clapp DW and Low PS (1999) Expression and functional characterization of the beta-isoform of the folate receptor on CD34(+) cells. *Blood* **93**(11): 3940-3948.

Reddy JA, Westrick E, Santhapuram HK, Howard SJ, Miller ML, Vetzel M, Vlahov I, Chari RV, Goldmacher VS and Leamon CP (2007) Folate receptor-specific antitumor activity of EC131, a folate-maytansinoid conjugate. *Cancer Res* **67**(13): 6376-6382.

Rhee MS, Galivan J, Wright JE and Rosowsky A (1994) Biochemical studies on PT523, a potent nonpolyglutamatable antifolate, in cultured cells. *Mol Pharmacol* **45**(4): 783-791.

Rijnboutt S, Jansen G, Posthuma G, Hynes JB, Schornagel JH and Strous GJ (1996) Endocytosis of GPI-linked membrane folate receptor-alpha. *The Journal of cell biology* **132**(1-2): 35-47.

Roberts JD, Poplin EA, Tombes MB, Kyle B, Spicer DV, Grant S, Synold T and Moran R (2000a) Weekly lometrexol with daily oral folic acid is appropriate for phase II evaluation. *Cancer Chemother Pharmacol* **45**(2): 103-110.

Roberts JD, Shibata S, Spicer DV, McLeod HL, Tombes MB, Kyle B, Carroll M, Sheedy B, Collier MA, Pithavala YK, Paradiso LJ and Clendeninn NJ (2000b) Phase I study of AG2034, a targeted GARFT inhibitor, administered once every 3 weeks. *Cancer Chemother Pharmacol* **45**(5): 423-427.

Rosowsky A, Bader H, Cucchi CA, Moran RG, Kohler W and Freisheim JH (1988) Methotrexate analogues. 33. N delta-acyl-N alpha-(4-amino-4-deoxypteroyl)-L-ornithine derivatives: synthesis and in vitro antitumor activity. *J Med Chem* **31**(7): 1332-1337.

Rosowsky A, Bader H, Wright JE, Keyomarsi K and Matherly LH (1994) Synthesis and biological activity of N omega-hemiphthaloyl-alpha,omega- diaminoalkanoic acid analogues of aminopterin and 3',5-dichloroaminopterin. *J Med Chem* **37**(14): 2167-2174.

Ross JF, Chaudhuri PK and Ratnam M (1994) Differential regulation of folate receptor isoforms in normal and malignant tissues in vivo and in established cell lines. Physiologic and clinical implications. *Cancer* **73**(9): 2432-2443.

Ross JF, Wang H, Behm FG, Mathew P, Wu M, Booth R and Ratnam M (1999) Folate receptor type beta is a neutrophilic lineage marker and is differentially expressed in myeloid leukemia. *Cancer* **85**(2): 348-357.

Rothbart SB, Racanelli AC and Moran RG (2010) Pemetrexed indirectly activates the metabolic kinase AMPK in human carcinomas. *Cancer Res* **70**(24): 10299-10309.

Rothem L, Ifergan I, Kaufman Y, Priest DG, Jansen G and Assaraf YG (2002) Resistance to multiple novel antifolates is mediated via defective drug transport resulting from clustered mutations in the reduced folate carrier gene in human leukaemia cell lines. *Biochem J* **367**(Pt 3): 741-750.

Rubio-Aliaga I and Daniel H (2002) Mammalian peptide transporters as targets for drug delivery. *Trends in pharmacological sciences* **23**(9): 434-440.

Rubio-Aliaga I, Frey I, Boll M, Groneberg DA, Eichinger HM, Balling R and Daniel H (2003) Targeted disruption of the peptide transporter Pept2 gene in mice defines its physiological role in the kidney. *Mol Cell Biol* **23**(9): 3247-3252.

Russ WP and Engelman DM (2000) The GxxxG motif: a framework for transmembrane helix-helix association. *J Mol Biol* **296**(3): 911-919.

Sabharanjak S and Mayor S (2004) Folate receptor endocytosis and trafficking. *Adv Drug Deliv Rev* **56**(8): 1099-1109.

Sadasivan E and Rothenberg SP (1989) The complete amino acid sequence of a human folate binding protein from KB cells determined from the cDNA. *J Biol Chem* **264**(10): 5806-5811.

Sadlish H, Williams FM and Flintoff WF (2002) Functional role of arginine 373 in substrate translocation by the reduced folate carrier. *J Biol Chem* **277**(44): 42105-42112.

Salojin KV, Cabrera RM, Sun W, Chang WC, Lin C, Duncan L, Platt KA, Read R, Vogel P, Liu Q, Finnell RH and Oravecz T (2011) A mouse model of hereditary folate malabsorption: deletion of the PCFT gene leads to systemic folate deficiency. *Blood* **117**(18): 4895-4904.

Scagliotti G, Hanna N, Fossella F, Sugarman K, Blatter J, Peterson P, Simms L and Shepherd FA (2009) The differential efficacy of pemetrexed according to NSCLC histology: a review of two Phase III studies. *Oncologist* **14**(3): 253-263.

Scagliotti GV, Parikh P, von Pawel J, Biesma B, Vansteenkiste J, Manegold C, Serwatowski P, Gatzemeier U, Digumarti R, Zukin M, Lee JS, Mellemgaard A, Park K, Patil S, Rolski J, Goksel T, de Marinis F, Simms L, Sugarman KP and Gandara D (2008) Phase III study comparing cisplatin plus gemcitabine with cisplatin plus pemetrexed in chemotherapy-naive patients with advanced-stage non-small-cell lung cancer. *Journal of clinical oncology : official journal of the American Society of Clinical Oncology* **26**(21): 3543-3551.

Schirch L (1978) Formyl-methenyl-methylenetetrahydrofolate synthetase from rabbit liver (combined). Evidence for a single site in the conversion of 5,10-

methylenetetrahydrofolate to 10-formyltetrahydrofolate. *Arch Biochem Biophys* **189**(2): 283-290.

Schirch V and Strong WB (1989) Interaction of folylpolyglutamates with enzymes in one-carbon metabolism. *Arch Biochem Biophys* **269**(2): 371-380.

Schmid FA, Sirotnak FM, Otter GM and DeGraw JI (1985) New folate analogs of the 10-deaza-aminopterin series: markedly increased antitumor activity of the 10-ethyl analog compared to the parent compound and methotrexate against some human tumor xenografts in nude mice. *Cancer treatment reports* **69**(5): 551-553.

Scholze P, Freissmuth M and Sitte HH (2002) Mutations within an intramembrane leucine heptad repeat disrupt oligomer formation of the rat GABA transporter 1. *J Biol Chem* **277**(46): 43682-43690.

Schulz J, Keller A, Canfield V, Parker G and Douglass E (2004) ZD9331 as second- or third-line therapy in patients with advanced colorectal cancer: a phase II multicenter trial. *American journal of clinical oncology* **27**(4): 337-342.

Scotti M, Stella L, Shearer EJ and Stover PJ (2013) Modeling cellular compartmentation in one-carbon metabolism. *Wiley Interdiscip Rev Syst Biol Med* **5**(3): 343-365.

Seal RP and Amara SG (1998) A reentrant loop domain in the glutamate carrier EAAT1 participates in substrate binding and translocation. *Neuron* **21**(6): 1487-1498.

Sega EI and Low PS (2008) Tumor detection using folate receptor-targeted imaging agents. *Cancer Metastasis Rev* **27**(4): 655-664.

Seither RL, Trent DF, Mikulecky DC, Rape TJ and Goldman ID (1989) Folate-pool interconversions and inhibition of biosynthetic processes after exposure of L1210 leukemia cells to antifolates. Experimental and network thermodynamic analyses of the

role of dihydrofolate polyglutamylates in antifolate action in cells. *J Biol Chem* **264**(29): 17016-17023.

Sennoune SR, Bakunts K, Martinez GM, Chua-Tuan JL, Kebir Y, Attaya MN and Martinez-Zaguilan R (2004) Vacuolar H+-ATPase in human breast cancer cells with distinct metastatic potential: distribution and functional activity. *Am J Physiol Cell Physiol* **286**(6): C1443-1452.

Shane B (1989) Folylpolyglutamate synthesis and role in the regulation of one-carbon metabolism. *Vitam Horm* **45**: 263-335.

Sharina IG, Zhao R, Wang Y, Babani S and Goldman ID (2001) Mutational analysis of the functional role of conserved arginine and lysine residues in transmembrane domains of the murine reduced folate carrier. *Mol Pharmacol* **59**(5): 1022-1028.

Sharma I, EA S, P L, NJ V, WE S, K C, K F, S B and M R (2010) A phase I study of EC0225 administered weeks 1 and 2 of a 4-week cycle. *ASCO Annual Meeting*.

Shen F, Ross JF, Wang X and Ratnam M (1994) Identification of a novel folate receptor, a truncated receptor, and receptor type beta in hematopoietic cells: cDNA cloning, expression, immunoreactivity, and tissue specificity. *Biochemistry* **33**(5): 1209-1215.

Shen F, Wu M, Ross JF, Miller D and Ratnam M (1995) Folate receptor type gamma is primarily a secretory protein due to lack of an efficient signal for glycosylphosphatidylinositol modification: protein characterization and cell type specificity. *Biochemistry* **34**(16): 5660-5665.

Shih C, Barnett, C. J., Grindey, G. B., Pearce, H. L., Engelhardt, J. A., Todd, G. C., Rinzel, S. M., Worzalla, J. F., Gossett, L. S., Everson, T. P., Wilson, T. M., Kobierski, M. E., Winter, M. A., Moran, R. G., Kuhnt, D., Taylor, E. C. (1993) Structural Features That

Determine the Biological Activity of Pyrrolo[2,3-d]pyrimidine Based Antifolates, in *The 10th International Symposium, Chemistry and Biology of Pteridines and Folates*, Orange Beach, AL.

Shih C, Chen VJ, Gossett LS, Gates SB, MacKellar WC, Habeck LL, Shackelford KA, Mendelsohn LG, Soose DJ, Patel VF, Andis SL, Bewley JR, Rayl EA, Moroson BA, Beardsley GP, Kohler W, Ratnam M and Schultz RM (1997) LY231514, a pyrrolo[2,3-d]pyrimidine-based antifolate that inhibits multiple folate-requiring enzymes. *Cancer Res* **57**(6): 1116-1123.

Shin DS, Mahadeo K, Min SH, Diop-Bove N, Clayton P, Zhao R and Goldman ID (2011) Identification of novel mutations in the proton-coupled folate transporter (PCFT-SLC46A1) associated with hereditary folate malabsorption. *Mol Genet Metab* **103**(1): 33-37.

Shin DS, Min SH, Russell L, Zhao R, Fiser A and Goldman ID (2010) Functional roles of aspartate residues of the proton-coupled folate transporter (PCFT-SLC46A1); a D156Y mutation causing hereditary folate malabsorption. *Blood* **116**(24): 5162-5169.

Shin DS, Zhao R, Fiser A and Goldman ID (2013) Role of the fourth transmembrane domain in proton-coupled folate transporter function as assessed by the substituted cysteine accessibility method. *Am J Physiol Cell Physiol* **304**(12): C1159-1167.

Shin DS, Zhao R, Yap EH, Fiser A and Goldman ID (2012) A P425R mutation of the proton-coupled folate transporter causing hereditary folate malabsorption produces a highly selective alteration in folate binding. *Am J Physiol Cell Physiol*.

Siegel BA, Dehdashti F, Mutch DG, Podoloff DA, Wendt R, Sutton GP, Burt RW, Ellis PR, Mathias CJ, Green MA and Gershenson DM (2003) Evaluation of 111In-DTPA-folate as

a receptor-targeted diagnostic agent for ovarian cancer: initial clinical results. *Journal of nuclear medicine : official publication, Society of Nuclear Medicine* **44**(5): 700-707.

Siegel RL, Miller KD and Jemal A (2016) Cancer statistics, 2016. *CA Cancer J Clin* **66**(1): 7-30.

Sierra EE, Brigle KE, Spinella MJ and Goldman ID (1997) pH dependence of methotrexate transport by the reduced folate carrier and the folate receptor in L1210 leukemia cells. Further evidence for a third route mediated at low pH. *Biochem Pharmacol* **53**(2): 223-231.

Sierra EE and Goldman ID (1998) Characterization of folate transport mediated by a low pH route in mouse L1210 leukemia cells with defective reduced folate carrier function. *Biochem Pharmacol* **55**(9): 1505-1512.

Sigmond J, Backus HH, Wouters D, Temmink OH, Jansen G and Peters GJ (2003) Induction of resistance to the multitargeted antifolate Pemetrexed (ALIMTA) in WiDr human colon cancer cells is associated with thymidylate synthase overexpression. *Biochem Pharmacol* **66**(3): 431-438.

Sirotnak FM, Chello PL, Moccio DM, Kisliuk RL, Combepine G, Gaumont Y and Montgomery JA (1979) Stereospecificity at carbon 6 of fomyltetrahydrofolate as a competitive inhibitor of transport and cytotoxicity of methotrexate in vitro. *Biochem Pharmacol* **28**(19): 2993-2997.

Sirotnak FM, DeGraw JI, Colwell WT and Piper JR (1998) A new analogue of 10-deazaaminopterin with markedly enhanced curative effects against human tumor xenografts in mice. *Cancer Chemother Pharmacol* **42**(4): 313-318.

Sirotnak FM, DeGraw JI, Schmid FA, Goutas LJ and Moccio DM (1984) New folate analogs of the 10-deaza-aminopterin series. Further evidence for markedly increased antitumor

efficacy compared with methotrexate in ascitic and solid murine tumor models. *Cancer Chemother Pharmacol* **12**(1): 26-30.

Sirotnak FM, Kurita S and Hutchison DJ (1968) On the nature of a transport alteration determining resistance to amethopterin in the L1210 leukemia. *Cancer Res* **28**(1): 75-80.

Sirotnak FM, Moccio DM, Kelleher LE and Goutas LJ (1981) Relative frequency and kinetic properties of transport-defective phenotypes among methotrexate-resistant L1210 clonal cell lines derived in vivo. *Cancer Res* **41**(11 Pt 1): 4447-4452.

Sirotnak FM, Otter GM and Schmid FA (1993) Markedly improved efficacy of edatrexate compared to methotrexate in a high-dose regimen with leucovorin rescue against metastatic murine solid tumors. *Cancer Res* **53**(3): 587-591.

Sitte HH, Farhan H and Javitch JA (2004) Sodium-dependent neurotransmitter transporters: oligomerization as a determinant of transporter function and trafficking. *Molecular interventions* **4**(1): 38-47.

Siu MK, Kong DS, Chan HY, Wong ES, Ip PP, Jiang L, Ngan HY, Le XF and Cheung AN (2012) Paradoxical impact of two folate receptors, FRalpha and RFC, in ovarian cancer: effect on cell proliferation, invasion and clinical outcome. *PloS one* **7**(11): e47201.

Smith D and Gallagher N (2003) A phase II/III study comparing intravenous ZD9331 with gemcitabine in patients with pancreatic cancer. *Eur J Cancer* **39**(10): 1377-1383.

Smith GK, Bigley JW, Dev IK, Duch DS, Ferone R and Pendergast W (1999) A Potent, Noncopetitive Thymidylate Synthase Inhibitor-Preclinical and Preliminary Clinical Studies in *Anticancer Drug Development Guide: Antifolate Drugs in Cancer Therapy* (Jackman AL ed) pp 59-100, Humana Press, Inc. , Totowa, NJ.

Smith GK, Mueller WT, Benkovic PA and Benkovic SJ (1981) On the cofactor specificity of glycinamide ribonucleotide and 5-aminoimidazole-4-carboxamide ribonucleotide transformylase from chicken liver. *Biochemistry* **20**(5): 1241-1245.

Smith GK, Mueller WT, Wasserman GF, Taylor WD and Benkovic SJ (1980) Characterization of the enzyme complex involving the folate-requiring enzymes of de novo purine biosynthesis. *Biochemistry* **19**(18): 4313-4321.

Srimatkandada S, Schweitzer BI, Moroson BA, Dube S and Bertino JR (1989) Amplification of a polymorphic dihydrofolate reductase gene expressing an enzyme with decreased binding to methotrexate in a human colon carcinoma cell line, HCT-8R4, resistant to this drug. *J Biol Chem* **264**(6): 3524-3528.

Stokstad ELR (ed) (1990) *Historical Perspective on Key Advances in the Biochemistry and Physiology of Folates*. Wiley-Liss, New York.

Stuwe L, Muller M, Fabian A, Waning J, Mally S, Noel J, Schwab A and Stock C (2007) pH dependence of melanoma cell migration: protons extruded by NHE1 dominate protons of the bulk solution. *The Journal of physiology* **585**(Pt 2): 351-360.

Subramanian VS, Marchant JS and Said HM (2008) Apical membrane targeting and trafficking of the human proton-coupled transporter in polarized epithelia. *Am J Physiol Cell Physiol* **294**(1): C233-240.

Sun Y, Sun J, Shi S, Jing Y, Yin S, Chen Y, Li G, Xu Y and He Z (2009) Synthesis, transport and pharmacokinetics of 5'-amino acid ester prodrugs of 1-beta-D-arabinofuranosylcytosine. *Molecular pharmaceutics* **6**(1): 315-325.

Surmont VF and van Meerbeeck JP (2011) Raltitrexed in mesothelioma. *Expert review of anticancer therapy* **11**(10): 1481-1490.

Taber LD, O'Brien P, Bowsher RR and Sportsman JR (1991) Competitive particle concentration fluorescence immunoassay for measuring 5,10-dideaza-5,6,7,8-tetrahydrofolic acid (lometrexol) in serum. *Clinical chemistry* **37**(2): 254-260.

Taylor EC (1993) Design and synthesis of inhibitors of folate-dependent enzymes as antitumor agents. *Advances in experimental medicine and biology* **338**: 387-408.

Taylor EC, Harrington PJ, Fletcher SR, Beardsley GP and Moran RG (1985) Synthesis of the antileukemic agents 5,10-dideazaaminopterin and 5,10-dideaza-5,6,7,8-tetrahydroaminopterin. *J Med Chem* **28**(7): 914-921.

Taylor EC, Kuhnt D, Shih C, Rinzel SM, Grindey GB, Barredo J, Jannatipour M and Moran RG (1992) A dideazatetrahydrofolate analogue lacking a chiral center at C-6, N-[4-[2-(2-amino-3,4-dihydro-4-oxo-7H-pyrrolo[2,3-d]pyrimidin-5- yl)ethyl]benzoyl]-L-glutamic acid, is an inhibitor of thymidylate synthase. *J Med Chem* **35**(23): 4450-4454.

Temkin SM, Tanner EJ, Dewdney SB and Minasian LM (2016) Reducing Overtreatment in Gynecologic Oncology: The Case for Less in Endometrial and Ovarian Cancer. *Frontiers in oncology* **6**: 118.

Theti DS, Bavetsias V, Skelton LA, Titley J, Gibbs D, Jansen G and Jackman AL (2003) Selective delivery of CB300638, a cyclopenta[g]quinazoline-based thymidylate synthase inhibitor into human tumor cell lines overexpressing the alpha-isoform of the folate receptor. *Cancer Res* **63**(13): 3612-3618.

Thigpen AE, West MG and Appling DR (1990) Rat C1-tetrahydrofolate synthase. cDNA isolation, tissue-specific levels of the mRNA, and expression of the protein in yeast. *J Biol Chem* **265**(14): 7907-7913.

Thompson CA (2009) FDA approves pralatrexate for treatment of rare lymphoma. *American journal of health-system pharmacy : AJHP : official journal of the American Society of Health-System Pharmacists* **66**(21): 1890.

Tibbetts AS and Appling DR (2010) Compartmentalization of Mammalian folate-mediated one-carbon metabolism. *Annu Rev Nutr* **30**: 57-81.

Toffoli G, Cernigoi C, Russo A, Gallo A, Bagnoli M and Boiocchi M (1997) Overexpression of folate binding protein in ovarian cancers. *Int J Cancer* **74**(2): 193-198.

Tomasini P, Greillier L, Khobta N and Barlesi F (2013) The place of pemetrexed in the management of non-small-cell lung cancer patients. *Expert review of anticancer therapy* **13**(3): 257-266.

Toner LE, Vrhovac R, Smith EA, Gardner J, Heaney M, Gonen M, Teruya-Feldstein J, Sirotnak F and O'Connor OA (2006) The schedule-dependent effects of the novel antifolate pralatrexate and gemcitabine are superior to methotrexate and cytarabine in models of human non-Hodgkin's lymphoma. *Clin Cancer Res* **12**(3 Pt 1): 924-932.

Tong Y, Liu-Chen X, Ercikan-Abali EA, Zhao SC, Banerjee D, Maley F and Bertino JR (1998) Probing the folate-binding site of human thymidylate synthase by site-directed mutagenesis. Generation of mutants that confer resistance to raltitrexed, Thymitaq, and BW1843U89. *J Biol Chem* **273**(47): 31209-31214.

Trent JM, Buick RN, Olson S, Horns RC, Jr. and Schimke RT (1984) Cytologic evidence for gene amplification in methotrexate-resistant cells obtained from a patient with ovarian adenocarcinoma. *Journal of clinical oncology : official journal of the American Society of Clinical Oncology* **2**(1): 8-15.

Turek JJ, Leamon CP and Low PS (1993) Endocytosis of folate-protein conjugates: ultrastructural localization in KB cells. *Journal of cell science* **106 (Pt 1)**: 423-430.

Umapathy NS, Gnana-Prakasam JP, Martin PM, Mysona B, Dun Y, Smith SB, Ganapathy V and Prasad PD (2007) Cloning and functional characterization of the proton-coupled electrogenic folate transporter and analysis of its expression in retinal cell types. *Invest Ophthalmol Vis Sci* **48**(11): 5299-5305.

Unal ES, Zhao R, Chang MH, Fiser A, Romero MF and Goldman ID (2009a) The functional roles of the His247 and His281 residues in folate and proton translocation mediated by the human proton-coupled folate transporter SLC46A1. *J Biol Chem* **284**(26): 17846-17857.

Unal ES, Zhao R and Goldman ID (2009b) Role of the glutamate 185 residue in proton translocation mediated by the proton-coupled folate transporter SLC46A1. *Am J Physiol Cell Physiol* **297**(1): C66-74.

Unal ES, Zhao R, Qiu A and Goldman ID (2008) N-linked glycosylation and its impact on the electrophoretic mobility and function of the human proton-coupled folate transporter (HsPCFT). *Biochim Biophys Acta* **1778**(6): 1407-1414.

Urquhart BL, Gregor JC, Chande N, Knauer MJ, Tirona RG and Kim RB (2010) The human proton-coupled folate transporter (hPCFT): modulation of intestinal expression and function by drugs. *Am J Physiol Gastrointest Liver Physiol* **298**(2): G248-254.

van der Wilt CL, Backus HH, Smid K, Comijn L, Veerman G, Wouters D, Voorn DA, Priest DG, Bunni MA, Mitchell F, Jackman AL, Jansen G and Peters GJ (2001) Modulation of both endogenous folates and thymidine enhance the therapeutic efficacy of thymidylate synthase inhibitors. *Cancer Res* **61**(9): 3675-3681.

Vardy E, Arkin IT, Gottschalk KE, Kaback HR and Schuldiner S (2004) Structural conservation in the major facilitator superfamily as revealed by comparative modeling. *Protein science : a publication of the Protein Society* **13**(7): 1832-1840.

Varela-Moreiras G and Selhub J (1992) Long-term folate deficiency alters folate content and distribution differentially in rat tissues. *J Nutr* **122**(4): 986-991.

Veggian R, Fasolato S, Menard S, Minucci D, Pizzetti P, Regazzoni M, Tagliabue E and Colnaghi MI (1989) Immunohistochemical reactivity of a monoclonal antibody prepared against human ovarian carcinoma on normal and pathological female genital tissues. *Tumori* **75**(5): 510-513.

Vergote I and Leamon CP (2015) Vintafolide: a novel targeted therapy for the treatment of folate receptor expressing tumors. *Therapeutic advances in medical oncology* **7**(4): 206-218.

Vergote IB, Marth C and Coleman RL (2015) Role of the folate receptor in ovarian cancer treatment: evidence, mechanism, and clinical implications. *Cancer Metastasis Rev* **34**(1): 41-52.

Vilasco M, Communal L, Mourra N, Courtin A, Forgez P and Gompel A (2011) Glucocorticoid receptor and breast cancer. *Breast cancer research and treatment* **130**(1): 1-10.

Visentin M, Chang MH, Romero MF, Zhao R and Goldman ID (2012) Substrate- and pH-Specific Antifolate Transport Mediated by Organic Anion-Transporting Polypeptide 2B1 (OATP2B1-SLCO2B1). *Mol Pharmacol* **81**(2): 134-142.

Visentin M, Unal ES, Najmi M, Fiser A, Zhao R and Goldman ID (2015) Identification of Tyr residues that enhance folate substrate binding and constrain oscillation of the proton-coupled folate transporter (PCFT-SLC46A1). *Am J Physiol Cell Physiol* **308**(8): C631-641.

Visentin M, Unal ES, Zhao R and Goldman ID (2013) The membrane transport and polyglutamation of pralatrexate: a new-generation dihydrofolate reductase inhibitor. *Cancer Chemother Pharmacol* **72**(3): 597-606.

Vlahov IR, Santhapuram HK, Kleindl PJ, Howard SJ, Stanford KM and Leamon CP (2006) Design and regioselective synthesis of a new generation of targeted chemotherapeutics. Part 1: EC145, a folic acid conjugate of desacetylvinblastine monohydrazide. *Bioorganic & medicinal chemistry letters* **16**(19): 5093-5096.

Volk EL and Schneider E (2003) Wild-type breast cancer resistance protein (BCRP/ABCG2) is a methotrexate polyglutamate transporter. *Cancer Res* **63**(17): 5538-5543.

Wang L, Cherian C, Kugel Desmoulin S, Mitchell-Ryan S, Hou Z, Matherly LH and Gangjee A (2012) Synthesis and biological activity of 6-substituted pyrrolo[2,3-d]pyrimidine thienoyl regioisomers as inhibitors of de novo purine biosynthesis with selectivity for cellular uptake by high affinity folate receptors and the proton-coupled folate transporter over the reduced folate carrier. *J Med Chem*.

Wang L, Cherian C, Kugel Desmoulin S, Polin L, Deng Y, Wu J, Hou Z, White K, Kushner J, Matherly LH and Gangjee A (2010) Synthesis and antitumor activity of a novel series of 6-substituted pyrrolo[2,3-d]pyrimidine thienoyl antifolate inhibitors of purine biosynthesis with selectivity for high affinity folate receptors and the proton-coupled folate transporter over the reduced folate carrier for cellular entry. *J Med Chem* **53**(3): 1306-1318.

Wang L, Desmoulin SK, Cherian C, Polin L, White K, Kushner J, Fulterer A, Chang MH, Mitchell-Ryan S, Stout M, Romero MF, Hou Z, Matherly LH and Gangjee A (2011) Synthesis, biological, and antitumor activity of a highly potent 6-substituted pyrrolo[2,3-

d]pyrimidine thienoyl antifolate inhibitor with proton-coupled folate transporter and folate receptor selectivity over the reduced folate carrier that inhibits beta-glycinamide ribonucleotide formyltransferase. *J Med Chem* **54**(20): 7150-7164.

Wang L, Wallace A, Raghavan S, Deis SM, Wilson MR, Yang S, Polin L, White K, Kushner J, Orr S, George C, O'Connor C, Hou Z, Mitchell-Ryan S, Dann CE, 3rd, Matherly LH and Gangjee A (2015) 6-Substituted Pyrrolo[2,3-d]pyrimidine Thienoyl Regioisomers as Targeted Antifolates for Folate Receptor alpha and the Proton-Coupled Folate Transporter in Human Tumors. *J Med Chem* **58**(17): 6938-6959.

Wang W, Marsh S, Cassidy J and McLeod HL (2001) Pharmacogenomic dissection of resistance to thymidylate synthase inhibitors. *Cancer Res* **61**(14): 5505-5510.

Wang X, Shen F, Freisheim JH, Gentry LE and Ratnam M (1992) Differential stereospecificities and affinities of folate receptor isoforms for folate compounds and antifolates. *Biochem Pharmacol* **44**(9): 1898-1901.

Wang Y, Zhao R and Goldman ID (2004) Characterization of a folate transporter in HeLa cells with a low pH optimum and high affinity for pemetrexed distinct from the reduced folate carrier. *Clin Cancer Res* **10**(18 Pt 1): 6256-6264.

Webb BA, Chimenti M, Jacobson MP and Barber DL (2011) Dysregulated pH: a perfect storm for cancer progression. *Nature reviews Cancer* **11**(9): 671-677.

Weitman SD, Frazier KM and Kamen BA (1994) The folate receptor in central nervous system malignancies of childhood. *Journal of neuro-oncology* **21**(2): 107-112.

Weitman SD, Lark RH, Coney LR, Fort DW, Frasca V, Zurawski VR, Jr. and Kamen BA (1992a) Distribution of the folate receptor GP38 in normal and malignant cell lines and tissues. *Cancer Res* **52**(12): 3396-3401.

Weitman SD, Weinberg AG, Coney LR, Zurawski VR, Jennings DS and Kamen BA (1992b) Cellular localization of the folate receptor: potential role in drug toxicity and folate homeostasis. *Cancer Res* **52**(23): 6708-6711.

Wessels JA, Huizinga TW and Guchelaar HJ (2008) Recent insights in the pharmacological actions of methotrexate in the treatment of rheumatoid arthritis. *Rheumatology* **47**(3): 249-255.

Westerhof GR, Schornagel JH, Kathmann I, Jackman AL, Rosowsky A, Forsch RA, Hynes JB, Boyle FT, Peters GJ, Pinedo HM and et al. (1995) Carrier- and receptor-mediated transport of folate antagonists targeting folate-dependent enzymes: correlates of molecular-structure and biological activity. *Mol Pharmacol* **48**(3): 459-471.

Wettergren Y, Odin E, Nilsson S, Willen R, Carlsson G and Gustavsson B (2005) Low expression of reduced folate carrier-1 and folylpolyglutamate synthase correlates with lack of a deleted in colorectal carcinoma mRNA splice variant in normal-appearing mucosa of colorectal carcinoma patients. *Cancer detection and prevention* **29**(4): 348-355.

Whetstine JR, Flatley RM and Matherly LH (2002a) The human reduced folate carrier gene is ubiquitously and differentially expressed in normal human tissues: identification of seven non-coding exons and characterization of a novel promoter. *Biochem J* **367**(Pt 3): 629-640.

Whetstine JR, Witt TL and Matherly LH (2002b) The human reduced folate carrier gene is regulated by the AP2 and sp1 transcription factor families and a functional 61-base pair polymorphism. *J Biol Chem* **277**(46): 43873-43880.

White JC, Bailey BD and Goldman ID (1978) Lack of stereospecificity at carbon 6 of methyltetrahydrofolate transport in Ehrlich ascites tumor cells. Carrier-mediated transport of both stereoisomers. *J Biol Chem* **253**(1): 242-245.

White JC and Goldman ID (1981) Methotrexate resistance in al L1210 cell line resulting from increased dihydrofolate reductase, decreased thymidylate synthetase activity, and normal membrane transport. Computer simulations based on network thermodynamics. *J Biol Chem* **256**(11): 5722-5727.

Whittington DA, Waheed A, Ulmasov B, Shah GN, Grubb JH, Sly WS and Christianson DW (2001) Crystal structure of the dimeric extracellular domain of human carbonic anhydrase XII, a bitopic membrane protein overexpressed in certain cancer tumor cells. *Proceedings of the National Academy of Sciences of the United States of America* **98**(17): 9545-9550.

Wielinga P, Hooijberg JH, Gunnarsdottir S, Kathmann I, Reid G, Zelcer N, van der Born K, de Haas M, van der Heijden I, Kaspers G, Wijnholds J, Jansen G, Peters G and Borst P (2005) The human multidrug resistance protein MRP5 transports folates and can mediate cellular resistance against antifolates. *Cancer Res* **65**(10): 4425-4430.

Williams FM and Flintoff WF (1995) Isolation of a human cDNA that complements a mutant hamster cell defective in methotrexate uptake. *J Biol Chem* **270**(7): 2987-2992.

Wilson MR, Hou Z and Matherly LH (2014) Substituted cysteine accessibility reveals a novel transmembrane 2-3 reentrant loop and functional role for transmembrane domain 2 in the human proton-coupled folate transporter. *J Biol Chem* **289**(36): 25287-25295.

Wilson MR, Hou Z, Wilson LJ, Ye J and Matherly LH (2016a) Functional and mechanistic roles of the human proton-coupled folate transporter transmembrane domain 6-7 linker. *Biochem J*.

Wilson MR, Hou Z, Yang S, Polin L, Kushner J, White K, Huang J, Ratnam M, Gangjee A and Matherly LH (2016b) Targeting Nonsquamous Nonsmall Cell Lung Cancer via the Proton-Coupled Folate Transporter with 6-Substituted Pyrrolo[2,3-d]Pyrimidine Thienoyl Antifolates. *Mol Pharmacol* **89**(4): 425-434.

Wilson MR, Kugel S, Huang J, Wilson LJ, Wloszczynski PA, Ye J, Matherly LH and Hou Z (2015) Structural determinants of human proton-coupled folate transporter oligomerization: role of GXXXG motifs and identification of oligomeric interfaces at transmembrane domains 3 and 6. *Biochem J* **469**(1): 33-44.

Witt TL, Stapels SE and Matherly LH (2004) Restoration of transport activity by co-expression of human reduced folate carrier half-molecules in transport-impaired K562 cells: localization of a substrate binding domain to transmembrane domains 7-12. *J Biol Chem* **279**(45): 46755-46763.

Wollack JB, Makori B, Ahlawat S, Koneru R, Picinich SC, Smith A, Goldman ID, Qiu A, Cole PD, Glod J and Kamen B (2008) Characterization of folate uptake by choroid plexus epithelial cells in a rat primary culture model. *Journal of neurochemistry* **104**(6): 1494-1503.

Wong SC, Proefke SA, Bhushan A and Matherly LH (1995) Isolation of human cDNAs that restore methotrexate sensitivity and reduced folate carrier activity in methotrexate transport-defective Chinese hamster ovary cells. *J Biol Chem* **270**(29): 17468-17475.

Wong SC, Zhang L, Proefke SA, Hukku B and Matherly LH (1998) Gene amplification and increased expression of the reduced folate carrier in transport elevated K562 cells. *Biochem Pharmacol* **55**(7): 1135-1138.

Worm J, Kirkin AF, Dzhandzhugazyan KN and Guldberg P (2001) Methylation-dependent silencing of the reduced folate carrier gene in inherently methotrexate-resistant human breast cancer cells. *J Biol Chem* **276**(43): 39990-40000.

Wright JE, Vaidya CM, Chen Y and Rosowsky A (2000) Efficient utilization of the reduced folate carrier in CCRF-CEM human leukemic lymphoblasts by the potent antifolate N(alpha)-(4-amino-4-deoxypteroyl)-N(delta)-hemiphthaloyl-L- ornithine (PT523) and its B-ring analogues. *Biochem Pharmacol* **60**(1): 41-46.

Wu M, Fan J, Gunning W and Ratnam M (1997) Clustering of GPI-anchored folate receptor independent of both cross-linking and association with caveolin. *The Journal of membrane biology* **159**(2): 137-147.

Wu M, Gunning W and Ratnam M (1999) Expression of folate receptor type alpha in relation to cell type, malignancy, and differentiation in ovary, uterus, and cervix. *Cancer epidemiology, biomarkers & prevention : a publication of the American Association for Cancer Research, cosponsored by the American Society of Preventive Oncology* **8**(9): 775-782.

Xia W and Low PS (2010) Folate-targeted therapies for cancer. *J Med Chem* **53**(19): 6811-6824.

Yan C and Luo J (2010) An analysis of reentrant loops. *The protein journal* **29**(5): 350-354.

Yang R, Sowers R, Mazza B, Healey JH, Huvos A, Grier H, Bernstein M, Beardsley GP, Krailo MD, Devidas M, Bertino JR, Meyers PA and Gorlick R (2003) Sequence alterations in the reduced folate carrier are observed in osteosarcoma tumor samples. *Clin Cancer Res* **9**(2): 837-844.

Yin MB, Voigt W, Panadero A, Vanhoefer U, Frank C, Pajovic S, Azizkhan J and Rustum YM (1997) p53 and WAF1 are induced and Rb protein is hypophosphorylated during cell

growth inhibition by the thymidylate synthase inhibitor ZD1694 (Tomudex). *Mol Pharmacol* **51**(4): 630-636.

Zain J and O'Connor O (2010a) Pralatrexate: basic understanding and clinical development. *Expert opinion on pharmacotherapy* **11**(10): 1705-1714.

Zain JM and O'Connor O (2010b) Targeted treatment and new agents in peripheral T-cell lymphoma. *International journal of hematology* **92**(1): 33-44.

Zeng H, Chen ZS, Belinsky MG, Rea PA and Kruh GD (2001) Transport of methotrexate (MTX) and folates by multidrug resistance protein (MRP) 3 and MRP1: effect of polyglutamylation on MTX transport. *Cancer Res* **61**(19): 7225-7232.

Zhao R, Diop-Bove N, Visentin M and Goldman ID (2011a) Mechanisms of membrane transport of folates into cells and across epithelia. *Annu Rev Nutr* **31**: 177-201.

Zhao R, Gao F and Goldman ID (2001) Marked suppression of the activity of some, but not all, antifolate compounds by augmentation of folate cofactor pools within tumor cells. *Biochem Pharmacol* **61**(7): 857-865.

Zhao R, Gao F, Hanscom M and Goldman ID (2004a) A prominent low-pH methotrexate transport activity in human solid tumors: contribution to the preservation of methotrexate pharmacologic activity in HeLa cells lacking the reduced folate carrier. *Clin Cancer Res* **10**(2): 718-727.

Zhao R and Goldman ID (2003) Resistance to antifolates. *Oncogene* **22**(47): 7431-7457.

Zhao R and Goldman ID (2007) The molecular identity and characterization of a Proton-coupled Folate Transporter--PCFT; biological ramifications and impact on the activity of pemetrexed. *Cancer Metastasis Rev* **26**(1): 129-139.

Zhao R, Hanscom M, Chattopadhyay S and Goldman ID (2004b) Selective preservation of pemetrexed pharmacological activity in HeLa cells lacking the reduced folate carrier: association with the presence of a secondary transport pathway. *Cancer Res* **64**(9): 3313-3319.

Zhao R, Matherly LH and Goldman ID (2009a) Membrane transporters and folate homeostasis: intestinal absorption and transport into systemic compartments and tissues. *Expert Rev Mol Med* **11**: e4.

Zhao R, Min SH, Qiu A, Sakaris A, Goldberg GL, Sandoval C, Malatack JJ, Rosenblatt DS and Goldman ID (2007) The spectrum of mutations in the PCFT gene, coding for an intestinal folate transporter, that are the basis for hereditary folate malabsorption. *Blood* **110**(4): 1147-1152.

Zhao R, Min SH, Wang Y, Campanella E, Low PS and Goldman ID (2009b) A role for the proton-coupled folate transporter (PCFT-SLC46A1) in folate receptor-mediated endocytosis. *J Biol Chem* **284**(7): 4267-4274.

Zhao R, Najmi M, Fiser A and Goldman ID (2016) Identification of an Extracellular Gate for the Proton-coupled Folate Transporter (PCFT-SLC46A1) by Cysteine Cross-linking. *J Biol Chem* **291**(15): 8162-8172.

Zhao R, Qiu A, Tsai E, Jansen M, Akabas MH and Goldman ID (2008) The proton-coupled folate transporter: impact on pemetrexed transport and on antifolates activities compared with the reduced folate carrier. *Mol Pharmacol* **74**(3): 854-862.

Zhao R, Sharina IG and Goldman ID (1999) Pattern of mutations that results in loss of reduced folate carrier function under antifolate selective pressure augmented by chemical mutagenesis. *Mol Pharmacol* **56**(1): 68-76.

Zhao R, Shin DS, Diop-Bove N, Ovits CG and Goldman ID (2011b) Random mutagenesis of the proton-coupled folate transporter (SLC46A1), clustering of mutations, and the bases for associated losses of function. *J Biol Chem* **286**(27): 24150-24158.

Zhao R, Shin DS, Fiser A and Goldman ID (2012) Identification of a functionally critical GXXG motif and its relationship to the folate binding site of the proton-coupled folate transporter (PCFT-SLC46A1). *Am J Physiol Cell Physiol* **303**(6): C673-681.

Zhao R, Unal ES, Shin DS and Goldman ID (2010) Membrane topological analysis of the proton-coupled folate transporter (PCFT-SLC46A1) by the substituted cysteine accessibility method. *Biochemistry* **49**(13): 2925-2931.

ABSTRACT

STRUCTURAL CHARACTERIZATION AND THERAPEUTIC UTILITY OF THE PROTON-COUPLED FOLATE TRANSPORTER

by

MICHAEL ROY WILSON

December 2016

Advisor: Dr. Larry H. Matherly

Major: Cancer Biology

Degree: Doctor of Philosophy

Folate is a B9 vitamin essential to DNA synthesis. The proton-coupled folate transporter (PCFT) is a newly discovered proton/folate symporter with an acidic pH optimum and broad expression across a variety of solid tumor types, with limited expression in normal tissues. Several antifolate molecules have been developed as cancer therapeutics, although these classical antifolates display numerous off-target effects due to transport by the ubiquitous reduced folate carrier (RFC). In this dissertation, we determine the roles of multiple PCFT structure/function domains, and develop PCFT-specific antifolates to target solid tumors. We utilize substituted cysteine accessibility methods (SCAM) to identify a novel reentrant loop structure between the second and third transmembrane domains (TMDs), which is critical to PCFT function, using membrane-impermeable thiol-reactive reagent MTSEA-biotin. We also utilize SCAM to identify and characterize the PCFT oligomerization interface at TMDs 3 and 6 via crosslinking reagent MTS-6-MTS. By the development of PCFT and ThTr1 chimera molecules, creation of PCFT half molecules, and cysteine- and alanine-scanning mutagenesis, we determined the purely structural role of the TMD6-7 connecting loop region. We studied novel 6-substituted pyrrolo[2,3-*d*]pyrimidine thienoyl regioisomers related to pemetrexed (PMX), a standard NS-

NSCLC treatment. [AGF94 (2',5') and AGF154 (2',4')], which showed potencies comparable to PMX toward six NS-NSCLC cell lines. Uptake of [^{3}H]AGF154 was comparable to that of [^{3}H]PMX at acidic pH. *De novo* purine biosynthesis inhibition by AGF94/154 was confirmed by an *in situ* assay which measures incorporation of [^{14}C]glycine into formyl GAR. *In vivo* efficacy of AGF94 was seen toward H460 tumor xenografts in severe-combined immunodeficient mice. Additonal antifolates were synthesized through the addition of fluorine to existing molecules and studied for their transport specifiticies correlating with anti-proliferative effects. In particular, AGF278 displayed increased specificity to PCFT, while also being very potent toward ovarian cancer cell lines. In conclusion, we established the role of three key structural domains of PCFT while also developing several novel PCFT-targeted antifolates for use as cancer therapeutics for NS-NSCLC and ovarian cancer. These novel antifolates are targeted to the acidic tumor microenvironment via selective transport by PCFT.

AUTOBIOGRAPHICAL STATEMENT

EDUCATION

Wayne State University 2011-2016
Doctor of Philosophy: Cancer Biology
Grand Valley State University 2007-2011
Bachelor of Science: Cell & Molecular Biology (Minors in Chemistry, Philosophy)

GRANTS

T-32 Training Grant- National Institute of Health (NIH) 2013-2015
Rumble Fellowship- Wayne State University 2015-2016

SELECTED PUBLICATIONS

Wilson M.R., Hou Z., Wilson L.J., Ye J., Matherly L.H. Determining the role of the transmembrane domain 6/7 linker of the proton-coupled folate transporter via folate transporter/thiamine transporter chimeras. [ePub ahead of print] **2016.**

Golani L.K., Wallace-Povirk A., Deis S.M., Wong J.E., Ke J., Gu X., Raghavan S., **Wilson M.R.**, Li X., Polin L., Waal P.W., White K., Kushner J., O'Connor C., Hou Z., Xu H.E., Melcher K., Dann III C.E., Matherly L.H., and Gangjee A. Tumor targeting with novel 6-Substituted pyrrolo [2,3-*d*] pyrimidine antifolates with heteroatom bridge substitutions via cellular uptake by folate receptor α and the proton-coupled folate transporter and inhibition of *de novo* purine nucleotide biosynthesis. [ePub ahead of print] **2016.**

Wilson M.R., Hou Z., Yang S., Polin L., Kushner J., White K., Huang J., Ratnam M., Gangjee A., Matherly L.H. Targeting non-squamous non-small cell lung cancer via the proton-coupled folate transporter with 6-substituted pyrrolo[2,3-*d*]pyrimidine thienoyl antifolates. Mol Pharmacol. 89(4):425-34. **2016.**

Wang L., Wallace A., Raghavan S., Deis S.M., **Wilson M.R.**, Yang S., Polin L., White K., Kushner J., Orr S., George C., O'Connor C., Hou Z., Mitchell-Ryan S., Dann C.E. 3rd, Matherly L.H., Gangjee A. 6-Substituted pyrrolo[2,3-*d*]pyrimidine thienoyl regioisomers as targeted antifolates for folate receptor α and the proton-coupled folate transporter in human tumors. J Med Chem. 58(17):6938-59. **2015.**

Wilson M.R., Kugel S., Huang J., Wilson L.J., Wloszczynski P.A., Ye J., Matherly L.H., Hou Z. Structural determinants of human proton-coupled folate transporter oligomerization: role of GXXXG motifs and identification of oligomeric interfaces at transmembrane domains 3 and 6. Biochem J. 469(1):33-44. **2015.**

Golani L.K., George C., Zhao S., Raghavan S., Orr S., Wallace A., **Wilson M.R.**, Hou Z., Matherly L.H., Gangjee A. Structure-activity profiles of novel 6-substituted pyrrolo[2,3-*d*]pyrimidine thienoyl antifolates with modified amino acids for cellular uptake by folate receptors α and β and the proton-coupled folate transporter. J Med Chem. 57(19):8152-66. **2014.**

Wilson, M.R., Hou, Z., & Matherly, L.H. Substituted cysteine accessibility reveals a novel transmembrane 2-3 reentrant loop and functional role for transmembrane domain 2 in the human proton-coupled folate transporter. J Biol Chem. 289(36):25287-95. **2014.**